

Characterization of Wood Sheathed Cold-Formed Steel Diaphragms Under in Plane Loading (Phase 2 of Diaphragm Research Program)

By

Patrick Latreille



Department of Civil Engineering and Applied Mechanics

McGill University, Montreal, Canada

August 2016

A thesis submitted to McGill University
in partial fulfillment of the requirements of
the degree of Master of Engineering

©Patrick Latreille, 2016

Abstract

There exists a desire to better understand the in-plane response of cold-formed steel (CFS) framed diaphragms subjected to seismic loading. At present, the diaphragm design information available in the North American design standards (AISI S240, AISI S400) is not applicable in Canada and is of limited scope in the United States and Mexico. These design provisions are based largely on basic principles of engineering and the extrapolation of design methods used for wood diaphragms. Few full-scale tests have been performed to validate the accuracy of these design values and equations for real world application. Furthermore, the effect of non-structural components on the in-plane strength and stiffness of the diaphragm component has yet to be explored. In an effort to provide insight into the complex nature of the diaphragm structure and the influence of non-structural components, a research program was initiated in the Jamieson Structures Laboratory at McGill University focusing on the characterization of the behaviour of CFS framed - wood sheathed diaphragms under in-plane loading. A total of six 3.7m x 6.1m CFS diaphragm specimens with oriented strand board sheathing were tested following the cantilever test method. Three of these diaphragms focused on the effects of structural changes, while the remaining three were used to investigate the effects of incorporating non-structural elements in the construction.

This thesis contains a detailed account of these six tests, including their design, construction and the overall results and observations. The tests focusing on structural changes, demonstrated that the orientation of the joists with respect to loading had little effect on the overall diaphragm response, strap blocking for panel edges was shown to be just as effective as full blocking and an upper threshold for shear strength and stiffness was reached by reducing the spacing of the perimeter fasteners. The tests of diaphragms built having non-structural elements demonstrated that both the addition of a single layer of gypsum panels to the underside of the diaphragm and a

19mm gypcrete topping poured on top of the wood sheathing had a significant strengthening and stiffening impact on the overall diaphragms response. Design predictions were calculated using the AISI S400 Standard for both deflection and shear strength. Meaningful comparisons were only realized for design deflection when the equation for shear walls was used with the values adjusted to remove inelastic behaviour, while no meaningful comparisons were realized for shear strength due to the limited information available within the S240 and S400 standards.

Résumé

Il y a actuellement un manque de compréhension concernant la réaction des diaphragmes en acier formé à froid (AFF) soumis à un chargement sismique. Les informations contenues dans les normes de conception nord-américaines (AISI S240, AISI S400) concernant la conception des diaphragmes ne sont pas applicables au Canada et sont limitées à une utilisation aux États-Unis et au Mexique. Ces dispositions de conception sont basées en grande partie sur des principes fondamentaux d'ingénierie et l'extrapolation des méthodes de conception utilisées pour les diaphragmes en bois. Peu de tests à grande échelle ont été réalisés pour valider l'exactitude de ces équations pour une application en situation réelle. En outre, l'effet des éléments non structuraux sur la résistance latérale et la rigidité du diaphragme n'a pas encore été exploré. Dans le but de mieux comprendre la complexité de la structure des diaphragmes et l'influence des éléments non structuraux, un programme expérimental a été initié dans le laboratoire de Structures Jamieson de L'Université McGill. Le programme est centré sur la caractérisation des diaphragmes avec cadre en AFF et platelage en bois soumis à des charges latérales. Un total de six spécimens de diaphragmes 3.7m par 6.1m en AFF avec des panneaux de lamelles orientées (OSB) ont été testés avec la méthode du porte-à-faux. Trois de ces diaphragmes ont été utilisés pour examiner les effets des changements structurels et les trois autres pour étudier les effets de l'intégration des éléments non structurels dans la construction.

Cette thèse contient un compte détaillé de ces six essais incluant leur conception, leur construction ainsi que les résultats et observations globales. Les tests centrés sur les changements structurels ont démontré que l'orientation des solives par rapport au chargement a un effet mineur sur la réponse globale du diaphragme. Le blocage réalisé avec des sangles a été aussi efficace que le blocage complet. En diminuant les espaces entre les vis sur le périmètre des panneaux, la résistance

et la rigidité ont été augmentées. Les tests des diaphragmes construits avec des éléments non-structuraux ont démontré que l'addition d'une seule couche de panneaux de gypse sur la face inférieure du diaphragme et une garniture de gypcrete de 19mm versée sur le dessus du platelage de bois a eu un impact significatif sur la résistance et la rigidité des diaphragmes. Un dimensionnement préliminaire a été effectué avec la Norme AISI S400 afin de comparer la résistance et les déformations obtenues lors des tests. Des résultats satisfaisants ont été atteints pour les déformations lorsque l'équation pour les murs de cisaillement a été utilisée, ajustée d'un comportement élastique. Par contre, les résultats des tests ne corroboraient pas aux valeurs théoriques fournies par la norme pour la résistance au cisaillement, notamment à cause du manque d'information disponible dans les normes S240 et S400.

Acknowledgements

I would like to extend my most sincere gratitude to Colin Rogers for all of the guidance and support he has given me as mentor of my Master's program and also as the professor of some of my favorite courses taken at McGill. His attention to detail and his ability to take a complicated subject and present it in a way that is easy to understand are traits that I admire and hope to bring with me into my working career as a structural engineer.

A special thanks to Evelina Nikolaidou, whose patience with me was surpassed by none. It was a true blessing to have been able to work beside someone with so much wisdom on such an interesting project.

I would also like to thank Dr. Bill Cook and John Bartczak for all the help they provided in the lab as well as to all my friends who worked directly on the project, Andrea Iachetta, David Pizzuto, Rico Massa, Chas Morin, Keith Lee and Nick Adomat. It was an absolute pleasure to work beside every one of you and I wish you the best in your studies and future careers.

To all my friends and family which made the whole experience one that I will never forget. I wish to express my gratitude to Robert Rizk, Veronica Santos, Jinghui Ding, Waqas Ahmed, Vincent Briere and Julien Cravero who made going to class and working in the lab always something to look forward to. To my loving girlfriend Julia Boland, who was always there for me, through final exams and deadlines, who helped motivate and inspire me, I simply could not have done it without you.

Finally, a thank you to all of the organizations who financially supported this project to make it possible. The Natural Sciences and Engineering Research Council of Canada (NSERC), the Canadian Sheet Steel Building Institute (CSSBI) and the American Iron and Steel Institute (AISI).

A special thank you is extended to Bailey Metal Products Ltd., Simpson Strong-Tie Co. Inc., Ontario Tools and Fasteners Ltd, le Groupe Beauchesne, Maxxon Corporation, Beton Autonivelant SGI, ArcelorMittal and Construction Proco Inc. for the all the materials and tools that they provided. Lastly, I would like to express my gratitude to the Pierre Arbour Foundation and Hewitt Equipment Ltd. for believing in me as a student and for providing me the financial assistance which allowed me to focus on my studies and ultimately succeed in my academic endeavours.

Table of Contents

Abstract.....	i
Résumé.....	iii
Acknowledgements.....	v
Table of Contents.....	vii
List of Figures.....	ix
List of Tables.....	xii
Chapter 1 Introduction.....	1
1.1 General Overview.....	1
1.2 Statement of Problem.....	4
1.3 Research Objectives.....	4
1.4 Scope of Study.....	5
1.5 Literature Review.....	7
1.5.1 Summary of Research on CFS Framed Diaphragms.....	7
1.5.2 Design Deflection Equations.....	11
1.5.3 Phase 1 of the CFS Diaphragm Research Program at McGill University.....	18
Chapter 2 Test Program.....	25
2.1 Test Apparatus.....	25
2.2 Test Diaphragms.....	28
2.2.1 (11-RALT-M) Roof Alternate Direction Joists - Monotonic Loading.....	30
2.2.2 (12-RSTRAP-M) Roof Strap Blocking - Monotonic Loading.....	30
2.2.3 (13-FB4-M) Floor Blocked (100mm / 300mm) Spacing - Monotonic Loading.....	31
2.2.4 (14-RGYP-M & 15-RGYP-C) Roof with Gypsum Ceiling - Monotonic & Reversed Cyclic Loading.....	31
2.2.5 (16-FCRETE-M) Floor with 19mm Gypcrete Topping.....	33
2.3 Diaphragm Construction.....	35
2.4 Instrumentation.....	47
2.5 Loading Protocol.....	49
2.5.1 Monotonic.....	49
2.5.2 Reversed Cyclic.....	49
Chapter 3 Test Results and Observations.....	52
3.1 Material Properties.....	52
3.1.1 Steel.....	52

3.1.2 OSB and Gypsum.....	54
3.1.3 Gypcrete.....	56
3.1.4 Sheathing-to-Frame Connection Tests.....	57
3.2 Diaphragm Test Results and Observations	62
3.2.1 (11-RALT-M) Roof Alternate Direction Joists – Monotonic Loading.....	62
3.2.2 (12-RSTRAP-M) Roof Strap Blocking – Monotonic Loading.....	67
3.2.3 (13-FB4-M) Floor Blocked (100mm / 300mm) Spacing – Monotonic Loading	69
3.2.4 (14-RGYP-M) Roof with Gypsum Ceiling – Monotonic Loading.....	76
3.2.5 (15-RGYP-C) Roof with Gypsum Ceiling – Reversed Cyclic Loading	79
3.2.6 (16-FCRETE-M) Floor with Gypcrete Topping – Monotonic Loading	82
3.3 Design Predictions	86
3.3.1 In-Plane Deflection	86
3.3.2 Shear Strength.....	98
3.4 Comparison of Test Results Between Phase 1 and Phase 2.....	100
3.4.1 11-RALT-M vs. 7-RB-M ; Direction of Joists.....	101
3.4.2 12-RSTRAP-M vs. 7-RB-M ; Type of Panel Edge Blocking.....	104
3.4.3 13-FB4-M vs. 9-F#12-M ; Maximized Shear Resistance	106
3.4.4 14-RGYP-M & 15-RGYP-C vs. 3-RU-M & 4-RU-C ; Installation of Gypsum Ceiling	107
3.4.5 16-FCRETE-M vs. 9-F#12-M ; Installation of Gypcrete Topping	109
Chapter 4 Conclusions and Recommendations.....	112
4.1 Conclusion	112
4.2 Recommendations for Future Research	114
References.....	117
APPENDIX A:.....	120
APPENDIX B:.....	151
APPENDIX C:.....	162
APPENDIX D:.....	172

List of Figures

Figure 1.1: Illustration of Joist to Rim Joist Configuration	2
Figure 1.2: Illustration of Blocked and Unblocked Diaphragms	3
Figure 1.3: Testing Configuration Used by NAHBRC (NAHBRC 1999).....	9
Figure 1.4: Schematic of CFS-NEES Test Structure (Peterman 2014).....	11
Figure 1.5: Illustration of Diaphragm Deflection (Serrette and Chau 2003)	15
Figure 1.6: Illustration of Shear Wall Deflection (Serrette and Chau 2003)	18
Figure 1.7: Illustration of Cantilever Diaphragm Test Apparatus (Phase 1)	20
Figure 1.8: Comparison of Shear Force vs. Rotation for Tests Performed in Phase 1: a) and b) Show the Monotonic and Cyclic Tests Performed for the Roof Specimen (Unblocked vs. Blocked) c) and d) Show the Monotonic and Cyclic Tests Performed for the Floor Specimen (#10 vs. #12 Fasteners) (Nikolaidou et al. 2015)	21
Figure 1.9: Photo of Bending Action of the Diaphragm After Sheathing Failure (Sheathing Removed to Show Frame) (Nikolaidou et al. 2015).....	22
Figure 2.1 Illustration of Test Apparatus	27
Figure 2.2: Photograph of Diaphragm Test Apparatus with Rim Joists Bolted to Fixed and Free Ends....	27
Figure 2.3: (Left) Greased Rollers on Distribution Beam (Right) Actuator to Distribution Beam Connection	28
Figure 2.4: (Left) Fixed End Connection (Right) Pre-Tensioned 38mm Threaded Rods.....	28
Figure 2.5: Bare Frame and Frame with Sheathing: Specimen 11-RALT-M	30
Figure 2.6: Bare Frame and Frame with Sheathing: Specimen 12-RSTRAP-M	31
Figure 2.7: Bare Frame and Frame with Sheathing: Specimen 13-FB4-M	31
Figure 2.8: Bare Frame and Frame with Sheathing: Specimen 14-RGYP-M and 15-RGYP-C	32
Figure 2.9: Specimen 14-RGYP-M Before and After Joint Tape and Compound was Placed Between Panels and at Screw Locations.....	33
Figure 2.10: Bare Frame and Frame with Sheathing: Specimen 16-FCRETE-M	34
Figure 2.11: (Left) 25mm Boarder Surrounding Perimeter of Diaphragm (Right) Application of Primer to OSB.....	34
Figure 2.12: (Left) Drilling Holes with Magnetic Drill (Right) Snug-Tightening Rim Joist to Frame Using Elongated Ratchet	36
Figure 2.13: Roof Specimen Joist to Rim Joist Connection	37
Figure 2.14: Diaphragm Specimen After Installation of Rim Joists and Joists	38
Figure 2.15: (Left) Unblocked Specimen (14-RGYP-M) (Right) Web-Stiffener to Joist Connection (Closed Face)	39
Figure 2.16: Frame of Specimen 13-FB4-M.....	40
Figure 2.17: (Left) Alternating Blocking Members (Right) Blocking Connected to Joist (Open Face)	40
Figure 2.18: Frame of Specimen 12-RSTRAP-M	41
Figure 2.19: Strap Splice Interface at Mid-Span of Blocking Member	42
Figure 2.20: (Left) Square Edge Roof OSB (Right) Tongue-and-Groove Floor OSB	43
Figure 2.21: (Left) Initial Lift of Specimen 14-RGYP-M Using I-Hooks (Right) Applying Joint Tape and Compound to Panel Interface.....	44
Figure 2.22: Application of First Coat of Floor Primer to OSB Sheathing	46
Figure 2.23: (Left) Photo of GYP-CRETE2000®/3.2K (Right) Photo of Barrel Batch Mixing Process....	46

Figure 2.24: (Left) Progress after 2/3 of Gypcrete Had Been Poured (Right) Photo Immediately After Pour	47
Figure 2.25: Placement of String Potentiometers	48
Figure 2.26: Placement of Linear Variable Differential Transformers (LVDTs)	48
Figure 2.27: Displacement vs Time for Specimen 15-RGYP-C	50
Figure 3.1: (Left) Photo of 150 KN MTS Sintech Machine (Right) Tensile Coupon Samples	53
Figure 3.2: Engineering Stress-Strain Curve of Roof Joist Sample 1	54
Figure 3.3: Single Shear Screw-Fastened Connection Test Set Up (Tao et al. 2016) and Specimen Dimensions (in mm) and Construction (Tao et al. 2016).....	59
Figure 3.4: Backbone Curve Nomenclature (Tao et al. 2016)	60
Figure 3.5: (a) Dowel Bearing Test Setup and (b) Sheathing Specimen Dimensions for Bearing Tests (Tao et al. 2016)	61
Figure 3.6: Progression Damage to Connection between Rim Joist and C-Shaped Section: a) Initial Position b) Position at Which Test was Stopped c) Position Where Connection Had Failed Completely d) Final Position	63
Figure 3.7: 11-RALT-M Contact Zone Caused by Lateral Displacement of Distribution Beam	64
Figure 3.8: Shear Force vs. Rotation (displacement) for 11-RALT-M.....	65
Figure 3.9: Sheathing Failure along Fixed End of 11-RALT-M	66
Figure 3.10: Hinge in Blocking to Joist Connection of Specimen 11-RALT-M	66
Figure 3.11: Post-Test Blocking Connections along Fixed End (Damage)	66
Figure 3.12: (Left) Original Shear Force vs. Rotation (Displacement) for 11-RALT-M (Right) Modified Shear Force vs. Rotation (Displacement) for 11-RALT-M	67
Figure 3.13: Shear Force vs. Rotation (Displacement) for 12-RSTRAP-M	68
Figure 3.14: (Left) Isolation of South-West Corner Panel of 12-RSTRAP-M (Right) Close Up of Tear-out Fastener Failures	68
Figure 3.15: Bending of CFS Joist at Hinge Location Created After Sheathing Failure	69
Figure 3.16: Tilting of Sheathing Fasteners Due to Shear Forces	69
Figure 3.17: Illustration of Specimen 13-FB4-M with Predicted Axial Forces of Joist Members	71
Figure 3.18: Reinforcements for Critical Connections	72
Figure 3.19: Shear Force vs. Rotation (displacement) for 13-FB4-M	72
Figure 3.20: Gaps Between OSB Panels During Testing of Specimen 13-FB4-M	74
Figure 3.21: Illustration of Compression/Tension Field in Diaphragm Specimen 13-FB4-M	74
Figure 3.22: Damage to Frame Members of Specimen 13-FB4-M Caused by Compression Field in CFS Structure.....	75
Figure 3.23: (Left) Original Shear Force vs. Rotation (Displacement) for Specimen 13-FB4-M (Right) Modified Shear Force vs. Rotation (Displacement) for Specimen 13-FB4-M	75
Figure 3.24: Lift Off of OSB Panels After Failure of Sheathing Fasteners	77
Figure 3.25: (Left) Displacement of Sheathing and Bending of Double Joist (Right) Tear-out of Sheathing Fasteners and Gypsum Failure.....	77
Figure 3.26: 14-RGYP-M Specimen Post-Test with OSB Panels Removed.....	78
Figure 3.27: (Left) Tilted Gypsum Fastener, Gypsum Panel Had Fallen (Right) Tear out of Gypsum Fastener at Corner Location.....	78
Figure 3.28: Shear Force vs. Rotation (displacement) for Diaphragm Specimen 14-RGYP-M.....	79
Figure 3.29: Specimen 15-RGYP-C Sheathing Failure Across Both Panel Row Interfaces	80
Figure 3.30: Connection Failures of Gypsum Panels for Specimen 15-RGYP-C	81

Figure 3.31: Shear Force vs. Rotation (displacement) for Specimen 15-RGYP-C.....	81
Figure 3.32: Progression of Crack Propagation of Gypcrete Topping (16-FCRETE-M).....	83
Figure 3.33: Extensive Deformation at North-East Joist – Rim Joist Connection.....	84
Figure 3.34: Separation of Panels with Increased In-plane Displacement (Post-Peak Loading).....	84
Figure 3.35: Tension Fracture of Gypcrete Topping with Tear out Failure of Sheathing Fasteners	85
Figure 3.36: Illustration of Tension Field on Specimen 16-FCRETE-M	85
Figure 3.37: Shear Force vs. Rotation (displacement) for Specimen 16-FCRETE-M	86
Figure 3.38: Table A Used to Approximate Shear Modulus, G (TECO, 2008).....	89
Figure 3.39: Elastic Deflection for Specimen 12-RSTRAP-M.....	95
Figure 3.40: Table F2.4-1 in AISI S400 (2015).....	99
Figure 3.41: Comparison of 11-RALT-M with 7-RB-M ; Direction of Joists.....	102
Figure 3.42: Comparison of Axial Forces in Framing Members between Specimens 7-RB-M and 11-RALT-M	103
Figure 3.43: Comparison of 12-RSTRAP-M with 7-RB-M ; Type of Panel Edge Blocking	105
Figure 3.44: Comparison of Sheathing Failures ; a) 12-RSTRAP-M and b) 7-RB-M	105
Figure 3.45: Comparison of Hinges Developed in CFS ; a) 12-RSTRAP-M and b) 7-RB-M	106
Figure 3.46: Comparison of 13-FB4-M with 9-F#12-M ; Maximized Shear Resistance	107
Figure 3.47: Comparison of 14-RGYP-M with 3-RU-M ; Installation of Gypsum Ceiling.....	108
Figure 3.48: Comparison of Sheathing Failures ; a) 14-RGYP-M and b) 3-RU-M.....	109
Figure 3.49: Comparison of 15-RGYP-C with 4-RU-C ; Installation of Gypsum Ceiling.....	109
Figure 3.50: Comparison of 16-FCRETE-M with 9-F#12-M ; Installation of Gypcrete Topping	110
Figure 3.51: Sheathing Separation Comparison : a) 9-F#12-M b) 16-FCRETE-M.....	111

List of Tables

Table 1.1: Components of CFS-NEES Building Roof and Floor	19
Table 2.1: Phase 1 Diaphragm Specimen Nomenclature.....	29
Table 2.2: Phase 2 Diaphragm Specimen Nomenclature.....	29
Table 2.3: Summary of Components Used for Diaphragms in Phase 2.....	35
Table 2.4: CUREE Loading Protocol Used for Specimen 15-RGY-P-C	51
Table 3.1: Tensile Coupon Test Results	53
Table 3.2: Moisture Content of OSB and Gypsum Panels Using ASTM D442 Standard (2007)	55
Table 3.3: Gypcrete Cube Compression Test Results.....	56
Table 3.4: Gypcrete Cylindrical Tensile Tests Results.....	57
Table 3.5: Summary of Connection Test Results (Backbone Curve Parameters)	60
Table 3.6: Summary of Dowel Bearing Test Results.....	61
Table 3.7: Comparison of Calculated Deflections Using Equation 3.1 vs. Measured Deflections.....	88
Table 3.8: Comparison of Calculated Deflections Using Equation 3.2 vs. Measured Deflections.....	92
Table 3.9: Summary of General Properties from Phase 2 Diaphragm Tests	96
Table 3.10: Comparison of Calculated Deflections Using Eq. 3.2 vs. Elastic Deflection Values.....	97
Table 3.11: Comparison of Shear Strength Design Values vs. Measured Shear Strength Values.....	99

Chapter 1 Introduction

1.1 General Overview

Cold-formed steel (CFS) is a product where a thin sheet of steel, typically in the range of 0.3 – 6 mm is formed into various shapes at room temperature. CFS can be formed into virtually unlimited different geometric configurations, allowing for it to be applicable in many different areas. A major application for CFS is for structural purposes, predominately used for roofing and framing of low to mid-rise residential and commercial buildings. The main advantage of a CFS structure is that it has the strength of a steel product with the versatility and construction process similar to a wood framed structure. The thin members allow for a very high strength-to-weight ratio, while being formed at room temperature reduces the manufacturing costs. When it comes to construction, CFS members are easy to transport, move around on site, and install without the use of heavy machinery similar to wood framing. Unlike wood framing, CFS members are not affected by insects, nor humidity, making CFS structures very popular in regions where rot or insect damage is a prevalent issue.

A CFS diaphragm is a flat structural unit which is typically incorporated into the design of the floors and roof of a structure in order to transfer in-plane loads from wind or earthquakes to vertical resisting members. One of the more common designs for CFS diaphragms is to have regularly spaced joists connected to rim joists with the use of self-drilling screws (Figure 1.1), upon which wood sheathing, typically plywood or oriented strand board (OSB) panels are screw fastened. The strength of a diaphragm is influenced by the steel frame thickness and joist spacing, the sheathing type and thickness, the fastener type, size and spacing, and whether the edges of the panels are blocked or unblocked. “Blocking” refers in this case to how the wood sheathing is connected, particularly in regards to how the panel edges are fastened. In an unblocked diaphragm, the

sheathing is fastened to the underlying steel frame along two opposite edges while the adjacent edges are fastened only where a joist runs underneath. In a blocked diaphragm, steel blocking is placed between joists in order to provide support around the full perimeter of each panel allowing for all four edges to be fastened (Figure 1.2).

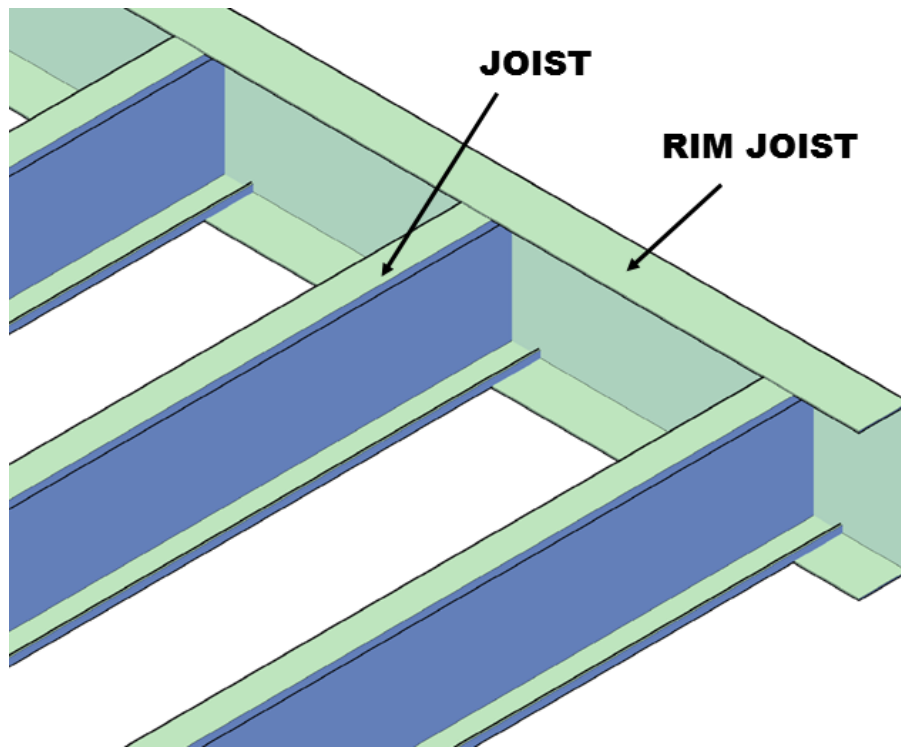


Figure 1.1: Illustration of Joist to Rim Joist Configuration

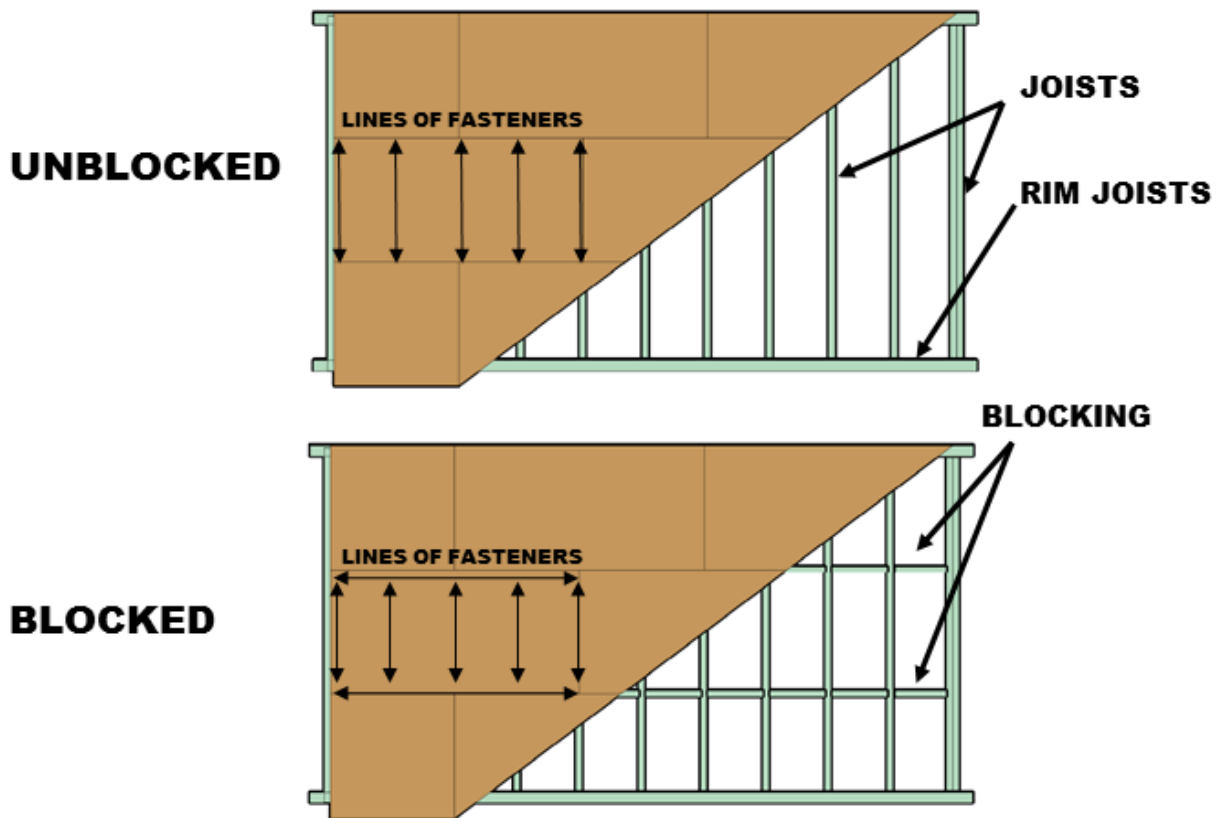


Figure 1.2: Illustration of Blocked and Unblocked Diaphragms

Currently, the design of the lateral force resisting system of cold-formed steel buildings revolves around shear walls, as there is very little research surrounding CFS diaphragms. As a consequence, in Canada there are currently no design provisions for this type of CFS diaphragm (AISI S400, AISI S240). In the US, there exist limited resources for diaphragm design which are mostly based on experimental work done on wood diaphragms. Furthermore, the effect that commonly used non-structural components such as gypsum panels and gypcrete topping have on the overall diaphragm strength and stiffness has yet to be investigated. Therefore, the need to perform research to better understand the behaviour under loading of CFS diaphragms is evident in order to assist professional engineers design safer and more economical CFS structures.

1.2 Statement of Problem

The most current North American Standard for the seismic design of CFS structural systems does not include diaphragm design provisions for use in Canada (AISI S400 2015). The standard does include provisions which can be used in the US and Mexico, however, the provisions offered are limited due to the overall lack of research in this area. In comparison to the design guidelines for hot-rolled steel, concrete and wood, the design deficiencies of the CFS standards become evident (CSA S16-14 2014, CSA A23.3-14 2014, CSA 086-14 2014).

In order to give practicing engineers the toolset to design and create economical and safe CFS structures, a comprehensive design guide needs to be created. To do so, research must be conducted to better understand several aspects of CFS structures, particularly the CFS diaphragm where limited resources currently exist. Experiments on isolated CFS diaphragms under in-plane loading will need to be performed in order to assess the impact of these systems on the overall lateral resisting system. Furthermore, currently existing provisions available for use in the US and Mexico need to be examined to verify their accuracy and comprehensiveness such that they can be adopted for use in Canada. Non-structural elements and the impact they have on the diaphragm's response to in-plane loads also need to be investigated because, currently, no information on the subject exists.

1.3 Research Objectives

The objectives of this research are as follows:

- Perform a literature review on the research related to CFS framed diaphragms, including wood diaphragms on which many of the design provisions are based.
- Summarize the testing done at McGill University during Phase 1 of the diaphragm research program.

- Create and conduct Phase 2 of the diaphragm research program to better understand the in-plane response of various types of CFS diaphragms including the addition of non-structural elements.
- Provide a detailed account of test results and notable observations from the Phase 2 tests.
- Compare the in-plane deflection and shear strength observed in the tests to calculated values as per the design provisions in the AISI S400 Standard (for use in the US and Mexico).
- Draw relevant conclusions by examining the test results and through comparisons to diaphragms tested in Phase 1.

1.4 Scope of Study

Six different wood-sheathed CFS framed diaphragm specimens were tested for the completion of Phase 2 of an ongoing CFS diaphragm study at McGill University. Phase 1, which was carried out by Nikolaidou et al. (2015) primarily consisted of testing a ‘basic’ configuration for both a roof and floor diaphragm, as well as two additional configurations which featured a single structural change. The basic configuration of the CFS frame was designed based on the research performed at the Johns Hopkins University (Peterman 2014, Madsen et al. 2011), where a full scale two-storey CFS wood-sheathed structure was tested under earthquake loading. This design choice was made with the prospect that future researchers could compare the data from the two sets of research and through computer modeling, describe the diaphragm’s impact on the overall response of the lateral force resisting system to load. Phase 1 is described in detail in Section 1.5.2. The diaphragm test specimens were 6.1m by 3.5m which were based on the design space available in the Jamieson Structures Laboratory at McGill University. Budgetary and time constraints allowed for a total of six specimens to be tested in Phase 2. It was decided, based on the results from Phase 1 that it would be more beneficial to test several different configurations under monotonic loading alone. In Phase 1 each diaphragm configuration was tested under both monotonic and cyclical loading

which would require a total of two specimens for each configuration. Hence, Phase 2 consisted of five different configurations tested under monotonic loading with one configuration repeated under reversed cyclic loading. Out of the five configurations, three focused on structural changes while the last two focused on the impact of non-structural elements. Each diaphragm configuration was designed specifically to test the effect of changing a single parameter. This was achieved by designing each specimen to be identical to a diaphragm tested in Phase 1 with the addition of a single change. In doing this, a direct comparison could be made using the results from both tests to observe the effect that the change had on the overall diaphragm response. The parameters tested in this thesis were as follows:

- The impact of the direction of loading with respect to the joist direction
- The comparison of full panel blocking versus strap-blocking
- Estimating an upper limit for the design strength of wood-sheathed CFS framed diaphragms
- The influence of non-structural gypsum ceiling panels on the overall shear strength and stiffness of the diaphragm; and
- The influence of non-structural gypcrete topping on the overall shear strength and stiffness of the diaphragm.

This thesis contains a description of all of the tests performed in Phase 2, as well as a comparison between the results obtained from these tests and the calculated design predictions using the most current standard for the design of CFS structural systems presented in the AISI S400 Standard. Auxiliary tests included within this thesis are the material tests performed for the steel, wood, gypsum and gypcrete as well as a summary of the connection tests performed at Virginia Polytechnic Institute and State University.

1.5 Literature Review

1.5.1 Summary of Research on CFS Framed Diaphragms

The Light Gauge Steel Engineers Association (LGSEA) were among the first groups to begin researching wood-sheathed CFS framed diaphragms. In their 1998 Technical Note the LGSEA states “While tables of service load diaphragm values exist in the various codes for plywood attached to wood framing, values for plywood attached to cold-formed steel framing were not available in any of the nationally recognized building codes at the time of this writing.” (LGSEA 1998). Building upon the works done by Tissell and Elliot on wood diaphragms with wood sheathing and using basic principles of engineering, the LGSEA developed an allowable design strength table for cold-formed steel framed diaphragms (Tissell and Elliot 2004). This table was created by calculating the individual fastener strength and then multiplying it by factors based on grade, spacing and type of sheathing. A slightly modified version of the table developed by the LGSEA is included in the AISI S213 Standard as Table D2-1 (2007), and is also found in the new AISI S400 (2015) Standard as Table F2.4-1.

In 1999 the National Association of Home Builders Research Center (NAHBRC) performed what is believed to be the first full scale horizontal diaphragm test of a cold-formed steel framed structure (NAHBRC 1999). The test was conducted in order to obtain values to be used for empirical design, since none were available at the time that the research was conducted. The testing program consisted of a total of four diaphragm specimens which were 3.6m x 7.2m in size. Out of the four diaphragms, two different configurations were chosen, one that was built with 800S162-43 joists while the other was constructed with thicker 1200S162-54 joists. These two different configurations were chosen to test the influence of joist size and thickness on the overall shear capacity and stiffness of the diaphragm. Each diaphragm consisted of 13 joists placed at the

maximum recommended spacing of 610mm on-centre. The joists were sheathed with 18.3mm thick OSB panels in a staggered arrangement. Finally, the sheathing was attached to the CFS frame via #8 self-drilling, tapping screws which were spaced at 152mm along all edges and 305mm in the field. All diaphragms were designed to be unblocked; the original design from the NAHBRC report is shown in Figure 1.3. The tests were conducted under monotonic loading cycles in accordance with the APA Report 138 recommended test sequence for wood diaphragms (Tissell and Elliot 1993¹). The diaphragms were loaded by a hydraulic cylinder at four equally spaced locations with concentrated loads of equal magnitude. The failure mechanisms of the diaphragms were noted to be very similar between the two different configurations. The failures were characterized by the separation of OSB panels on the tensile side of the diaphragm followed by the screws tearing through the outer edges of wood, which completely separated the sheathing from the diaphragm. The individual fastener responses were examined in order to determine if a good estimate for the diaphragms shear capacity can be obtained by multiplying the connection capacity by the number of fasteners. This method was concluded to be effective based on their test results. It was also concluded that the size and/or thickness of the CFS joists does not have a significant influence on the shear capacity of the diaphragm. Lastly, the NAHBRC formulated a deflection equation for simply supported diaphragms by modifying an existing equation used for shear walls in the *AISI Shear Wall Design Guide* (AISI 1998). This deflection equation was further modified by Serrette and Chau (2003) into what is available today in the current North American CFS standards (AISI S240, AISI S400).

¹ The APA Report 138 has since been revised twice to its current 2004 edition, the 1993 has since been superseded. The reference used herein belongs to the 2004 revision of Report 138

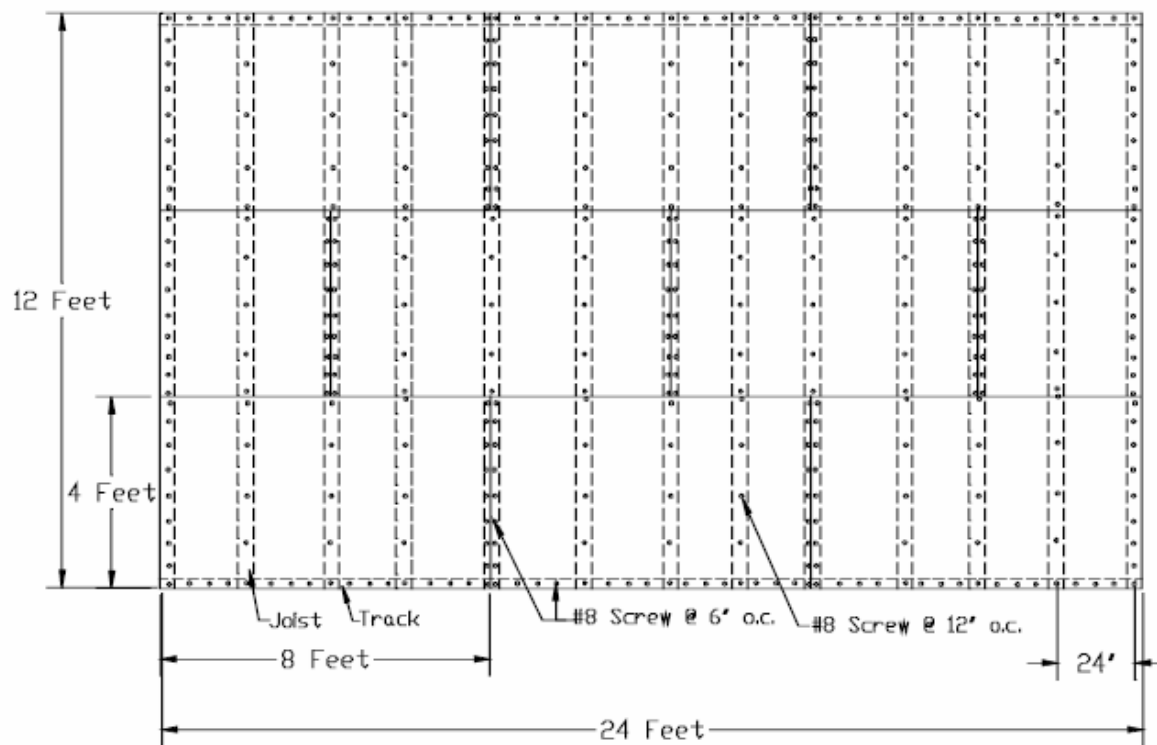


Figure 1.3: Testing Configuration Used by NAHBRC (NAHBRC 1999)

More recently, a full scale experimental work has taken place at John Hopkins University called the CFS-NEES project (Madsen et al. 2011). The main goal of this research was to practice seismic performance-based design of CFS buildings as well as to spur innovation in the field of seismic design of CFS systems. The research was focused on the two full scale, two-storey, CFS-framed structures with wood sheathed shear walls that were designed and constructed based on common design practice in order to observe their overall seismic response. The structures were tested on shake tables at the University of Buffalo using recorded ground motions from the 1994 Northridge earthquake. The two structures were built to be nominally identical with the exception that the first would be tested with the structural system only, while the second was to be fully finished with the inclusion of non-structural components. The structures were designed based on the International Building Code (IBC 2009) along with support from industry professionals through an industry

advisory board. The structure itself was a two-storey ledger framing system with the lateral system being composed of diaphragms idealized as being flexible and OSB sheathed shear walls shown in Figure 1.4 (Peterman 2014). Unfortunately, due to the diaphragms being designed to have complete elastic behaviour, little information could be extracted in regards to diaphragm design. While the experiment pushed the boundaries of our current knowledge of CFS-framed systems, it was noted that more research is required on isolated diaphragms in order to better understand the entirety of the system. The CFS-NEES project showed that non-structural elements had a significant effect on the overall shear capacity and stiffness of the building structure. This was investigated further in the numerical works of Shamim and Rogers (2013, 2015) which showed that adding a single 12.5mm layer of gypsum to shear walls led to benefits in both seismic capacity and a more favourable response to ground motions. Lu's work on CFS strap braced walls showed that installing two layers of gypsum on both sides of a wall can almost double the shear strength of the system (Lu 2015). In many ways a CFS diaphragm can be compared to a horizontal CFS shear wall, while no research has been conducted to analyze the effect of non-structural components on CFS diaphragms, the similarities between a shear wall and a diaphragm may suggest similar benefits.

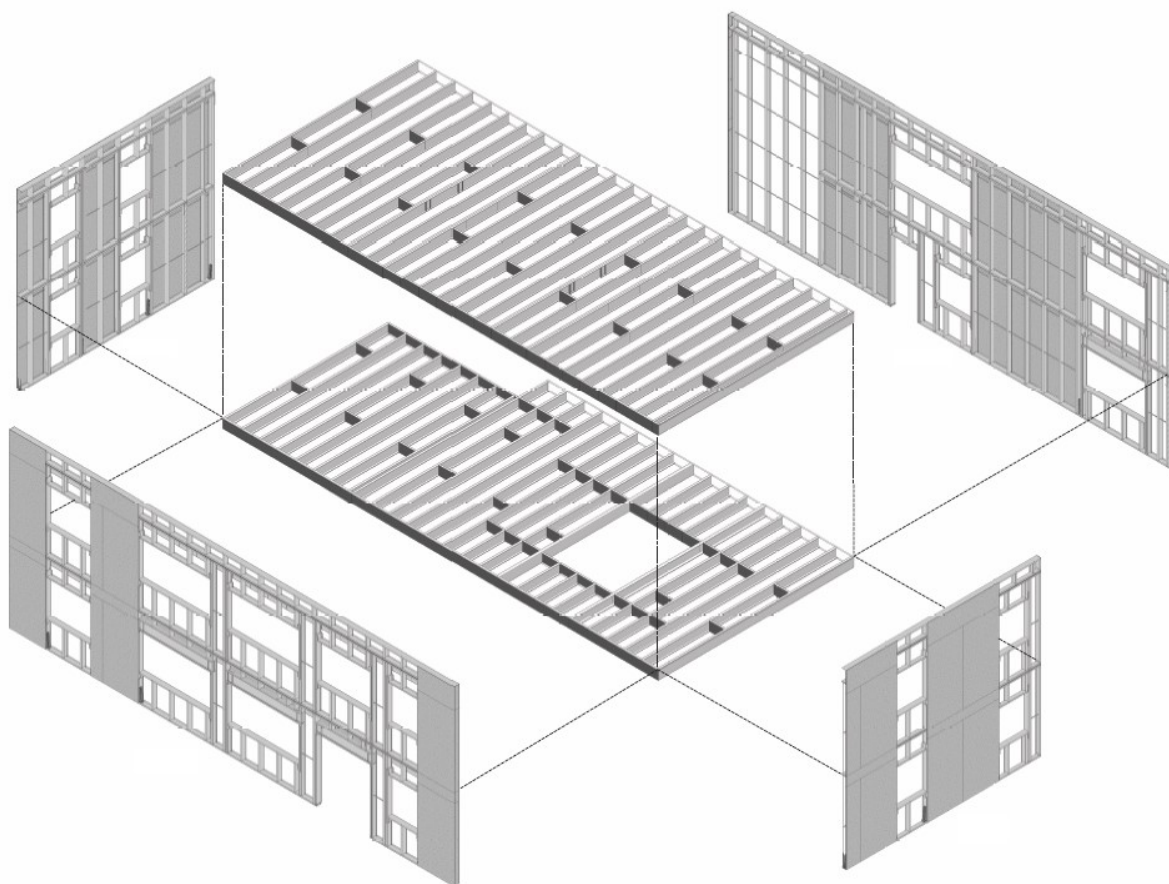


Figure 1.4: Schematic of CFS-NEES Test Structure (Peterman 2014)

The current standards in Canada do not address the seismic design of wood sheathed CFS framed diaphragms (NBCC 2010, CSA S136, AISI S400) while the CFS diaphragm related design provisions available in the US and Mexico are limited at best and have yet to be verified by large scale testing. Furthermore, in all of North America, the effect that non-structural components have on the overall response of the diaphragm component has yet to be explored.

1.5.2 Design Deflection Equations

As mentioned, the AISI S400 Standard includes design provisions which are available to be used in the United States and Mexico. This section describes in greater detail the two deflection equations used within this thesis.

Diaphragm Deflection Equation (Equation C-F2.4.3-1 in AISI S400)

The first attempt at constructing a diaphragm deflection equation for CFS framed structures was by the NAHBRC (1999). This was largely based on the methodology described in the APA's Design and Fabrication of All-Plywood Beams (1995). This methodology outlines how to calculate the deflection of a beam at allowable load. The reason a deflection equation for a beam is adequate for a diaphragm is because a structural diaphragm can be analyzed using a beam analogy. In this analogy, the floor of the diaphragm would represent the web of a wide-flange beam which is assumed to carry the shear forces. The edge of the diaphragm, which would typically be walls, would act as the beam flanges which are assumed to carry the flexural stresses. By taking the methodology for deflection equations provided by the APA for plywood beams, the NAHBRC came up with the following formula:

$$\frac{5VL^3}{8EAb} + \frac{VL}{4Gt} + 0.23Le_n + \frac{\sum(\Delta_c X)}{2b} = \Delta \quad (\text{Eq. 1-1})$$

The diagram shows four boxes below the equation, each connected by a line to a specific term in the equation:

- Bending deflection** is connected to the first term: $\frac{5VL^3}{8EAb}$
- Shear deflection** is connected to the second term: $\frac{VL}{4Gt}$
- Deflection due to screw slip** is connected to the third term: $0.23Le_n$
- Deflection due to track splice slip** is connected to the fourth term: $\frac{\sum(\Delta_c X)}{2b}$

Where,

- V = maximum unit shear in the direction under consideration, in pounds per linear foot
- L = diaphragm length, in feet
- b = diaphragm width, in feet
- A = net area of track cross section, in square inches
- E = elastic modulus of joist, in pounds per square inch
- G = modulus of rigidity of sheathing, in pounds per square inch
- t = effective thickness of sheathing for shear, in inches
- e_n = screw joint slippage at load per screw on perimeter of interior panel, in inches

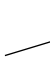
$\Sigma(\Delta_c X)$ = sum of individual joist splice slip values on both sides of the diaphragm, each multiplied by its distance in feet to the nearest support

Δ = calculated deflection at mid-point of diaphragm, in inches


The only difference between Eq. 1-1 and the formula used for wood-framed diaphragms at the time was a modification to the screw slip coefficient (third term). In the wood frame diaphragm this coefficient was taken to be 0.188 (Tissell and Elliot 1993²).

Four years later, Serrette and Chau (2003) proposed a major change to the cold-formed steel diaphragm deflection equation. This proposal was still based on the wood-framed diaphragm equation, but added new coefficients to account for fastener spacing, thickness of CFS-framing, type of wood sheathing as well as a non-uniform fastener pattern. It was considered to be applicable for both unblocked and blocked diaphragms. This equation was adapted for use with both imperial and S.I. units, and has since been implemented into the current North American CFS design standards (AISI S240, AISI S400). This CFS deflection equation is presented below as Eq. 1-2 and is intended to calculate the deflection of the mid span of a simply supported diaphragm (Figure 1.5):


$$\delta = \frac{0.052vL^3}{E_s A_c b} + \frac{\omega_1 \omega_2 v L}{\rho G t_{sheathing}} + \omega_1^4 \omega_2 (\alpha) \left(\frac{v}{2\beta} \right)^2 + \frac{\sum_{j=1}^n \Delta_{ci} X_i}{2b} \quad (\text{Eq. 1-2})$$



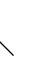
Bending deflection



Shear deflection



Deflection due to screw slip



Deflection due to track (chord) splice slip

Where,

A_c = Gross cross-sectional area of chord member, in square inches (mm²)

b = Diaphragm depth parallel to direction of load, in inches (mm)

E_s = Modulus of elasticity of steel 29,500,000 psi (203,000 MPa)

² The APA Report 138 has since been revised twice to its current 2004 edition, the 1993 has since been superseded. The reference used herein belongs to the 2004 revision of Report 138

G	= Shear modulus of sheathing material, in pounds per square inch (MPa)
L	= Diaphragm length perpendicular to direction of load, in inches (mm)
n	= Number of chord splices in diaphragm (considering both diaphragm chords)
s	= Maximum fastener spacing at panel edges, in inches (mm)
$t_{\text{sheathing}}$	= Nominal panel thickness, in inches (mm)
t_{stud}	= Nominal framing thickness, in inches (mm)
v	= Shear demand ($V/2b$), in pounds per linear inch (N/mm)
V	= Total lateral load applied to the diaphragm, in pounds (N)
X	= Distance between the “ith” chord-splice and the nearest support (braced wall line), in inches (mm)
α	= Ratio of the average load per fastener based on a non-uniform fastener pattern to the average load per fastener based on a uniform fastener pattern (= 1 for a uniformly fastened diaphragm)
β	= 67.5 for plywood and 55 for OSB for U.S. Customary ($\text{lb/in}^{1.5}$) 2.35 for plywood and 1.91 for OSB for SI units ($\text{N/mm}^{1.5}$)
δ	= Calculated deflection, in inches (mm)
Δ_{ci}	= Deformation value associated with “ith” chord splice, in inches (mm)
ρ	= 1.85 for plywood and 1.05 for OSB
ω_1	= $s/6$ (for s in inches) = $s/152.4$ (for s in mm)
ω_2	= $0.033/t_{\text{stud}}$ (for t_{stud} in inches) = $0.838/t_{\text{stud}}$ (for t_{stud} in mm)

For unblocked diaphragms, δ is multiplied by 2.50. This factor comes from the wood industry where testing on wood diaphragms suggests that the deflection of an unblocked diaphragm at its tabulated allowable shear capacity will be about 2.5 times the deflection of a similarly constructed blocked diaphragm at the same shear capacity (SEAOC 1999).

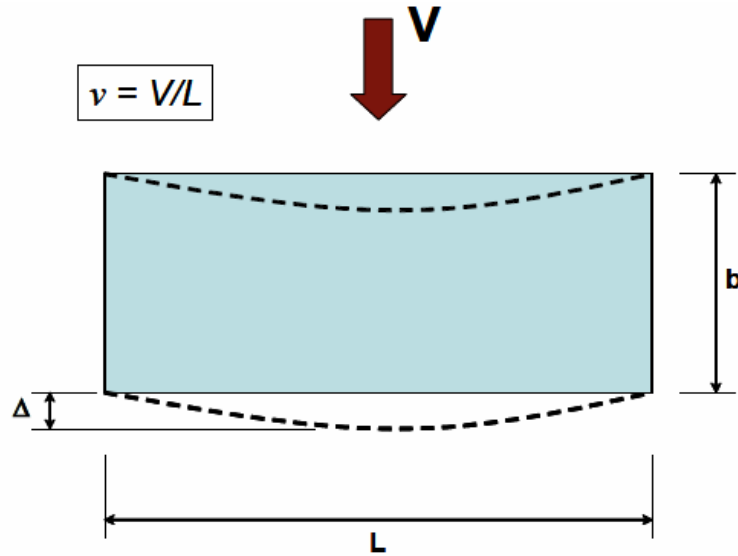


Figure 1.5: Illustration of Diaphragm Deflection (Serrette and Chau 2003)

Shear Wall Deflection Equation (Equation E2.4.1.4-1 in AISI S400)

It was found that due to the cantilever loading configuration used in the testing of the diaphragm specimens, the shear wall deflection equation may be applicable for calculating the design deflection for comparison purposes. This is described in greater detail in Section 3.3.

Similar to the diaphragm deflection equation, the shear wall deflection equation also originated from the wood industry. Equation 1-3 is the wood-framed diaphragm deflection equation taken from the 2003 International Building Code, from which the current CFS shear wall deflection equation is based:

$$\frac{8vh^3}{EAb} + \frac{Vh}{Gt} + 0.75he_n + d_a = \Delta \quad (\text{Eq. 1-3})$$

Bending deflection

Shear deflection

Deflection due to fastener slip


Deflection due to anchorage details

Where,

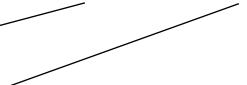
A	= Area of boundary element (vertical element at shear wall boundary) cross section, in square inches
b	= Wall width, in feet
d _a	= Deflection due to anchorage details (rotation and slip at tie-down bolts), in inches
E	= Elastic modulus of boundary element, in pounds per square inch
e _n	= Deformation of mechanically fastened connections, in inches
G	= Modulus of rigidity of wood structural panel, in pounds per square inch
h	= Wall height, in feet
t	= Effective thickness of wood structural panel for shear, in inches
v	= Maximum shear due to design loads at the top of the wall, in pounds per linear foot
Δ	= Calculated deflection, in inches

Serrette and Chau (2003) proposed modifications to this equation so that it could be used to determine the deflection for CFS-framed shear walls. By analyzing reversed cyclic test data from CFS-framed shear walls, Serrette and Chau proposed to add modification factors to account for variables such as fastener spacing, thickness of CFS framing, aspect ratio and type of sheathing (plywood, OSB or sheet steel). The proposals were accepted and the new equation was adapted to be used with both imperial and S.I. units, and has since been implemented into the current North American CFS design standards (AISI S240, AISI S400). The present version of the CFS-framed shear wall deflection is presented in Equation 1-4 and is intended to calculate the deflection of a Type 1 blocked CFS-framed shear wall (Figure 1.6):


$$\delta = \frac{2vh^3}{3E_s A_c b} + \frac{\omega_1 \omega_2 v h}{\rho G t_{sheathing}} + \omega_1^{\frac{5}{4}} \omega_2 \omega_3 \omega_4 \left(\frac{v}{\beta}\right)^2 + \frac{h}{b} \delta_v \quad (\text{Eq. 1-4})$$



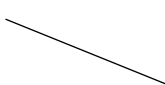
Bending deflection



Shear deflection



Overall nonlinear effects



Deflection due to anchorage details

Where,

A_c	= Gross cross-sectional area of chord member, in square inches (mm^2)
b	= Width of the shear wall, in inches (mm)
E_s	= Modulus of elasticity of steel 29,500 ksi (203,000 MPa)
G	= Shear modulus of sheathing material, in pounds per square inch (MPa)
h	= Wall height, in inches (mm)
s	= Maximum fastener spacing at panel edges, in inches (mm)
$t_{\text{sheathing}}$	= Nominal panel thickness, in inches (mm)
t_{stud}	= Nominal framing thickness, in inches (mm)
v	= Shear demand (V/b), in pounds per linear inch (N/mm)
V	= Total in-plane load applied to the diaphragm, in pounds (N)
β	= 67.5 for plywood and 55 for OSB for U.S. Customary ($\text{lb/in}^{1.5}$) = 2.35 for plywood and 1.91 for OSB for SI units ($\text{N/mm}^{1.5}$)
δ	= Calculated deflection, in inches (mm)
δ_v	= Vertical deformation of anchorage / attachment details, in inches (mm)
ρ	= 1.85 for plywood and 1.05 for OSB
ω_1	= $s/6$ (for s in inches) = $s/152.4$ (for s in mm)
ω_2	= $0.033/t_{\text{stud}}$ (for t_{stud} in inches) = $0.838/t_{\text{stud}}$ (for t_{stud} in mm)
ω_3	= $\sqrt{\frac{h}{b}}$
ω_4	= 1 for wood with structural panels

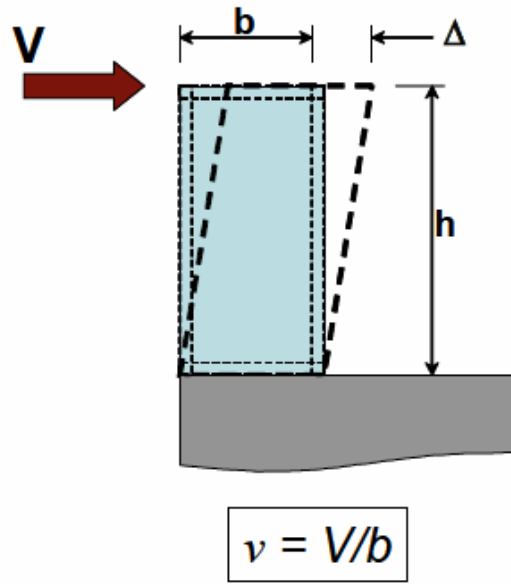


Figure 1.6: Illustration of Shear Wall Deflection (Serrette and Chau 2003)

1.5.3 Phase 1 of the CFS Diaphragm Research Program at McGill University

Upon completion of the CFS - NEES project it was noted that further study should be performed in order to better understand the effects that the CFS diaphragm has on the structure (Peterman 2014). This task was undertaken in 2015 at McGill University with the CFS diaphragm research program carried out by Nikolaidou et al. (2015). The program consisted of a total of ten tests which were performed on isolated OSB sheathed CFS diaphragms, which were designed to replicate the basic roof and floor configurations used in the CFS - NEES building. A summary of the components is provided in Table 1.1. Of the ten tests that were performed, the first two were utilized to measure the corresponding stiffness of the underlying bare CFS frame. It was found that the bare steel frame's contribution to the overall shear strength and rigidity was negligible. The remaining eight tests consisted of four different diaphragm configurations tested both monotonically and cyclically following the CUREE (Consortium of Universities for Research in Earthquake Engineering) controlled loading protocol (Krawinkler et al. 2000). The first two

configurations, i.e. those matching what were found in the CFS-NEES structure, are itemized in Table 1.1. The remaining two configurations featured a unique structural change. In the roof diaphragm, full panel edge blocking was installed, and in the floor diaphragm the gauge of the sheathing fasteners was increased from #10 to #12. All tests were performed in the Jamieson Structures laboratory at McGill University using a cantilever configuration. The test apparatus was designed to perform as a self-reacting braced frame, which was loaded evenly using an actuator attached to a distribution beam. An illustration of the test apparatus is shown in Figure 1.7. A comparison of the shear force vs. diaphragms rotation results obtained from the tests in Phase 1 is shown in Figure 1.8.

Table 1.1: Components of CFS-NEES Building Roof and Floor

Element	Basic Roof Configuration	Basic Floor Configuration
Joists	1200S200-54	1200S250-97
Rim Joists	1200T200-68	1200T200-97
Joist connectors	L 38.1x38.1x1.37mm	L 38.1x38.1x1.37mm
Joist blocking	1200S162-54	1200S200-54
Blocking connectors	L 38.1x101.6x1.37mm	L 38.1x101.6x1.37mm
Joist bracing straps	38.1x1.37mm	38.1x1.37mm
Sheathing self-drilling screws (150mm/300mm spacing)	#8	#10/#12
OSB panels	2440x1220x11.11mm	2440x1220x18.25mm
#10 flat head self-drilling screws : all joist to rim joist flange connections		
#10 hex head self-drilling screws : all joist to rim joist web angle & joist bracing connections		

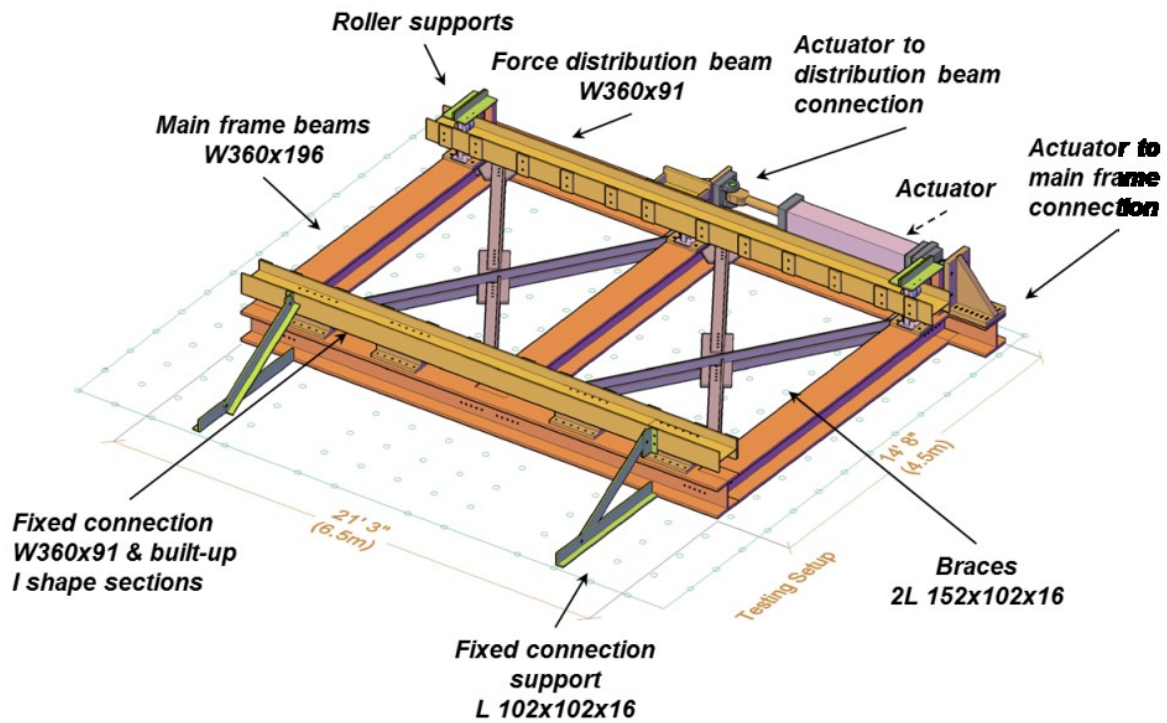


Figure 1.7: Illustration of Cantilever Diaphragm Test Apparatus (Phase 1)

In the roof diaphragm (Figure 1.8a & 1.8b) a 130% increase in shear resistance and a 70% increase in overall stiffness was observed when full panel blocking was added to the diaphragm. When a larger sheathing fastener size was used in the floor diaphragm (Figure 1.8c & 1.8d), an increase of 50% of shear resistance was observed along with a more desirable failure mode, i.e. wood bearing vs. screw shear fracture.

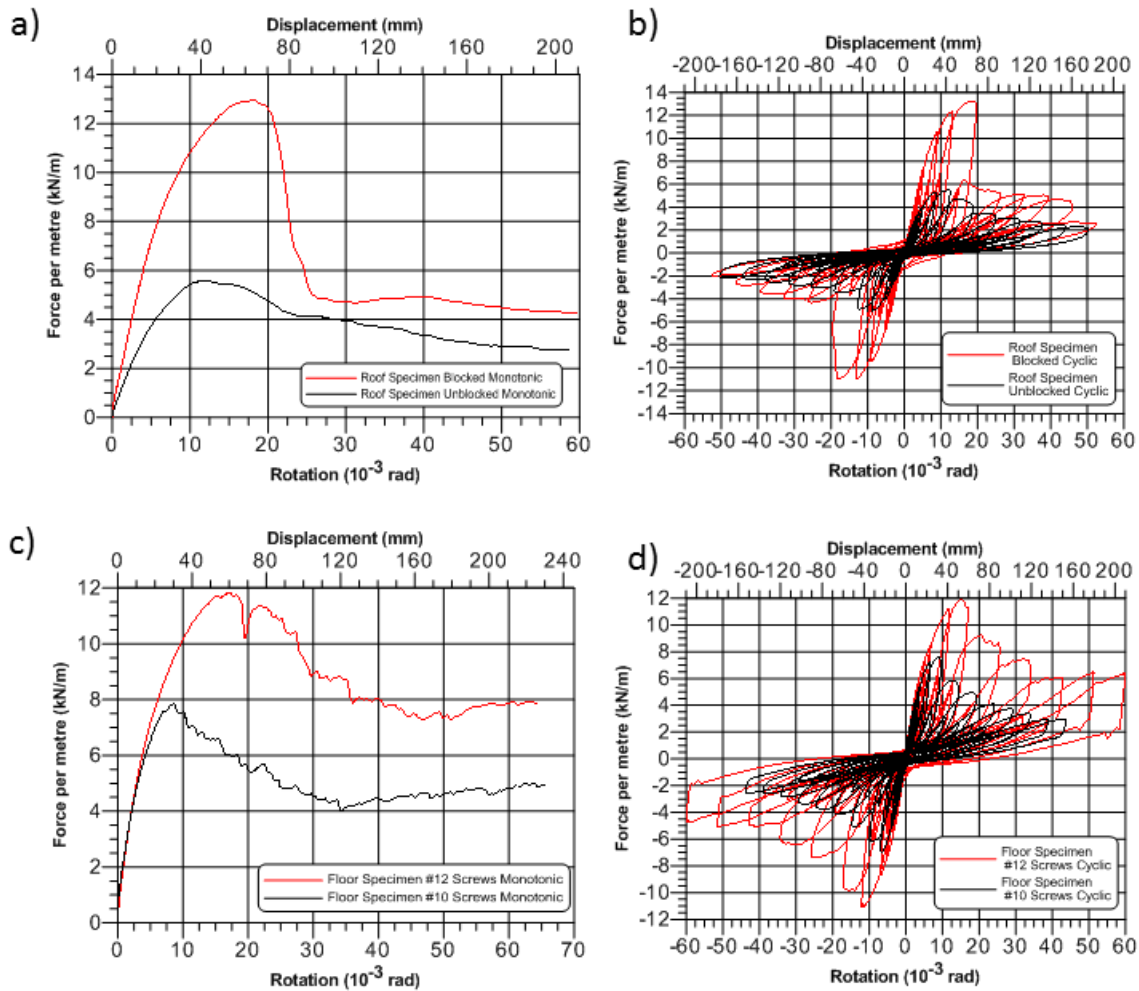


Figure 1.8: Comparison of Shear Force vs. Rotation for Tests Performed in Phase 1: a) and b) Show the Monotonic and Cyclic Tests Performed for the Roof Specimen (Unblocked vs. Blocked) c) and d) Show the Monotonic and Cyclic Tests Performed for the Floor Specimen (#10 vs. #12 Fasteners) (Nikolaidou et al. 2015)

The failure method for the unblocked roof diaphragm was concentrated in the middle row of panels; this was expected because fewer fasteners were located in the middle row due to the diaphragm being unblocked. The failure started with wood bearing followed by the fasteners pulling through the OSB and tearing out along the edges perpendicular to the direction of loading. The blocked roof diaphragm was able to reach a much higher peak load than the unblocked case, at which a sudden loss in resistance occurred. Shearing of the fasteners was observed in the blocked

diaphragm case along with tear outs and pull throughs similar to what was observed in the unblocked diaphragm. The sheared fasteners were mostly observed in areas where the fasteners penetrated two layers of steel (joist to rim joist connection locations). Once the entire row of OSB sheathing had failed, the diaphragm was observed to sustain a level of resistance by means of bending action of the frame shown in Figure 1.9.

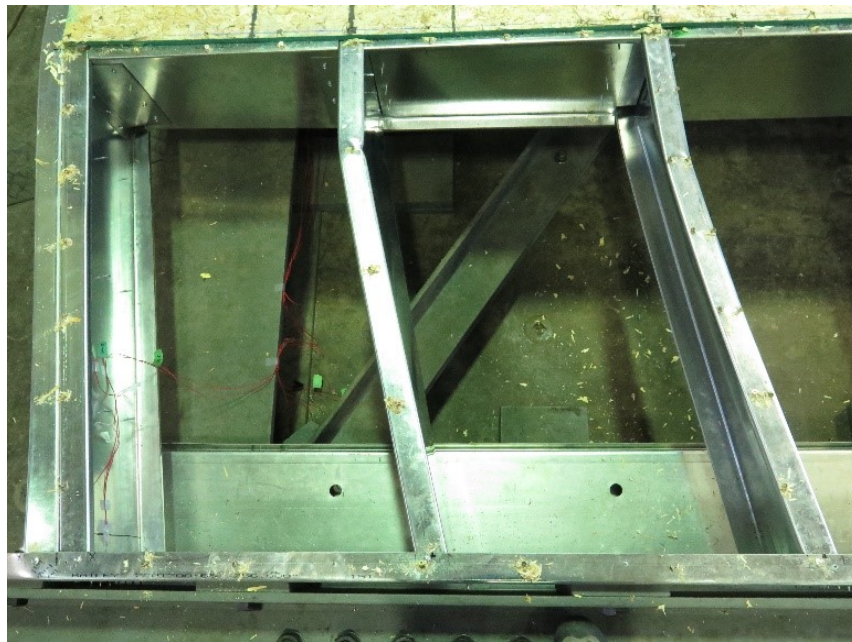


Figure 1.9: Photo of Bending Action of the Diaphragm After Sheathing Failure (Sheathing Removed to Show Frame) (Nikolaidou et al. 2015)

In the floor diaphragm specimen with the #10 gauge screws, once peak load was reached the fasteners began to shear in rapid succession. After the failure of the first fastener, a series of failures followed indicating the diaphragm's inability to redistribute the forces. Only minor damage was observed to the OSB sheathing. It was noted that the tongue and groove characteristic of the floor sheathing allowed for contact friction between the edges of the OSB panels to occur which led to a higher shear resistance to be reached after failure than what was observed in the roof specimens.

The floor diaphragm with the #12 gauge screws failed in a similar way to that with the #10 gauge screws, with the exception that the larger fasteners were much better at redistributing force demands once initial sheathing connection failure occurred. The time between screw shear failures was significantly longer than what was observed during the test with the #10 fasteners. A combination of shear and tensile forces were observed to have taken place resulting in the fasteners tilting before shear failure occurred. In some locations wood panel edge contact/bearing (friction) action took place after the sheathing fasteners failed resulting in the load stabilizing towards the end of the test.

After the Phase 1 tests, design predictions were calculated based on the AISI S400 Standard. It was found that formula C-F2.4.3-1 in the AISI S400 Standard typically used for calculating the design deflection in diaphragms, should not be used due to the cantilever loading configuration. Instead, the design deflection for shear walls was utilized, i.e. equation E2.4.1.4-1 from the AISI S400 Standard, because it better represented the testing situation. In the end both equations consistently led to calculated deflections with a percent of error of over 50% from the deflections observed during testing. The equivalent elastic deflections of the test results were then calculated based on the observed rigidity of the specimens and compared to the previously calculated design predictions. Upon comparing these results the error decreased in all cases, and was nearly zero in the blocked specimen. This error reduction was thought to indicate that the empirical factors designed to account for inelastic behaviour in the equation may not be adequate when used to calculate the deflections for diaphragms. It was concluded that given the current design provisions in the North American design standard, no design procedure for deflections could accurately predict the observed deflections and further investigation would have to be done. Shear predictions were also carried out according to the AISI S400 Standard using Table F2.4-1 where the table was

found to be limited in terms of design choices. The table only contains design values for a total of three different sheathing thicknesses and provides no method to account for the fastener size. These limitations limited the proper use of the table to only two out of the four test diaphragm configurations, while assumptions were required for the remaining two configurations. In cases where the table was directly applicable it was shown to provide reasonable estimates for overall shear strength. It was concluded that the scope of the design table would have to be expanded to include more variety within diaphragm configurations. In the end, the major findings of Phase 1 of the diaphragm research project were threefold:

- Blocking the edges of the OSB panels leads to a large increase in both shear resistance and stiffness
- The size of the fastener not only affects the shear capacity but can also leads to changes in the overall failure mode leading to a different diaphragm response.
- The current standard (AISI S400) is inadequate for determining the deflection and shear resistance of the majority of CFS-framed wood sheathed diaphragms due to the limited information available.

Chapter 2 Test Program

2.1 Test Apparatus

The test apparatus was initially designed in 2015 by Nikolaidou et al. (2015) in order to carry out Phase 1 of the diaphragm test program. The test apparatus was designed as a self-reacting braced frame. The design was made not only for the test configurations planned in 2015 but also for the possibility of works in the future with diaphragm configurations of higher resistance. The major objectives of the frame design were that it would behave in an elastic manner at all times and to be as stiff as possible to obtain the minimum amount of deformations during testing. By investigating the peak loads from the works outlined in the literature review (NAHBRC 1999, Madsen et al. 2011), as well as the peak loads found in CFS framed shear wall testing performed at McGill University (Branston 2004, Chen 2004, Boudreault 2005, Rokas 2005, Blais 2006) it was found that in all cases, the estimated peak load of the diaphragm was always below 200kN. Thus, it was decided to base the design of the test apparatus around the maximum forces which could be generated by the actuator used for loading. The actuator had a tensile capacity of 450kN and a compressive capacity of 650kN. A safety factor of 1.2 was implemented, and the final design was built to withstand a maximum load of 540kN. Due to the space limitations of the Jamieson Structures Laboratory at McGill, all of the diaphragm specimens were to be tested in a cantilever fashion with dimensions of 3.6x6.1m. The dimensions for the test frame were chosen to be 4.5x6.5m in order to support the diaphragms. The complete test frame design is shown in Figure 2.1 and Figure 2.2. In order to obtain a cantilever loading situation; one end of the diaphragm was completely fixed to the frame while the other end was able to move freely along the plane of loading. The fixed end was realized by bolting the rim joist of one side of the diaphragm into the

flange of a W360x91 beam, the web of that beam was then bolted to four smaller built up I-beams which were directly bolted to the frame. The free end was created by resting the web of another W360x91 beam along three sets of rollers. Near the ends of the beam, rollers were placed on the top and bottom of the beam in order to prevent any vertical displacement. The third set of rollers was placed at mid-span of the beam to prevent any vertical deformations caused by the self-weight of the set up. High performance rollers with greased surfaces were used throughout which provided for minimal resistance due to friction during loading. The loading was provided by an MTS actuator attached at the midpoint of the W360x91 beam, which transferred the load uniformly across the rim joist of the diaphragm specimens. The frame underneath was composed of W360x196 members which were anchored to the floor using pre-tensioned 38mm threaded rods that were designed to resist a maximum shear capacity of 50kN. It is important to note that theoretically, all of the in-plane forces should have been contained within the frame and ideally, the threaded rods would not experience any shear loading. Double angle braces L152x102x16 with a 25.4mm spacing were chosen in order to minimize any movement of the frame and to ensure elastic behaviour. Lastly L102x102x16 vertical brace supports were installed at both ends of the fixed connection in order to prevent any rotation of the fixed end during loading. SAP2000 commercial software (CSI 2009) was used in order to analyze and design the frame and all calculations were done according to Canadian design standards (NBCC 2010, CSA S16 2014). Figures 2.3 and 2.4 show photos of the various parts of the test apparatus used during Phase 2. The data captured by the instrumentation showed that during all of the tests performed, there were no notable movements of the frame. However, despite the vertical bracing, some problems did emerge with regards to rotation of the fixed end connection as well as the sliding of the distribution beam which is further discussed in Chapter 3.

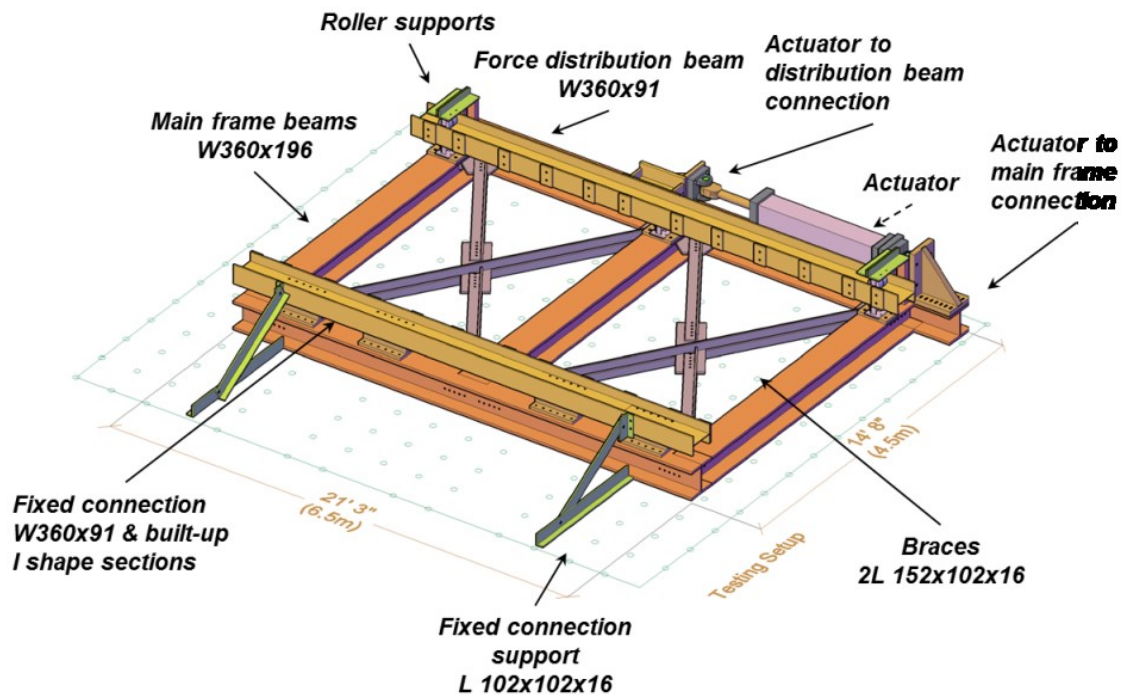


Figure 2.1 Illustration of Test Apparatus

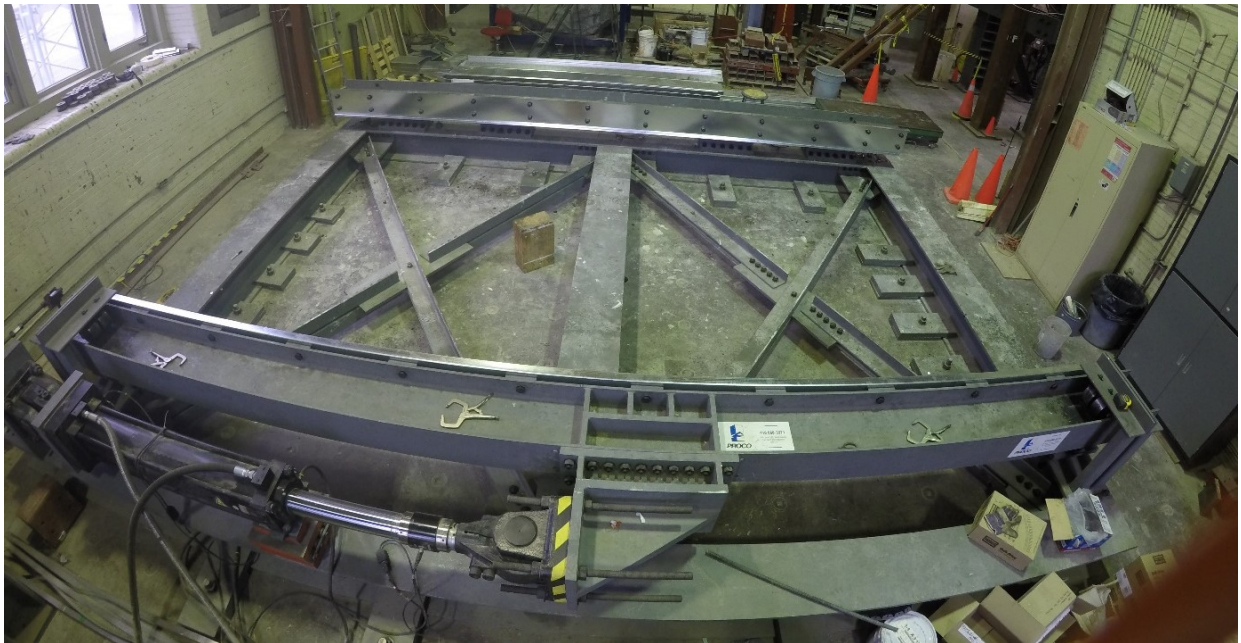


Figure 2.2: Photograph of Diaphragm Test Apparatus with Rim Joists Bolted to Fixed and Free Ends

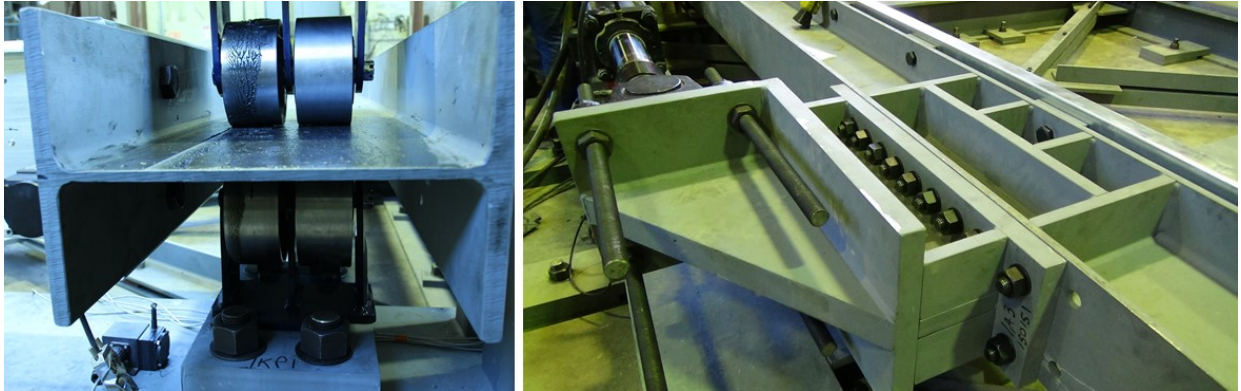


Figure 2.3: (Left) Greased Rollers on Distribution Beam (Right) Actuator to Distribution Beam Connection



Figure 2.4: (Left) Fixed End Connection (Right) Pre-Tensioned 38mm Threaded Rods

2.2 Test Diaphragms

In Phase 2 of the CFS diaphragm research program at McGill University, time and budgetary constraints allowed for a total of six new diaphragms to be tested. In Phase 1 each diaphragm configuration was tested under both monotonic and reversed cyclic loading, which required the construction of two identical specimens per configuration. It was decided that due to the vastly unexplored nature of CFS diaphragms it would be more beneficial to test a larger variety of diaphragm configurations under monotonic loading alone. Therefore, in Phase 2 a total of five different configurations were designed for monotonic loading while one specimen was also tested

under reverse cyclic conditions. The diaphragm configurations were based on the unmodified CFS-NEES building design for both the floor and roof specimens. These are referred to as the basic roof and floor designs which were tested during Phase 1 (Nikolaidou et al. 2015) and are described in detail in Section 1.5.3. With the testing information of the basic roof and floor diaphragm readily available, Phase 2 focused on diaphragm configurations featuring a single alteration so that the effect could be easily compared to the results of the basic configurations from Phase 1. Tables 2.1 and 2.2 contain an inclusive list of nomenclature for all diaphragms tested in Phases 1 and 2. The configurations tested in Phase 2 are described in detail in this section and are illustrated in Figures 2.5 through 2.10.

Table 2.1: Phase 1 Diaphragm Specimen Nomenclature

Specimen	Description
1-RF-M	Roof Bare Steel Frame : Monotonic
2-FF-M	Floor Bare Steel Frame : Monotonic
3-RU-M	Roof Unblocked : Monotonic
4-RU-C	Roof Unblocked : Reversed Cyclic
5-F#10-M	Floor #10 Screws : Monotonic
6-F#10-C	Floor #10 Screws : Reversed Cyclic
7-RB-M	Roof Blocked : Monotonic
8-RB-C	Roof Blocked : Reversed Cyclic
9-F#12-M	Floor #12 Screws : Monotonic
10-F#12-C	Floor #12 Screws : Reversed Cyclic

Table 2.2: Phase 2 Diaphragm Specimen Nomenclature

Specimen	Description
11-RALT-M	Roof Blocked Alternate Direction Joists : Monotonic
12-RSTRAP-M	Roof Strap Blocking : Monotonic
13-FB4-M	Floor #12 Screws Blocked (100mm/300mm) Spacing : Monotonic
14-RGYP-M	Roof with Gypsum Ceiling : Monotonic
15-RGYP-C	Roof with Gypsum Ceiling : Reversed Cyclic
16-FCRETE-M	Floor with 1-inch Gypcrete Topping : Monotonic

2.2.1 (11-RALT-M) Roof Alternate Direction Joists - Monotonic Loading

Specimen 11-RALT-M was the same as the blocked roof specimen tested in Phase 1 (7-RB-M) with a 90 degree change in orientation of the joists (Figure 2.5). The main purpose of this configuration was to observe how the strength and stiffness would be affected if the load was applied parallel to the joists rather than perpendicular.

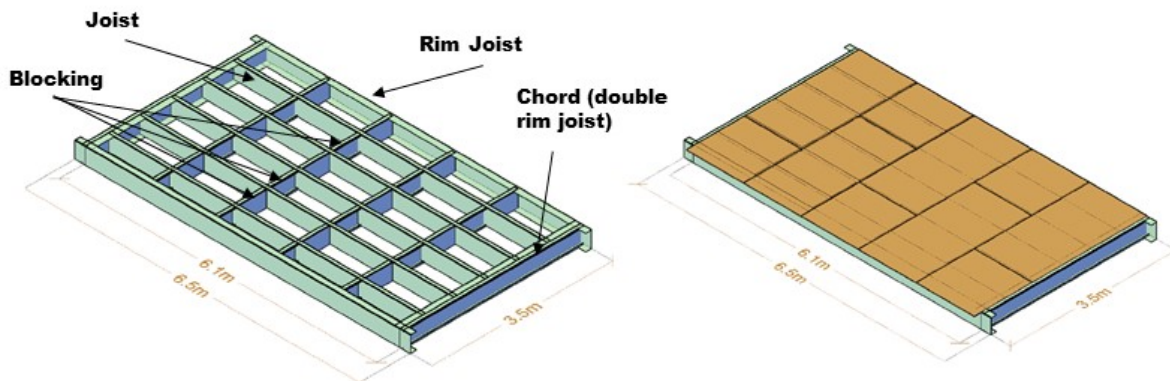


Figure 2.5: Bare Frame and Frame with Sheathing: Specimen 11-RALT-M

2.2.2 (12-RSTRAP-M) Roof Strap Blocking - Monotonic Loading

Specimen 12-RSTRAP-M was also similar to 7-RB-M, with the exception that the full blocking at the OSB panel edges was replaced with strap blocking. Two lines of blocking were installed which were each composed of four fully blocked segments and a continuous steel strap on the top and bottom (Figure 2.6). The main purpose of this configuration was to determine if strap blocking, which is less costly and easier to install, would be as effective as full blocking in terms of providing adequate support to the OSB panel edges to attain similar diaphragm shear strength and stiffness.

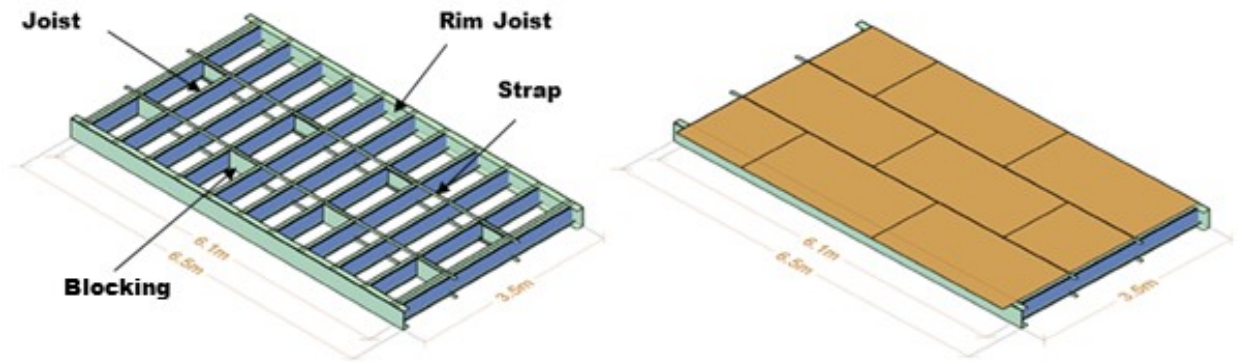


Figure 2.6: Bare Frame and Frame with Sheathing: Specimen 12-RSTRAP-M

2.2.3 (13-FB4-M) Floor Blocked (100mm / 300mm) Spacing - Monotonic Loading

Test specimen 13-FB4-M (Figure 2.7) was designed to maximise the shear resistance of a diaphragm given a basic floor configuration of a 2.5 mm thick steel frame and 18.3 mm thick OSB sheathing. It was decided to use a fully blocked floor specimen with a screw (#12 gauge) spacing of 100mm along all panel edges. The primary objective of this configuration was to obtain an upper estimate for the design strength of these diaphragms.

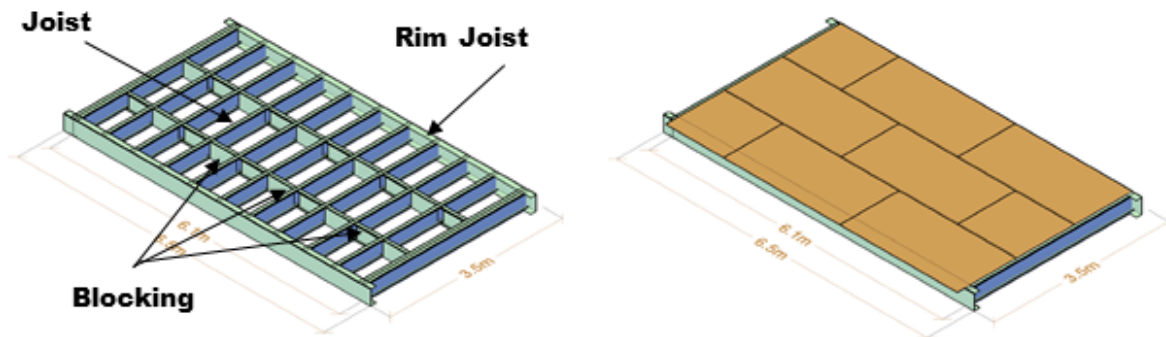


Figure 2.7: Bare Frame and Frame with Sheathing: Specimen 13-FB4-M

2.2.4 (14-RGYP-M & 15-RGYP-C) Roof with Gypsum Ceiling - Monotonic & Reversed Cyclic Loading

Test specimens 14-RGYP-M and 15-RGYP-C were comprised of a basic roof configuration (3-RU-M) with one layer of Type X, 16mm thick gypsum ceiling installed to the underside of the

frame (Figure 2.8). A gypsum ceiling is classified as a non-structural feature, which is mainly used for aesthetic purposes but also provides fire protection for the steel frame. This floor assembly would be expected to attain a fire resistance rating of 45mins to an hour (SFA 2013). The gypsum was directly attached to the underside of the CFS framing without the use of resilient channels. Lu (2015) showed that when resilient channels are used to attach gypsum panels to strap braced walls, the influence of the gypsum on the strength and stiffness is close to negligible because of the flexibility of the channels. Hence, because the intent was to identify the influence of the gypsum layer, it was attached directly to the CFS frame. The fasteners used to attach the gypsum panels to the framing were #6 32mm long Type S drywall screws, spaced at 305mm o/c throughout (perimeter and field). Joint compound and joint tape were applied at panel intersections and at screw locations in order to reinforce and conceal the joints and screw heads as shown in Figure 2.9. The main purpose was to examine the contribution of the non-structural gypsum panels to the shear strength and stiffness of the diaphragm. For this configuration a reversed cyclic test was desired to observe whether the potential strength increase would be retained if repeated cycles were applied, similar to what would occur during seismic loading.

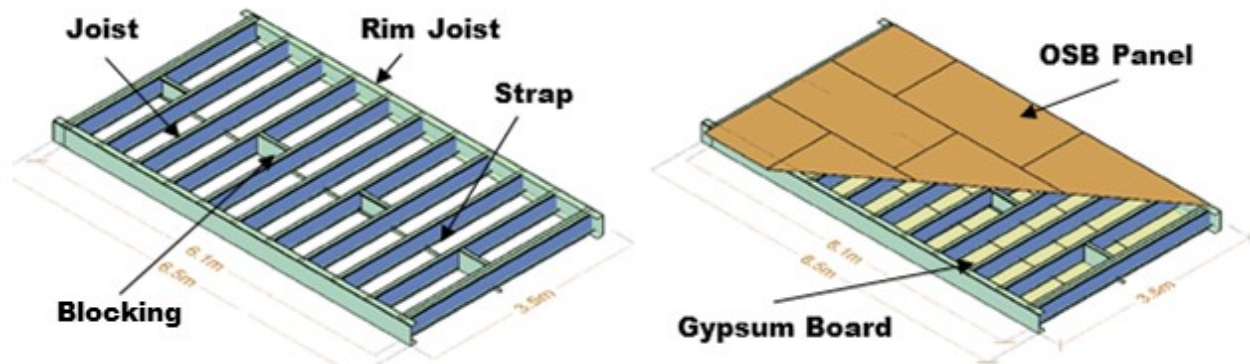


Figure 2.8: Bare Frame and Frame with Sheathing: Specimen 14-RGYP-M and 15-RGYP-C



Figure 2.9: Specimen 14-RGY-P-M Before and After Joint Tape and Compound was Placed Between Panels and at Screw Locations

2.2.5 (16-FCRETE-M) Floor with 19mm Gypcrete Topping - Monotonic Loading

Test specimen 16-FCRETE-M was comprised of a basic floor configuration using #12 screws (10-F#12-M) with a 19mm thick gypcrete topping installed on the surface of the OSB sheathing (Figure 2.10). GYP-CRETE2000[®]/3.2K was used, which is a commonly used, locally available gypcrete product. Gypcrete is often added to structures to provide sound insulation between floors and to improve the fire resistance rating. For this assembly, a minimum fire resistance rating of 1-hour would be obtained, provided that the underside would be covered by a minimum of two layers of type C, 13mm thick gypsum boards (Maxxon 2016). In order to obtain a uniform height across the diaphragm, a 25mm high plywood border was installed around the perimeter of the frame, shown in Figure 2.11. Prior to pouring, Maxxon[®] powder floor primer was applied at a concentration of approximately 7.3m²/L by means of a handheld roller shown in Figure 2.11. The primer was used to ensure that an adequate bond between the gypcrete and the underlying OSB was obtained. The gypcrete was mixed on site according to the mixing instructions provided by Maxxon and was poured evenly across the floor surface. Multiple gypcrete cylinders were cast during pouring which were later tested after a set time interval to determine when the gypcrete topping was at adequate strength for testing. The product design strength in compression was between 13.8-22.1MPa

(MAXXON 2016). The main purpose of this configuration was to examine the contribution of the non-structural gypcrete topping to the overall shear strength and stiffness of the diaphragm.

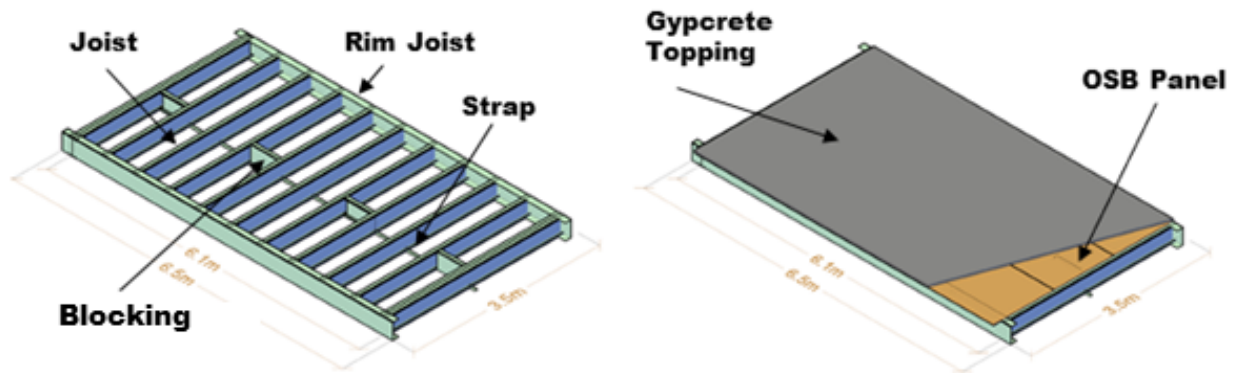


Figure 2.10: Bare Frame and Frame with Sheathing: Specimen 16-FCRETE-M

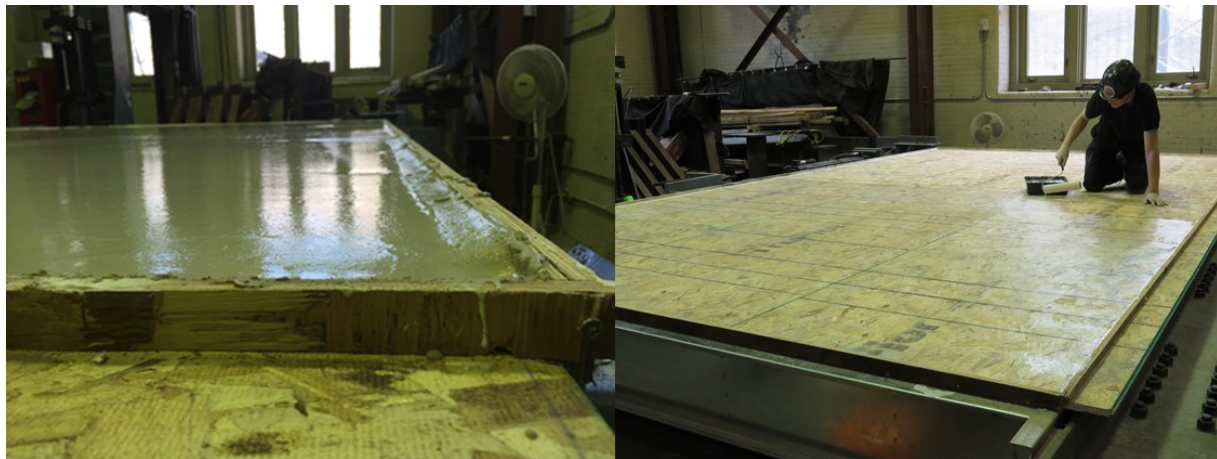


Figure 2.11: (Left) 25mm Boarder Surrounding Perimeter of Diaphragm (Right) Application of Primer to OSB

It should be noted that the double joist shown at the ends of each diaphragm configuration in Figures 2.5, 2.6, 2.7, 2.8 and 2.10 was placed in an effort to include the stiffening effect of a wall attached to the underside of the diaphragm. Also, to account for the ledger framing used in the CFS – NEES building, the sheathing had an extension of 152mm past the edge of the steel diaphragm frame to match the detail commonly used in construction. Lastly, the boundary conditions for both the gypsum and gypcrete tests were left free to move. This was considered to

be a conservative approach whereby the lowest increase in shear and stiffness would be obtained. Typically in practice, the edges of these systems would be restrained by the surrounding walls which would restrict movement. A more detailed overview of the construction including parts used and the connections can be found in Section 2.3.

2.3 Diaphragm Construction

All diaphragm specimens were designed according to the specifications of the CFS-NEES building, with the joists spaced at 610mm o/c and the steel components corresponding to those listed in Table 2.3.

Table 2.3: Summary of Components Used for Diaphragms in Phase 2

Element	Roof Configurations	Floor Configurations
Joists	1200S200-54	1200S250-97
Rim Joists	1200T200-68	1200T200-97
Joist connectors	L 38.1x38.1x1.37mm	L 38.1x38.1x1.37mm
Joist blocking ⁽¹⁾	1200S162-54	1200S200-97
Blocking connectors	L 38.1x101.6x1.37mm	L 38.1x101.6x1.37mm
Joist bracing straps ⁽¹⁾	38.1x1.37mm	38.1x1.37mm
Sheathing self-drilling screws (150mm/300mm spacing) ⁽²⁾	#8	#12
OSB panels	2440x1220x11.11mm	2440x1220x18.25mm
#10 flat head self-drilling screws : all joist to rim joist flange connections		
#10 hex head self-drilling screws : all joist to rim joist web angle & joist bracing connections		

⁽¹⁾ For blocked configurations 1200S250-54 / 1200S250-97 blocking was used

⁽²⁾ 12-RSTRAP-M used a 50.8x1.37mm strap

⁽³⁾ 13-FB4-M used 100/300mm spacing

Each specimen was constructed using the following four steps:

1. **Install rim joists:** Rim joists were installed by first placing the CFS member in position along the free and fixed end of the frame (flange of W360x71 beams). Once in place the rim joists were leveled using a Dakashi laser level and locked into position with c-clamps. The locations of all the bolts that connect the rim joists to the frame were marked and the rim joists were dismounted. Using a magnetic drill with a 27mm drill bit, holes were drilled at the marked locations. After all the marked locations had been drilled the rim joists were installed to the frame using 25mm bolts. All bolts were installed snug-tight using the full effort of a single worker with an elongated ratchet shown in Figure 2.12.



Figure 2.12: (Left) Drilling Holes with Magnetic Drill (Right) Snug-Tightening Rim Joist to Frame Using Elongated Ratchet

2. **Install joists:** Once the rim joists were installed to the frame the joists were installed. The first step to install the joists was to mark the positions along the top flange of the rim joist where the joists were to be placed. This was done by measuring the centre of each rim joist and then marking at 610mm intervals from the centre mark. The height of the joists were designed such that they were able to fit tightly between the flanges of the rim joist allowing for the joists to remain in place without any fasteners. Once all joists were placed, they were then leveled and #10 self-drilling screws were used to fasten the flanges of the joists to the flanges of the rim joists. Flat head fasteners were used for the top flange connection while #10 hex-head fasteners were used everywhere else. #10 Flat-head fasteners were

used for the top flange connection because they protruded far less than the hex-head fasteners which would have affected the placement of the OSB sheathing. Finally, joist connector angles (L38.1x38.1x1.37mm) were installed to connect the webs of the joists to the webs of the rim joists. Using the same screw pattern used in the CFS-NEES building a total of ten screws were used per web connection. For the roof specimens, seven screws attached the rim joist and three attached the joist, shown in Figure 2.13. The floor specimens had six screws through the rim joist with the remaining four through the joist. Figure 2.14 shows the frame after the completion of this step.

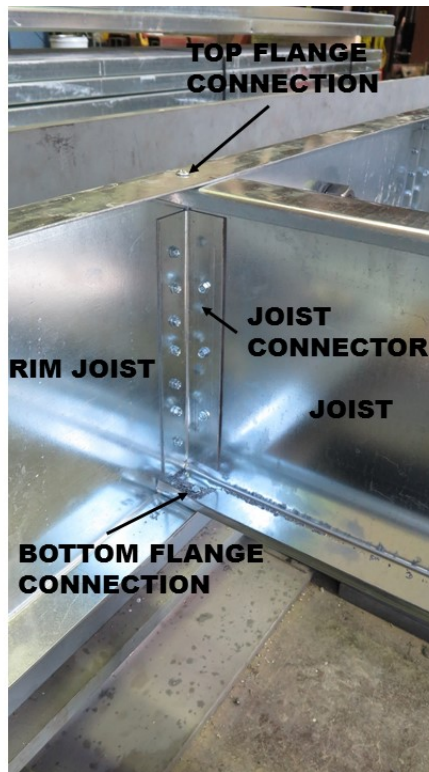


Figure 2.13: Roof Specimen Joist to Rim Joist Connection



Figure 2.14: Diaphragm Specimen After Installation of Rim Joists and Joists

3. **Install blocking:** Depending on the design of the specific configuration, there were three different types of blocking that were used for the six specimens tested in Phase 2.

Unblocked: For the unblocked diaphragms (14-RGYP-M, 15-RGYP-C, 16-FCRETE-M), no blocking was added to provide steel framing along the entire perimeter of the OSB sheathing panels. However, blocking members were used as lateral supports at every third joist spacing at the mid-span of the joist, shown in Figure 2.15. It is important to note that the OSB sheathing was not connected to these blocking members, nor were they positioned along the panel edges; the purpose of these members were solely to provide lateral support for the joists. The blocking members were designed to be the same size as the joists, only shorter in length. The connections were detailed according to the specifications provided by the CFS-NEES building design. These connections were nearly identical to the joist to rim joist connections with the exception that the blocking connectors used a total of eight fasteners, four in the web of the blocking and four in the web of the joist. Two types of

angles were used for the blocking members, an L38.1x38.1x1.37mm where the blocking was connected to the closed face of a joist (Figure 2.15) and an L38.1x101.6x1.37mm where the blocking was connected to the open face (Figure 2.17). A 38mm wide strap with the same thickness as the joists was then installed across the underside of the frame and fastened along each blocking member as well as each joist (Figure 2.15). The purpose of the strap was to provide some level of lateral support to the joists which had no blocking connected.



Figure 2.15: (Left) Unblocked Specimen (14-RGYP-M) (Right) Web-Stiffener to Joist Connection (Closed Face)

Blocked: For the blocked specimens (11-RALT-M, 13-FB4-M), complete lines of blocking were installed at every sheathing interface. The purpose of these blocks was not only to provide lateral support for the joists but also to support the edges of the OSB panels. For the 13-FB4-M specimen, two rows of blocking were required (Figure 2.16) While the 11-RALT-M specimen required four rows of blocking. The blocking members were installed between each joist in an alternating pattern (Figure 2.17). The reason for the alternating pattern was to avoid the fasteners in the blocking connectors from overlapping. Because the blocking spanned the entire diaphragm, every joist member had adequate lateral support and the need for straps was eliminated.



Figure 2.16: Frame of Specimen 13-FB4-M

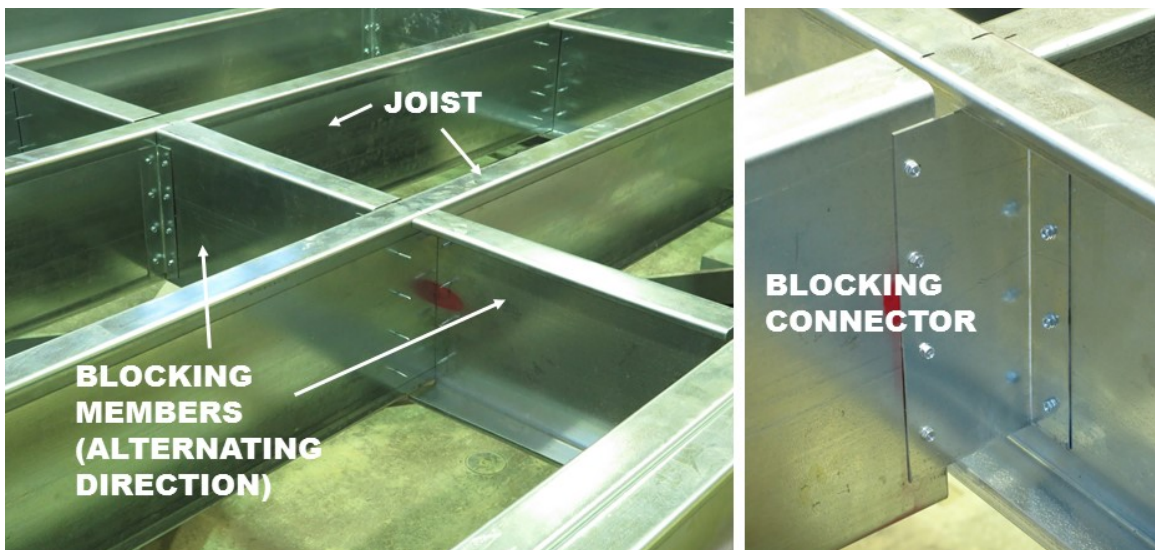


Figure 2.17: (Left) Alternating Blocking Members (Right) Blocking Connected to Joist (Open Face)

Strap-blocking: The strap blocked diaphragm (12-RSTRAP-M), used a combination of techniques from both the blocked and unblocked cases. The blocking were installed similar to an unblocked diaphragm with the exception that multiple rows of blocking were installed at the locations of the sheathing interfaces. In the strap-blocked case, after the 38mm wide

straps were installed along the underside of each row of blocking, an additional 50mm wide strap with the same thickness as the joists was fastened across the top (Figure 2.18). The top strap was intended to provide support for the edges of the OSB panels similar to a blocked diaphragm. The top strap was wider in order to ensure that proper edge distance was obtained when fastening the OSB sheathing into the straps. The wider straps were not available in adequate length to span the full length of the diaphragm (6.1m); hence, three separate straps were spliced together along their length. The straps were spliced at web stiffener locations without overlap to avoid protrusions as shown in Figure 2.19. Strap blocking was easier to install and less costly than the blocked frames, because of the challenge of fitting the full blocking between joists and the requirement for special blocking connectors and additional screws to connect them to the joists. Currently across North America, for all design calculations, a strap-blocked diaphragm is considered equivalent to a fully blocked diaphragm (AISI S240 2015, AISI S400 2015).



Figure 2.18: Frame of Specimen 12-RSTRAP-M



Figure 2.19: Strap Splice Interface at Mid-Span of Blocking Member

4. **Install Sheathing:** In Phase 2 only two types of OSB sheathing were used. An 11.1mm thick square edge OSB was used for roof configurations and a thicker 18.3mm thick tongue-and-groove OSB was used for floor configurations (Figure 2.20). The rows of sheathing were installed in an alternating pattern parallel to the direction of loading, excluding specimen 11-RALT-M for which the sheathing was installed perpendicular to the direction of loading. The sheathing was fastened to the frame with #8 and #12 self-drilling sheathing screws for the roof and floor, respectively. A consistent minimum edge distance of 13mm was used throughout, along with a screw spacing of 150mm along the perimeter and 300mm in the field. For specimen 13-FB4-M the perimeter screw spacing was reduced to 100mm while the field spacing remained at 300 mm. For blocked and strap-blocked diaphragms, all four edges of each OSB panel were fastened using the perimeter spacing. For unblocked specimens, two edges were fastened using the perimeter spacing while the rest of the panel was fastened along the underlying joists at 610mm spacing. A detailed look at the screw placements and how they failed can be found in APPENDIX A for each specimen.

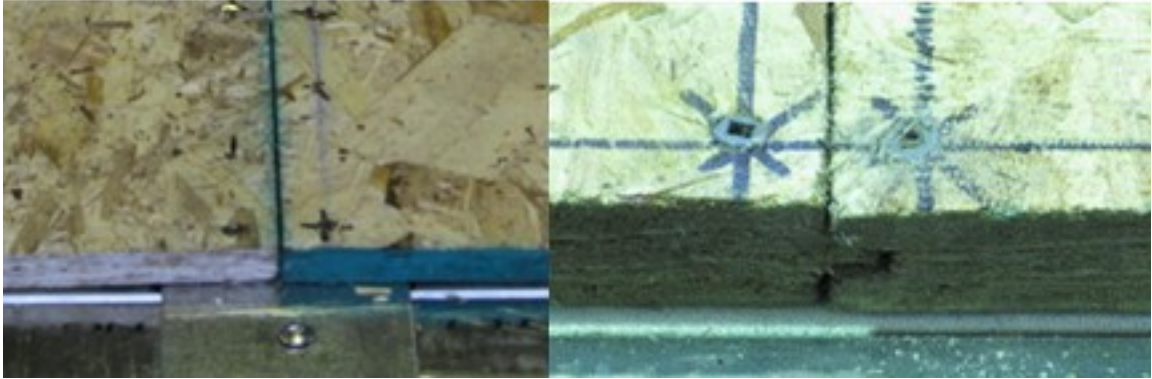


Figure 2.20: (Left) Square Edge Roof OSB (Right) Tongue-and-Groove Floor OSB

Configurations Including Non-Structural Elements

An additional step was required for the builds which incorporated non-structural elements. For specimens 14-RGYP-M and 15-RGYP-C gypsum panels were attached to the underside of the frame, and for specimen 16-FCRETE-M a 19mm thick gypcrete topping was poured on top of the OSB. A description of the installation method for the non-structural elements is as follows:

Gypsum: Due to the limited working space underneath the diaphragm test specimen, the frame had to be lifted by crane in order to install the gypsum boards to the underside of the CFS diaphragm. This was ultimately achieved by first constructing the entire CFS frame, and then by removing all but two of the bolts which connected the end of the rim joists of the diaphragm to the frame, and then using the overhead crane to lift the entire diaphragm which rotated about the two remaining bolts. The magnetic drill was used to drill holes into the double joists at each end of the diaphragm so that a pair of eye-bolts could be used with a lifting strap to raise up the frame, shown in Figure 2.21. Temporary bracing channels were fastened in an X pattern to the top of the joists to prevent damage to the frame during the lifting process and to force it to remain square. The gypsum panels were Type X, 16mm thick, which were installed with type S drywall screws using the same methods as was used

to install the sheathing (unblocked) with the exception that a constant 300mm spacing was used throughout. A minimum edge distance of 13mm was respected for all panels. Once the panels were installed, joint tape and joint compound were used to seal the joints between the panels as well as to cover the screw heads as is done in common practice (Figure 2.21).



Figure 2.21: (Left) Initial Lift of Specimen 14-RGYP-M Using I-Hooks (Right) Applying Joint Tape and Compound to Panel Interface

Gypcrete: In order to pour the gypcrete, first a 25mm border was built around the perimeter of the entire diaphragm. The border was constructed of plywood and attached to the underlying OSB sheathing using wood screws. The OSB sheathing was then cleaned in order for a primer to be applied. The primer used for this specimen was called Maxxon[®] Powder Floor Primer, which was provided by Maxxon, the company that also supplied the gypcrete. The powder primer was mixed with water and stirred vigorously until the blend was lump free; the ratio of water to primer powder was 13.24L to 2.72kg powder as was recommended by Maxxon. Two coats of primer were applied to the OSB surface using a hand roller shown in Figure 2.22 in order to satisfy the recommended application rate of

7.3m²/L. The floor was then given 24 hours to dry before the gypcrete was poured. The gypcrete used was GYP-CRETE2000[®]/3.2K; the mixing instructions were provided by Maxxon[®]. The gypcrete was mixed by a barrel batching process using the following steps:

- 1) Place approximately 16L of water into the mixing drum
- 2) Empty a 80lb bag of Maxxon GYP-CRETE2000[®]
- 3) Add approximately 45L of sand aggregate supplied by Maxxon[®]
- 4) Mix until lump free and slump tests yield results between 8-10inches (203-254mm), add more sand or water as needed
- 5) Empty barrel onto floor and immediately repeat process until pour is complete

This mixing process is shown in Figures 2.22 through 2.24. Once the pour was complete, adequate time was provided for the gypcrete to reach its intended design strength (13.8-22.1MPa) (MAXXON 2016). Prior to testing, the border was removed to ensure the gypcrete was not restricted from moving. This configuration will provide for a lower bound shear strength because the boundary edges of the gypcrete were not restrained. Ultimately, the test was carried out with a gypcrete topping thickness of 19mm \pm 1mm.



Figure 2.22: Application of First Coat of Floor Primer to OSB Sheathing



Figure 2.23: (Left) Photo of GYP-CRETE2000®/3.2K (Right) Photo of Barrel Batch Mixing Process

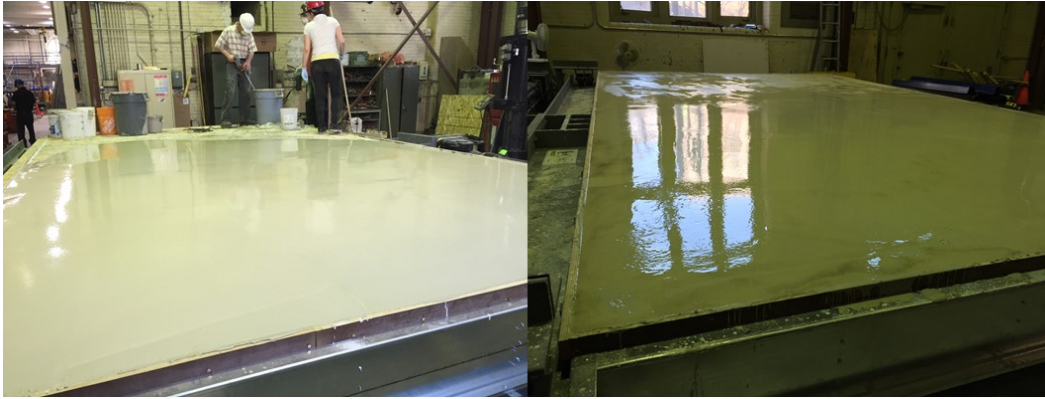


Figure 2.24: (Left) Progress after 2/3 of Gypcrete Had Been Poured (Right) Photo Immediately After Pour

2.4 Instrumentation

The instrumentation used in the Phase 2 diaphragm tests consisted of four string potentiometers as well as eight linear variable differential transformers (LVDTs). Out of the four string potentiometers there were two 254mm stroke and two 508mm stroke. The main purpose of the string potentiometers was to capture the in-plane displacement and overall shear deformation of the diaphragm specimens. The string potentiometers were set up exactly as they were in Phase 1, which is shown in Figure 2.25. The LVDTs were $\pm 15\text{mm}$ stroke and used to measure local in-plane displacement. Eight LVDTs were used in Phase 2, three on the joist members, two on the frame, two on the fixed connection supports and one to measure the displacement of the rim joist at the fixed end (Figure 2.26). In addition, the displacement and force generated by the actuator was recorded by internal LVDT and load cell devices that were monitored during testing. All instruments, including the instruments within the actuator, were connected to Vishay Model 5100B scanners that were used to record the data using Vishay System 5000 StrainSmart software.

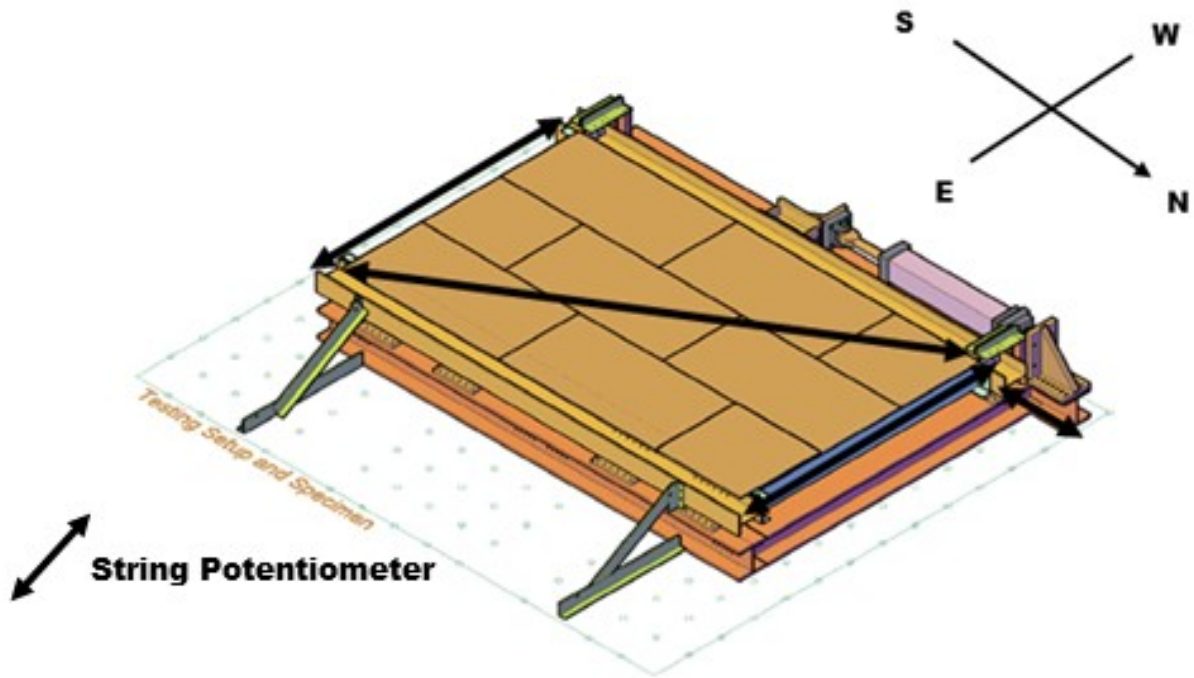


Figure 2.25: Placement of String Potentiometers

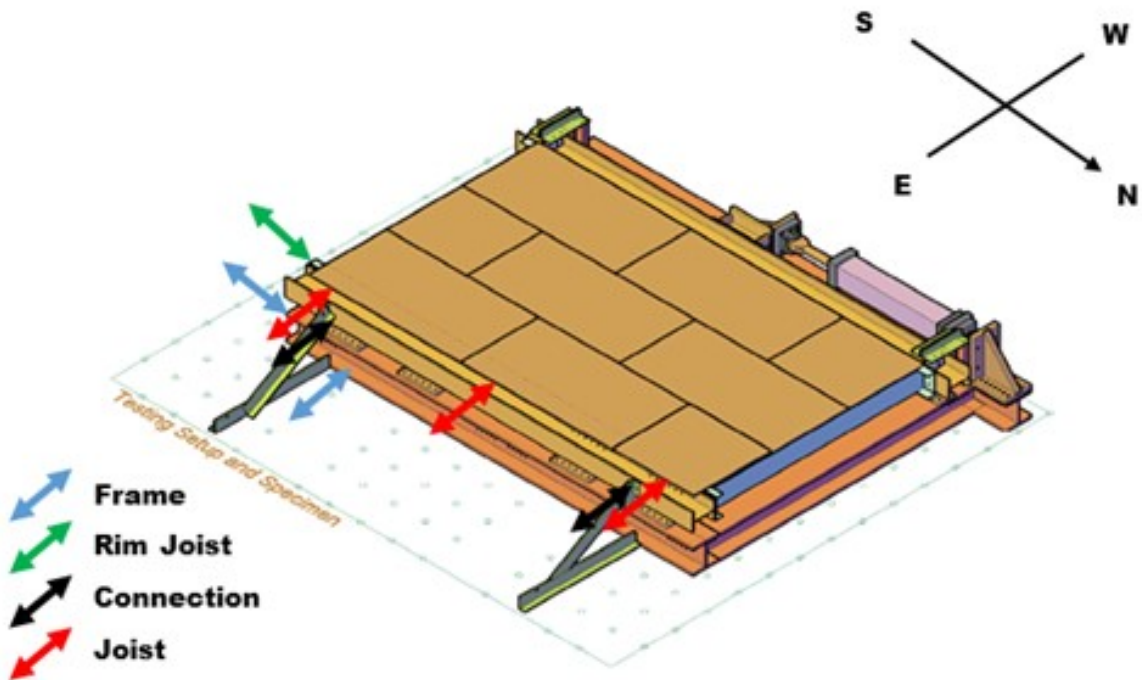


Figure 2.26: Placement of Linear Variable Differential Transformers (LVDTs)

2.5 Loading Protocol

2.5.1 Monotonic

In all of the monotonic tests, the edge of the diaphragm was displaced at a consistent rate of 5mm/min. The loading was applied until a post-peak plateau was observed and the overall displacement exceeded 200mm, which was based on the 2.5% storey drift ratio of the diaphragm given the cantilever loading conditions.

2.5.2 Reversed Cyclic

Specimen 15-RGYP-C was tested under reversed cyclic loading conditions following the Consortium of Universities for Research in Earthquake Engineering (CUREE) loading protocol (Krawinkler et al. 2000). The loading history for ordinary ground motions (basic loading history) was used, which was consistent with the protocol used throughout Phase 1 for all specimens tested under reversed cyclic conditions. The CUREE protocol is based on three types of loading known as initiation cycles, primary cycles and trailing cycles. A loading cycle is completed once the desired amplitude has been reached in both the positive and negative direction and the frame has been restored to its initial position. Initiation cycles are executed at the beginning of the loading history to serve as a check for the measurement devices, loading equipment and the force-deformation response at small amplitudes. The primary cycles are a single cycle which is larger than all of the preceding cycles. The trailing cycles follow the primary cycles at an amplitude of 75% of the preceding primary cycle and are repeated between two to six cycles before the next primary cycle occurs. All amplitudes are based off of a reference displacement (Δ_m) which is obtained from performing a monotonic test with a nominally identical configuration. Δ_m is defined as the deformation at which the applied load drops for the first time, below 80% of the maximum load that was applied to the specimen (F_{um}). The value Δ_m is then multiplied by the reduction

factor γ which decreases the peak value taken from the monotonic test in order to account for the expected deterioration caused by the repeated cycles during the reverse cyclic test. Table 2.4 shows the complete protocol used for the 15-RGYP-C test, while Figure 2.27 is a graph showing the displacement versus time of the protocol. The rate of loading used for the cyclic test began at 15mm/min and was increased to 60mm/min at the start of the 1.5 Δ primary cycle. The test was stopped at the end of the 4.0 Δ primary cycle because at this point the sheathing and gypsum had both failed, and the loads were being resisted solely by frame action which is described in depth in Chapter 3.

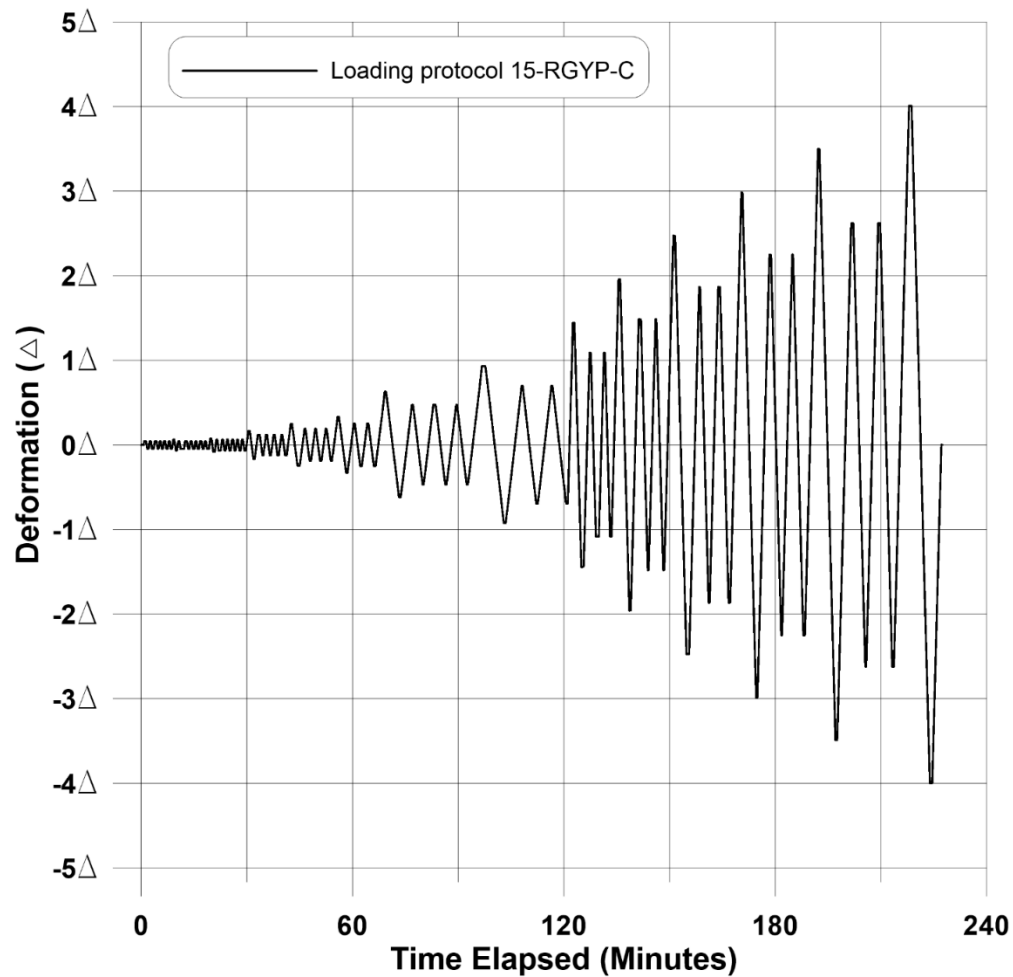


Figure 2.27: Displacement vs Time for Specimen 15-RGYP-C

Table 2.4: CUREE Loading Protocol Used for Specimen 15-RGYP-C

F_u	53.7	KN	15-RGYP-C
Δ_m	65.0	mm	
γ	0.6	reduction factor	
Amplitudes of cycles		Target Displacement (mm)	Number of Cycles
0.05	Δ	1.9	6
0.075	Δ	2.9	1
0.056	Δ	2.1	6
0.1	Δ	3.8	1
0.075	Δ	2.9	6
0.2	Δ	7.7	1
0.15	Δ	5.7	3
0.3	Δ	11.5	1
0.225	Δ	8.6	3
0.4	Δ	15.3	1
0.3	Δ	11.5	2
0.7	Δ	26.8	1
0.525	Δ	20.1	2
1	Δ	38.3	1
0.75	Δ	28.7	2
1.5	Δ	57.4	1
1.125	Δ	43.0	2
2	Δ	76.5	1
1.5	Δ	57.4	2
2.5	Δ	95.7	1
1.875	Δ	71.7	2
3	Δ	114.8	1
2.25	Δ	86.1	2
3.5	Δ	133.9	1
2.625	Δ	100.4	2
4	Δ	153.0	1
3	Δ	114.8	2
4.5	Δ	172.2	1
3.375	Δ	129.1	2
5	Δ	191.3	1

Chapter 3 Test Results and Observations

3.1 Material Properties

This section describes the auxiliary tests performed on the materials used in the diaphragm configurations. A description of each type of test and the standard that they conform to is presented along with a summary of the results obtained. Lastly, a summary is presented of the OSB sheathing to CFS frame connection tests performed at Virginia Polytechnic Institute and State University.

3.1.1 Steel

To test the material properties of the steel, which made up the underlying frame of the diaphragm specimens, tensile coupon tests were performed as per the ASTM A370 Standard (2016). Three coupons for each CFS element were tested so that an average could be obtained. In each set, one coupon was fixed with strain gauges (Figure 3.1) so that the Young's modulus could be accurately obtained. During testing, the elongation of each specimen was recorded by an extensometer with a gauge length of 50mm which was attached to the middle of each specimen. In addition, a secondary method to measure the elongation was also implemented where the coupons were punch-marked prior to testing at a constant distance. This distance was then measured once again after the test was completed to obtain the general elongation. The coupons were all tested in the 150kN capacity MTS Sintech universal test machine shown in Figure 3.1. During loading three different displacement rates were used. The loading rates for the elastic range, the plateau region and for the remainder of the test once strain hardening was initiated, were 0.002mm/s, 0.01mm/s and 0.1mm/s respectively. Prior to testing, the width and thickness of each specimen was measured in three separate locations with digital calipers and a micrometer. After testing the specimens were immersed in a solution of 15% hydrochloric acid to remove the zinc coating in order to measure the base metal thickness. All stress values calculated herein were determined using the base metal

thickness. The yield stress was obtained using the autographic diagram method (Davis, 2004) where the yield point is taken at the first instance where the stress is recorded to decrease (Figure 3.2). A summary of the averaged results obtained from the tensile coupon tests are shown in Table 3.1. Figure 3.2 shows an example of one of the engineering stress-strain curves.

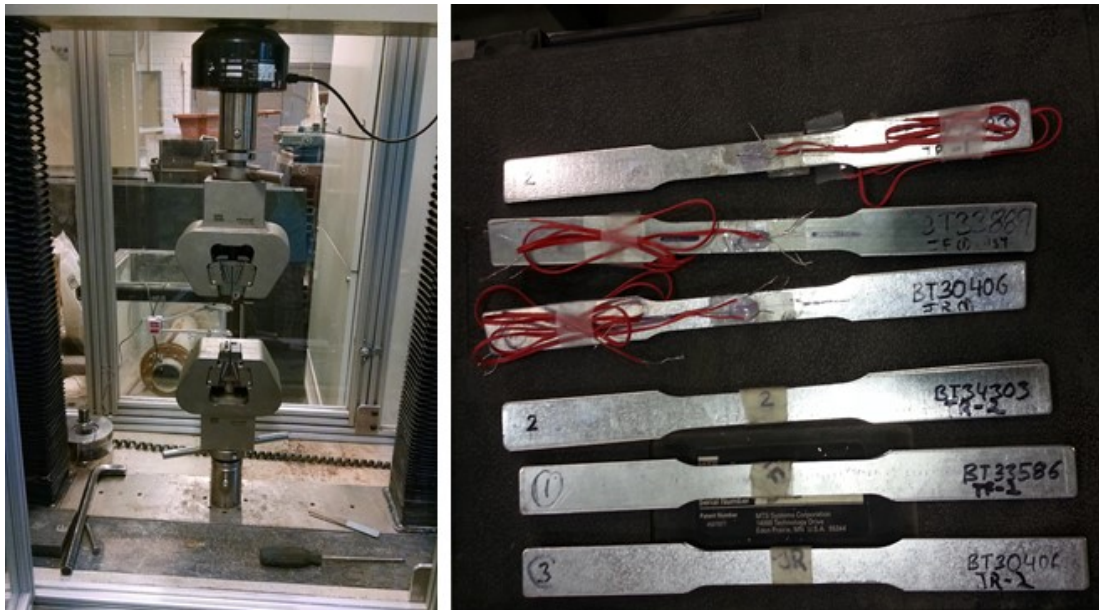


Figure 3.1: (Left) Photo of 150 KN MTS Sintech Machine (Right) Tensile Coupon Samples

Table 3.1: Tensile Coupon Test Results

Specimens	Steel Thickness (mm)	E (MPa)	F _y (MPa)	ε _y (mm/mm)	F _u (MPa)	ε _u (mm/mm)	F _u /F _y	Elongation (%)
Roof Joist	1.37	208400	375	0.00383	466	0.196	1.24	31.8
Floor Joist	2.46	207500	397	0.00514	473	0.177	1.19	32.3
Roof Rim Joist	1.73	204800	398	0.00311	474	0.155	1.19	30.3
Floor Rim Joist	2.46	201400	384	0.00531	454	0.174	1.18	31.9
11-RALT-M Joist-Rim Joist	1.37	203200	437	0.00464	516	0.170	1.18	26.9
11-RALT-M Chord-Joist	1.73	194700	377	0.00391	523	0.192	1.39	32.3

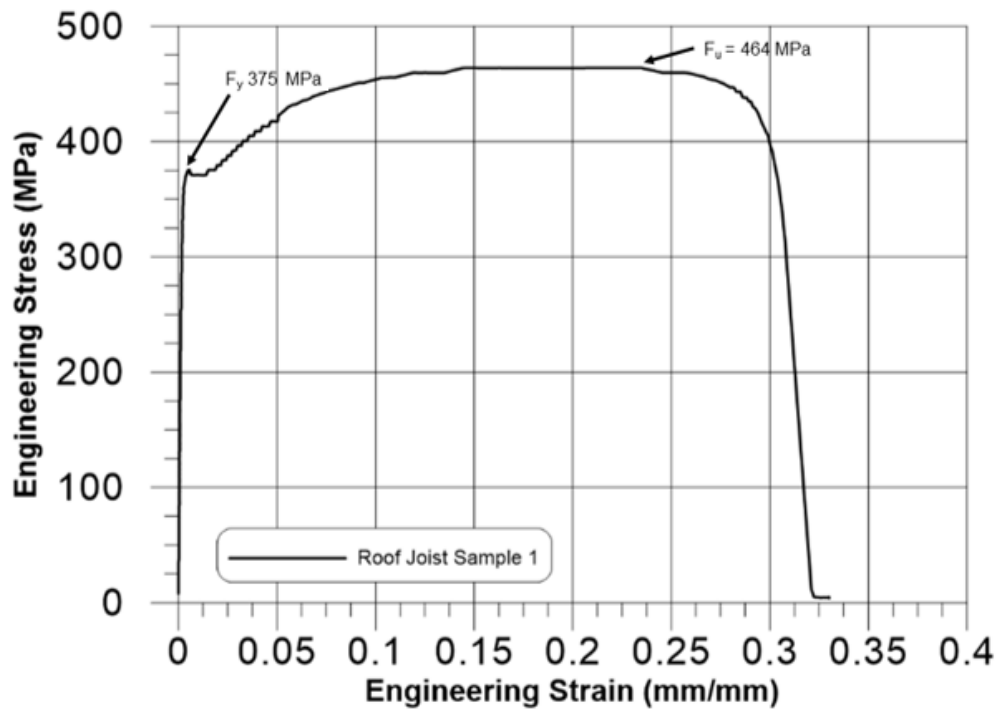


Figure 3.2: Engineering Stress-Strain Curve of Roof Joist Sample 1

The engineering stress-strain curve of all coupon tests along with the complete results can be found in APPENDIX B. The steel used for all of the CFS elements were Grade 50ksi with a nominal yield strength of 345MPa. The tensile coupon tests performed demonstrated that the yield strength for all of the steel elements used within the diaphragm specimens were greater than the nominal value.

3.1.2 OSB and Gypsum

The moisture content for both the OSB and gypsum panels was verified following the oven-drying method of the ASTM D4442 Standard (2015). Three round specimens (100mm diameter) from three separate panels were extracted from each diaphragm immediately after testing using a hand drill. The perimeter of each specimen was brushed in order to clean off loose fragments and the

initial mass was measured. The specimens were then placed in an oven at a temperature of 103°C for at least 24 hours, after which they were taken out and weighed to obtain the oven dry mass.

Finally the moisture content for each specimen was calculated using the following formula:

$$MC = \frac{\text{Initial mass} - \text{Oven dry mass}}{\text{Oven dry mass}} \times 100\%$$

The results of the three specimens were averaged to obtain a final moisture content which is presented in Table 3.2.

Table 3.2: Moisture Content of OSB and Gypsum Panels Using ASTM D442 Standard (2007)

Test	Specimen	Initial Mass (g)	Oven Dry Mass (g)	MC (%)	Average MC (%)
11-RALT-M	1	49.4	47.5	4.0	4.0
	2	55.2	53.1	4.0	
	3	49.5	47.6	3.9	
12-RSTRAP-M	1	57.5	55.2	4.1	4.2
	2	52.9	50.8	4.2	
	3	46.1	44.3	4.2	
13-FB4-M	1	72.3	69.8	3.6	3.6
	2	82.0	79.2	3.6	
	3	74.9	72.3	3.7	
14-RGYP-M (OSB)	1	50.1	48.0	4.2	4.2
	2	50.2	48.2	4.3	
	3	56.8	54.5	4.3	
14-RGYP-M (Gypsum)	1	79.9	65.7	21.6	21.6
	2	83.8	68.9	21.6	
	3	81.6	67.1	21.5	
15-RGYP-C (OSB)	1	49.1	47.1	4.3	4.3
	2	51.2	49.1	4.2	
	3	51.1	48.9	4.3	
15-RGYP-C (Gypsum)	1	87.7	72.4	21.2	21.5
	2	89.4	73.5	21.8	
	3	84.2	69.2	21.6	
16-FCRETE-M	1	77.7	74.4	4.5	4.6
	2	81.8	78.2	4.6	
	3	68.7	65.6	4.6	

It is shown that the moisture content for all of the OSB is well below 15% ensuring that the OSB sheathing was tested under dry conditions. The gypsum panels recorded a moisture content between 21-22%. This is considered as dry conditions for gypsum panels as naturally, gypsum is comprised of 21% water by weight (Encyclopedia Britannica, 2011).

3.1.3 Gypcrete

Tests following the guidelines of MAXXON, the gypcrete supplier, were carried out to obtain the compressive strength of the gypcrete topping. The specifications used were a modified version of the ASTM C-472 Standard (2014). During the pour of the gypcrete topping onto the diaphragm, three two-inch cubic molds were filled using the same batch of gypcrete. The cubes were given 90 minutes to set and then were then taken out of the mold and left in an area beside the diaphragm so that they were both exposed to the same conditions. On the same day that the diaphragm was tested the cubes were also tested using the 150 kN capacity MTS Sintech universal test machine. Each of the cubes was placed into the centre of the compression platens and loaded at a constant rate of 0.01mm/s until failure. The results of the compression tests are summarized in Table 3.3:

Table 3.3: Gypcrete Cube Compression Test Results

Specimen	Area (mm²)	Force (kN)	Compressive Strength (MPa)	Average Compression Strength (MPa)
1	2633	48.0	18.2	19.2
2	2633	52.4	19.9	
3	2614	50.5	19.3	

The compressive strength obtained by the cube compression tests of 19.2MPa placed the gypcrete in the upper end of the nominal range given by the manufacturer (13.8 MPa to 22.1 MPa).

Splitting tensile strength tests were conducted using gypcrete cylinders which were also cast during the pour and left in the same area to cure as the cubic molds for the compression tests. The cylindrical specimens had dimensions of 200mm in length and 100mm in diameter. The tests were carried out according to the ASTM C496 Standard (2011). The results of these tests are summarized in Table 3.4. No specification for the nominal tensile strength value is given for this product, however comparable fast drying commercial toppings from MAXXON have nominal tensile strengths of 3.2MPa after 28 days (MAXXON 2016).

Table 3.4: Gypcrete Cylindrical Tensile Tests Results

Specimen	Area (mm²)	Force (kN)	Tensile Strength (MPa)	Average Tensile Strength (MPa)
1	7854	70.1	8.92	8.10
2	7854	60.1	7.65	
3	7854	60.6	7.72	

3.1.4 Sheathing-to-Frame Connection Tests

All sheathing-to-frame connection tests were performed at Virginia Polytechnic Institute and State University by Robert Cole and Francis Li. The tests were conducted under the supervision of Fannie Tao, Aritra Chatterjee and Professor Cristopher D. Moen, following the procedures used for the single shear screw-fastened connection experimental program (Tao et al. 2016). A total of six different connection configurations were tested, where the results were obtained from an average of three identical tests performed per configuration. For all fastener gauges used in the diaphragm research program (#8, #10, #12) the appropriate sized OSB sheathing to joist connection and OSB sheathing to rim joist connection was tested. An illustration of the test set up, as well as the specimen dimensions and fastener location is shown in Figure 3.3. All tests were

performed using a cyclic loading protocol adopted from the FEMA 461 quasi-static cyclic deformation-controlled testing protocol (Tao et al. 2016). A backbone curve inspired by the Ibarra-Medina-Krawinkler model based on the reversed cyclic test results was used to characterize the cyclic fastener load-deformation responses (Figure 3.4). A summary of the averaged connection test results is presented in Table 3.5. The load vs. deformation responses of all connection tests can be found in APPENDIX C.

Dowel bearing strength tests were also conducted on the sheathing in accordance with the ASTM D5764 Standard (ASTM 2013) to obtain the ultimate stress and modulus of elasticity of the OSB panels. The set up used for the bearing tests is shown in Figure 3.5 with the exception that the dowel used across all tests had a diameter of 6.2mm rather than the 9.5mm shown in the figure. The results from the dowel bearing strength tests are summarised in Table 3.6. The load vs. deformation responses of all dowel bearing strength tests can be found in APPENDIX D.

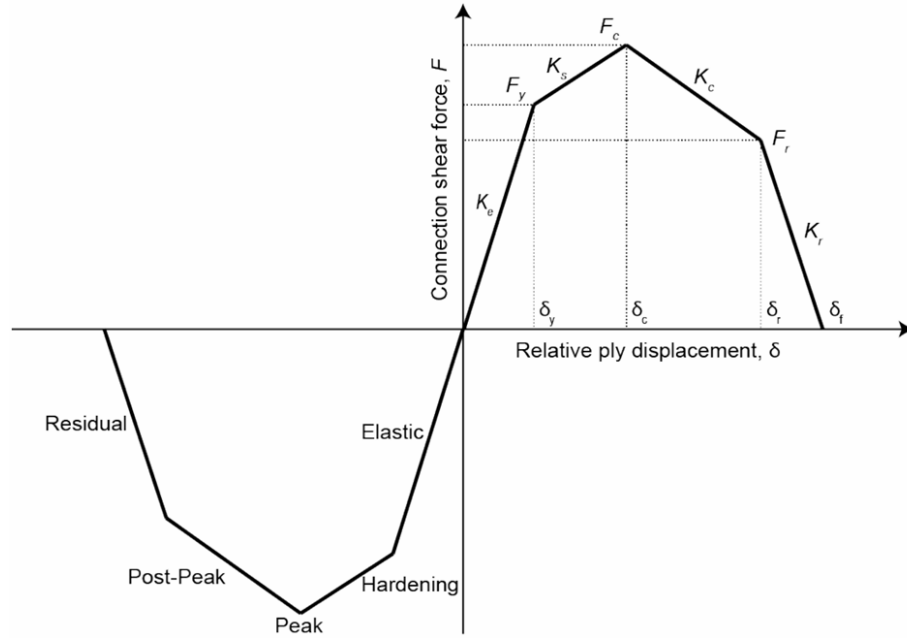


Figure 3.4: Backbone Curve Nomenclature (Tao et al. 2016)

Table 3.5: Summary of Connection Test Results (Backbone Curve Parameters)

Connection Type	Fastener Gauge	F _y (kN)	F _c (kN)	F _r (kN)	δ _y (mm)	δ _c (mm)	δ _r (mm)	δ _f (mm)	F _u (sheathing) (MPa)	F _{ss} (fastener shear strength) (MPa)
Roof OSB/Joist	#8	1.06	2.21	1.77	0.47	4.2	9.7	21	23.2	4.9
Roof OSB/Rim Joist		1.38	2.17	1.6	0.8	6.1	8.5	13	23.2	4.9
Floor OSB/Joist	#10	1.43	2.55	1.77	0.31	5.6	6	6.7	40.3	8.2
Floor OSB/Rim Joist		1.2	2.55	2.5	0.18	5.7	6	7.3	40.3	8.2
Floor OSB/Joist	#12	2.33	4.36	4.03	0.59	7.9	11	12	40.3	11.1
Floor OSB/Rim Joist		2.1	4.37	4.09	0.72	8.3	11	12	40.3	11.1

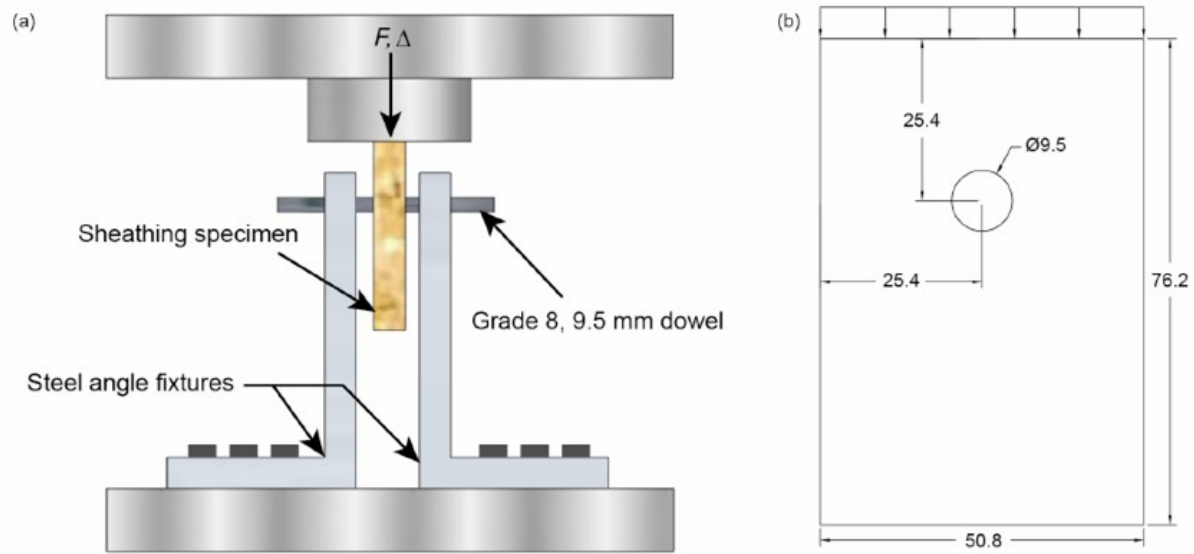


Figure 3.5: (a) Dowel Bearing Test Setup and (b) Sheathing Specimen Dimensions for Bearing Tests (Tao et al. 2016)

Table 3.6: Summary of Dowel Bearing Test Results

OSB Specimen	Length (mm)	Width (mm)	Thickness (mm)	Peak Load (kN)	Modulus of Elasticity, E (MPa)	Peak Stress, F_u (MPa)
Roof 1	75.9	48.3	10.9	1.60	538	23.6
Roof 2	75.9	48.3	10.6	1.94	562	29.5
Roof 3	75.7	49.0	10.7	1.07	394	16.1
Roof 4	75.5	48.3	10.8	2.01	763	29.9
Roof 5	76.0	48.3	11.0	1.15	268	16.7
Roof Average	75.8	48.4	10.8	1.55	505	23.2
Floor 1	76.2	48.8	18.0	6.46	827	57.7
Floor 2	75.3	46.8	18.0	4.57	450	40.7
Floor 3	75.1	46.6	17.7	4.56	274	41.5
Floor 4	76.0	46.5	17.7	3.38	399	30.7
Floor 5	75.8	47.3	17.9	3.41	773	30.5
Floor Average	75.7	47.2	17.9	4.48	545	40.3

3.2 Diaphragm Test Results and Observations

This section discusses the notable observations during the testing of the Phase 2 diaphragm specimens and presents the shear force vs. rotation graphs for each individual specimen.

3.2.1 (11-RALT-M) Roof Alternate Direction Joists – Monotonic Loading

Unlike any other configuration tested in either Phase 1 or Phase 2, the 11-RALT-M configuration did not have its rim joists bolted directly to the test apparatus. Instead, the rim joists were connected to C-shaped joists also referred to as chord elements which were bolted into the flanges of the W360x71 beams. This configuration resulted in high concentrated loads at these connections, particularly those at the fixed end. Due to the blocking members being significantly less stiff than the rim joist members, most of the east-west axial forces were directed into the rim joists and through the fixed end connections. Severe bending was observed at both of the fixed end connections in the C-shaped joists with one being in compression and the other in tension. The progression of bending of the C-shaped joist connection under tension at the north-east corner is shown in Figure 3.6. The high forces combined with the bending ultimately resulted in this connection failing and a separation observed between the previously connected members. As the connection began to fail, the rim joist began to pull away from the fixed end (west) causing the load distribution beam to move laterally. As the distribution beam continued to displace, it became apparent that contact was going to be made between the bolt heads on the support rollers and the bolt heads connecting the C-shaped section to the distribution beam (Figure 3.7). The potential for the two bolt heads making contact necessitated the test to be stopped. After the test was stopped, the frame was brought back to its initial position and the two bolts passing through the load distribution beam were removed to avoid conflict with the rollers. The test was then restarted from

the initial position. As the test specimen approached peak load, the north-east connection between the rim joist and C-shaped chord failed entirely which caused the distribution beam to laterally displace to the extent that the bolt heads on the edge of the rollers made contact with the inner flange of the distribution beam. The flange was greased to allow for it to act as a guide for the remainder of the test. Despite the failure of the rim joist connection, the ultimate resistance of the diaphragm was governed by the failure of the sheathing connections.

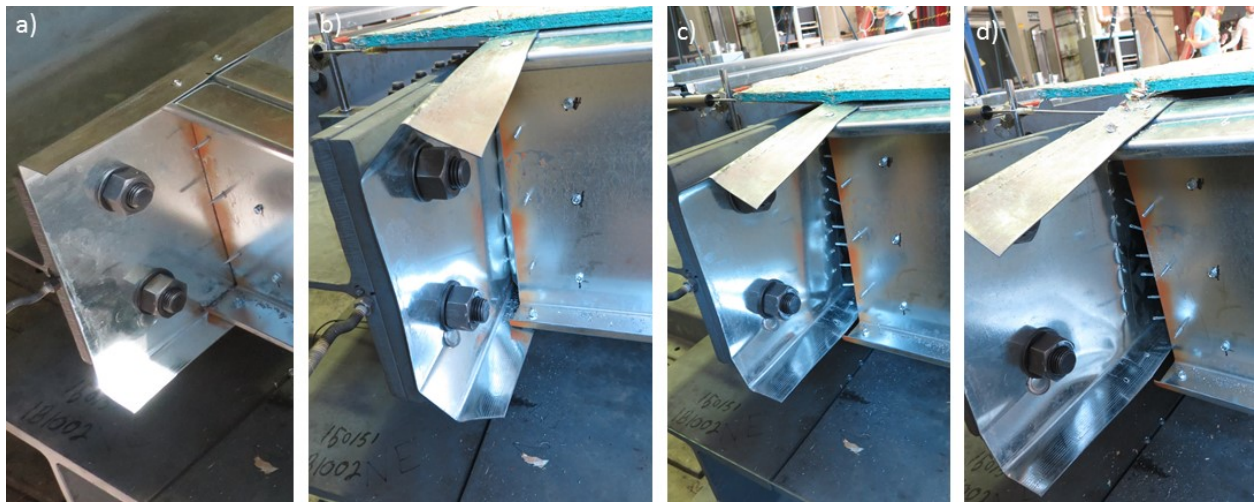


Figure 3.6: Progression Damage to Connection between Rim Joist and C-Shaped Section: a) Initial Position b) Position at Which Test was Stopped c) Position Where Connection Had Failed Completely d) Final Position

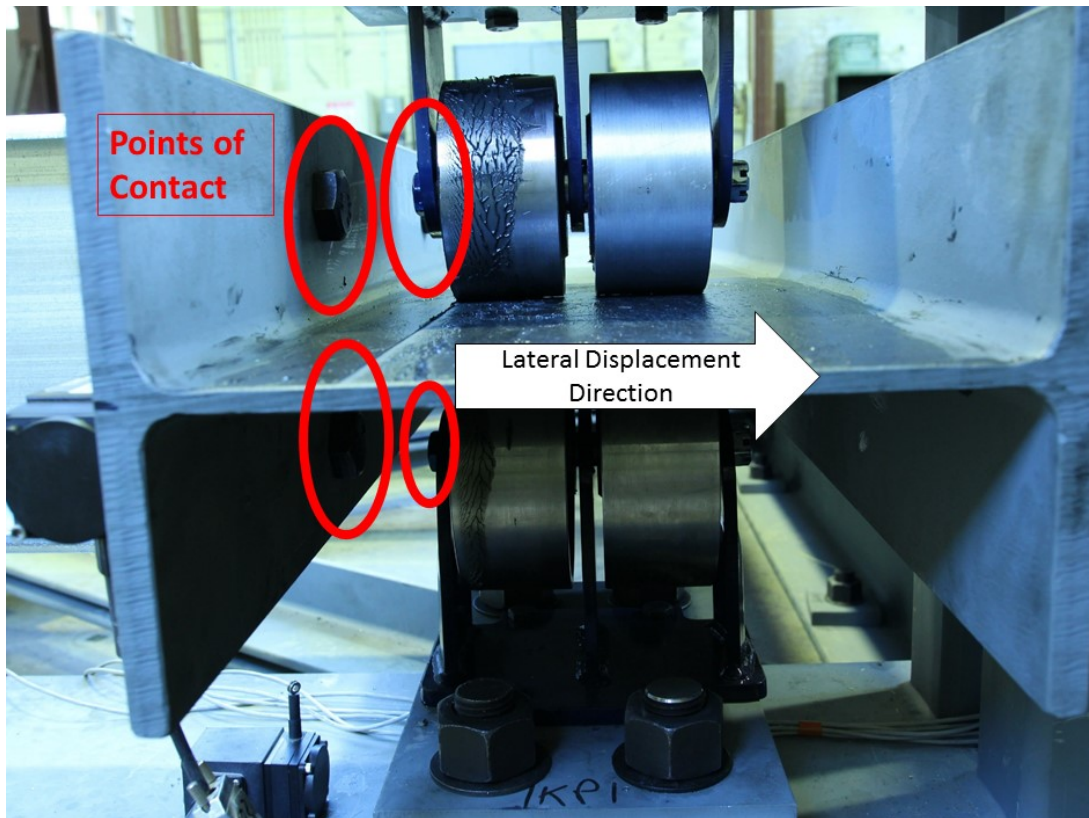


Figure 3.7: 11-RALT-M Contact Zone Caused by Lateral Displacement of Distribution Beam

The sheathing connection failure was concentrated along the fixed end of the diaphragm where the fasteners failed mainly due to tear out and pull through. The shear force vs. rotation curve is shown in Figure 3.8 with notable events numerically labeled. The sudden drop in resistance at Point 1 of Figure 3.8 was caused by the shear failure of the fasteners at the north-east rim joist to chord-joist connection. At this point more than half of the fasteners connecting the rim joist to the chord-joist had failed, and noticeable deformations of the connection could be observed (Figure 3.6 b). Once Point 2 was reached, it was decided to stop the test due to the potential of contact between the bolt heads. The frame was then brought back to its initial position corresponding to Point 3. At Point 4 the rim joist connection had failed completely (Figure 3.6 c) and the distribution beam was able to displace laterally until the inner flange made contact with the bolt heads of the rollers. Once the peak load was reached at Point 5, enough sheathing fasteners had failed in order to disconnect the

entire row of sheathing across fixed end (Figure 3.9) – it is assumed that had the failure at the north-east connection not occurred, a smooth curve would have been observed between Points 1 and 5. At Point 6, a hinge was developed in the connections between the first row of blocking and the joists adjacent to the fixed end shown in Figure 3.10. The damage caused to the blocking connections is shown in Figure 3.11. In order to provide clearer comparisons, it was decided to modify the original graph by removing the data points which corresponded to the stopping and restarting of the test. In Figure 3.12 the original and modified graphs are shown side by side; for all future references to specimen 11-RALT-M, the modified graph will be used.

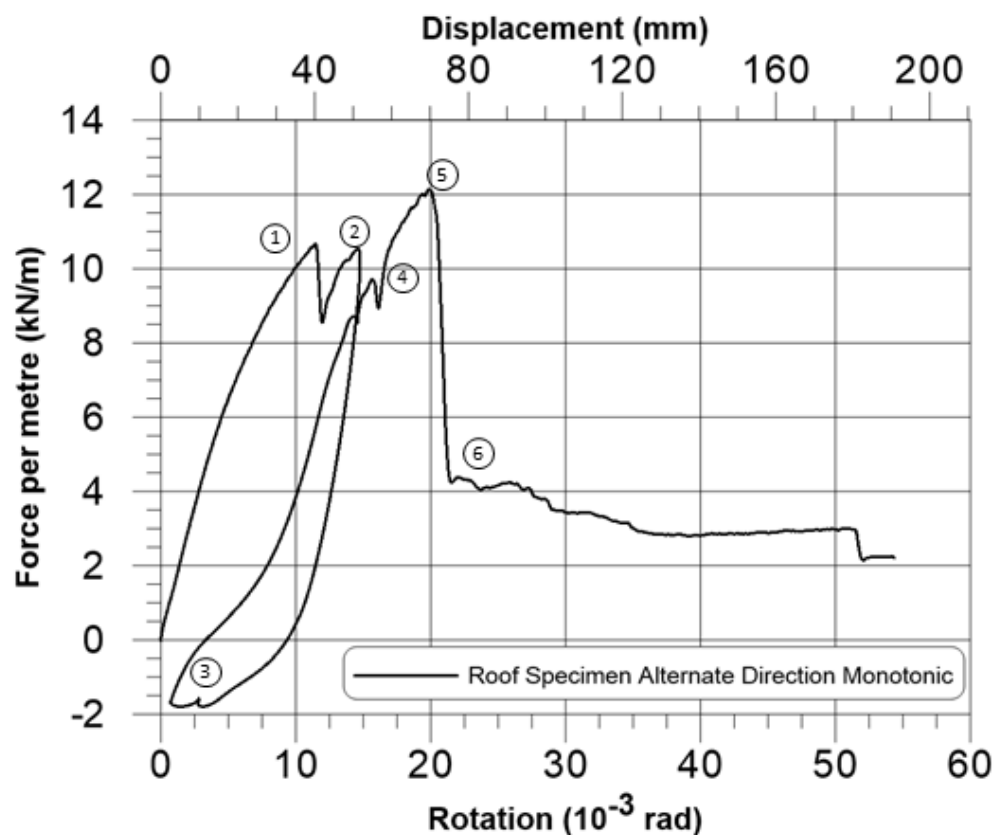


Figure 3.8: Shear Force vs. Rotation (displacement) for 11-RALT-M



Figure 3.9: Sheathing Failure along Fixed End of 11-RALT-M

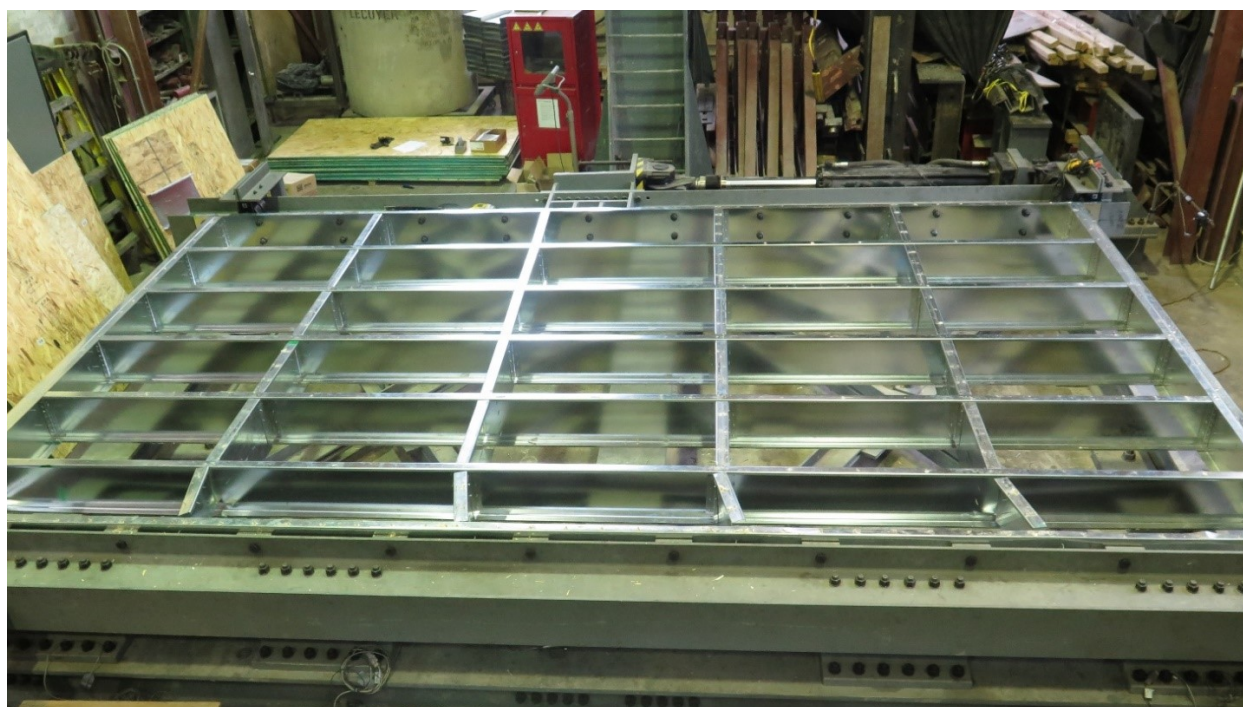


Figure 3.10: Hinge in Blocking to Joist Connection of Specimen 11-RALT-M



Figure 3.11: Post-Test Blocking Connections along Fixed End (Damage)

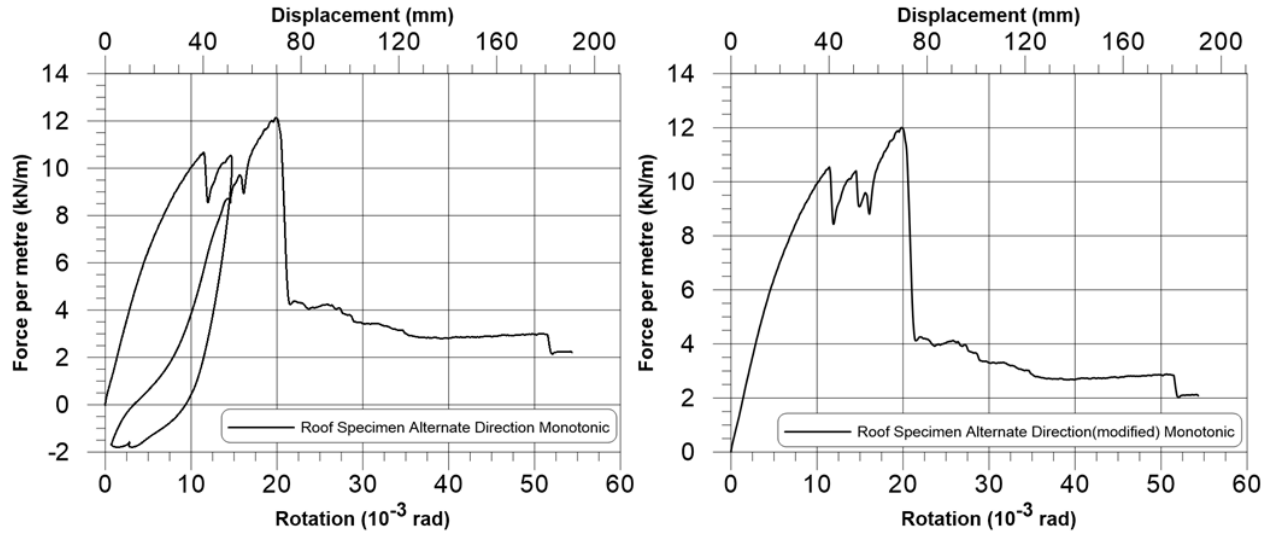


Figure 3.12: (Left) Original Shear Force vs. Rotation (Displacement) for 11-RALT-M (Right) Modified Shear Force vs. Rotation (Displacement) for 11-RALT-M

3.2.2 (12-RSTRAP-M) Roof Strap Blocking – Monotonic Loading

The 12-RSTRAP-M specimen experienced a smooth loading curve up until peak load as shown in Figure 3.13. At peak load a sudden failure of the sheathing fasteners was observed in the row of OSB panels beside the load distribution beam. Individual fastener shear failures happened in rapid succession which indicated the inability of the forces in the diaphragm to redistribute adequately between fastener failures. Tear out failures were also observed, particularly in the south-west corner panel (Figure 3.14) which essentially became isolated from the rest of the sheathing prior to peak loading. After sheathing failure occurred, a hinge was created at the interface between the first two rows of sheathing at the west end. The bending of the joist members after the hinge was created is shown in Figure 3.15. During the disassembly of the specimen, it was noted that the fasteners were significantly tilted (Figure 3.16). The tilts were more pronounced at sheathing interfaces, showing the high amount of shear forces placed upon these fasteners.

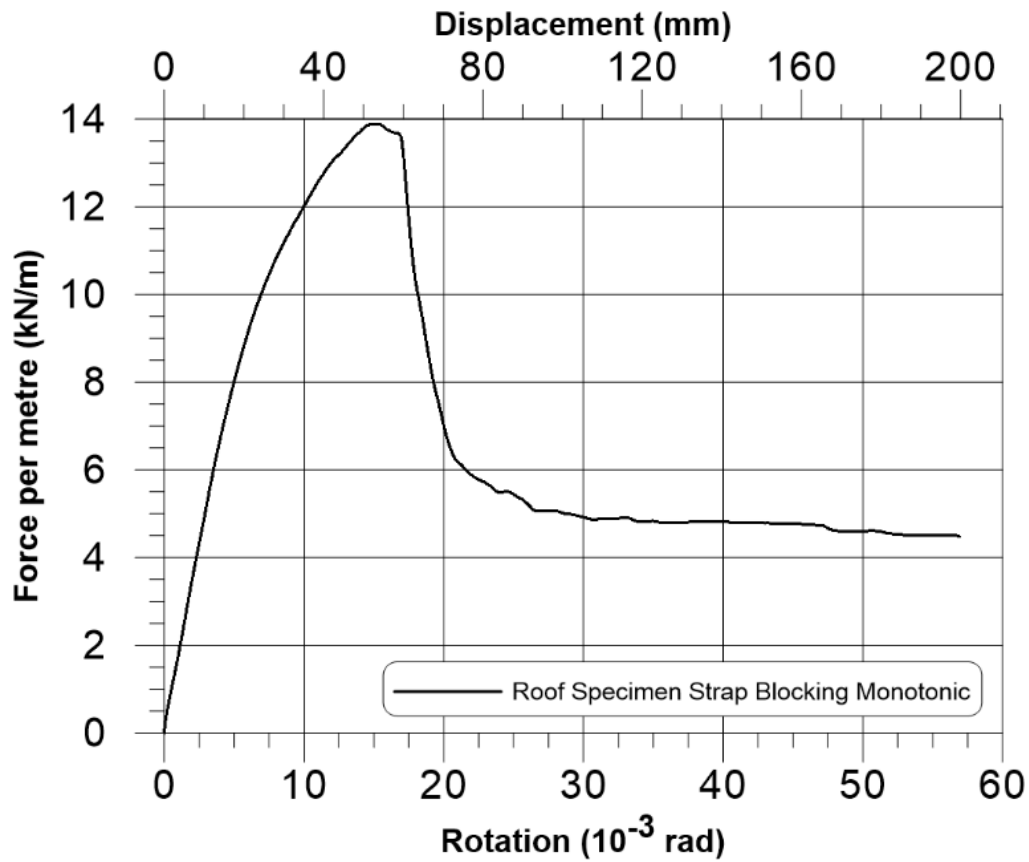


Figure 3.13: Shear Force vs. Rotation (Displacement) for 12-RSTRAP-M

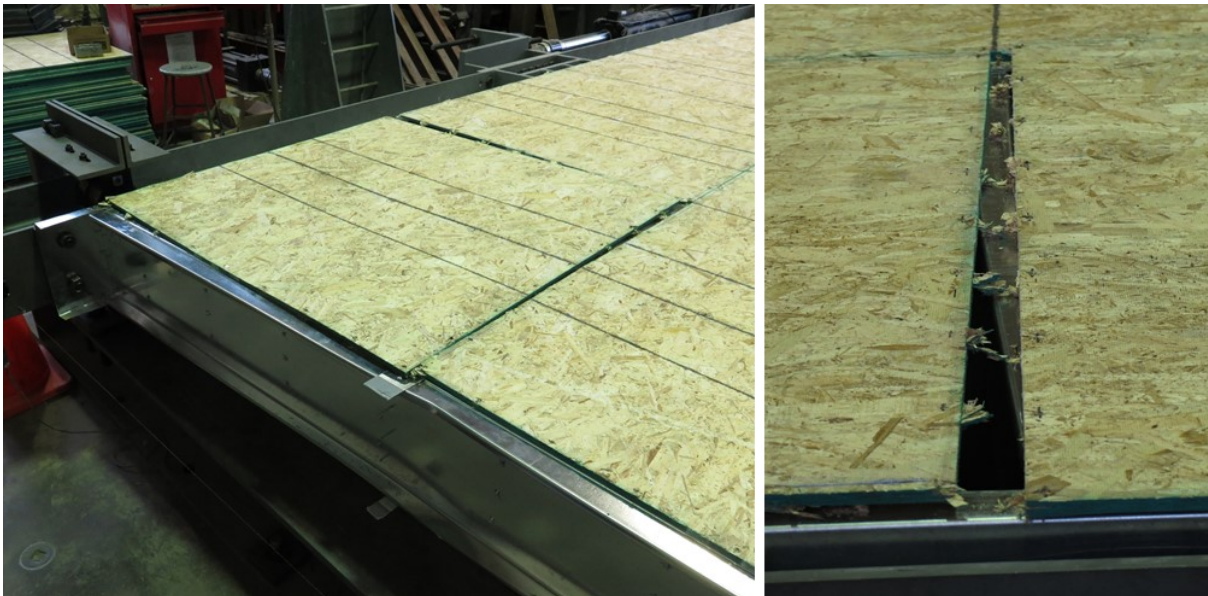


Figure 3.14: (Left) Isolation of South-West Corner Panel of 12-RSTRAP-M (Right) Close Up of Tear-out Fastener Failures

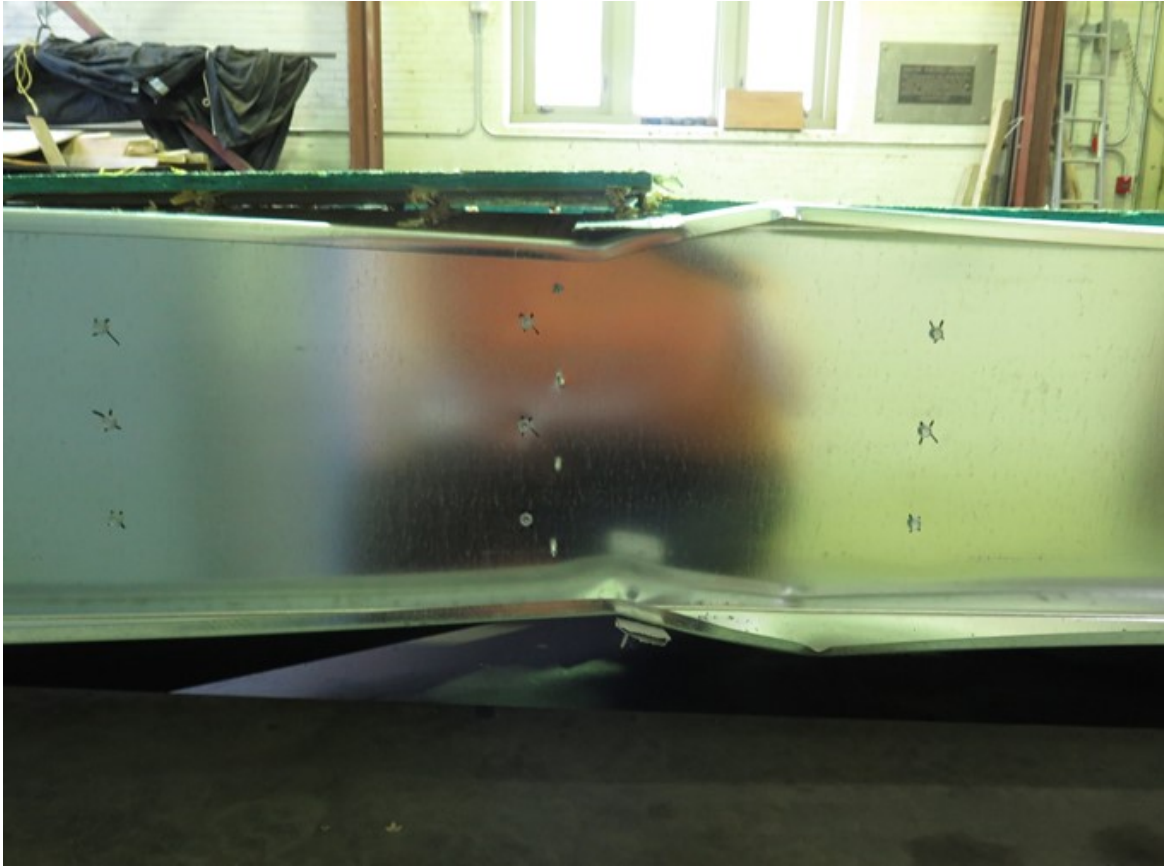


Figure 3.15: Bending of CFS Joist at Hinge Location Created After Sheathing Failure

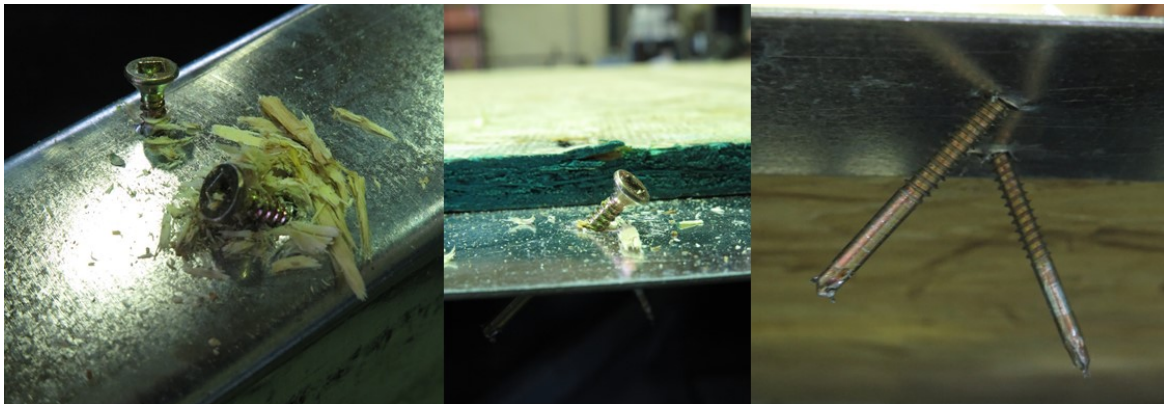


Figure 3.16: Tilting of Sheathing Fasteners Due to Shear Forces

3.2.3 (13-FB4-M) Floor Blocked (100mm / 300mm) Spacing – Monotonic Loading

Due to a problem that arose during the initial testing, the 13-FB4-M specimen was required to run through two separate tests; the first test was only partially completed, while the second test was

run to completion. During the first test, a connection issue occurred similar to what happened between the C-shaped chord-joist and rim joist connection as described for the 11-RALT-M specimen. In the 13-FB4-M specimen, severe bending of the north-east corner rim joist to joist connection allowed for the distribution beam to displace laterally. Unlike the 11-RALT-M case however, the test was not stopped prior to contact being made between the bolt heads of the rollers and those of the distribution beam. This point of contact began to resist the movement of the diaphragm and the perceived load began to increase rapidly. When the situation was realized, the test was stopped immediately and ultimately aborted and brought back to the initial position. The entirety of the OSB sheathing and underlying CFS-frame was examined and it was determined that while the sheathing had been damaged, the CFS-frame however, did not surpass the elastic range and therefore was able to be reused. All photos, results and graphs presented herein are of the second test. For the second test, it was decided to reinforce both corner connections of the fixed end as well as to reinforce the first three joist connections of the north-east end of the frame (Figure 3.17). The three connections at the north-east end of the frame were chosen as these connections were expected to experience the highest tensile forces which were the primary cause of the lateral displacement of the distribution beam. The last connection at the south-east corner was reinforced because it was expected to experience the highest compression forces. The reinforcements were done by fastening 175x175x1.37mm steel gusset plates to the bottoms of the joist to rim joist connections. Reinforcement plates were also fastened to the tops of the corner connections off to the side such that they would not interfere with the OSB sheathing (Figure 3.18). The size of the fasteners used in the angle clips were increased from 8 gauge to 10 gauge, and the number of fasteners in the angle clips increased from six fasteners in the rim joist and four in the joist to six fasteners in both. Finally, bearing plates were installed at the bolt locations on the tension side to

better distribute the forces in the rim joist at these connections (Figure 3.18). When installing the new sheathing for the second test, a system was required to avoid the holes created by the fasteners used in the first test. It was decided that all fastener locations were to be offset by 25mm except for those at the panel corner locations which were instead offset by 12.5mm. Figure 3.19 shows the force vs rotation for specimen 13-FB4-M with notable events numerically labeled.

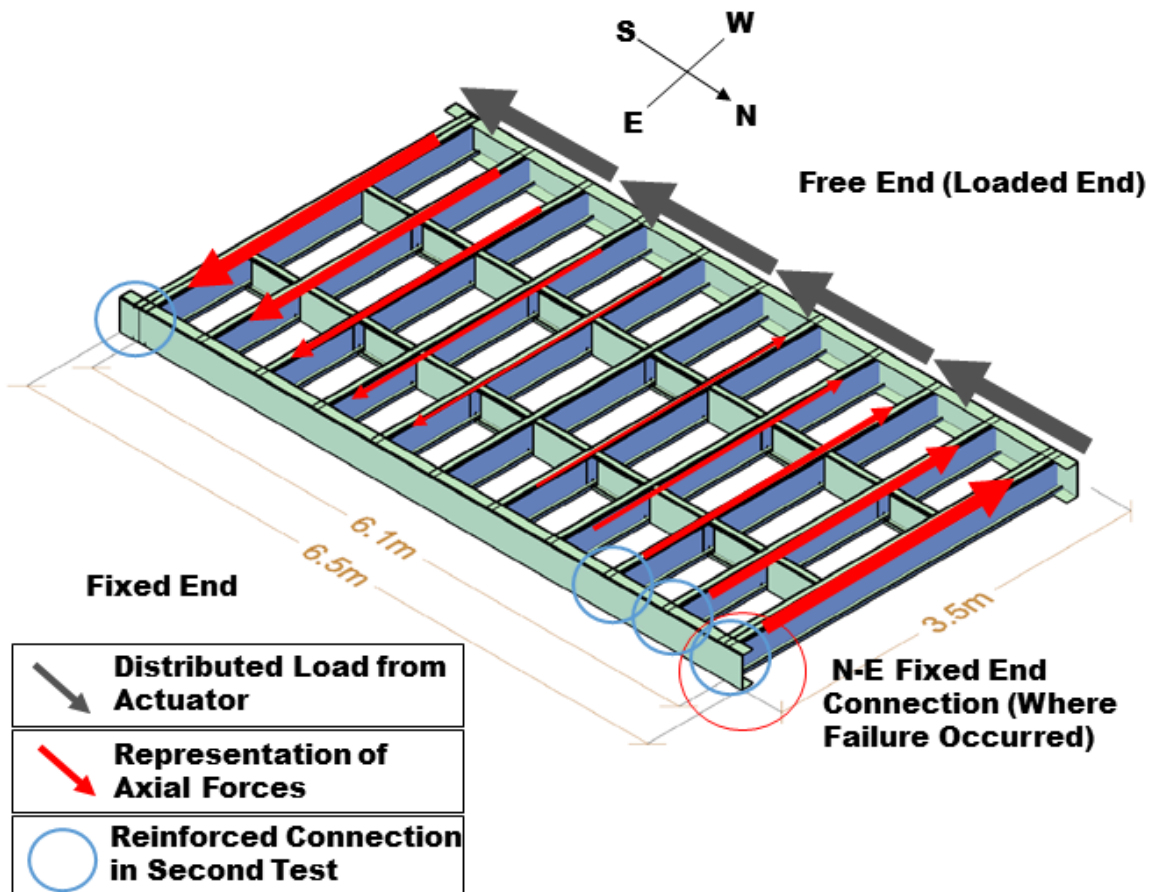


Figure 3.17: Illustration of Specimen 13-FB4-M with Predicted Axial Forces of Joist Members

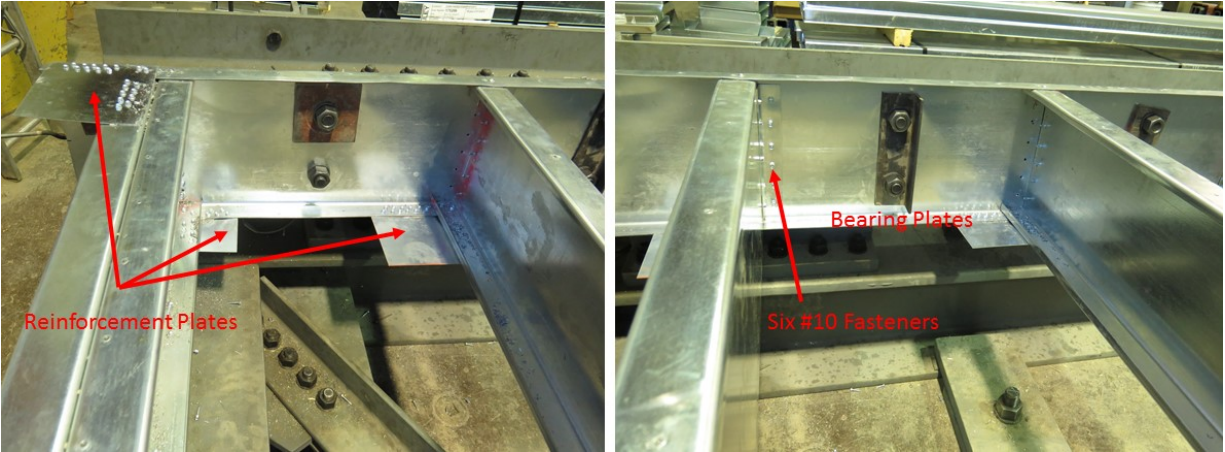


Figure 3.18: Reinforcements for Critical Connections

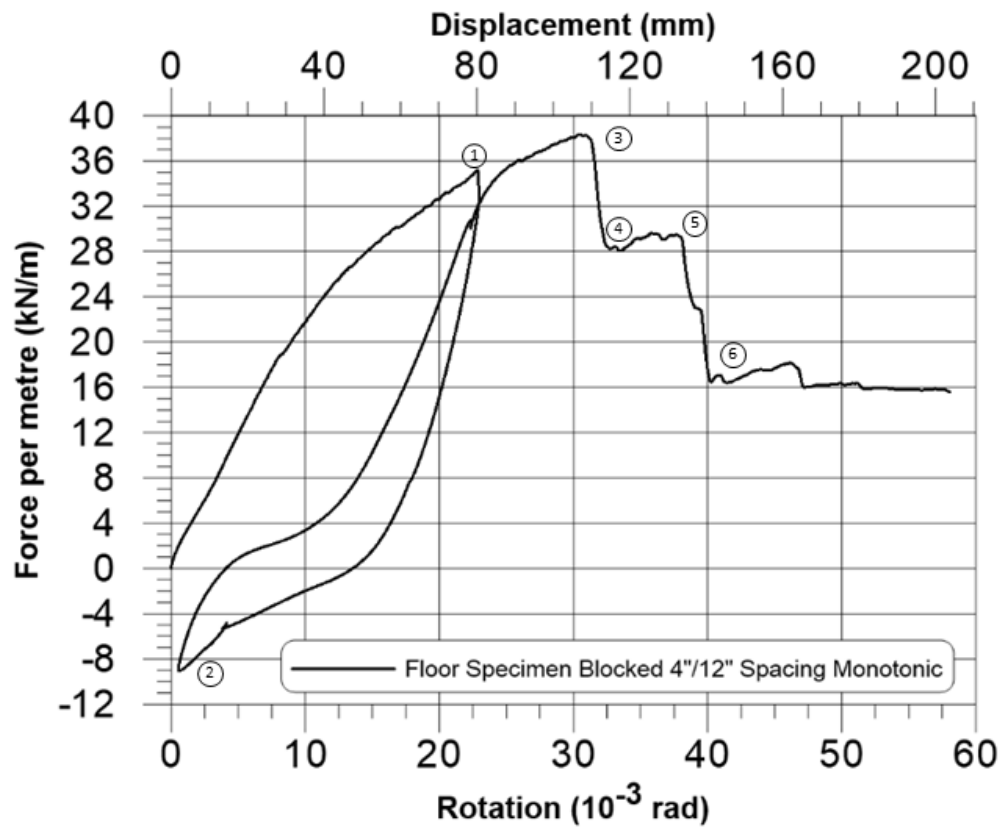


Figure 3.19: Shear Force vs. Rotation (displacement) for 13-FB4-M

While the added reinforcement did prevent the connection from failing, the high levels of forces caused extensive deformations at the north-east connections. These deformations combined with higher than normal rotations of the support frame necessitated a pause in the test. As a

precautionary measure, the test was stopped at Point 1 on Figure 3.19, and the diaphragm specimen was brought back to its initial position (Point 2). The bolts in the load distribution beam near the rollers were removed as had been done with specimen 11-RALT-M and the test was continued. Up until peak load (Point 3), only two sheathing fastener shears were observed, spaced far apart from one another. At peak load, shear failures of the sheathing fasteners occurred in rapid succession and two separate gaps began to form between the OSB panels as shown in Figure 3.20. At Point 4, the rapid shearing of sheathing fasteners began to slow down substantially. This continued until Point 5 where the rate of shearing fasteners increased once more similar to what was observed at peak load. At Point 6 the shearing failures slowed down once again. Shearing failures were still observed after Point 6 but the events were spaced far apart from one another (less than one failure every 30 seconds). After the test was ended and the sheathing panels were removed, it was noted that the diagonal compression field that developed across the diaphragm caused significant damage to the CFS frame (Figure 3.21). The joists as well as the blocking members were damaged following a path between the south-east and north-west corners as shown in Figure 3.22. Specimen 13-FB4-M was the only test where the steel frame and sheathing failed together, rather than the sheathing fasteners failing first, followed by the hinge action of the frame. Once again, as was done with specimen 11-RALT-M, a modified version of the shear force vs. rotation graph was made which omitted the data corresponding to the stopping and restarting of the test. Figure 3.23 shows a comparison between the original and modified graphs. It should be noted that despite the test being stopped and the bolts taken out, contact was never made throughout the test between the flange of the distribution beam and the bolt heads of the rollers.

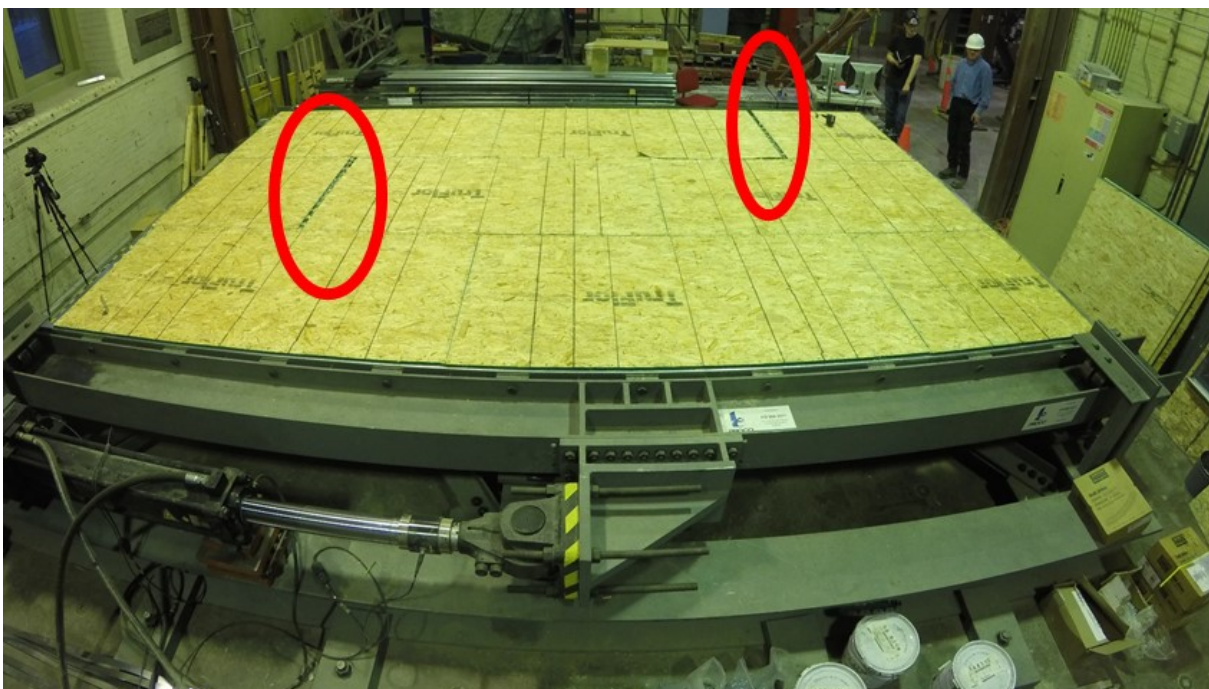


Figure 3.20: Gaps Between OSB Panels During Testing of Specimen 13-FB4-M

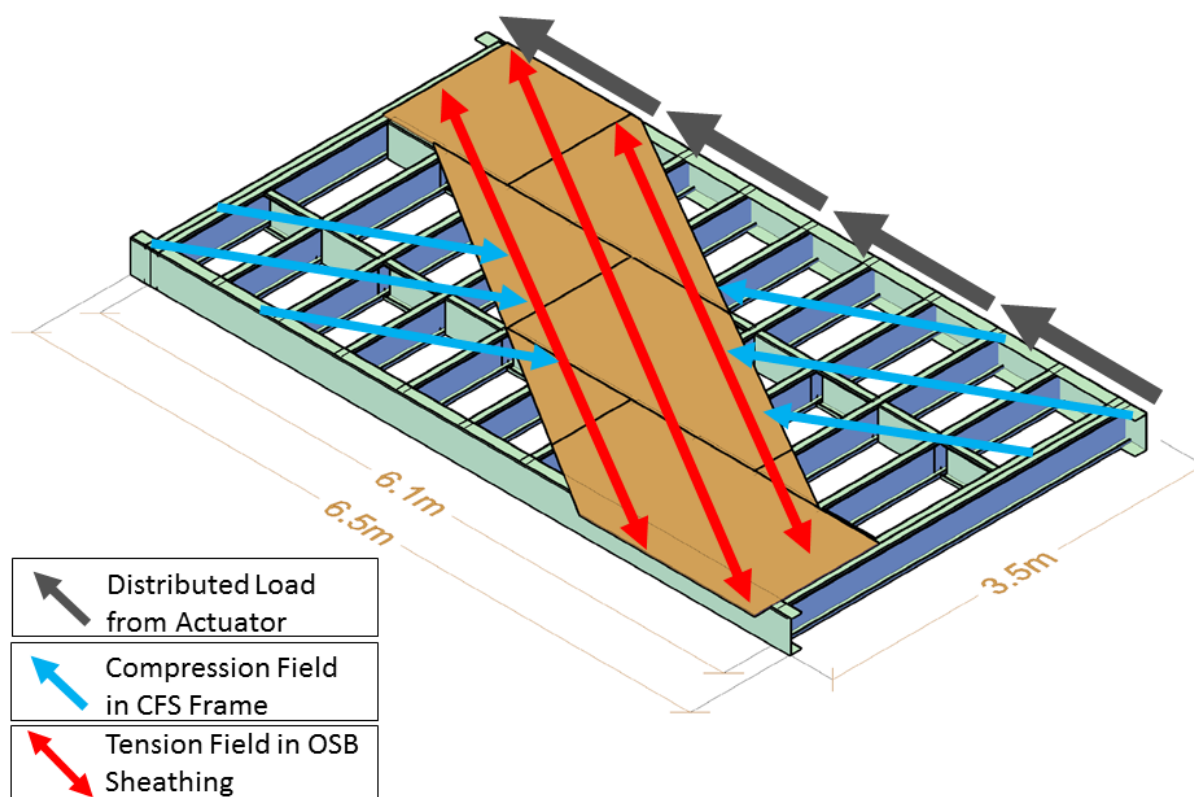


Figure 3.21: Illustration of Compression/Tension Field in Diaphragm Specimen 13-FB4-M



Figure 3.22: Damage to Frame Members of Specimen 13-FB4-M Caused by Compression Field in CFS Structure

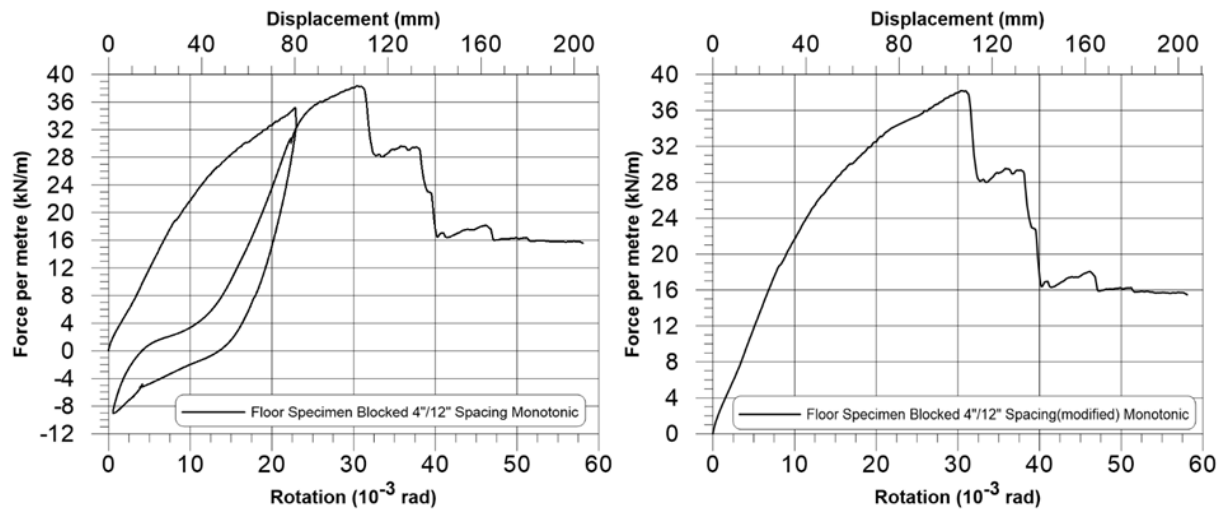


Figure 3.23: (Left) Original Shear Force vs. Rotation (Displacement) for Specimen 13-FB4-M
(Right) Modified Shear Force vs. Rotation (Displacement) for Specimen 13-FB4-M

3.2.4 (14-RGYP-M) Roof with Gypsum Ceiling – Monotonic Loading

Early on during the testing of specimen 14-RGYP-M, prior to peak load, cracking noises were heard from the underside of the frame. The sounds were believed to have been the joint compound used between the gypsum panels cracking under the minor deformations. Just prior to peak load, a small drop in shear resistance was observed which was due to some drywall fasteners failing in shear. At peak load, failure was caused by the fasteners of the OSB sheathing failing, mostly by means of tear out along the perimeter and a mix of partial and complete pull-through of the fasteners along the interface of the second and third rows (from west to east) of the sheathing panels. This type of failure was expected as the design for the unblocked diaphragm lacks framing support below the interior edges of the OSB panels which resulted in fewer fasteners along this interface. Lift off of the sheathing panels was observed in these locations (Figure 3.24). From direct observation and the subtle tilting of the gypsum panels, it was observed that all of the gypsum fasteners along this interface had failed near the time that peak load was reached. When the displacement reached approximately 85mm, the first gypsum panel was completely disconnected from the diaphragm (Figure 3.25). By the end of the test nearly half of all the gypsum panels had fallen from the diaphragm, Figure 3.26 is a photo of the diaphragm after testing with the OSB sheathing removed. The failures of the gypsum panels were caused by tear out or pull through of the fasteners; most of the fasteners were heavily tilted as shown in Figure 3.27. The joint tape and compound proved to provide little resistance to keep the gypsum panels from separating. The graph of shear force vs. rotation for the 14-RGYP-M specimen is shown in Figure 3.28.



Figure 3.24: Lift Off of OSB Panels After Failure of Sheathing Fasteners



Figure 3.25: (Left) Displacement of Sheathing and Bending of Double Joist (Right) Tear-out of Sheathing Fasteners and Gypsum Failure

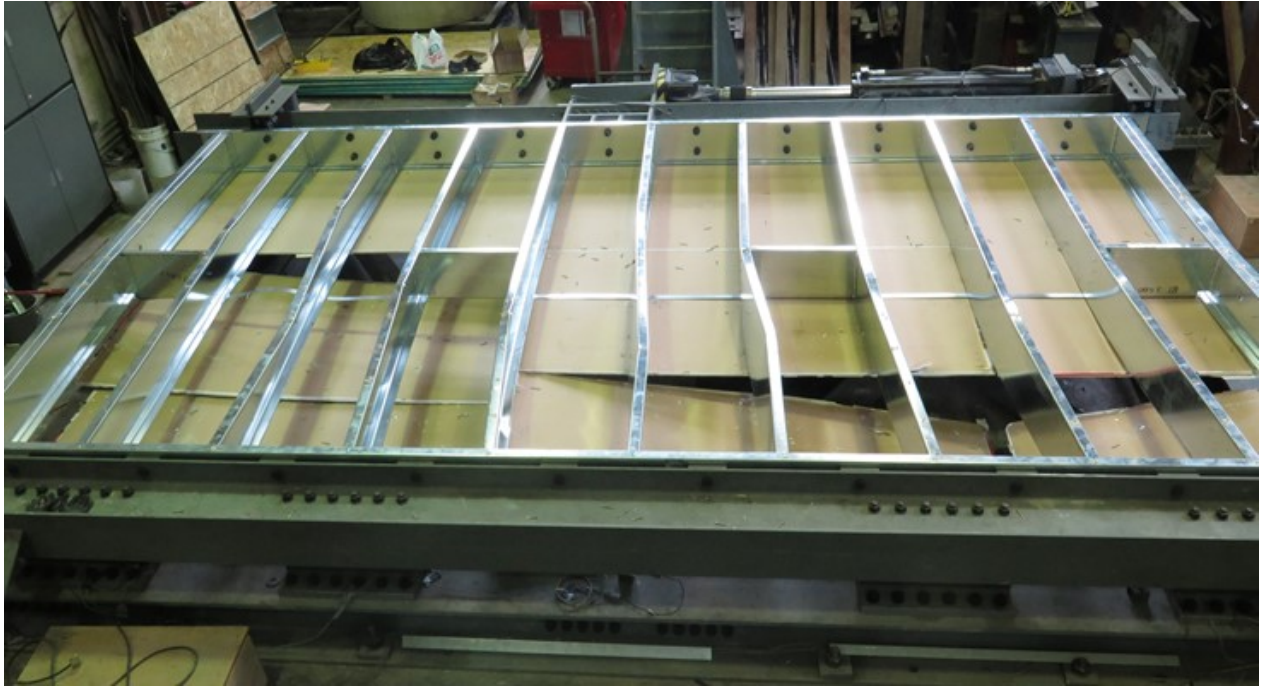


Figure 3.26: 14-RGYP-M Specimen Post-Test with OSB Panels Removed



Figure 3.27: (Left) Tilted Gypsum Fastener, Gypsum Panel Had Fallen (Right) Tear out of Gypsum Fastener at Corner Location

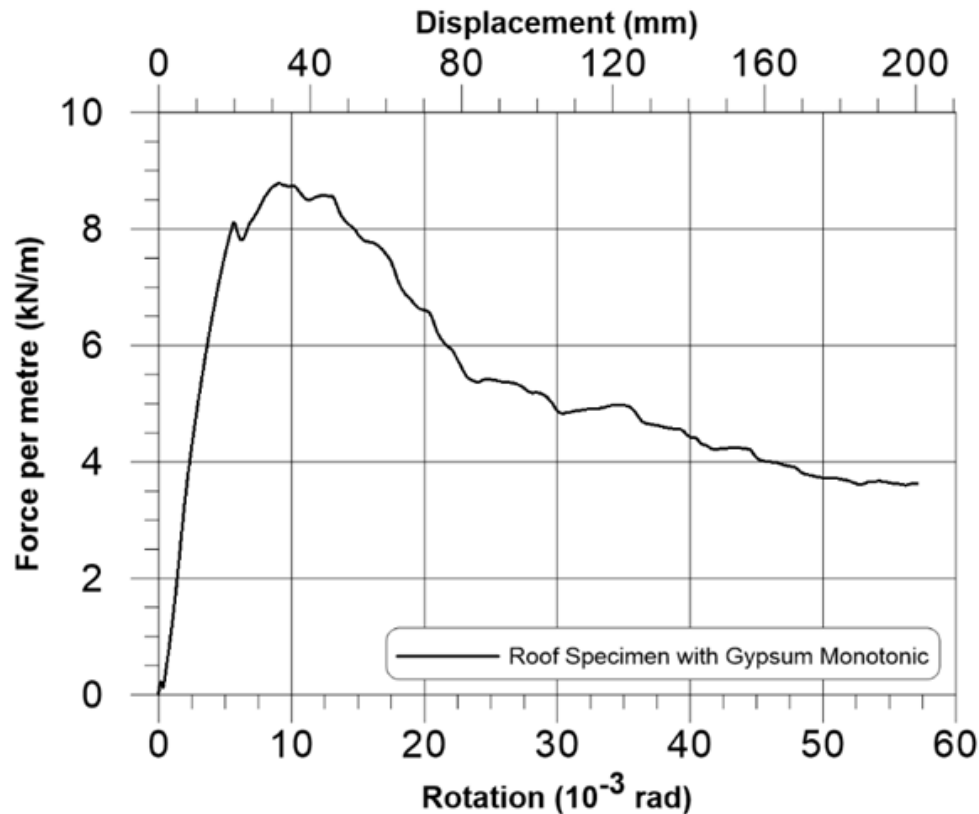


Figure 3.28: Shear Force vs. Rotation (displacement) for Diaphragm Specimen 14-RGYP-M

3.2.5 (15-RGYP-C) Roof with Gypsum Ceiling – Reversed Cyclic Loading

Being the same configuration as the 14-RGYP-M test, specimen 15-RGYP-C naturally had a very similar response. However, due to the numerous cycles of the reversed cyclic loading, the extent of the damage was increased. The failure mechanism was the same for specimen 15-RGYP-C as it had been described for the 14-RGYP-M test, with the exception that the failure occurred across both sheathing interfaces as shown in Figure 3.29 rather than just one. Once again the failure took place at the sheathing interfaces due to the lack of framing support along these panel edges. Contact forces on both sides of the centre panels caused them to bend in a U-shape ultimately causing pull through failures of all of the fasteners except for those which were located across the centre line of these panels. Over the course of the entire test, all of the gypsum panels became disconnected

from the CFS framing. Unlike the monotonic test where the gypsum panels failed without pattern, in the cyclic test failure of the gypsum panels began at the west end where shear failures were observed across the entire row. Following the shear failures, the combination of the reduced number of fasteners along with the forces generated in the test and the self-weight of the gypsum boards resulting in the remaining fasteners failing by pull through (Figure 3.30). The graph of shear force vs. rotation for the 15-RGYP-C specimen is shown in Figure 3.31.

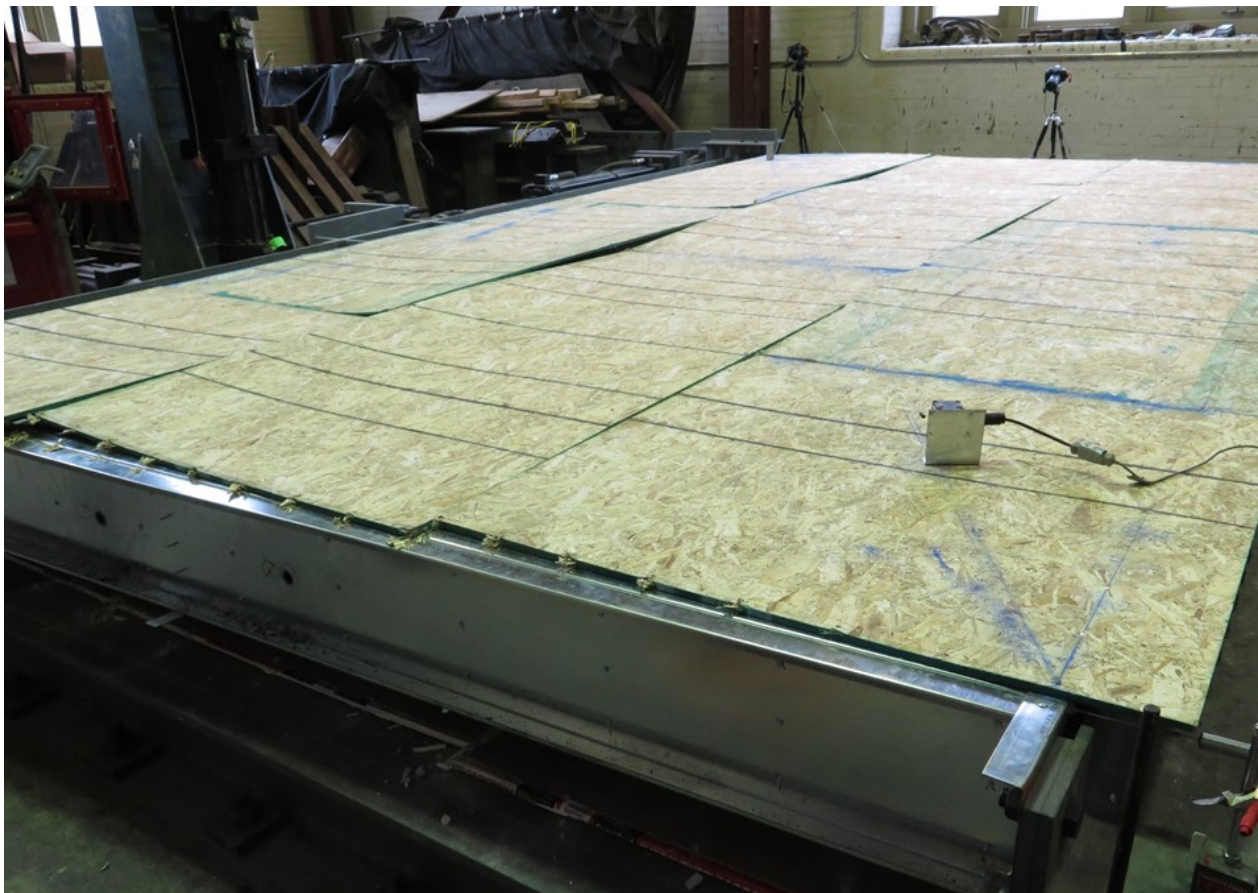


Figure 3.29: Specimen 15-RGYP-C Sheathing Failure Across Both Panel Row Interfaces



Figure 3.30: Connection Failures of Gypsum Panels for Specimen 15-RGYP-C

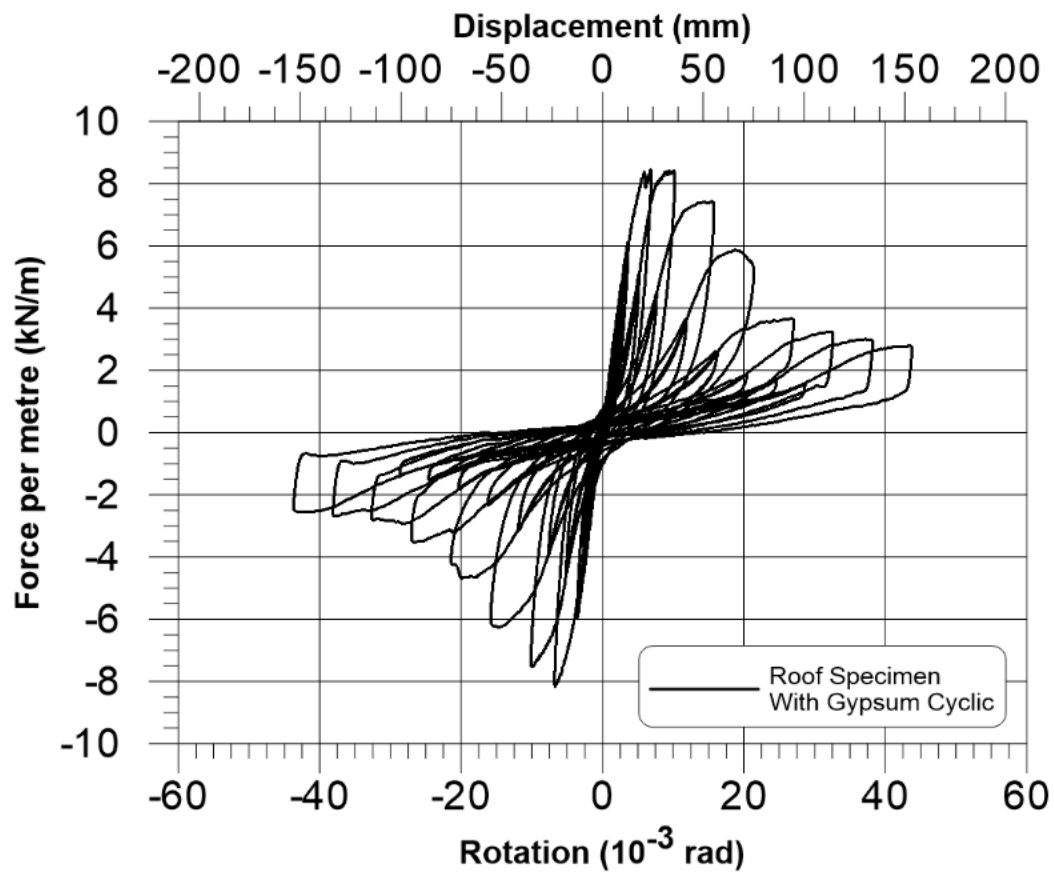


Figure 3.31: Shear Force vs. Rotation (displacement) for Specimen 15-RGYP-C

3.2.6 (16-FCRETE-M) Floor with Gypcrete Topping – Monotonic Loading

As specimen 16-FCRETE-M was being loaded, cracks in the gypcrete began to emerge. The cracking exactly followed the outlines of the underlying OSB sheathing panels. As the test continued the cracks propagated and grew wider, the progression of the gypcrete cracking can be seen in Figure 3.32. Prior to reaching peak load, two connection fastener shears were heard at the rim joist – joist connection at the north-east corner. Although the connection never failed entirely, extensive deformation at this connection was observed (Figure 3.33) which allowed for lateral displacement of the distribution beam, similar to what was observed in specimen 13-FB4-M. However, for specimen 16-FCRETE-M the bolts in the distribution beam which had caused problems for both the 11-RALT-M and 13-FB4-M specimens were taken out prior to testing. As the 16-FCRETE-M specimen approached peak load, sheathing fastener shearing could be heard in slow succession. Following peak load, more cracks emerged in the gypcrete topping, and the OSB panels began to separate from each other. Over time the distance of the panel separation increased, ultimately causing tear out failures of the sheathing fasteners, this can be seen in Figures 3.34 and 3.35. The gypcrete bonded integrally with the OSB panels, allowing it to behave as a composite sheathing which was much stronger and stiffer than the OSB alone. The gypcrete also restricted the movement of the heads of the sheathing screws; i.e. they were not able to tilt, instead they remained vertical which resulted in an increased connection resistance. Considering the tension field in the diaphragm as created by the shear loading that was applied, the cracking of the gypcrete perpendicular to the tension field was expected (Figure 3.36). The gap between wood panels at the edge locations required that any tension force in the composite sheathing be carried solely by the gypcrete alone. This tensile force at these locations ultimately caused visible cracking to occur in the gypcrete topping. After cracking of the gypcrete topping, the sheathing to CFS frame

connections failed at these locations via bearing failure of the screws (Figure 3.35). The shear force vs. rotation graph of the 16-FCRETE-M specimen is shown in Figure 3.37. It was noted during the disassembly how strong the bond between the OSB panels and gypcrete was. No delamination was observed despite the use of a powered jack hammer with flat-head bit applied directly to the gypcrete/OSB interface. The only method that proved effective to separate the two materials was to crush the gypcrete topping from above.

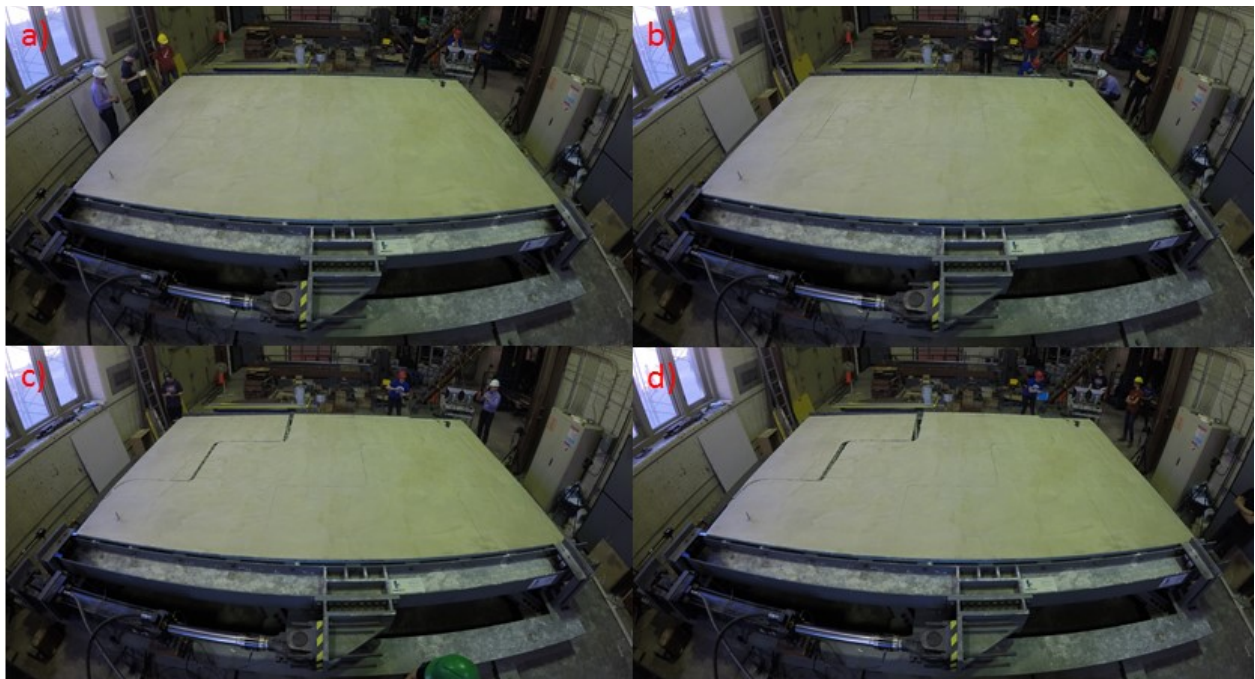


Figure 3.32: Progression of Crack Propagation of Gypcrete Topping (16-FCRETE-M)



Figure 3.33: Extensive Deformation at North-East Joist – Rim Joist Connection



Figure 3.34: Separation of Panels with Increased In-plane Displacement (Post-Peak Loading)



Figure 3.35: Tension Fracture of Gypcrete Topping with Tear out Failure of Sheathing Fasteners

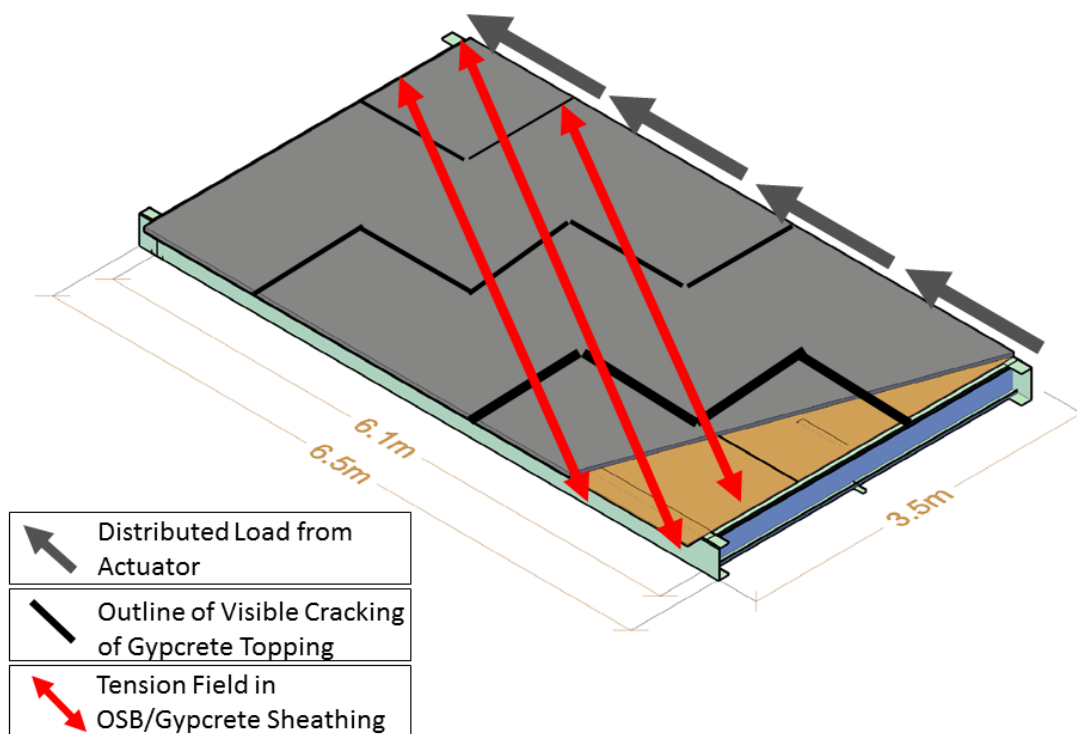


Figure 3.36: Illustration of Tension Field on Specimen 16-FCRETE-M

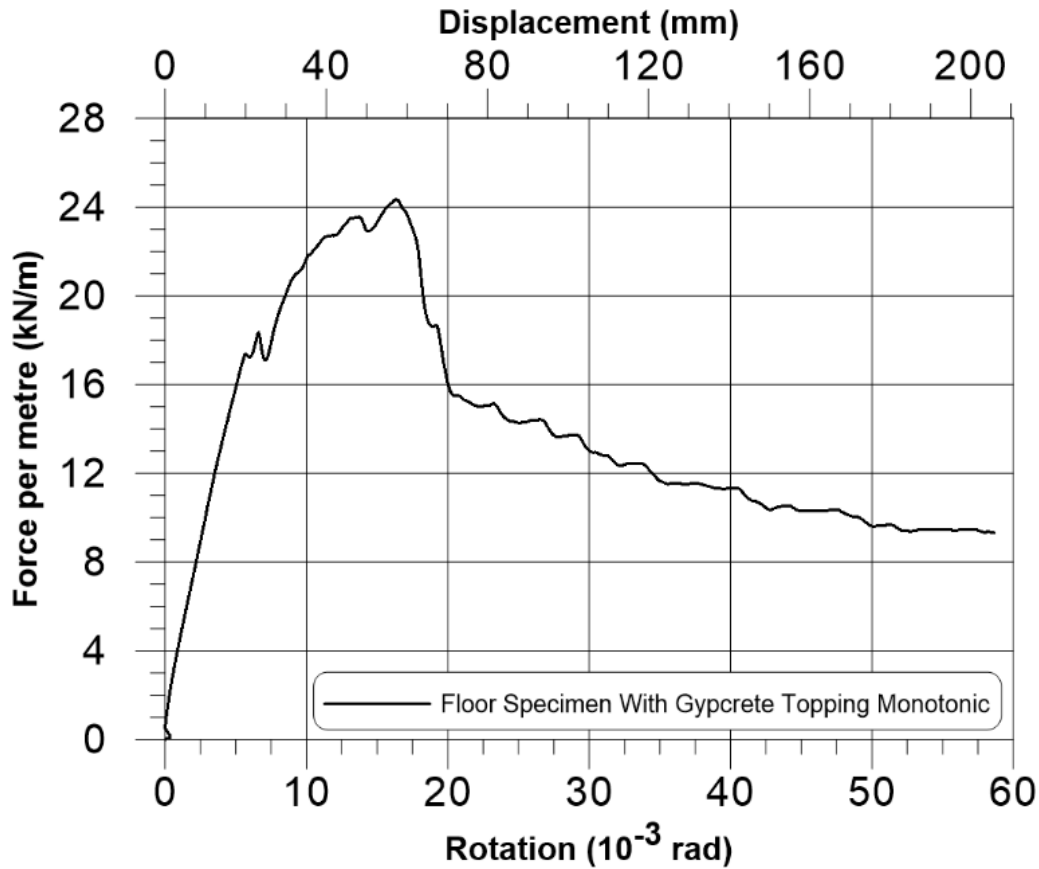


Figure 3.37: Shear Force vs. Rotation (displacement) for Specimen 16-FCRETE-M

3.3 Design Predictions

This section contains the design values for in-plane deflection and shear strength as well as the procedure for how the values were obtained. The methodology and formulas used in this section were taken from the AISI S400 Standard (2015). The predicted values are compared with the measured response of the diaphragm test specimens.

3.3.1 In-Plane Deflection

A total of three different methods were implemented to predict in-plane deflection values to compare with the measured displacement of the diaphragm test specimens. The first method was by using equation C-F2.4.3-1 from the AISI S400 Standard (2015) used for calculating design deflection in diaphragms for simple support conditions. The second method used equation

E2.4.1.4-1 from the same standard, which is a design deflection equation intended to be used for cantilever shear walls. The final method that was used was a variation of the second method where the results obtained from Eq. E2.4.1.4-1 were compared against the equivalent elastic in-plane deflection values of the test diaphragms.

Diaphragm Deflection Equation (C-F2.4.3-1)

For the first method, the diaphragm equation C-F2.4.3-1 from the AISI S400 Standard (2015) was used which is presented as Equation 3.1. This equation was designed for CFS wood or steel sheathed diaphragms under simple supported conditions. Due to the tests being performed under cantilever loading, the shear demand (v) and the length perpendicular to loading (L) were multiplied by a factor of two in an attempt to match a simple supported scenario. Table 3.7 summarises the results obtained using this method and compares them to the deflection observed during testing.

$$\delta = \frac{0.052vL^3}{E_s A_c b} + \frac{\omega_1 \omega_2 v L}{\rho G t_{sheathing}} + \omega_1^4 \omega_2 (\alpha) \left(\frac{v}{2\beta} \right)^2 + \frac{\sum_{j=1}^n \Delta_{ct} X_i}{2b} \quad (\text{Eq. 3.1})$$

where,

A_c	= Gross cross-sectional area of chord member, in square inches (mm^2)
b	= Diaphragm depth parallel to direction of load, in inches (mm)
E_s	= Modulus of elasticity of steel 29,500,000 psi (203,000 MPa)
G	= Shear modulus of sheathing material, in pounds per square inch (MPa)
L	= Diaphragm length perpendicular to direction of load, in inches (mm)
N	= Number of chord splices in diaphragm (considering both diaphragm chords)
s	= Maximum fastener spacing at panel edges, in inches (mm)
$t_{sheathing}$	= Nominal panel thickness, in inches (mm)
t_{stud}	= Nominal framing thickness, in inches (mm)
v	= Shear demand ($V/2b$), in pounds per linear inch (N/mm)

V	= Total lateral load applied to the diaphragm, in pounds (N)
X	= Distance between the “i th ” chord-splice and the nearest support (braced wall line), in inches (mm)
α	= Ratio of the average load per fastener based on a non-uniform fastener pattern to the average load per fastener based on a uniform fastener pattern (= 1 for a uniformly fastened diaphragm)
β	= 67.5 for plywood and 55 for OSB for U.S. Customary (lb/in ^{1.5}) 2.35 for plywood and 1.91 for OSB for SI units (N/mm ^{1.5})
δ	= Calculated deflection, in inches (mm)
Δ_{ci}	= Deformation value associated with “i th ” chord splice, in inches (mm)
ρ	= 1.85 for plywood and 1.05 for OSB
ω_1	= s/6 (for s in inches) = s/152.4 (for s in mm)
ω_2	= 0.033/t _{stud} (for t _{stud} in inches) = 0.838/ t _{stud} (for t _{stud} in mm)

For unblocked diaphragms, δ is multiplied by 2.50.

Table 3.7: Comparison of Calculated Deflections Using Equation 3.1 vs. Measured Deflections

Specimen	$\delta_{\text{Calculated}}$ (mm)	δ_{Test} (mm)	% Error
11-RALT-M	9.3	69.3	86.7
12-RSTRAP-M	12.0	52.4	77.2
13-FB4-M	23.1	108.7	78.8
14-RGYP-M	13.8	34.1	59.6
16-FCRETE-M	41.1	57.3	28.2

Sample Calculation

Deflection calculation using Eq. 3.1 for diaphragm specimen 12-RSTRAP-M

$$A_c = 1230 \text{ mm}^2 \text{ (2x 1200S200-54)}$$

$$b = 6096 \text{ mm (20ft)}$$

$$E_s = 203000 \text{ MPa}$$

$$G = \frac{G_v t_v}{t_{\text{sheathing}}} = \left(\frac{14629 \left(\frac{N}{mm} \right)}{11.11 mm} \right) = 1316 \text{ N/mm}^2 \text{ (24/16 rating OSB)}$$

the shear modulus, G, is

not a readily available value in most cases. Here G is approximated by dividing the through thickness shear rigidity ($G_v t_v$) by the nominal panel thickness ($t_{\text{sheathing}}$). The through thickness shear rigidity ($G_v t_v$) is taken from Table A (Shown in Figure 3.38). This table was obtained from TECO's document entitled *Design Capacities for Oriented Strand Board* (TECO, 2008). These values correspond with the values published in the 2005 edition of the AF&PA American Wood Council's *Allowable Stress Design (ASD)/LRFD Manual for Engineered Wood Construction*. It is important to note that the construction adjustment factor C_G was incorporated into the design values found in Table A.

Table A
Wood Structural Panel Design Capacities Based on Span Ratings^(a)

Span Rating	Strength							Planar Shear	Stiffness and Rigidity					
	Bending F _b S (lb-in/ft of width)		Axial Tension F _t A (lb/ft of width)		Axial Compression F _c A (lb/ft of width)		Shear through the thickness ^(b) F _v t _v (lb/in of shear-resisting panel length)	Planar Shear F _s (lb/Q) (lb/ft of width)	Bending EI (lb-in ² /ft of width)	Axial ^(a1) EA (lb/ft of width x 10 ⁶)		Rigidity through the thickness G _v t _v (lb/in of panel depth)		
	Capacities relative to strength axis ^(c)													
	0°	90°	0°	90°	0°	90°	0° / 90°	0° / 90°	0°	90°	0°	90°	0° / 90°	
Sheathing Span®														
24/0	300	97	2,300	780	2,850	2,500	155	130	60,000	11,000	3.35	2.50	77,500	
24/16	385	115	2,600	1,300	3,250	2,500	165	150	78,000	16,000	3.80	2.70	83,500	
32/16	445	165	2,800	1,650	3,550	3,100	180	165	115,000	25,000	4.15	2.70	83,500	
40/20	750	270	2,900	2,100	4,200	4,000	195	205	225,000	56,000	5.00	2.90	88,500	
48/24	1,000	405	4,000	2,550	5,000	4,300	220	250	400,000	91,500	5.85	3.30	96,000	
Floor Span®														
16 oc	500	180	2,600	1,900	4,000	3,600	170	205	150,000	34,000	4.50	2.70	83,500	
20 oc	575	250	2,900	2,100	4,200	4,000	195	205	210,000	40,500	5.00	2.90	87,000	
24 oc	770	385	3,350	2,550	5,000	4,300	215	250	300,000	80,500	5.85	3.30	93,000	
32 oc	1,050	685	4,000	3,250	6,300	6,200	230	300	650,000	235,000	7.50	4.20	110,000	
48 oc	1,900	1,200	5,600	4,750	8,100	6,750	305	385	1,150,000	495,000	8.20	4.60	155,000	

(a) The design values in this table correspond with those published in the 2005 edition of the AF&PA American Wood Council's *Allowable Stress Design (ASD)/LRFD Manual for Engineered Wood Construction* Tables M9.2.1- M9.2.4, which are available from the AF&PA American Wood Council.

(a1) In late January 2008, revised Axial EA 90° (perpendicular) values were submitted for modification to AF&PA based on an industry-wide consensus. The appropriate panel grade and construction adjustment factor, C_a , has already been incorporated into these design values—do not apply the C_a factor a second time. These values do not apply to Structural I panels. See Tables M9.2.1 – M9.2.4 for the appropriate multipliers for Structural I panels.

(b) Shear through the thickness design capacities are limited to sections two feet or less in width; wider sections may require further reductions.

(c) Strength axis is defined as the axis parallel to the face and back orientation of the flakes, which is generally the long panel direction, unless otherwise marked.

Figure 3.38: Table A Used to Approximate Shear Modulus, G (TECO, 2008)

As a reference value, the shear modulus calculated from the CSA O86 Standard (2014) assuming short term loading ($K_D = 1.15$) gives a value of $G = 1139 \text{ N/mm}^2$. The previously calculated value

($G = 1317 \text{ N/mm}^2$) is used as it is the value suggested by the OSB provider Norbord based on the testing of their products.

$$L = 2 \times 3505 \text{ mm} = 7010 \text{ mm (Dimension perpendicular to loading multiplied by 2)}$$

$$s = 152.4 \text{ mm (6in)}$$

$$t_{\text{sheathing}} = 11.1 \text{ mm (7/16in OSB)}$$

$$t_{\text{stud}} = 1.44 \text{ mm (1200S200-54)}$$

$$v = V/2b = \frac{172756 \text{ N}}{2 \times 6096 \text{ mm}} = 14.17 \text{ N/mm}$$

$$V = 2 \times 86378 \text{ N} = 172756 \text{ N (Maximum recorded shear force multiplied by 2)}$$

$$\beta = 1.91 \text{ N/mm}^{1.5} \text{ (Standard OSB)}$$

$$\rho = 1.05 \text{ (Standard OSB)}$$

$$\omega_1 = s/152.4 = 152.4/152.4 = 1.0$$

$$\omega_2 = 0.838/t_{\text{stud}} = 0.838/1.438 = 0.583$$

$$\delta = \frac{0.052vL^3}{E_s A_c b} + \frac{\omega_1 \omega_2 v L}{\rho G t_{\text{sheathing}}} + \omega_1^4 \omega_2 (\alpha) \left(\frac{v}{2\beta} \right)^2 = \frac{0.052 \left(\frac{14.17 \text{ N}}{\text{mm}} \right) (7010 \text{ mm})^3}{203000 \text{ Mpa} (1230 \text{ mm}^2) (6096 \text{ mm})} + 1 \text{ mm} * 0.583 \text{ mm} * \frac{\left(\frac{14.17 \text{ N}}{\text{mm}} \right) (7010 \text{ mm})}{1.05 \left(\frac{1317 \text{ N}}{\text{mm}^2} \right) (11.11 \text{ mm})} + 1 \text{ mm}^{\frac{5}{4}} * 0.583 \text{ mm} * 1.0 \left(\frac{\frac{14.17 \text{ N}}{\text{mm}}}{2 * \frac{1.91 \text{ N}}{\text{mm}^{1.5}}} \right)^2 = 12.0 \text{ mm}$$

$$\% \text{ Error} = \frac{|\delta_{\text{observed}} - \delta_{\text{calculated}}|}{\delta_{\text{observed}}} * 100 = \frac{|52.4 - 12.0|}{52.4} * 100\% = 77.2\%$$

Note: the 4th term in eq. C-F2.4.3-1 was omitted for all specimens, as no chord splices were included in the design.

The large percentage of error obtained may indicated that despite modifying the variables to account for the cantilever loading conditions, the equation remained inappropriate to use for the cantilever loading configuration used in this test program.

Shear Wall Deflection Equation (E1.4.1.4-1)

It was believed that the loading configuration was the main source of error while using the diaphragm equation presented in Eq. 3.1; thus, for the next method, the shear wall equation, E1.4.1.4-1 from the AISI S400 Standard (2015) was used. The shear wall equation is intended to be used with cantilever loading conditions, similar to what was used in Phase 2. The entire diaphragm could be thought of as a very large shear wall placed horizontally. Equation 3.2 presents the shear wall deflection equation and a comparison of the results calculated from this equation versus those observed during testing is summarised in Table 3.8.

$$\delta = \frac{2vh^3}{3E_s A_c b} + \frac{\omega_1 \omega_2 v h}{\rho G t_{sheathing}} + \omega_1^4 \omega_2 \omega_3 \omega_4 \left(\frac{v}{\beta}\right)^2 + \frac{h}{b} \delta_v \quad (\text{Eq. 3.2})$$

where,

- A_c = Gross cross-sectional area of chord member, in square inches (mm^2)
- b = Width of the shear wall, in inches (mm)
- E_s = Modulus of elasticity of steel 29,500 ksi (203,000 MPa)
- G = Shear modulus of sheathing material, in pounds per square inch (MPa)
- h = Wall height, in inches (mm)
- s = Maximum fastener spacing at panel edges, in inches (mm)
- $t_{sheathing}$ = Nominal panel thickness, in inches (mm)
- t_{stud} = Nominal framing thickness, in inches (mm)
- v = Shear demand (V/b), in pounds per linear inch (N/mm)
- V = Total in-plane load applied to the diaphragm, in pounds (N)
- β = 67.5 for plywood and 55 for OSB for U.S. Customary ($\text{lb/in}^{1.5}$)
= 2.35 for plywood and 1.91 for OSB for SI units ($\text{N/mm}^{1.5}$)
- δ = Calculated deflection, in inches (mm)
- δ_v = Vertical deformation of anchorage / attachment details, in inches (mm)
- ρ = 1.85 for plywood and 1.05 for OSB

$$\begin{aligned}\omega_1 &= s/6 \text{ (for } s \text{ in inches)} \\ &= s/152.4 \text{ (for } s \text{ in mm)} \\ \omega_2 &= 0.033/t_{\text{stud}} \text{ (for } t_{\text{stud}} \text{ in inches)} \\ &= 0.838/t_{\text{stud}} \text{ (for } t_{\text{stud}} \text{ in mm)} \\ \omega_3 &= \sqrt{\frac{h}{b}} \\ \omega_4 &= 1 \text{ for wood with structural panels}\end{aligned}$$

Table 3.8: Comparison of Calculated Deflections Using Equation 3.2 vs. Measured Deflections

Specimen	$\delta_{\text{Calculated}}$ (mm)	δ_{Test} (mm)	% Error
11-RALT-M	45.2	69.3	34.8
12-RSTRAP-M	32.1	52.4	37.3
13-FB4-M	62.6	108.7	42.4
14-RGYP-M	17.9	34.1	47.5
16-FCRETE-M	54.0	57.3	5.6

Sample Calculation

Deflection calculation using Eq. 3.2 for specimen 12-RSTRAP-M

$$\begin{aligned}A_c &= 1230 \text{ mm}^2 \text{ (2x 1200S200-54)} \\ b &= 6096 \text{ mm (20ft)} \\ E_s &= 203000 \text{ MPa} \\ G &= \frac{G_v t_v}{t_{\text{sheathing}}} = \left(\frac{14629 \left(\frac{N}{mm} \right)}{11.11 mm} \right) = 1317 \text{ N/mm}^2 \\ h &= 3505 \text{ mm} \\ s &= 152.4 \text{ mm (6in)} \\ t_{\text{sheathing}} &= 11.1 \text{ mm (7/16in OSB)} \\ t_{\text{stud}} &= 1.44 \text{ mm (1200S200-54)} \\ v &= V/b = \frac{86378 N}{6096 mm} = 14.2 \text{ N/mm} \\ V &= 86378 \text{ N} \\ \beta &= 1.91 \text{ N/mm}^{1.5} \text{ (Standard OSB)}\end{aligned}$$

$$\rho = 1.05 \text{ (Standard OSB)}$$

$$\delta_v = 23.5 \text{ mm (based on maximum value from string potentiometers)}$$

Currently there is no information for the vertical deformation of standard anchorage / attachment details, thus in order to obtain a value for δ_v , test results are required. For the results presented in this thesis, the maximum value recorded from the string potentiometers recording displacement in the east-west direction is used. It should be noted that until design values for δ_v are available, true design predictions (prior to testing) are unable to be obtained.

$$\omega_1 = s/152.4 = 152.4\text{mm}/152.4 = 1.0$$

$$\omega_2 = 0.838/t_{\text{stud}} = 0.838/1.44\text{mm} = 0.583$$

$$\omega_3 = \sqrt{\left(\frac{h}{b}\right)/2} = \sqrt{\left(\frac{7010}{6096}\right)/2} = 0.758$$

$$\omega_4 = 1 \text{ (wood structural panels)}$$

$$\begin{aligned} \delta &= \frac{2vh^3}{E_s A_c b} + \frac{\omega_1 \omega_2 v h}{\rho G t_{\text{sheathing}}} + \omega_1^{\frac{5}{4}} \omega_2 \omega_3 \omega_4 \left(\frac{v}{\beta}\right)^2 + \frac{h}{b} \delta_v \\ &= \frac{2 \left(\frac{14.2\text{N}}{\text{mm}}\right) (3505\text{mm})^3}{203000\text{Mpa} (1230\text{mm}^2) (6096\text{mm})} + 1\text{mm} * 0.583\text{mm} \\ &\quad * \frac{\left(\frac{14.17\text{N}}{\text{mm}}\right) (3505\text{mm})}{1.05 \left(\frac{1317\text{N}}{\text{mm}^2}\right) (11.11\text{mm})} + 1.0^{\frac{5}{4}} * 0.583 * 0.758 * 1.0 \left(\frac{\frac{14.2\text{N}}{\text{mm}}}{\frac{1.91\text{N}}{\text{mm}^{1.5}}}\right)^2 \\ &\quad + \left(\frac{3505\text{mm}}{6096\text{mm}}\right) * 23.48\text{mm} = 32.9\text{mm} \end{aligned}$$

$$\% \text{ Error} = \frac{|\delta_{\text{observed}} - \delta_{\text{calculated}}|}{\delta_{\text{observed}}} * 100 = \frac{|52.4 - 32.9|}{52.4} * 100\% = 37.3\%$$

While a notable improvement across all configurations was observed when using the shear wall deflection equation (Eq. 3.2) versus the diaphragm deflection equation (Eq. 3.1), the percentage of error still remained quite large. A significant portion of the error was believed to have been caused by the diaphragm specimen's inelastic behaviour prior to reaching peak load.

Elastic Deflection ($\delta_{ELASTIC}$)

It was observed that across all specimens, the in-plane deflection was underestimated by Equation 3.2. Although Eq. 3.2 uses empirical factors to account for inelastic behaviour, these were believed to be inadequate for the test diaphragms based on the size and blocking conditions and were believed to be the primary cause of the underestimations. It was decided to calculate the equivalent elastic deflection for each specimen in order to compare the results with the deflections calculated using Eq. 3.2. If the calculated values from Eq. 3.2 overestimate the elastic deflection values, it would support the assertion that the empirical factors are inadequate to account for the inelastic behaviour of these larger specimens. The elastic deflection was calculated using the following steps:

1. The peak shear demand, (S_u) was obtained from the test data
2. The peak load per metre (v) was calculated by dividing S_u by the dimension of the diaphragm parallel to the force.
3. The peak load per metre v was multiplied by 0.4 to obtain 40% of the peak load per metre ($v_{0.4}$)
4. The in-plane lateral displacement of the wall corresponding to the load at $v_{0.4}$ was obtained from the test data ($\Delta_{0.4v}$)
5. The in-plane lateral elastic stiffness, K_e was calculated based on the formula:

$$K_e = \frac{v_{0.4}}{\Delta_{0.4v}}$$

$v_{0.4}$ = 40% of the peak shear demand per meter

$\Delta_{0.4v}$ = in-plane lateral displacement of the wall corresponding to $v_{0.4}$

6. The elastic deflection, $\delta_{ELASTIC}$ was calculated based on the formula

$$\delta_{Elastic} = \frac{v}{K_e}$$

v = peak shear demand per meter
 K_e = Elastic stiffness

Figure 3.39 shows the elastic deflection for the 12-RSTRAP-M specimen, while Table 3.9 displays the general properties for all specimens. A comparison of the elastic deflection to the deflection calculated by Eq. 3.2 is shown in Table 3.10.

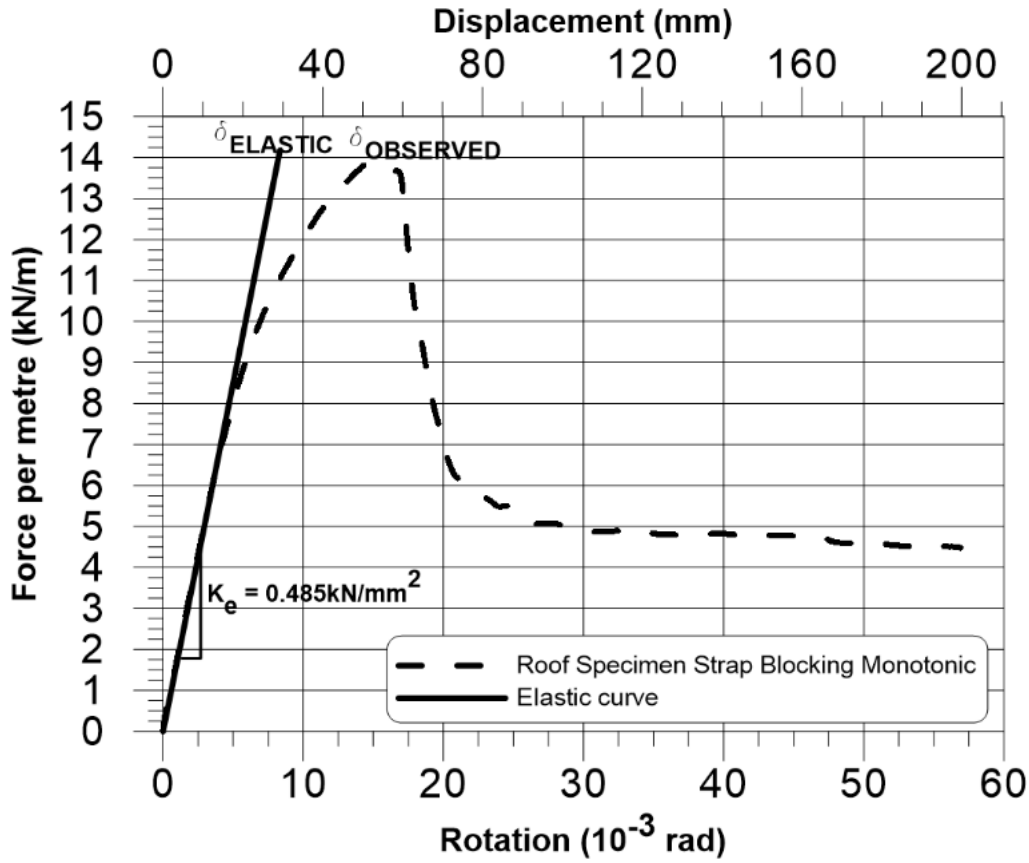


Figure 3.39: Elastic Deflection for Specimen 12-RSTRAP-M

Table 3.9: Summary of General Properties from Phase 2 Diaphragm Tests

Specimen	S_u (kN)	<i>v</i> (kN/m)	<i>v</i>_{0.4} (kN/m)	Δ_{0.4<i>v</i>} (mm)	K_e (kN/mm²)	Rigidity (kN/mm)	δ_{Elastic} (mm)
11-RALT-M	75.5	12.4	5.0	12.6	0.40	2.4	31.4
12-RSTRAP-M	86.4	14.2	5.7	11.7	0.49	3.0	29.2
13-FB4-M	235.9	38.7	15.5	22.8	0.68	4.1	56.9
14-RGY-P-M	54.8	9.0	3.6	7.0	0.51	3.1	17.6
15-RGY-P-C*	51.5	8.5	3.4	8.6	0.39	2.4	21.6
16-FCRETE-M	148.3	24.3	9.7	9.7	1.00	6.1	24.3

*Based on cycle where peak load was reached

Sample Calculation

Equivalent elastic deflection calculation for specimen 12-RSTRAP-M

$$v_{0.4} = 5.67 \text{ kN/mm}$$

$$\Delta_{0.4v} = 11.7 \text{ mm}$$

$$K_e = \frac{\frac{5.67 \text{ kN}}{\text{mm}}}{11.69 \text{ mm}} = \frac{0.485 \text{ kN}}{\text{mm}^2}$$

$$v = 14.2 \text{ kN/mm}$$

$$K_e = 2.96 \text{ kN/mm}^2$$

$$\delta_{\text{Elastic}} = \frac{\frac{14.17 \text{ kN}}{\text{mm}}}{\frac{0.485 \text{ kN}}{\text{mm}^2}} = 29.2 \text{ mm}$$

Table 3.10: Comparison of Calculated Deflections Using Eq. 3.2 vs. Elastic Deflection Values

Specimen	$\delta_{\text{Calculated}}$ (mm)	δ_{Elastic} (mm)	% Error
11-RALT-M	45.2	31.4	20.0
12-RSTRAP-M	32.1	29.2	6.9
13-FB4-M	62.6	56.9	5.2
14-RGYP-M	17.9	17.6	0.1
16-FCRETE-M	54.0	24.3	52.0

By comparing the design deflection values from the shear wall deflection equation with the elastic deflection for each specimen, a reasonably close approximation could be obtained for most specimens. The large percentage of error observed in specimen 16-FCRETE-M could be attributed to the increased stiffness provided by the gypcrete topping, which was not accounted for in the prediction. An identical frame tested during Phase 1 without the gypcrete topping had an elastic stiffness value, K_e of 0.504kN/mm² (Nikolaidou et al. 2015). If this stiffness value was used to calculate the elastic deflection, a result of 48.3mm would be found which would lead to an error of 11.9%. The error in 11-RALT-M could also be justified based on the high δ_v value used for the calculated deflection. Due to the failure at the north-east connection, the string potentiometers at the north end recorded the largest δ_v used across all specimens. If we take the δ_v value from the 13-FB4-M specimen where the north-east connection underwent large deformations but did not fail entirely, it would result in a calculated deflection of 33.1mm which would lower the calculated

error when compared to the elastic deflection to 2.5%. With these justifications it would appear that this method seems to be able to reasonably predict the in-plane deformation. However, it is important to note that for real world applications, values such as δ_v and K_e would not be readily available as engineers would typically not have access to full-scale test results. From the results shown in Table 3.10 it can be observed that the calculated deflection using Eq. 3.2 consistently overestimates the in-plane deflections compared to the elastic deflections. This is consistent with the conjecture of the inadequacy of the empirical factors used to account for inelastic behaviour for the larger diaphragm specimens.

3.3.2 Shear Strength

The design shear resistance was obtained from Table F2.4-1 (Figure 3.40) of the AISI S400 Standard (2015). The table provides design shear strength values for a limited number of diaphragm configurations with CFS framing and wood structural panel sheathing. A comparison is shown in Table 3.11 between the values obtained from Table F2.4-1 and the observed peak shear resistance values.

Table F2.4-1
Nominal Shear Strength (v_n) per Unit Length for Diaphragms Sheathed
With Wood Structural Panel Sheathing ^{1, 2}
U.S. and Mexico (lb/ft)

Sheathing	Thick- ness (in.)	Blocked				Unblocked	
		Screw spacing at diaphragm boundary edges and at all continuous panel edges (in.)				Screws spaced maximum of 6 in. on all supported edges	
		6	4	2.5	2	Load perpendicular to unblocked edges and continuous panel joints	All other configurations
		Screw spacing at all other panel edges (in.)					
		6	6	4	3		
Structural I	3/8	768	1022	1660	2045	685	510
	7/16	768	1127	1800	2255	755	565
	15/32	925	1232	1970	2465	825	615
C-D, C-C and other graded wood structural panels	3/8	690	920	1470	1840	615	460
	7/16	760	1015	1620	2030	680	505
	15/32	832	1110	1770	2215	740	555

1. For SI: 1" = 25.4 mm, 1 ft = 0.305 m, 1 lb = 4.45 N
2. For diaphragms sheathed with wood structural panels, tabulated R_n values are applicable for short-term load duration (seismic loads).

Figure 3.40: Table F2.4-1 in AISI S400 (2015)

Table 3.11: Comparison of Shear Strength Design Values vs. Measured Shear Strength Values

Specimen	V_{design} (kN/m)	V_{observed} (kN/m)	% Error
11-RALT-M	11.1	12.4	10.5
12-RSTRAP-M	11.1	14.2	21.8
13-FB4-M ⁽¹⁾⁽²⁾⁽³⁾	25.8	38.7	33.3
14-RGYP-M	7.4	9.0	17.8
15-RGYP-C	7.4	8.5	12.9
16-FCRETE-M ⁽¹⁾⁽²⁾	8.1	24.3	66.7

- (1) Due to lack of data, the design values taken correspond to an OSB thickness of 11.9mm when in reality 18.3mm was used.
- (2) Due to lack of data, the design values taken correspond to No. 10 fasteners being used when in reality No. 12 fasteners were used.
- (3) Due to lack of data, the design value taken corresponds to screw spacing around boundary edges of 63.5mm when in reality 101.6mm was used.

All OSB panels used in Phase 2 were classified as “rated sheathing” and were in conformance with DOC PS-2 which places them in the category of “other graded wood structural panels”. At present Table F2.4-1 limits the designer to No. 8 or No. 10 fasteners depending on the thickness of the CFS framing. No values are available for the larger No. 12 fasteners used in the floor configurations. Furthermore, no criteria exists for the incorporation of non-structural elements. Lastly, all design values in Table F2.4-1 (Figure 3.40) have been pre-adjusted by the short term duration factor ($k_d = 1.15$) as mentioned in note 2 below the table.

In all cases, it was found that the design values underestimate the observed shear strength of the diaphragms. The large percentage of error found in specimen 16-FCRETE-M can be attributed to the additional strength provided by the gypcrete topping. An identical diaphragm tested in Phase 1 without the gypcrete topping recorded a peak shear strength of 11.8kN/m which would correspond to an error of 21.2% (Nikolaidou et al. 2015). In tests 14-RGYP-M and 15-RGYP-C the gypsum panels were shown to increase the shear strength of both specimens by over 60%. It should be noted that because the table does not account for the addition of non-structural elements, had the gypsum panels not been installed there would have been no change to the design shear strength value. If a comparison is made to an identical diaphragm specimen without the gypsum panels tested in Phase 1, the observed shear strength for this configuration would be approximately 5.6kN/m (Nikolaidou et al. 2015). In this case the design values would over-estimate the shear strength by 51.8%. Based on the results obtained, no meaningful comparisons could be obtained with this table.

3.4 Comparison of Test Results Between Phase 1 and Phase 2

The majority of the configurations tested in Phase 2 of the diaphragm research program were designed with a single change, either structural or non-structural, so that they could be compared

with the tests performed in Phase 1 (Nikolaidou et al. 2015). In this section, comparisons between the Phase 1 and 2 tests will be made to highlight how the alteration affected the shear strength, rigidity and overall response to in-plane loading.

3.4.1 11-RALT-M vs. 7-RB-M ; Direction of Joists

Phase 2 specimen 11-RALT-M is compared with Phase 1 specimen 7-RB-M in order to determine the influence of the direction of joists with respect to the direction of loading. Figure 3.41 shows the impact of this change on the overall performance of the diaphragm. While the rigidity and peak load of specimen 11-RALT-M were reduced in comparison to the 7-RB-M test by 20% and 5%, respectively, the major difference between the two specimens was how the rim joist – joist connection at the north-east corner failed in specimen 11-RALT-M. The cause of this failure was due to how the axial forces were distributed within the CFS frame. In the 11-RALT-M test, the only members which spanned the east-west direction were the blocking members and the two rim joists. Due to the blocking members and their connections being significantly less stiff than the exterior rim joists, the majority of the east-west axial load was directed into the rim joists which in turn caused a higher load demand on the exterior chord-joist member connecting to the fixed end. This increased load is believed to have caused the failure in the north-east chord-to-rim joist connection, which resulted in the sudden drops in force prior to peak load shown in Figure 3.41. In the 7-RB-M specimen, the axial forces generated in the east-west direction were dispersed across the joist members which ran along this direction. Because all of the joist members shared a similar axial stiffness, the force was able to be distributed more evenly across the members; as such, the connection failure observed in the 11-RALT-M test did not occur. Figure 3.42 illustrates the difference in east-west axial forces experienced within the CFS frame for both specimens. It is hypothesized that if this chord to rim joist connection had been designed to carry the full in-plane

axial force, without the aid of the interior blocking lines, the shear vs. deformation response would have been similar for these two diaphragm specimens. The failed connection issue in the 11-RALT-M test shows the importance of anticipating the distribution of the in-plane axial forces and detailing the framing connections for the forces arriving from different loading directions on a building's diaphragm structures accordingly. Despite the connection failure that occurred prior to peak load in specimen 11-RALT-M, the failure mechanisms were similar in both specimens. Ultimately for both configurations, the failure was governed by the sheathing fasteners which failed mostly by means of shear, tear out and pull through failures. Once an entire row of sheathing had failed, a hinge was created in the CFS framing at the fixed end for both specimens. In the 11-RALT-M specimen the hinge was located in the blocking member connections, while in the 7-RB-M specimen the hinge was located in the joist members at the intersection of the sheathing panels.

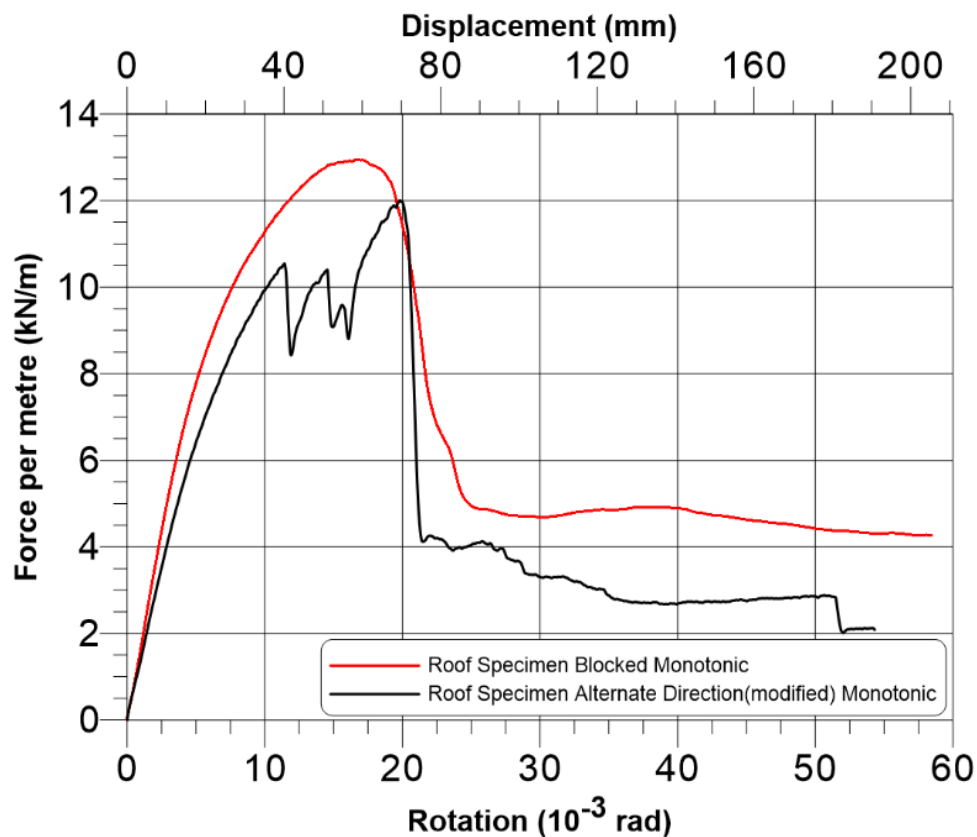
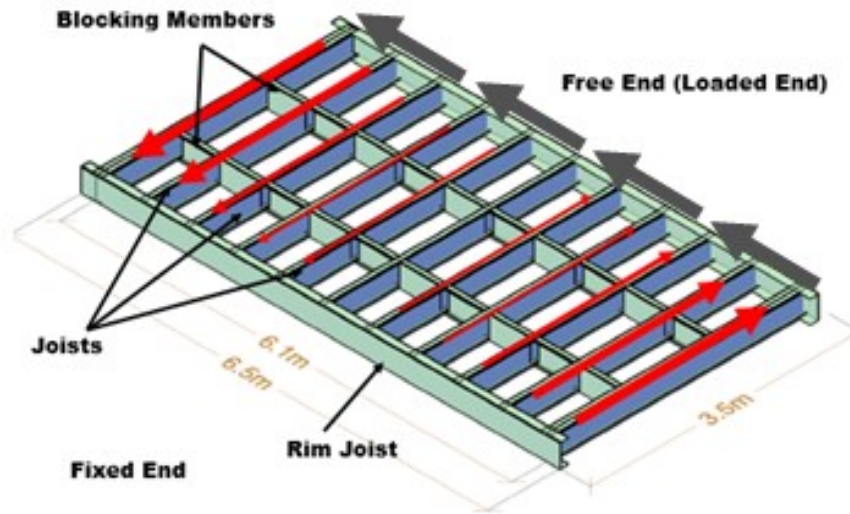
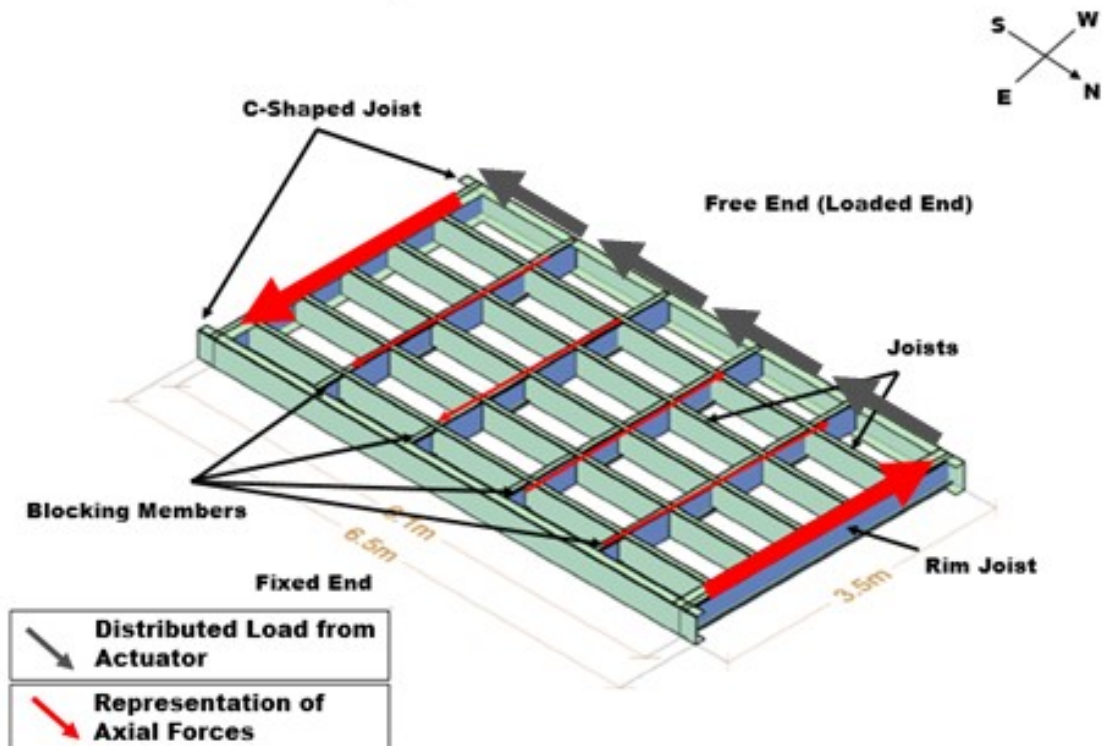


Figure 3.41: Comparison of 11-RALT-M with 7-RB-M ; Direction of Joists



Specimen 7-RB-M



Specimen 11-RALT-M

Figure 3.42: Comparison of Axial Forces in Framing Members between Specimens 7-RB-M and 11-RALT-M

3.4.2 12-RSTRAP-M vs. 7-RB-M ; Type of Panel Edge Blocking

Phase 2 specimen 12-RSTRAP-M is compared with Phase 1 specimen 7-RB-M in order to determine the effectiveness of strap blocking. It is demonstrated in Figure 3.43 how comparable strap blocking (Phase 2 12-RSTRAP-M) is to full-height blocking (Phase 1 7-RB-M) in terms of supporting the edges of the OSB panels and providing diaphragm shear resistance. The rigidity of both specimens were nearly identical, while their peak loads were within 10% of one another. It was initially assumed that the full blocking found in specimen 7-RB-M would be stiffer, and hence provide for slightly higher diaphragm shear resistance. After testing however, it was found that the shear resistance of the strap braced specimen was actually 8.9% higher than that measured for the full blocked diaphragm. The slightly increased peak load in the 12-RSTRAP-M case was most likely the result of minor changes in material properties of the OSB and CFS frame, which were sourced at different times. Given the observations and measurements of these two tests it can be concluded that the strap blocking (anchored to full-height blocking) provides equivalent support to the sheathing panel edges compared with the full-height blocking throughout the diaphragm. Both specimens showed similar behaviour while subjected to in-plane loading. The failure of both specimens was governed by the sheathing fasteners which failed mostly by shear, pull through and tear out failures (Figure 3.44). Once an entire row of fasteners had failed across the diaphragm, a hinge was created across the plane of failure within the CFS framing (Figure 3.45).

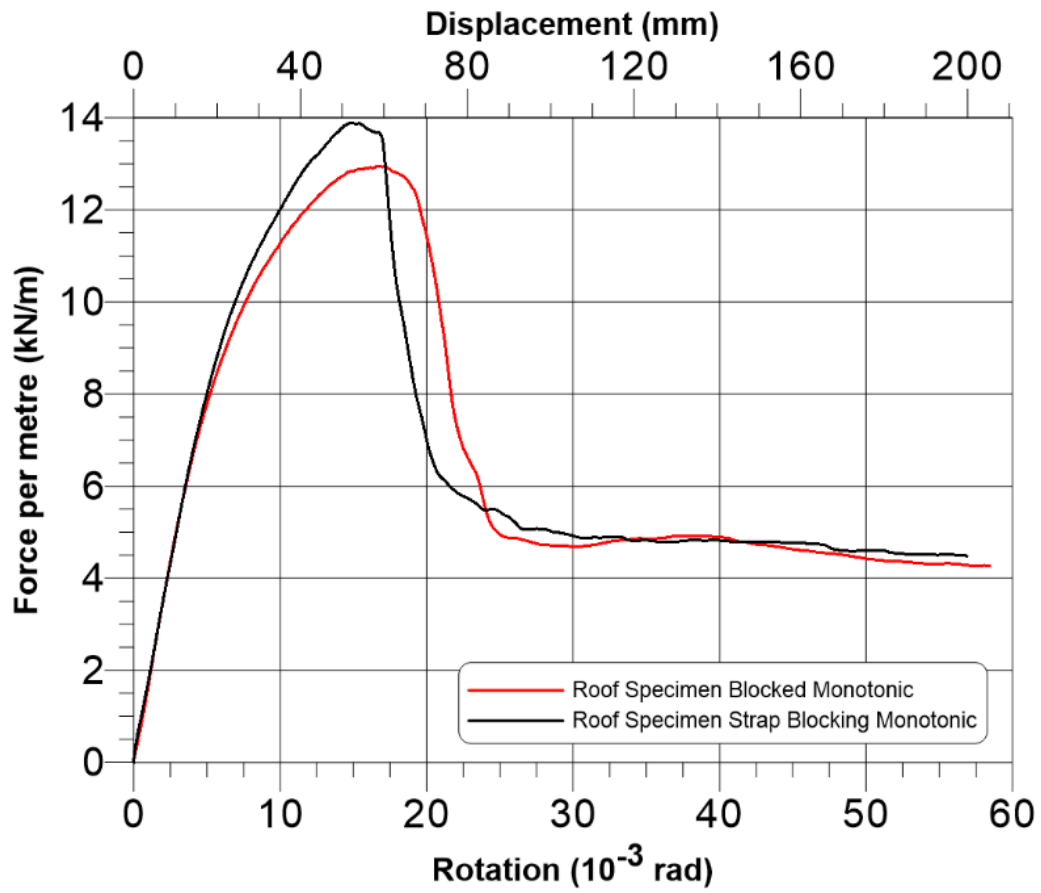


Figure 3.43: Comparison of 12-RSTRAP-M with 7-RB-M ; Type of Panel Edge Blocking

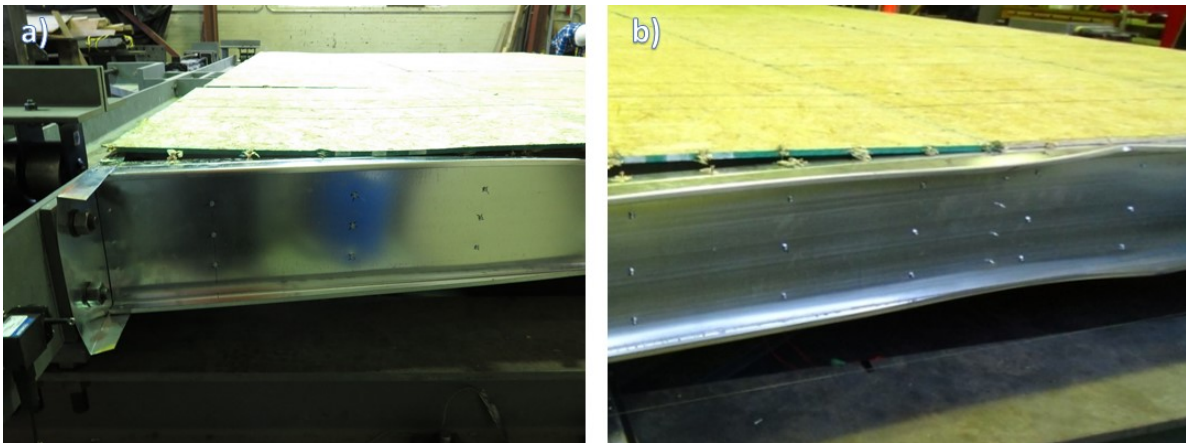


Figure 3.44: Comparison of Sheathing Failures ; a) 12-RSTRAP-M and b) 7-RB-M

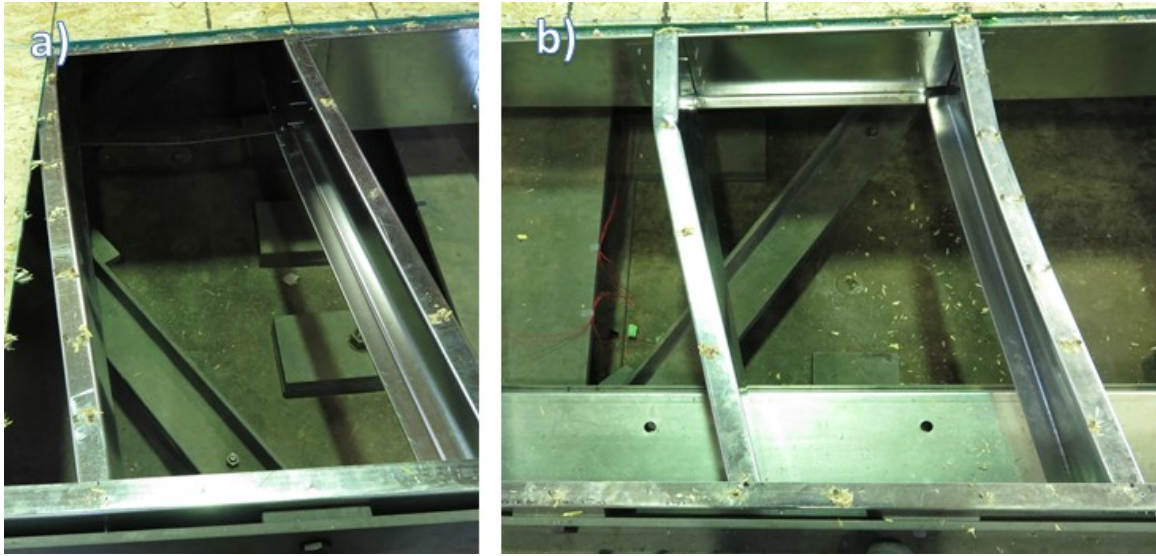


Figure 3.45: Comparison of Hinges Developed in CFS ; a) 12-RSTRAP-M and b) 7-RB-M

3.4.3 13-FB4-M vs. 9-F#12-M ; Maximized Shear Resistance

Phase 2 specimen 13-FB4-M is compared with Phase 1 specimen 9-F#12-M in order to demonstrate the difference in maximum shear resistance which can be obtained within a given configuration. The only differences between the two specimens is the blocking conditions and fastener spacing. 13-FB4-M is a fully blocked floor diaphragm with 100/300mm fastener spacing while 9-F#12-M is a partially blocked floor diaphragm with 150/300mm fastener spacing. By fastening the edges of all OSB panels to frame blocking and by reducing the spacing of the sheathing screw edge fasteners to 100mm, the maximum shear resistance was increased by over three times compared with the standard floor configuration from Phase 1 (9-F#12-M) (Figure 3.46). The reduced spacing of the sheathing fasteners increased the diaphragm shear rotation needed to cause failure by nearly double, while the rigidity was increased by just over 25% (Figure 3.46). Specimen 13-FB4-M also had a more preferable mode of failure , where the steel frame and sheathing failed together, rather than the sheathing connections failing first followed by the hinge action of the frame which was observed in 9-F#12-M. In 13-FB4-M there was no notable hinge

that developed in the CFS framing but instead the increased load caused localised buckling due to compression in the underlying joists. The blocking member connections were also damaged and two failed completely due to the compression fields which developed in the 13-FB4-M specimen.

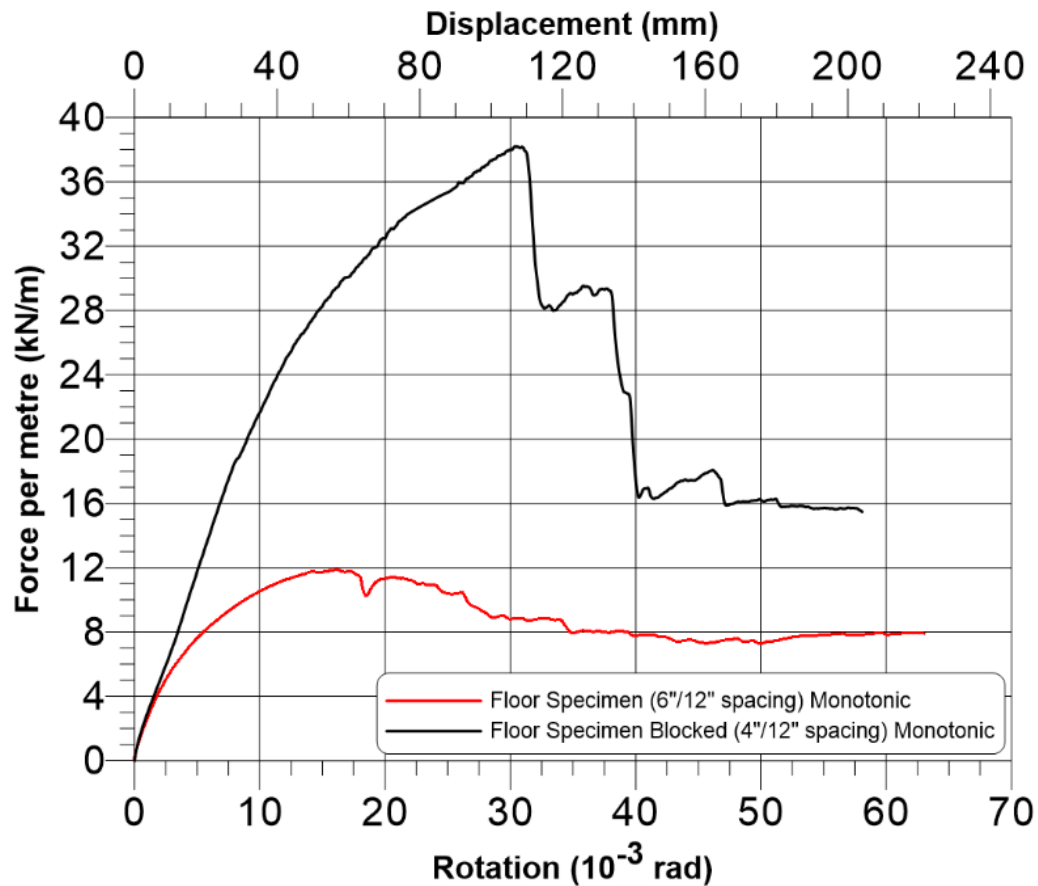


Figure 3.46: Comparison of 13-FB4-M with 9-F#12-M ; Maximized Shear Resistance

3.4.4 14-RGYP-M & 15-RGYP-C vs. 3-RU-M & 4-RU-C ; Installation of Gypsum Ceiling

Phase 2 specimens 14-RGYP-M and 15-RGYP-C are compared with Phase 1 specimens 3-RU-M and 4-RU-C to determine the effect of installing one layer of non-structural, 19mm thick gypsum panels to the underside of the diaphragm configuration. A 60% increase in shear strength and an approximate 105% increase in diaphragm rigidity were observed in tests 14-RGYP-M and 15-RGYP-C when compared against the standard roof configuration specimens tested in Phase 1 (3-RU-M and 4-RU-C) due to the addition of the gypsum panels (Figures 4.47 & 4.49). Overall, the

addition of the gypsum panels did not seem to have a large effect on the diaphragm's behaviour as all of the specimens failed in a similar fashion (Figure 4.48). In all cases, failure of the diaphragm was governed by the wood sheathing connections failing causing lift-off of the OSB panels, followed by hinge action of the CFS frame once a line of sheathing panels had disconnected. The failure for all specimens occurred at the interface between sheathing panels where there were less sheathing fasteners due to the unblocked configuration.

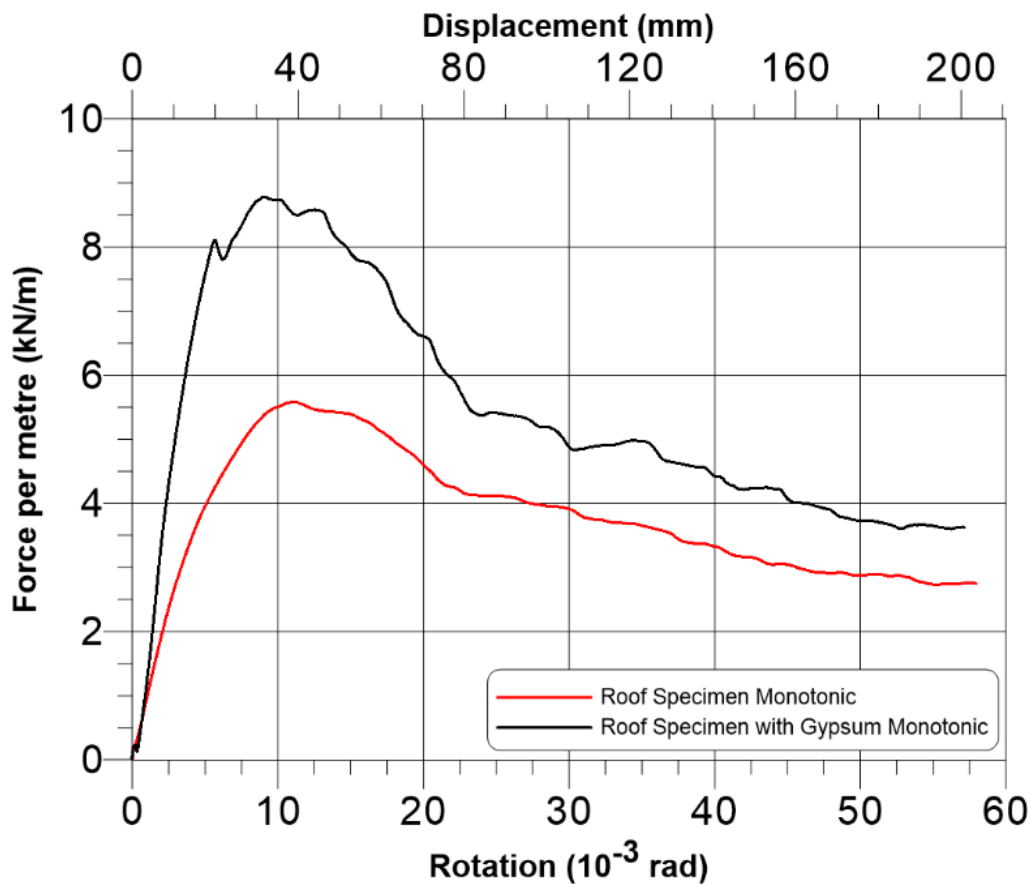


Figure 3.47: Comparison of 14-RGY-P-M with 3-RU-M ; Installation of Gypsum Ceiling

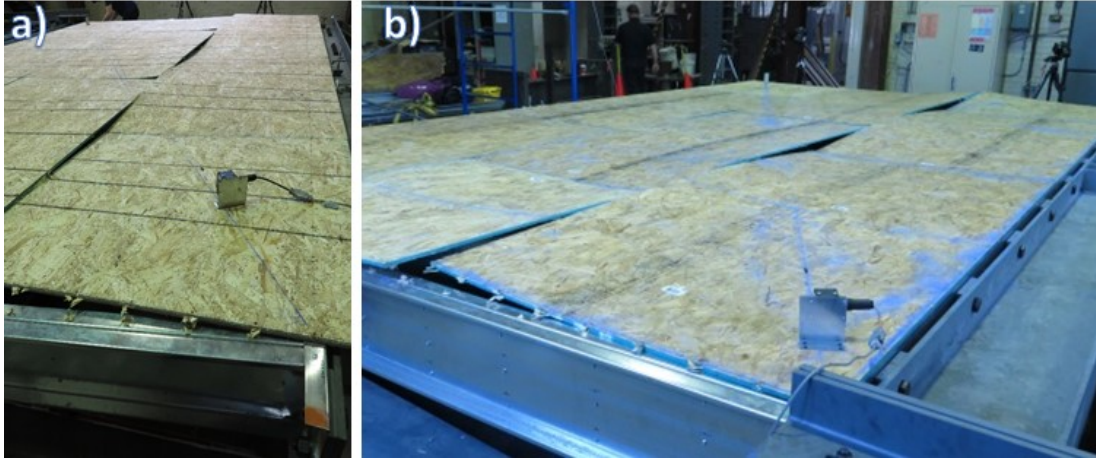


Figure 3.48: Comparison of Sheathing Failures ; a) 14-RGYP-M and b) 3-RU-M

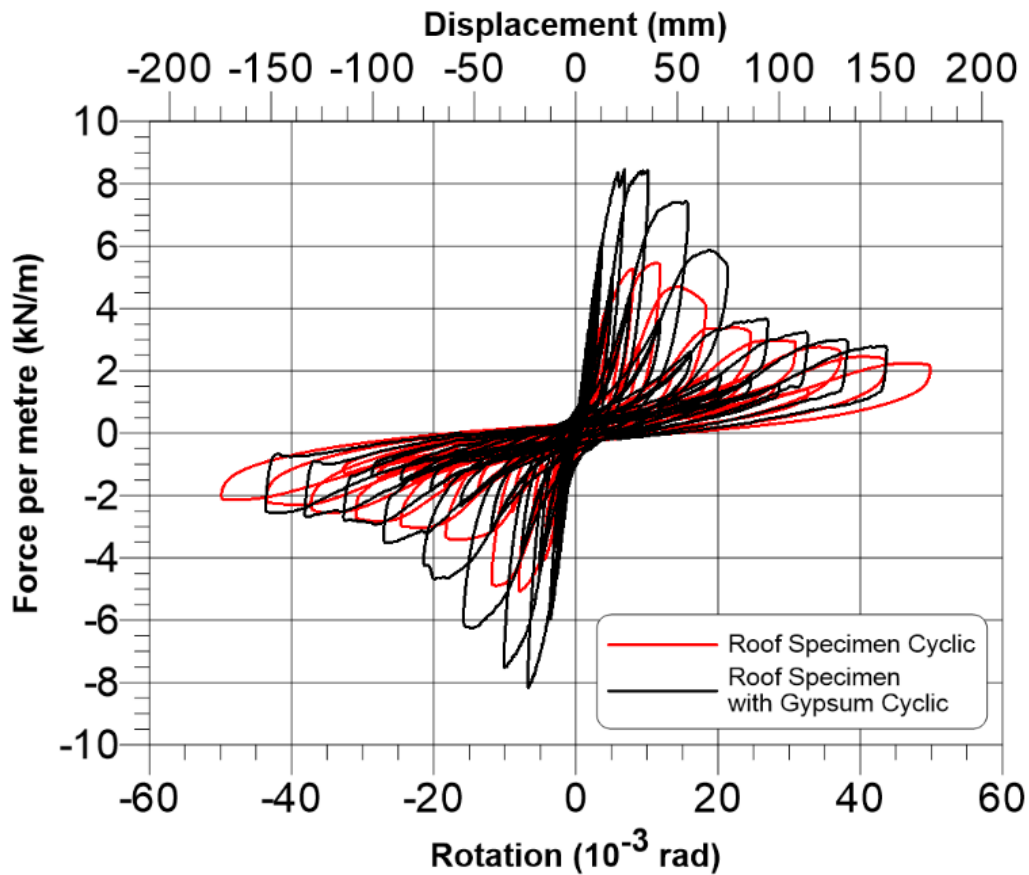


Figure 3.49: Comparison of 15-RGYP-C with 4-RU-C ; Installation of Gypsum Ceiling

3.4.5 16-FCRETE-M vs. 9-F#12-M ; Installation of Gypcrete Topping

Phase 2 specimen 16-FCRETE-M is compared with Phase 1 specimen 9-F#12-M to determine the effect of installing a 19mm thick gypcrete topping to the surface of the sheathing panels. The

addition of the gypcrete topping to specimen 16-FCRETE-M resulted in a doubling of both its maximum shear resistance and rigidity when compared to a nominally identical specimen without gypcrete (Figure 3.50). In both tests, following peak load, separation of the OSB panels was observed. In the specimen without gypcrete (9-F#12-M) these separations occurred at individual panel interfaces perpendicular to the load. In the 16-FCRETE-M test, the gypcrete and OSB developed a strong bond and behaved as a composite material. The gypcrete grouped several panels together which forced the panel separations to occur both parallel and perpendicular to the direction of loading (Figure 3.51). In both specimens the majority of the sheathing fasteners failed by shear failure and tear out, however the gypcrete topping seemed to prevent pull through failures of the fasteners which were observed in the 9-F#12-M specimen.

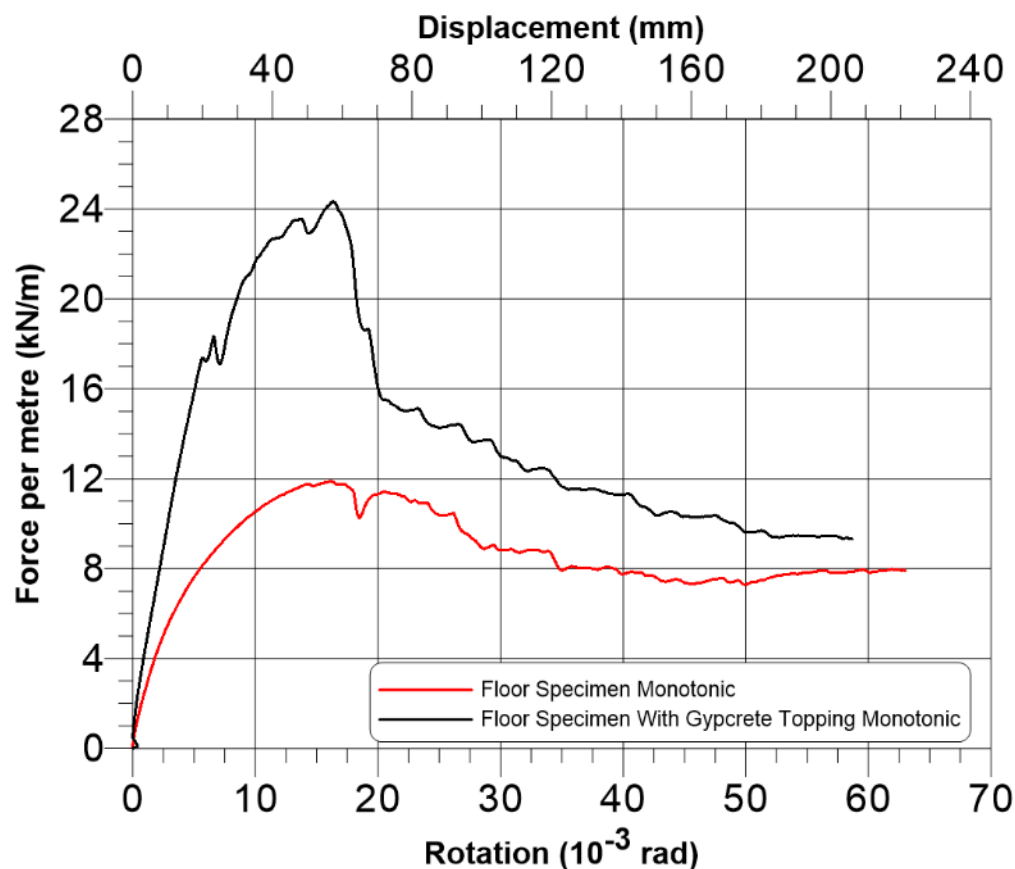


Figure 3.50: Comparison of 16-FCRETE-M with 9-F#12-M ; Installation of Gypcrete Topping

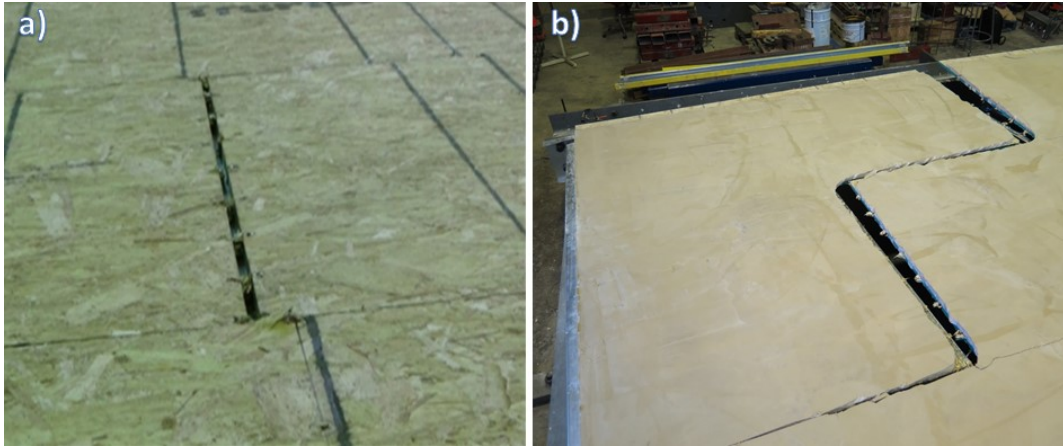


Figure 3.51: Sheathing Separation Comparison : a) 9-F#12-M b) 16-FCRETE-M

Chapter 4 Conclusions and Recommendations

4.1 Conclusion

The focus of this thesis was to characterize the in-plane behaviour of CFS framed/OSB sheathed diaphragms under monotonic and reversed cyclic loading. To do so, Phase 2 of the diaphragm research project was conducted in the winter of 2016 at McGill University in order to build upon what was accomplished in 2015 during Phase 1. A total of six diaphragm specimens with five different configurations were designed, constructed and tested. An examination of the following parameters was made possible by the completion of this laboratory test program:

- The effect of the joist orientation on the overall diaphragm response.
- The overall effectiveness of utilizing the strap method as blocking to support the edges of the OSB panels.
- An upper threshold for shear strength and stiffness in CFS/wood-sheathed diaphragms
- The effect on the overall diaphragm response of gypsum as a non-structural component when attached directly to the frame.
- The effect on the overall diaphragm response of gypcrete as a non-structural component when poured directly on top of the wood sheathing.

A complete summary of the tests performed during Phase 1 and a detailed account of the entirety of Phase 2 including the ancillary material tests were presented herein. Furthermore, design predictions were carried out in accordance to the methods available in the AISI S400 Standard (2015) for both the design deflection as well as the design shear strength for each specimen.

Upon completion of the Phase 2 tests, the results were analyzed and compared with those of the base configurations tested in Phase 1. The main findings of this analysis and comparison are summarized:

- ❖ The direction of loading was shown to have little effect on the shear strength and stiffness of the diaphragm, assuming that the increased in-plane axial forces are properly accounted for in the design of the CFS framing and connections. It was shown that in a typical roof configuration, the blocking members do not have adequate stiffness in order to distribute the in-plane axial forces across multiple joist members. Because of this, the engineer must design the external joist members and their connections to accommodate for these loads.
- ❖ Strap blocking of the OSB panel perimeters was shown to be just as effective as full blocking in terms of supporting the edges of the OSB panels and providing diaphragm shear resistance.
- ❖ In diaphragms where the sheathing fastener spacing is small and the shear demands are high, compression field action was shown to cause significant damage to the underlying CFS frame. This behaviour is not taken into account in any design documents that are currently available.
- ❖ Gypsum was shown to increase the shear strength and rigidity of an unblocked roof diaphragm by 60% and 105% respectively, but did not affect the overall failure mechanisms of the diaphragm test specimens.
- ❖ Gypcrete was shown to have a significant impact on shear strength and stiffness, increasing both by over 100% when compared to an identical unblocked floor specimen without the additional gypcrete topping. The addition of the gypcrete topping caused the sheathing to behave as a composite material.

In addition, using the shear wall deflection equation (E1.4.1.4-1) of the AISI S400 Standard led to a meaningful comparison between the calculated and observed data only by assuming elastic response of the diaphragm. The results from both Phase 1 and Phase 2 give support to the assertion that the empirical modification factors used to account for inelastic behaviour within Eq. E1.4.1.4-1 are inadequate when used for a larger shear wall (diaphragm). Lastly, the limited information available in the AISI S400 Standard did not allow for comparable design shear strength values to be obtained.

4.2 Recommendations for Future Research

Cold-formed steel is relatively new in terms of its use as a structural material. The first CFS design standard for North America to include design shear strengths as well as deflection equations for wood sheathed diaphragms was only published in 2004 in the AISI CFS lateral design standard (2004). Since then this Standard has been updated and expanded upon twice, first to the AISI S213 (2007) and then to the current version, the AISI S400 Standard (2015). With each version of the CFS lateral design standard, large strides to build and improve upon the previous are realised. However, in order to bring the CFS Standard up to the same level as what is offered for more established structural materials such as hot-rolled steel, concrete and wood, more research is required. While the recommendations that are given herein focus on the research surrounding the complicated nature of CFS diaphragm subsystems and how they interact with the global structure, it is important to note that there exists many areas within CFS design that also require research. Ultimately the goal would be to develop a comprehensive CFS design manual based off of these Standards that would allow for engineers to design economical and safe structures using this versatile structural material.

In this research it was shown how limited the resources are in the AISI S400 Standard in terms of calculating diaphragm shear resistance and in-plane displacement. Further research is required in order to expand the design shear resistance table to include factors that account for variables such as the size of fastener, as well as to include more options for sheathing thickness' and different fastener configurations. Furthermore, for calculating design deflection, the research presented in this thesis was unable to obtain comparable values by using the design deflection equation for diaphragms. It was believed that due to the loading configuration used, the diaphragm deflection equation was inappropriate for a cantilever loading configuration. Further research on CFS diaphragms should be conducted using a simple support configuration such that the accuracy of the diaphragm deflection equation could be verified.

Prior to this research, there was no information that existed in North America about the effects of non-structural elements on CFS-diaphragm systems. Currently, non-structural elements such as the gypsum panels and gypcrete topping used in this research are assumed to have no effect on the overall structure. This was shown to be incorrect; the addition of these non-structural components in both cases raised the stiffness and shear strength of the diaphragms significantly. More research into non-structural elements and their effects on the diaphragm structure needs to be conducted so that these types of systems can be better understood.

Further research can be conducted to expand on Phase 1 and 2 of the CFS diaphragm research program presented in this thesis. Aside from the addition of non-structural components, the effect that many different structural changes have on the overall diaphragm have yet to be observed. Structural changes such as the spacing of the joists, the orientation of wood sheathing on a blocked diaphragm and further exploration into the effect of fastener spacing are just a few examples of possibilities. It may be possible to create high fidelity finite element models of these diaphragms

which could be calibrated based on the data provided in Phase 1 and 2. These models could extrapolate based on the existing data to expand the database of these types of diaphragms. This would greatly reduce the time and cost required for this type of research.

References

- American Iron and Steel Institute (AISI). (2015). AISI S400-15. *North American Standard for Seismic Design of Cold-Formed Steel Structural Systems*. Washington, DC, USA.
- American Iron and Steel Institute (AISI). (2015). AISI S240-15. *North American Standard for Cold-Formed Steel Structural Framing*. Washington, DC, USA
- American Iron and Steel Institute (AISI). (2012). AISI S213-07/S1-09. *North American Standard for Cold-Formed Steel Structural Framing – Lateral Design 2007 Edition with Supplement No. 1*. Washington, DC, USA.
- American Iron and Steel Institute (AISI). (1998). AISI RG-9804. *Shear Wall Design Guide*. Washington, DC, USA.
- American Iron and Steel Institute (AISI). (2012). AISI S213-07/S1-09. *North American Standard for Cold-Formed Steel Structural Framing – Lateral Design 2007 Edition with Supplement No. 1*. Washington, DC, USA.
- American Iron and Steel Institute (AISI). (2004). AISI LATERAL-2004. *Standard for Cold-Formed Steel Framing – Lateral Design, 2004 Edition*. Washington, DC, USA.
- American Society for Testing and Materials (ASTM). (2013). ASTM D5764-97a. *Standard Test Method for Evaluating Dowel-Bearing Strength of Wood and Wood-Based Products*. West Conshohocken, PA, USA, ASTM International.
- American Society for Testing and Materials (ASTM). (2015). ASTM D4442–15. *Standard Test Methods for Direct Moisture Content Measurement of Wood and Wood Base Materials*. West Conshohocken, PA, USA, ASTM International.
- American Society for Testing and Materials (ASTM). (2014). ASTM C-472-99. *Standard Test Methods for Physical Testing of Gypsum, Gypsum Plasters and Gypsum Concrete*. West Conshohocken, PA, USA, ASTM International.
- American Society for Testing and Materials (ASTM). (2011). ASTM C496-11. *Standard Test Method for Splitting Tensile Strength of Cylindrical Concrete Specimens*. West Conshohocken, PA, USA, ASTM International.
- American Society for Testing and Materials (ASTM). (2016). A370-2016. *Standard Test Methods and Definitions for Mechanical Testing of Steel Products*. West Conshohocken, PA, USA, ASTM International.
- APA – The Engineering Wood Association. (2005). *Plywood Design Specification – Design and Fabrication of All-Plywood Beams*. Tacoma, Washington, USA.
- Blais, C. (2006). *Testing and Analysis of Light Gauge Steel Frame / 9mm OSB Wood Panel Shear Walls* (M.Eng. Thesis). Department of Civil Engineering & Applied Mechanics, McGill University, Montreal, QC, Canada.

- Boudreault, F.A. (2005). *Seismic Analysis of Steel Frame / Wood Panel Shear Walls* (M.Eng. Thesis) Department of Civil Engineering and Applied Mechanics, McGill University, Montreal, Qc, Canada.
- Branston, A.E. (2004). *Development of a Design Methodology for Steel Frame / Wood Panel Shear Walls* (M.Eng. Thesis). Department of Civil Engineering and Applied Mechanics, McGill University, Montreal, Qc, Canada.
- Canadian Standards Association (CSA). (2007). CSA S136-07. *North American Specification for the Design of Cold-Formed Steel Structural Members*. Mississauga, ON, Canada.
- Canadian Standards Association (CSA). (2014). CSA S16-14. *Design of steel structures*. Mississauga, ON, Canada.
- Canadian Standards Association (CSA). (2014). CSA A23.3-14. *Design of concrete structures*. Mississauga, ON, Canada.
- Canadian Standards Association (CSA). (2014). CSA O86-14. *Engineering design in wood*. Mississauga, ON, Canada.
- Chen, C.Y. (2004). *Testing and Performance of Steel Frame / Wood Panel Shear Walls* (M.Eng. Thesis). Department of Civil Engineering and Applied Mechanics, McGill University, Montreal, Qc, Canada.
- Computers and Structures, Inc. (CSI), SAP2000 V.14 (2009). *Linear and Non-linear Static and Dynamic Analysis and Design of Three-Dimensional Structures Basic Analysis Reference Manual*. Berkeley, California, USA.
- Davis, J. R. (2004). *Tensile testing Second Edition*. Materials Park, OH, USA. ASM International.
- Encyclopedia Britannica (2011). *Gypsum*. Retrieved October 12th, 2016 from <http://www.theodora.com/encyclopedia/g2/gypsum.html>.
- International Code Council (ICC). (2003). IBC-03. *International Building Code*. Falls Church, VA, USA.
- Krawinkler, H., Parisi, F., Ibarra, L., Ayoub, A. and Medina, R. (2000). *Development of a testing protocol for wood frame structures. Report W-02 covering Task 1.3.2*. CUREE/Caltech Woodframe Project. Consortium of Universities for Research in Earthquake Engineering (CUREE). Richmond, CA, USA.
- Light Gauge Steel Engineers Association (LGSEA). (1998). Tech Note 558b-1. *Lateral load resisting elements: Diaphragm design values*. Washington, DC, USA.
- Lu, S. (2015). *The Influence of gypsum sheathing on the lateral resistance of cold-formed steel shear walls* (M.Eng. Thesis). Department of Civil Engineering and Applied Mechanics, McGill University, Montreal, Qc, Canada.
- Madsen, R.L., Nakata, N., Schafer, B.W. (2011). CFS-NEESRR01c. *CFS-NEES Building Structural Design Narrative*. Corvallis, OR, USA.

- MAXXON (2016). *Gyp-Crete Fire Ratings/Detail Drawings*. Retrieved May 24th, 2016 from <http://www.maxxon.com/gyp-crete/drawings>.
- MAXXON (2016). *Commercial Topping Data Sheet*. Retrieved July 28th, 2016 from http://www.maxxon.ca/commercial_topping/data.
- National Association of Home Builders (NAHB). (1999). *Innovative residential floor construction: Horizontal diaphragm values for cold-formed steel framing*. Department of Housing and Urban Development, MD, USA.
- National Research Council of Canada (NRCC). (2010). *National Building Code of Canada 2010, 13th Edition*. Ottawa, ON, Canada.
- Nikolaidou, V., Latreille, P., Rogers, C. and Lignos, D (2015). *Characterization of CFS framed diaphragm behavior Report CM – 432*. American Iron and Steel Institute, Washington, USA.
- Peterman, K.D. (2014). *Behavior of full-scale cold-formed steel buildings under seismic excitations* (PhD Thesis). Johns Hopkins University, Baltimore, Maryland, USA.
- Rokas, D. (2005). *Testing of Steel Frame / 9.5 mm CSP Wood Panel Shear Walls* (Project Report). Department of Civil Engineering and Applied Mechanics, McGill University, Montreal, Qc, Canada.
- Serrette, R.L., and Chau, K. (2003). *Estimating the response of cold-formed steel-frame shear walls*. Santa Clara University. Santa Clara. CA
- Shamim, I., Rogers, C.A., (2013). *Steel sheathed / CFS framed shear walls under dynamic loading: numerical modelling and calibration*. Thin-Walled Structures 71: 57-71.
- Shamim, I., Rogers, C.A. (2015). *Numerical evaluation : AISI S400 steel-sheathed CFS framed shear wall seismic design method*. Thin-Walled Structures 95: 48-59.
- Steel Framing Alliance (SFA). (2013). *A guide to fire and acoustic data for cold-formed steel floor, wall & roof assemblies*. Washington, DC, USA.
- Structural Engineers Association of California (SEAOC). (1999). *The Blue Book. Recommended Lateral Force Requirements and Commentary*. Sacramento, CA, USA.
- Tao, F., Chatterjee, A. and Moen, C.D. (2016). *Monotonic and cyclic backbone response of single shear cold-formed steel-to-steel and sheathing-to-steel connections*. Blacksburg, Virginia, USA.
- TECO (2008). *TECHTIP. Design Capacities for Oriented Strand Board*. Retrieved October 30th, 2015, from http://www.tecotested.com/techtips/pdf/tt_osbdesigncapacities.
- Tissell, J. R. and Elliot, J. R. (2004). *APA – The Engineering Wood Association Research Report 138 “Plywood Diaphragms”*. Tacoma, Washington, USA.

APPENDIX A:

Failure Modes of Sheathing Fasteners

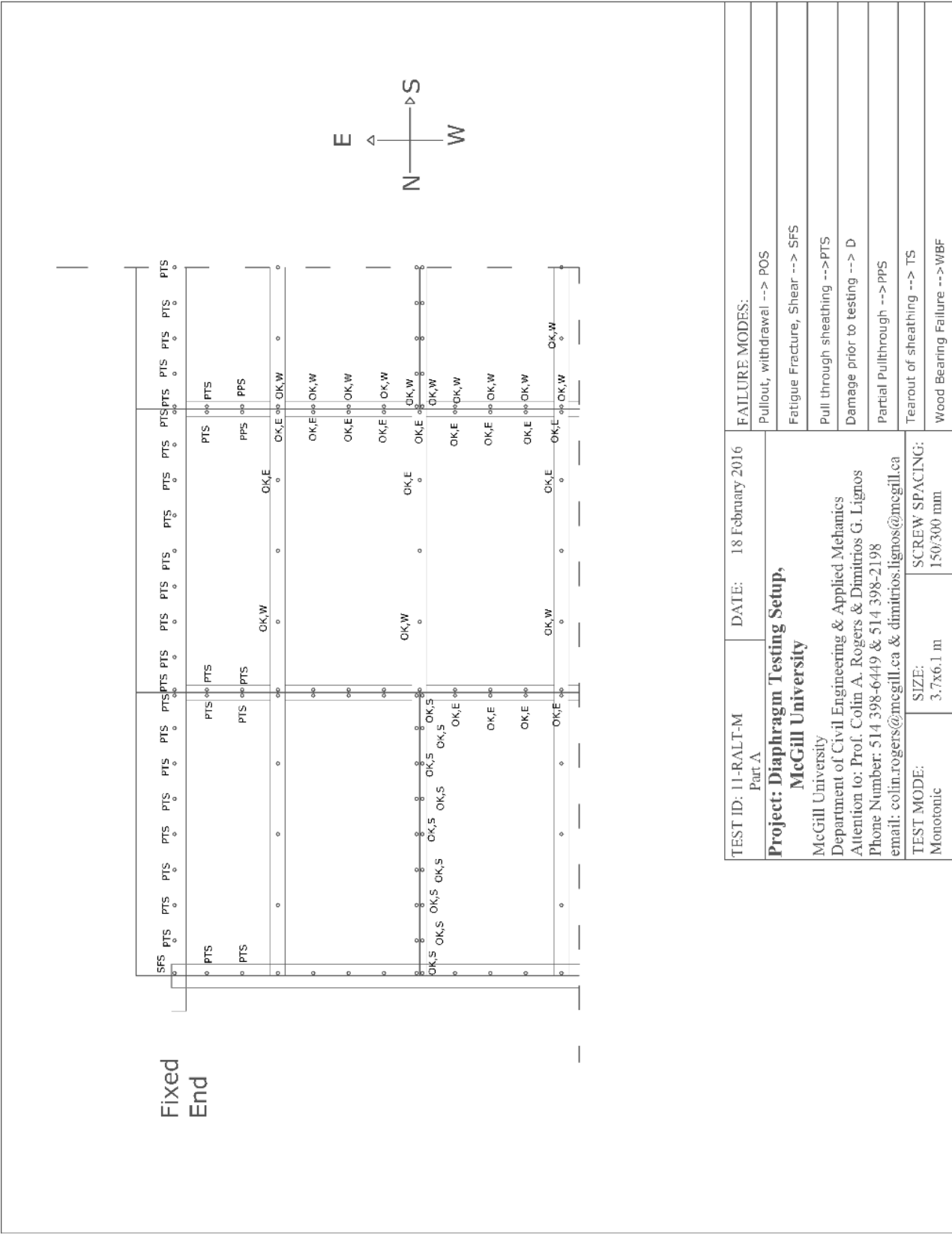
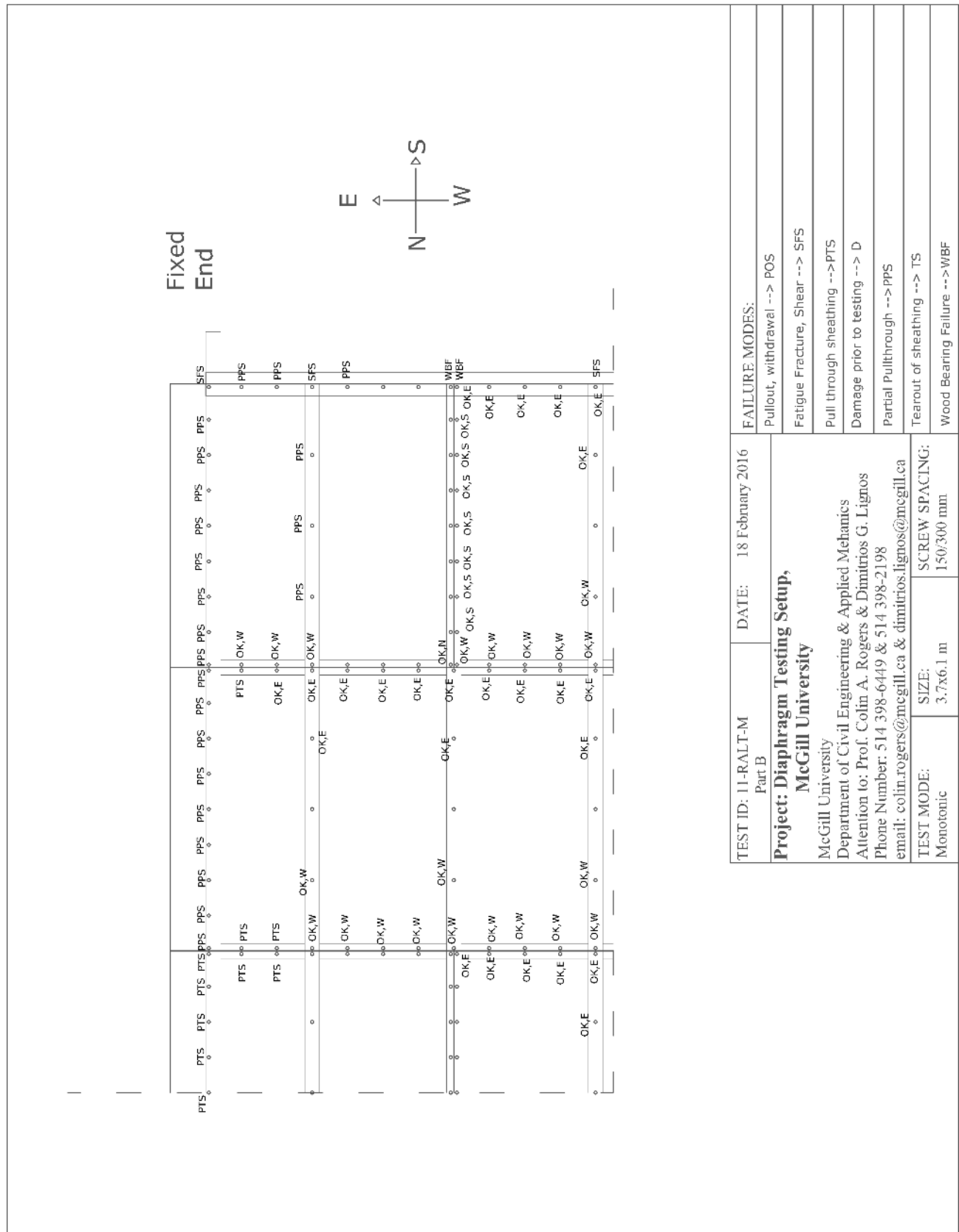


Figure A.2: Sheathing Fastener Failure Modes Part A Specimen 11-RALT-M



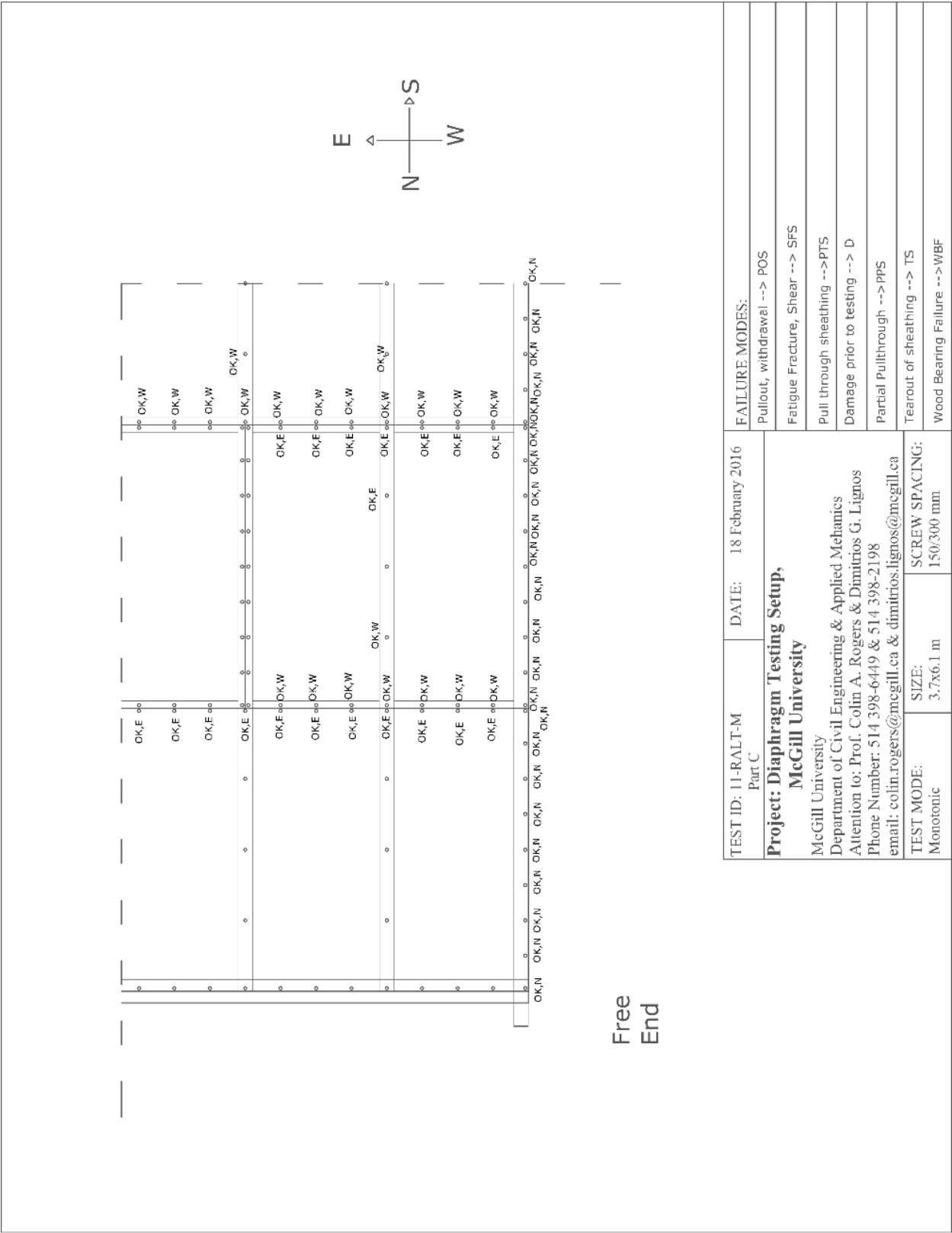


Figure A.4: Sheathing Fastener Failure Modes Part C Specimen 11-RALT-M

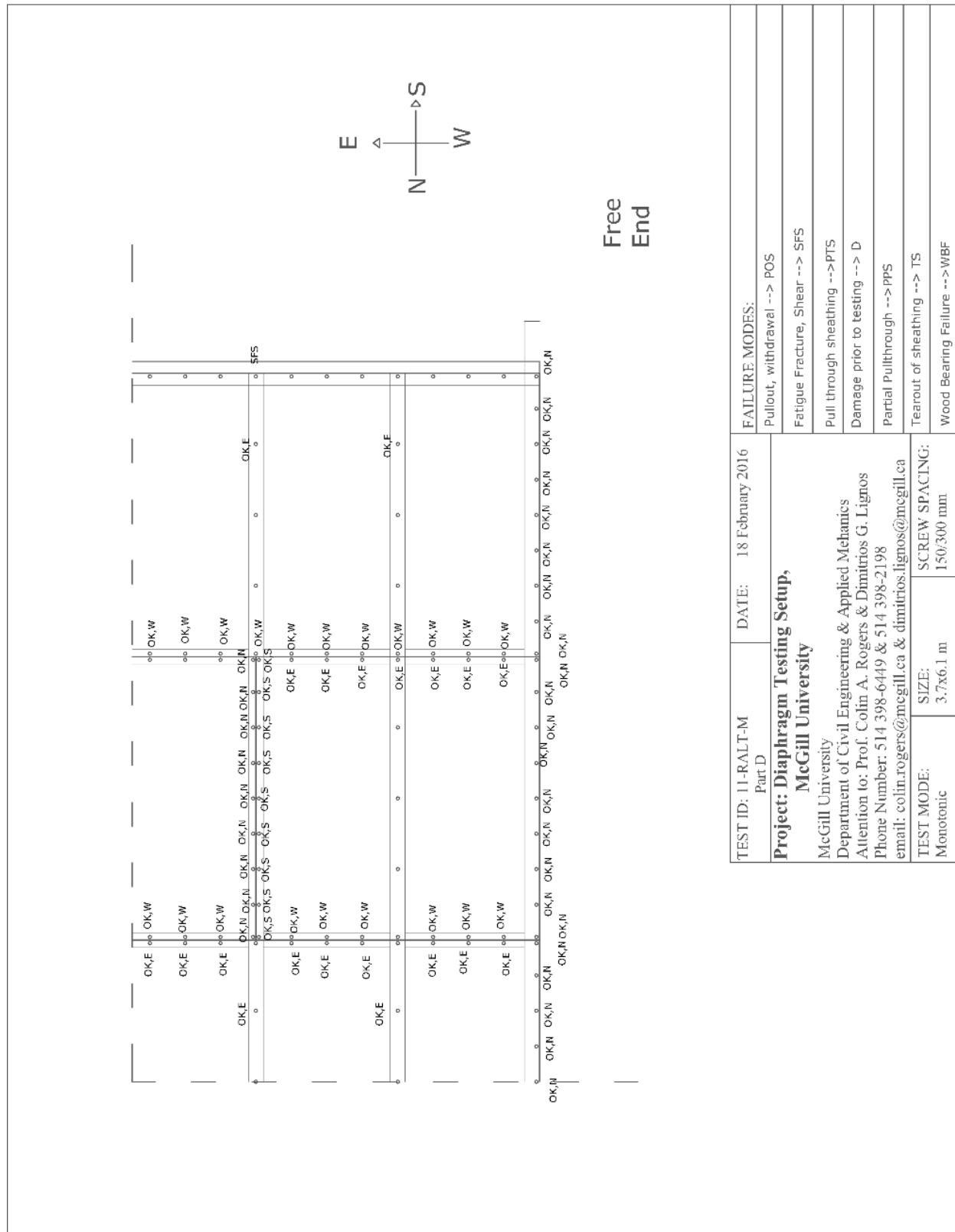


Figure A.5: Sheathing Fastener Failure Modes Part D Specimen 11-RALT-M

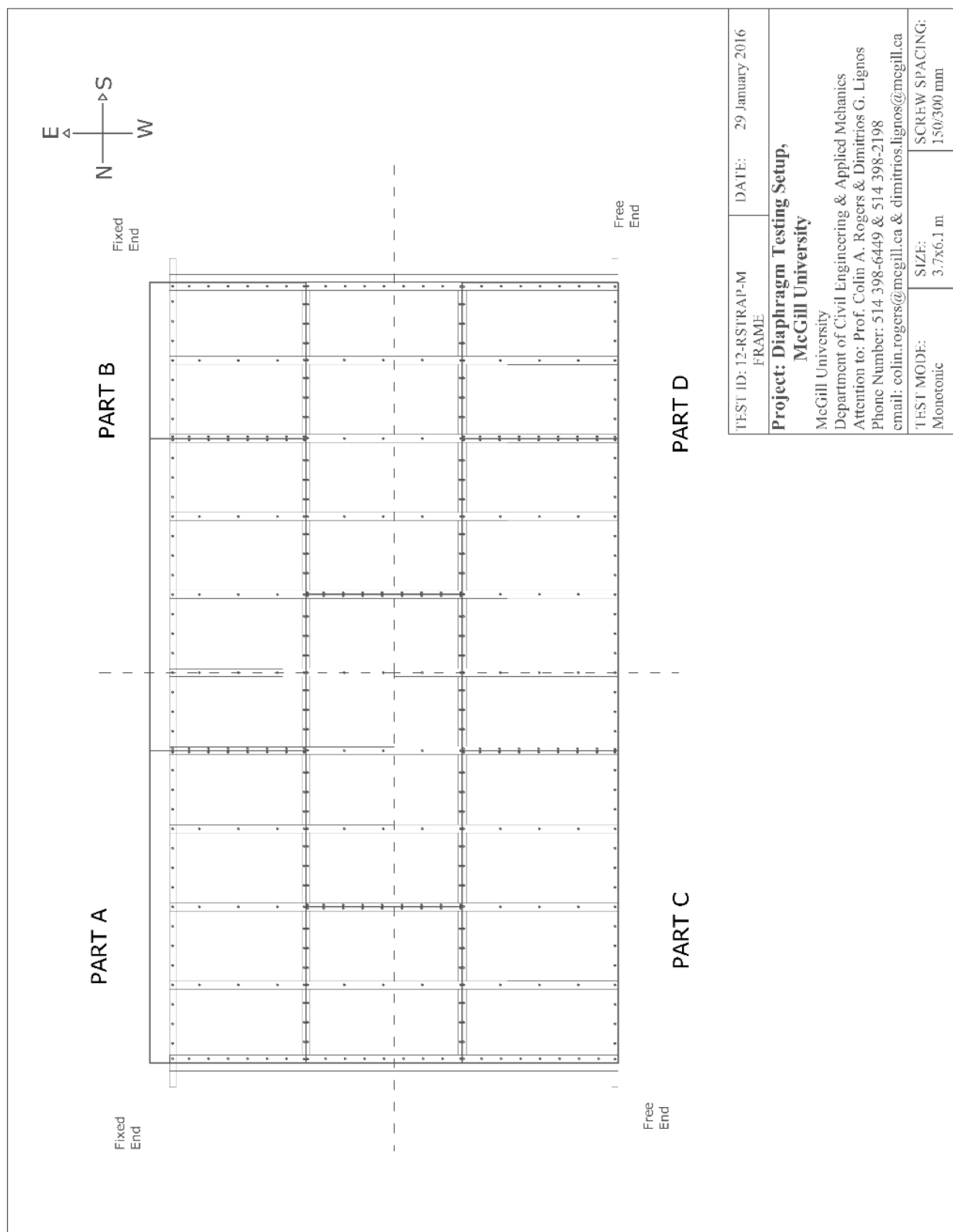


Figure A.6: Sheathing Fastener Placement for Specimen 12-RSTRAP-M

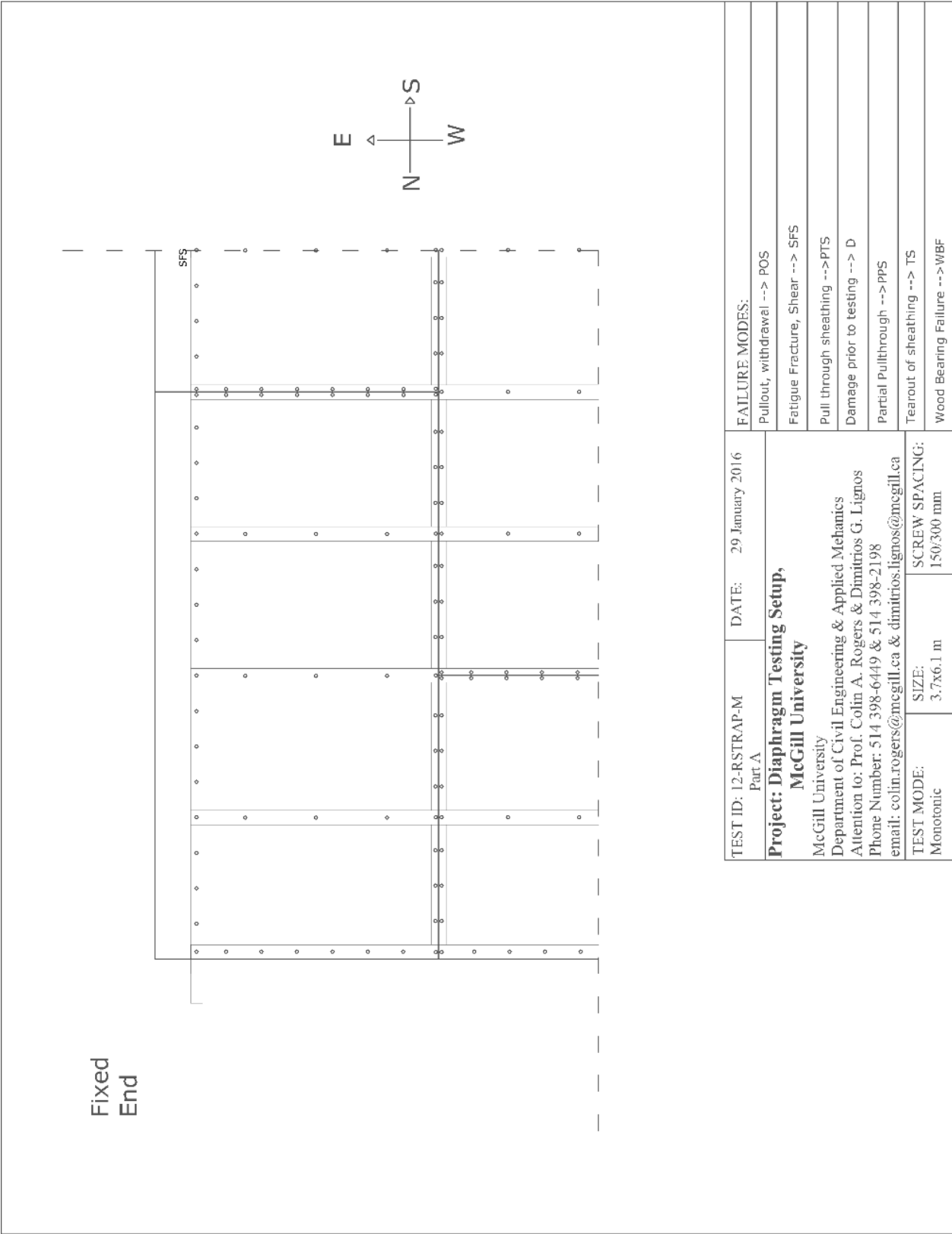


Figure A.7: Sheathing Fastener Failure Modes Part A Specimen 12-RSTRAP-M

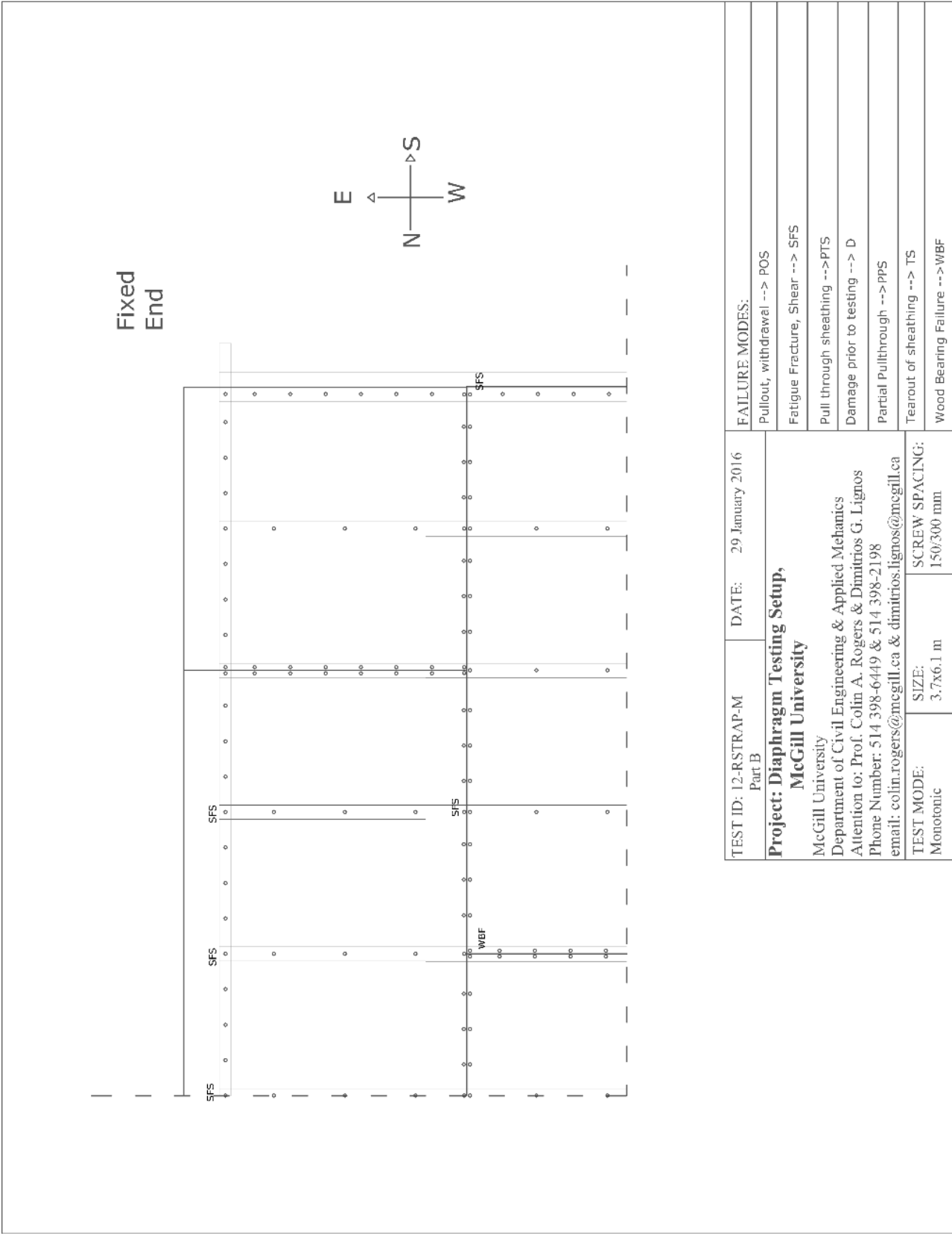


Figure A.8: Sheathing Fastener Failure Modes Part B Specimen 12-RSTRAP-M

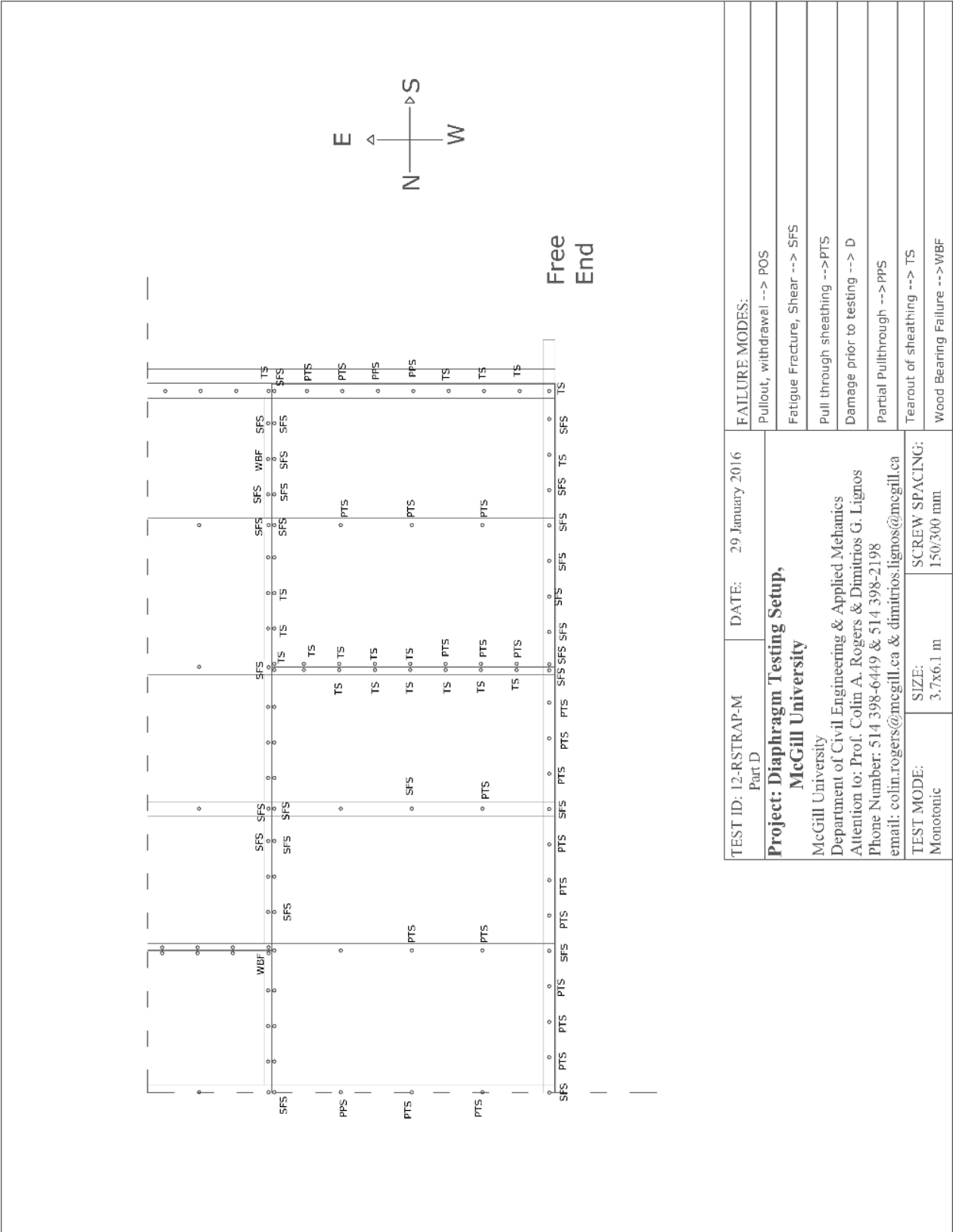


Figure A.10: Sheathing Fastener Failure Modes Part D Specimen 12-RSTRAP-M

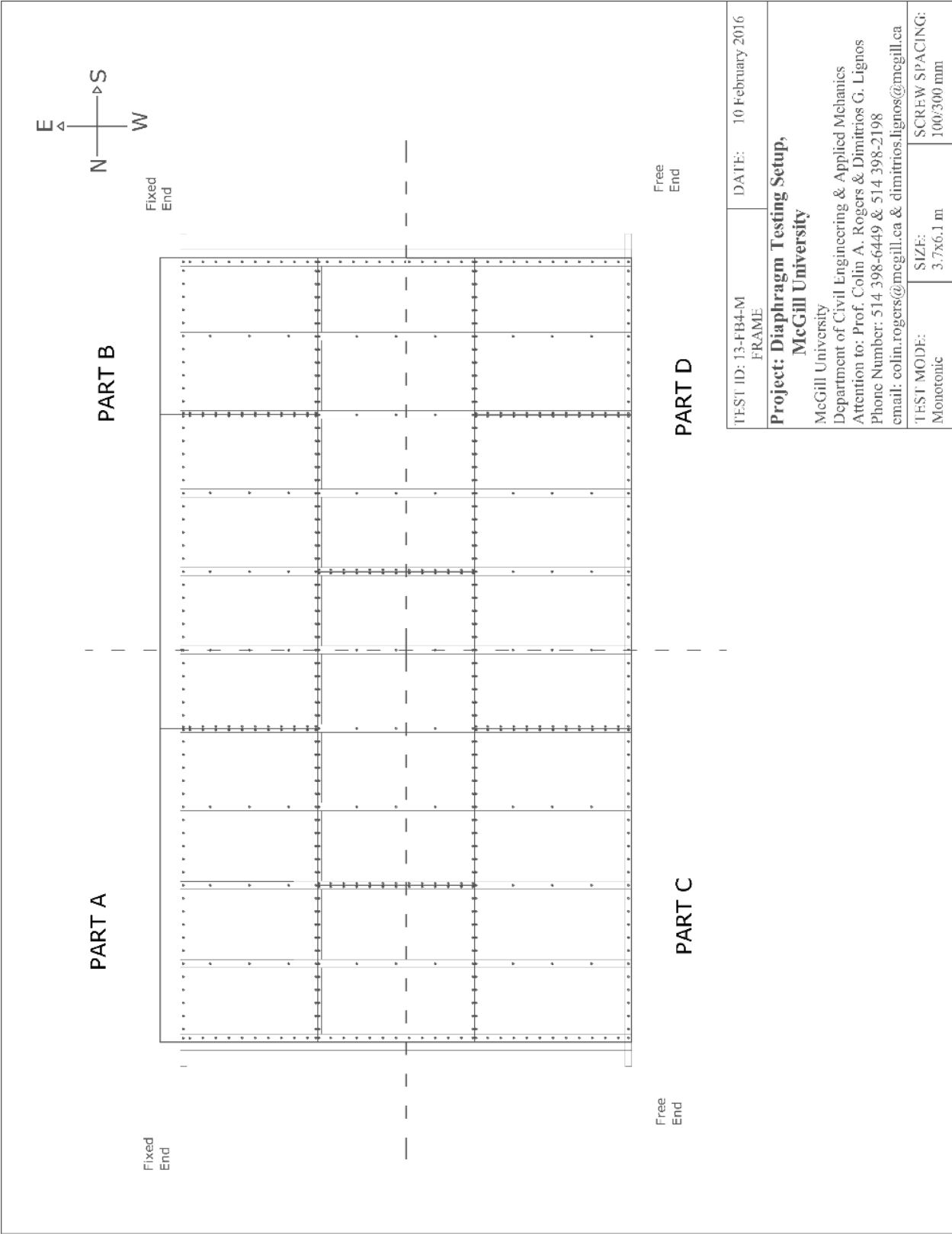


Figure A.11: Sheathing Fastener Placement for Specimen 13-FB4-M

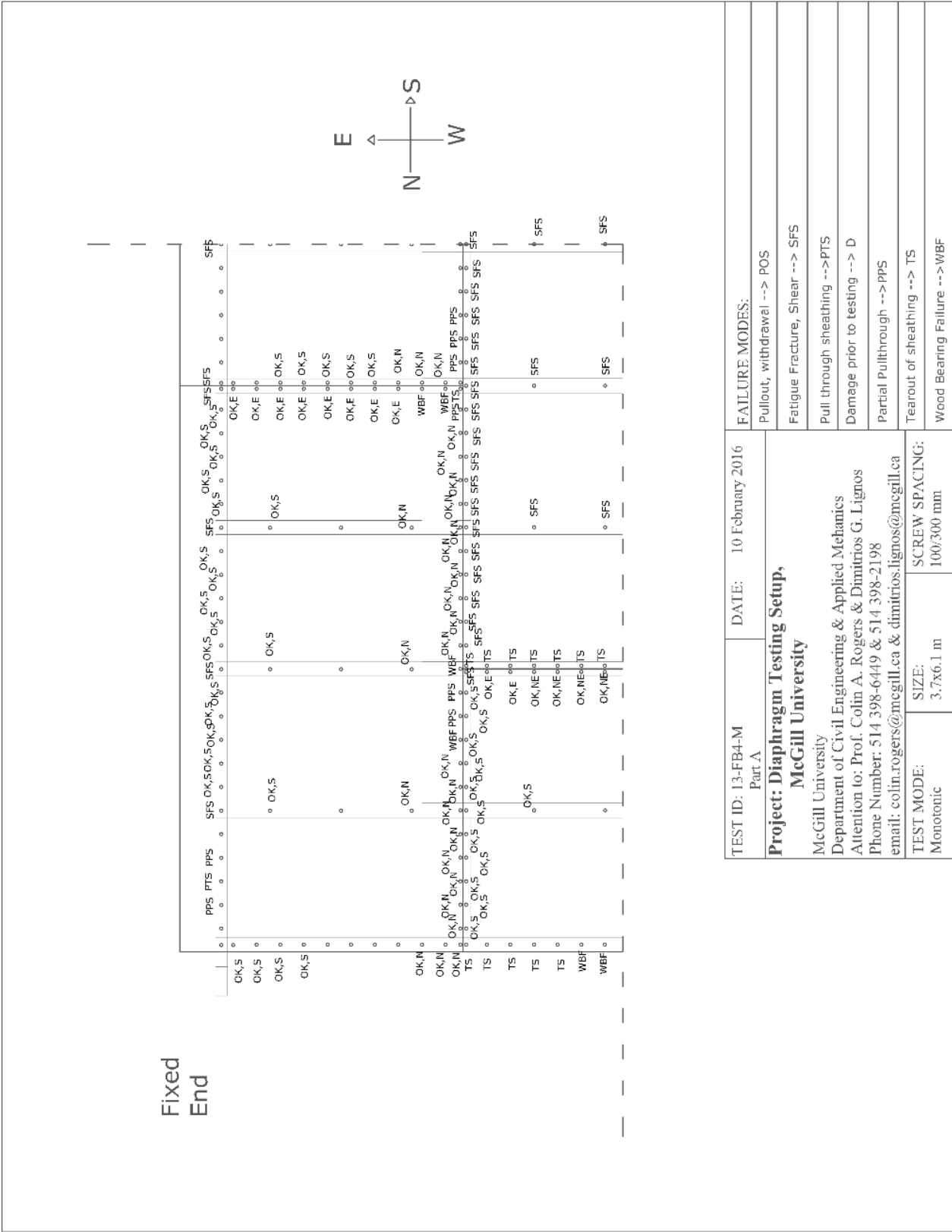


Figure A.12: Sheathing Fastener Failure Modes Part A Specimen 13-FB4-M

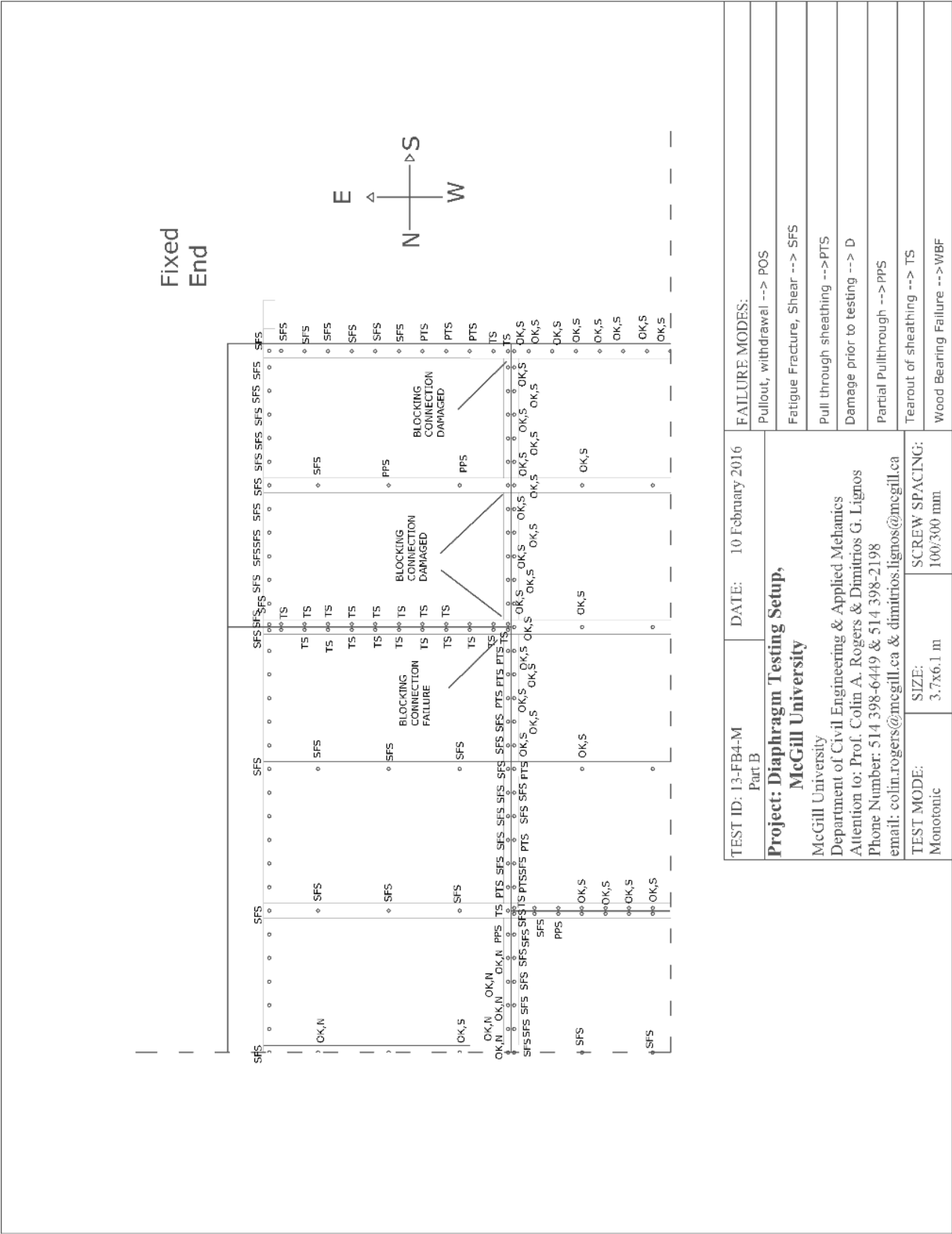


Figure A.13: Sheathing Fastener Failure Modes Part B Specimen 13-FB4-M

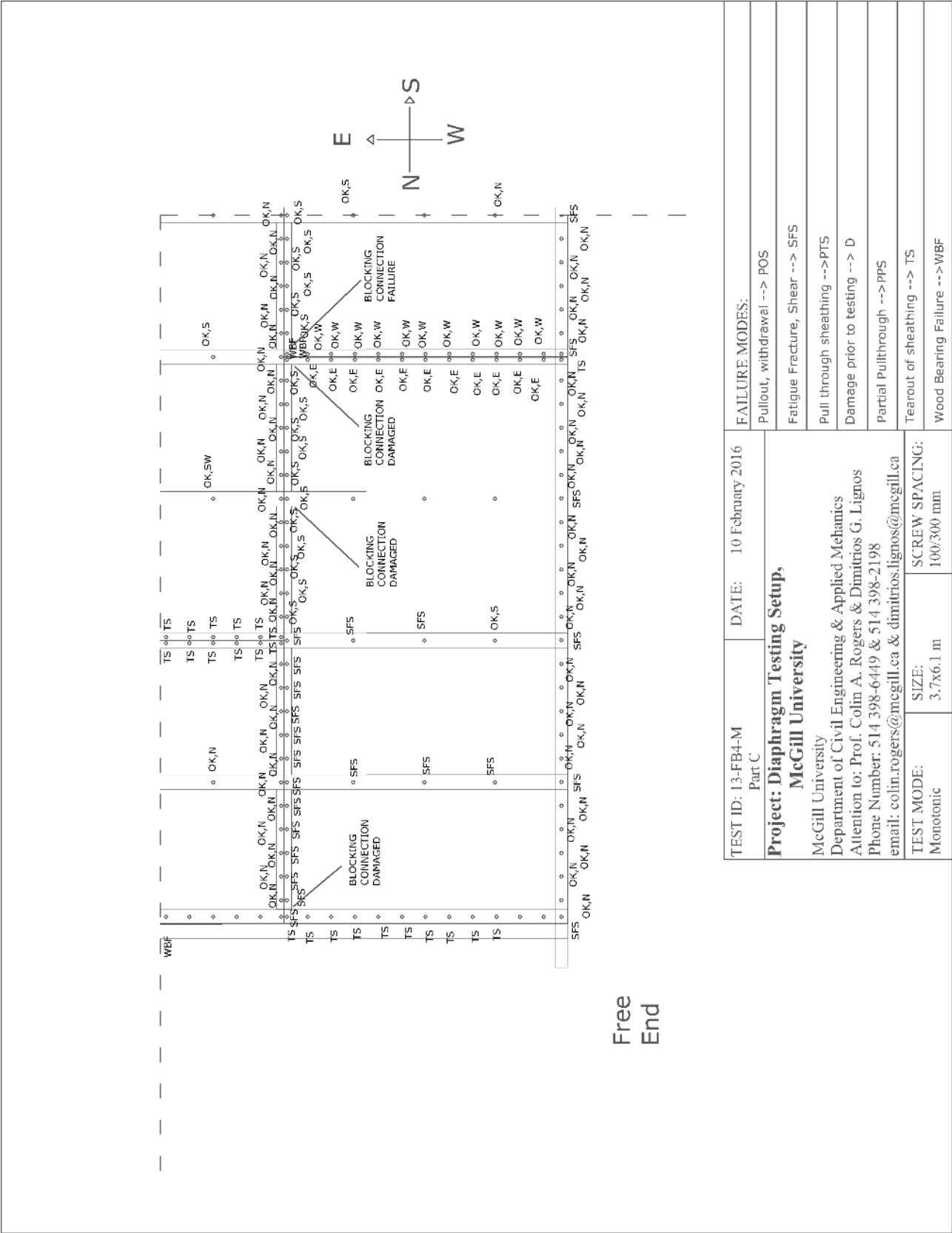


Figure A.14: Sheathing Fastener Failure Modes Part C Specimen 13-FB4-M

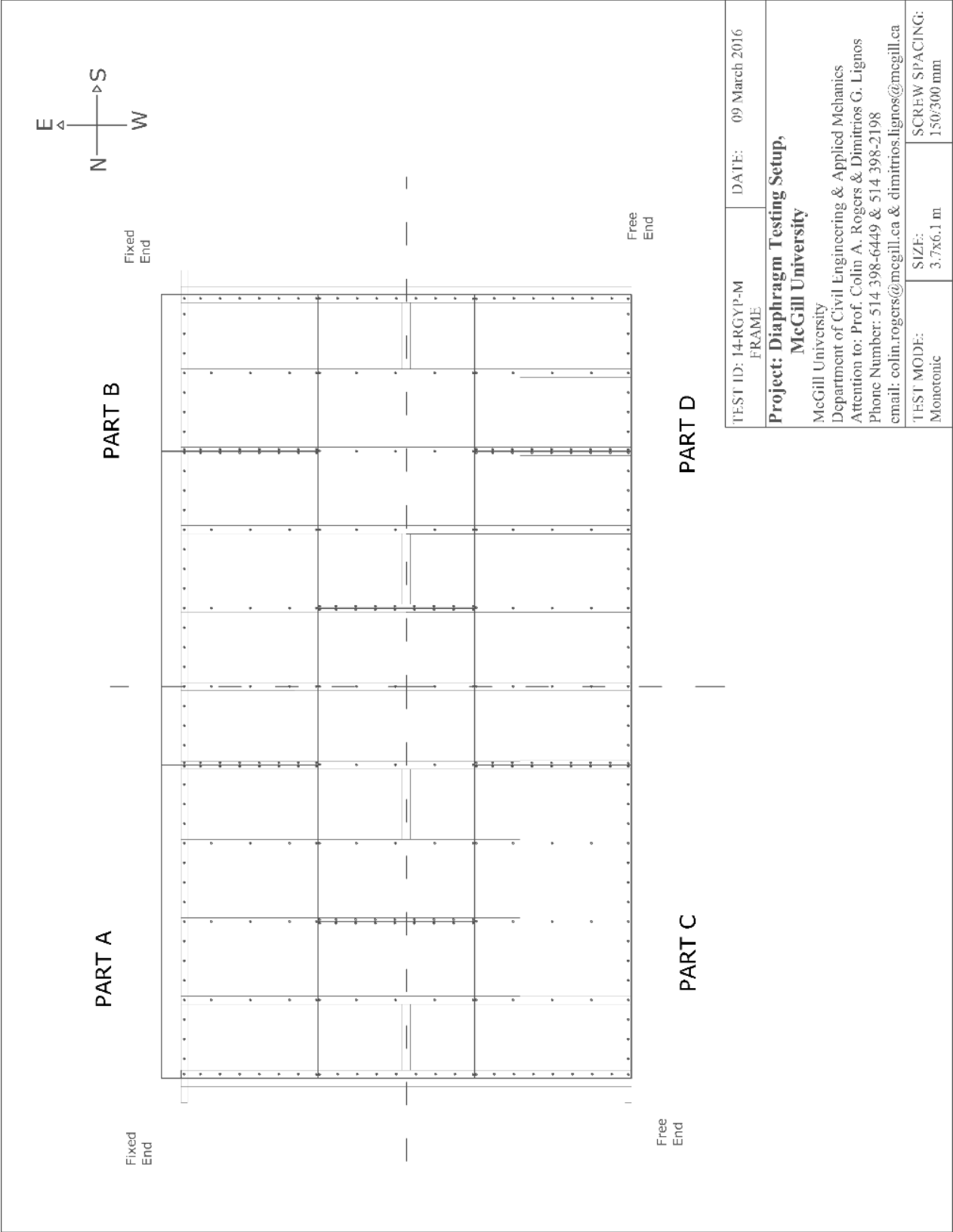


Figure A.16: Sheathing Fastener Placement for Specimen 14-RGY-P-M

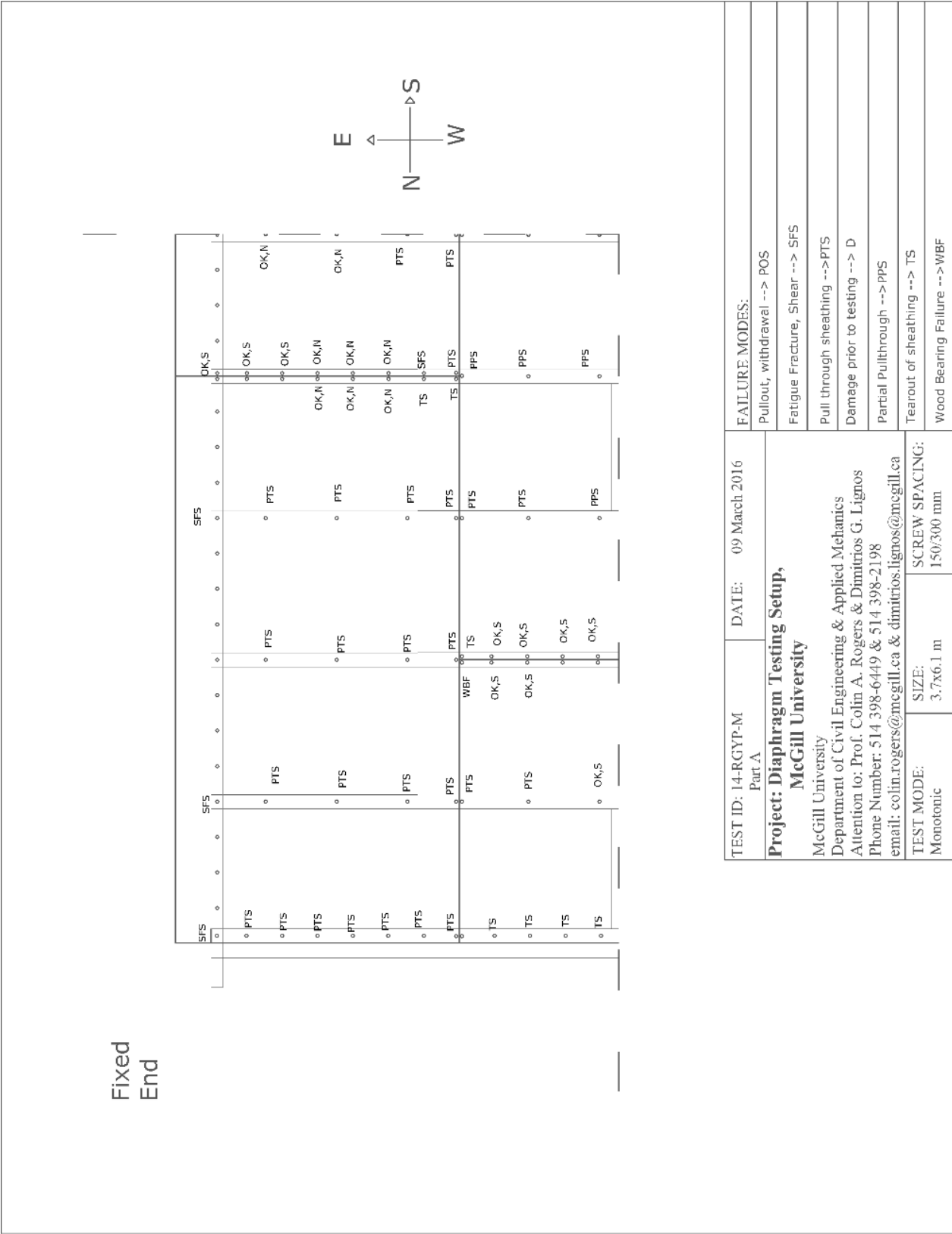


Figure A.17: Sheathing Fastener Failure Modes Part A Specimen 14-RGYP-M

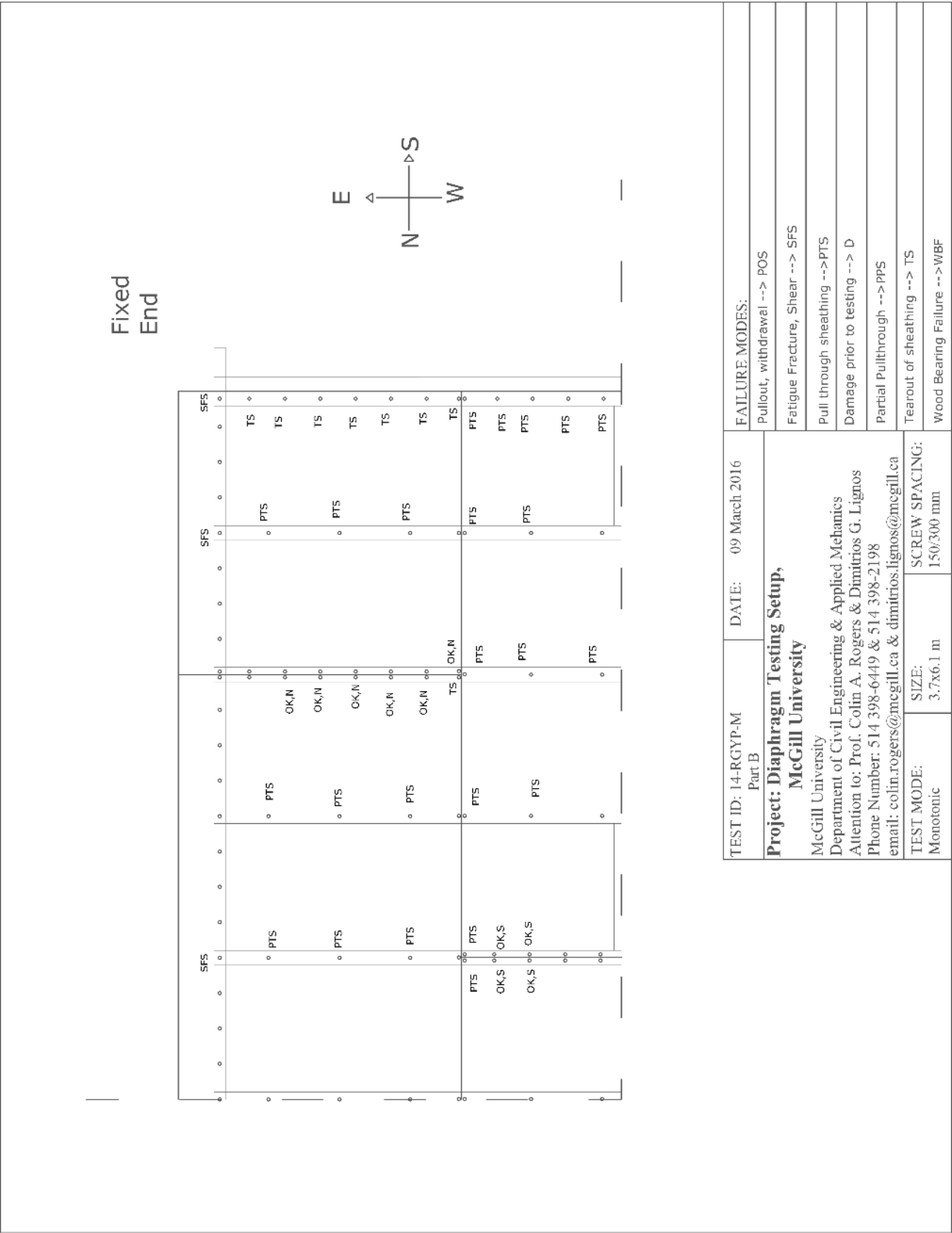


Figure A.18: Sheathing Fastener Failure Modes Part B Specimen 14-RGYP-M

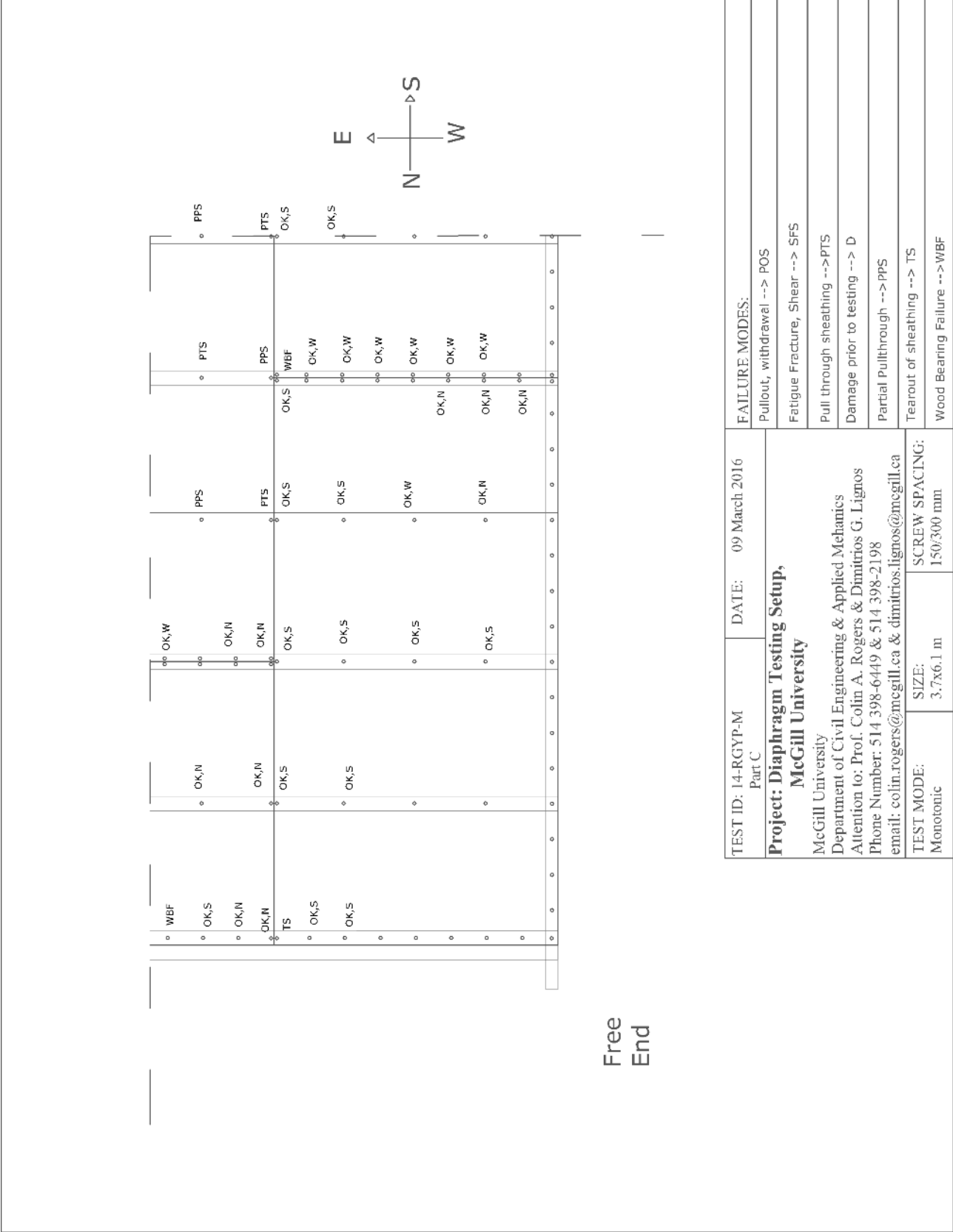


Figure A.19: Sheathing Fastener Failure Modes Part C Specimen 14-RGYP-M

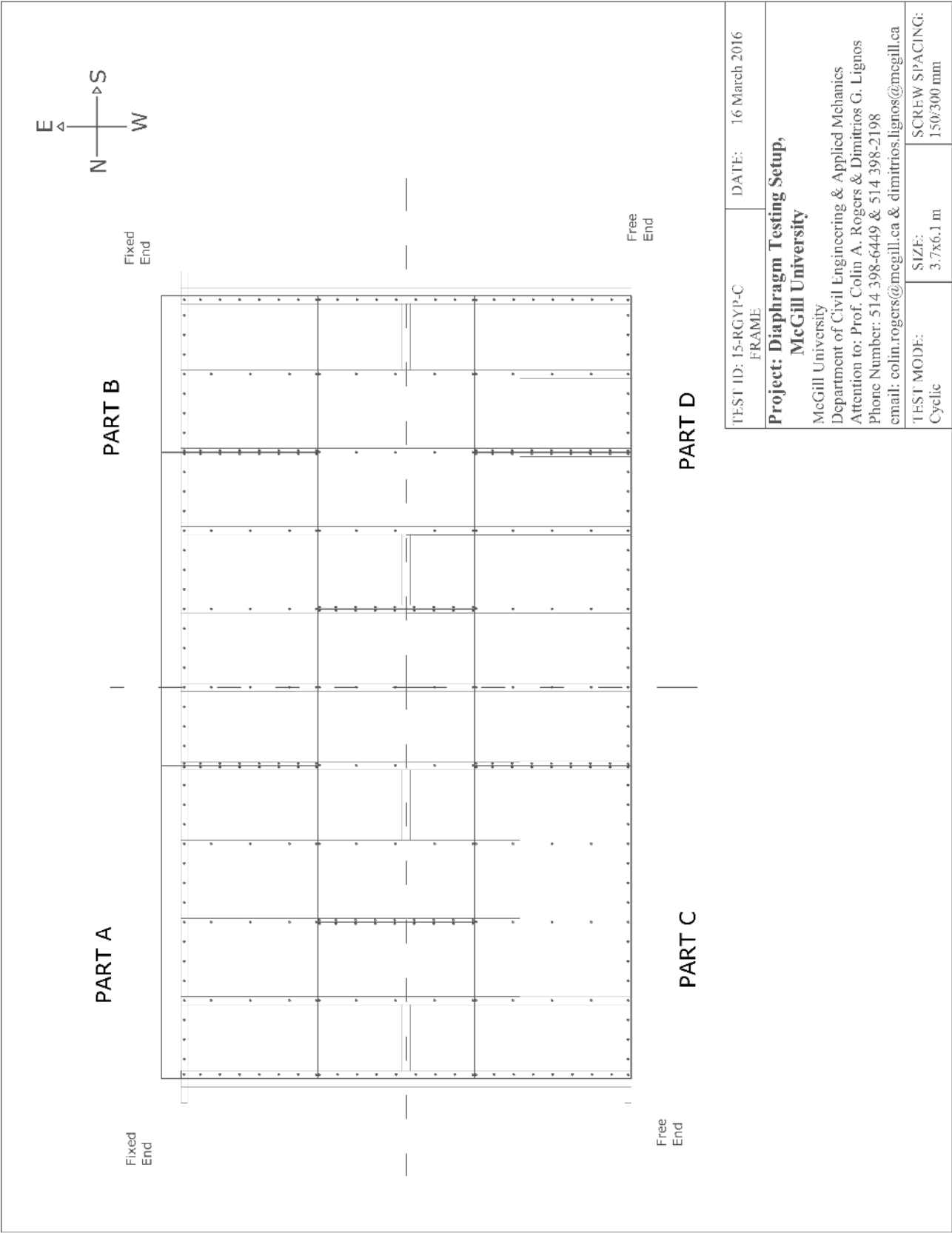


Figure A.21: Sheathing Fastener Placement for Specimen 15-RGYP-C

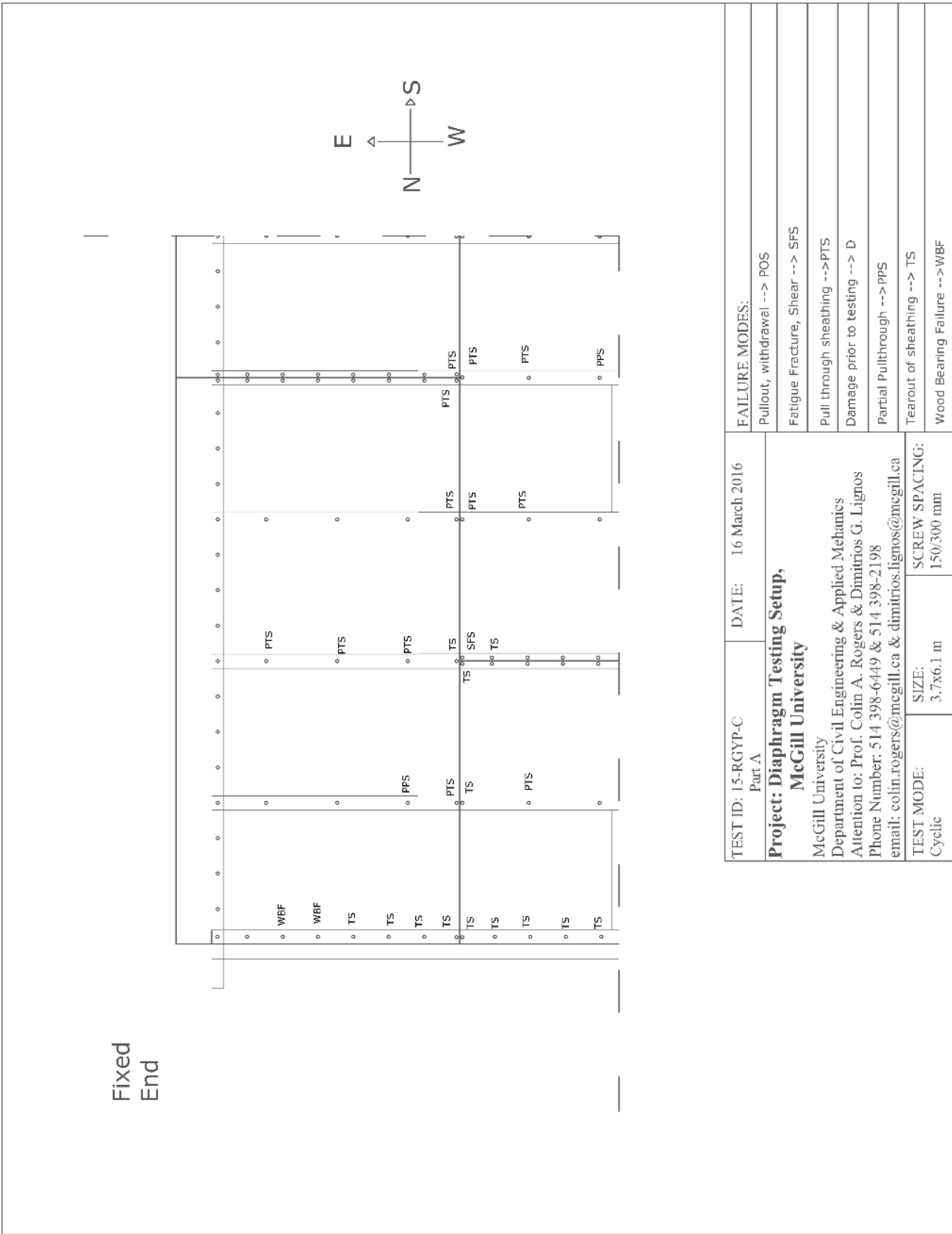


Figure A.22: Sheathing Fastener Failure Modes Part A Specimen 15-RGYP-C

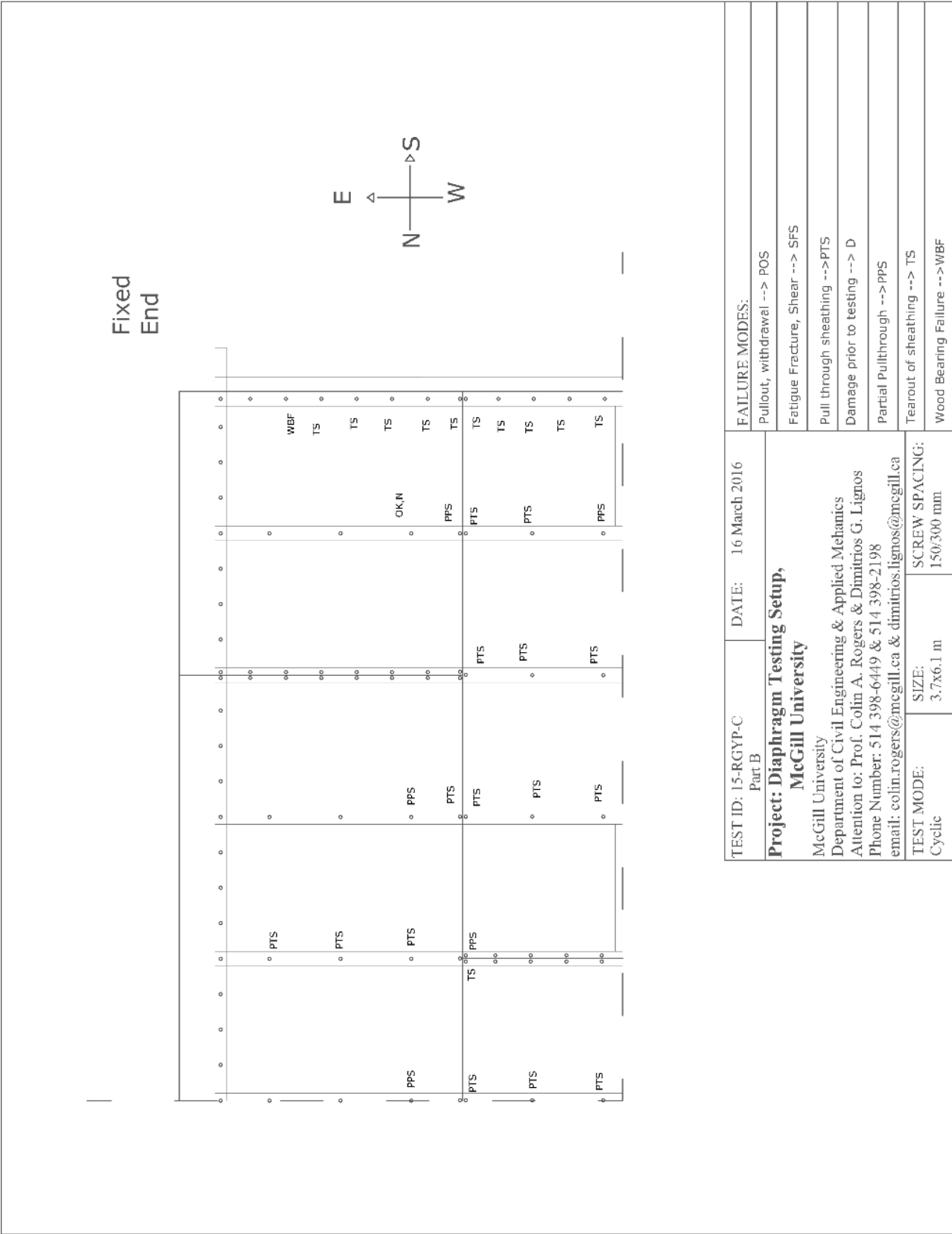
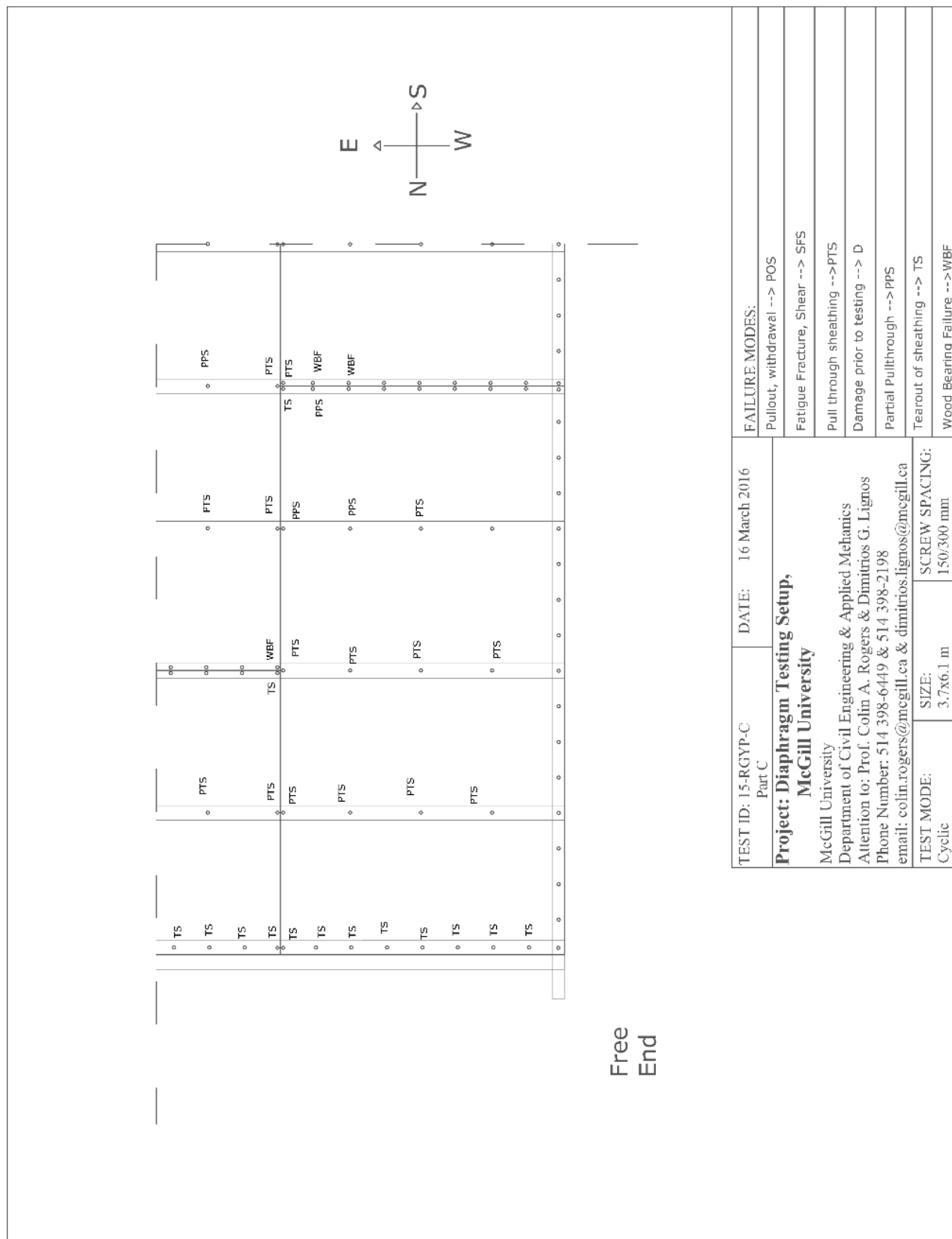


Figure A.23: Sheathing Fastener Failure Modes Part B Specimen 15-RGYP-C



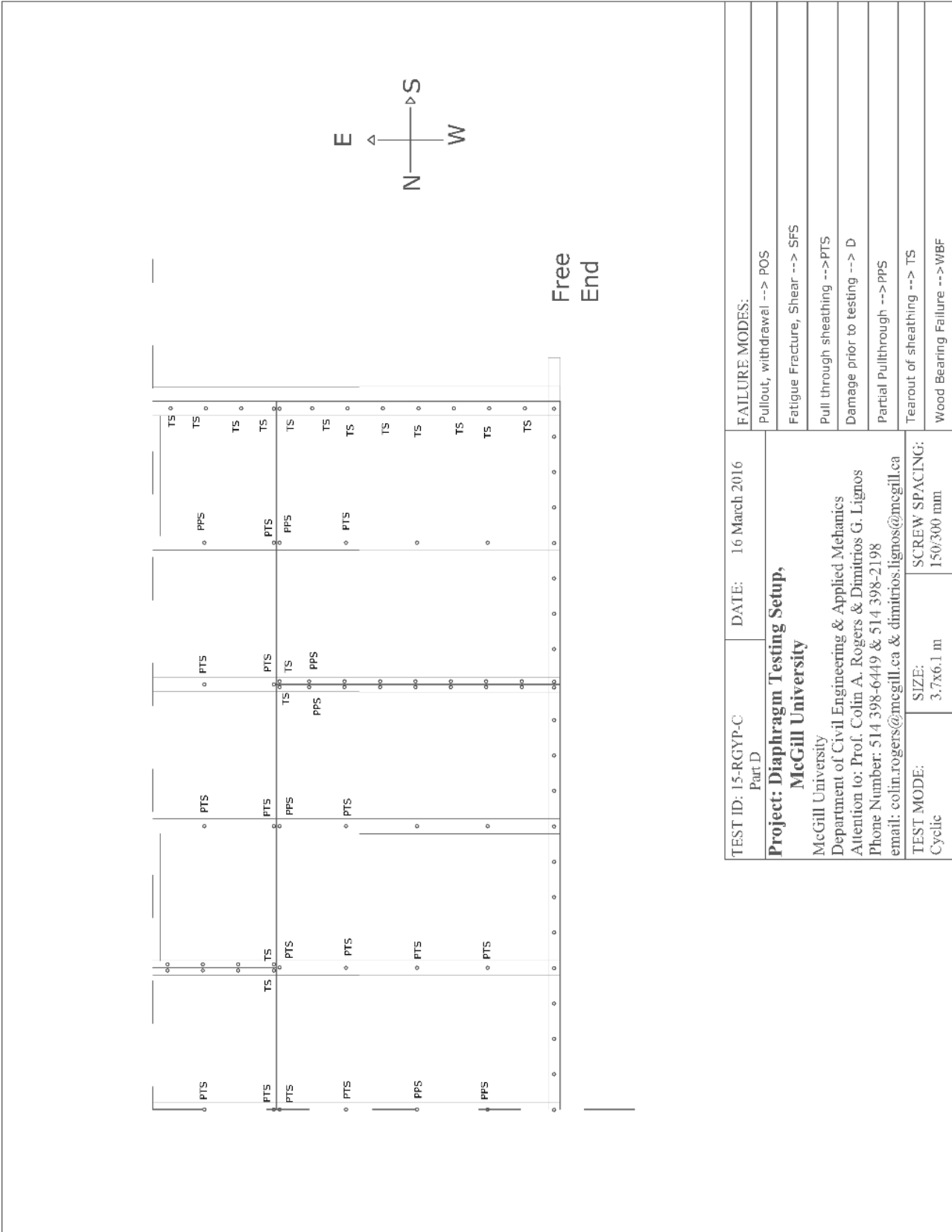


Figure A.25: Sheathing Fastener Failure Modes Part D Specimen 15-RGYP-C

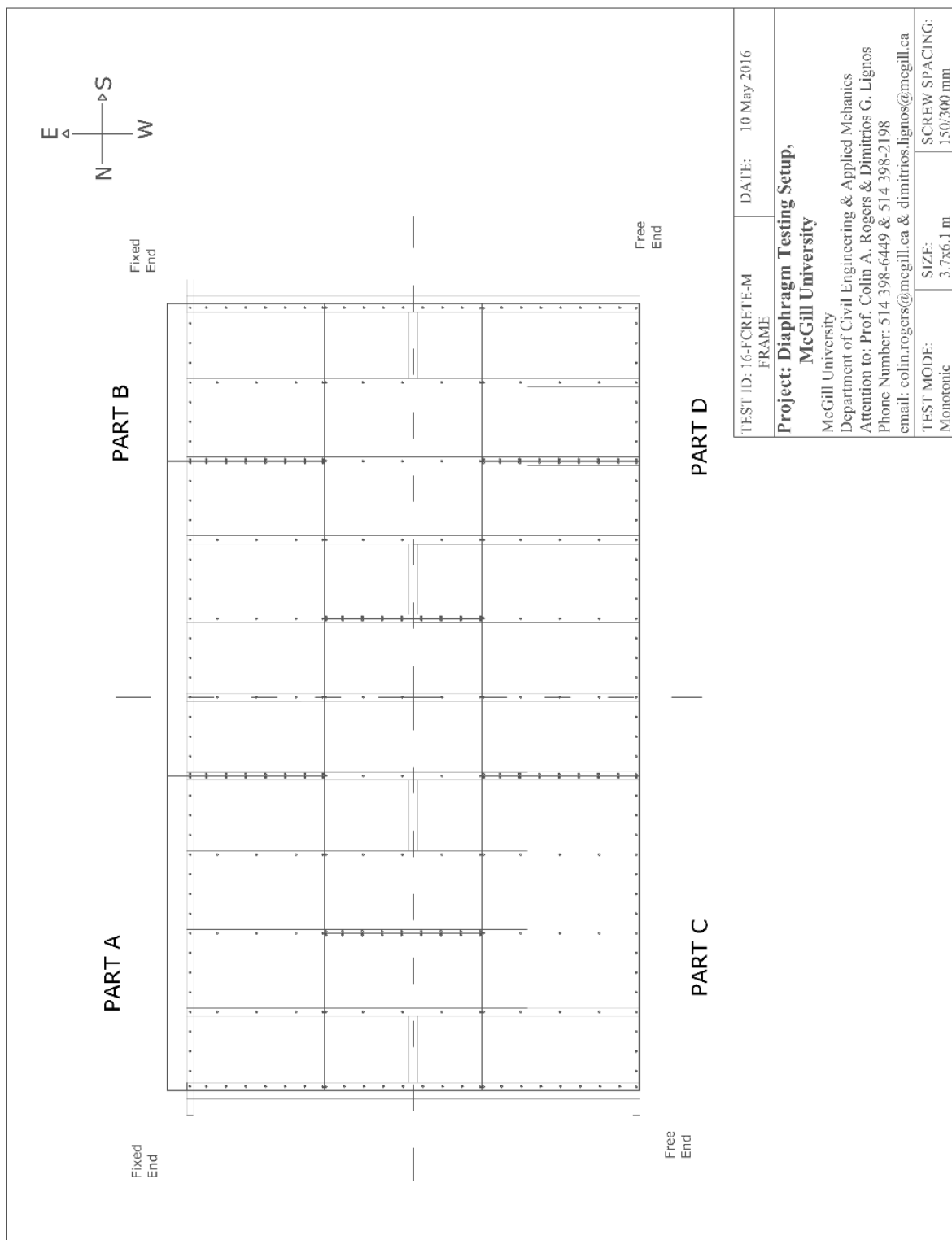


Figure A.26: Sheathing Fastener Placement for Specimen 16-FCRETE-M

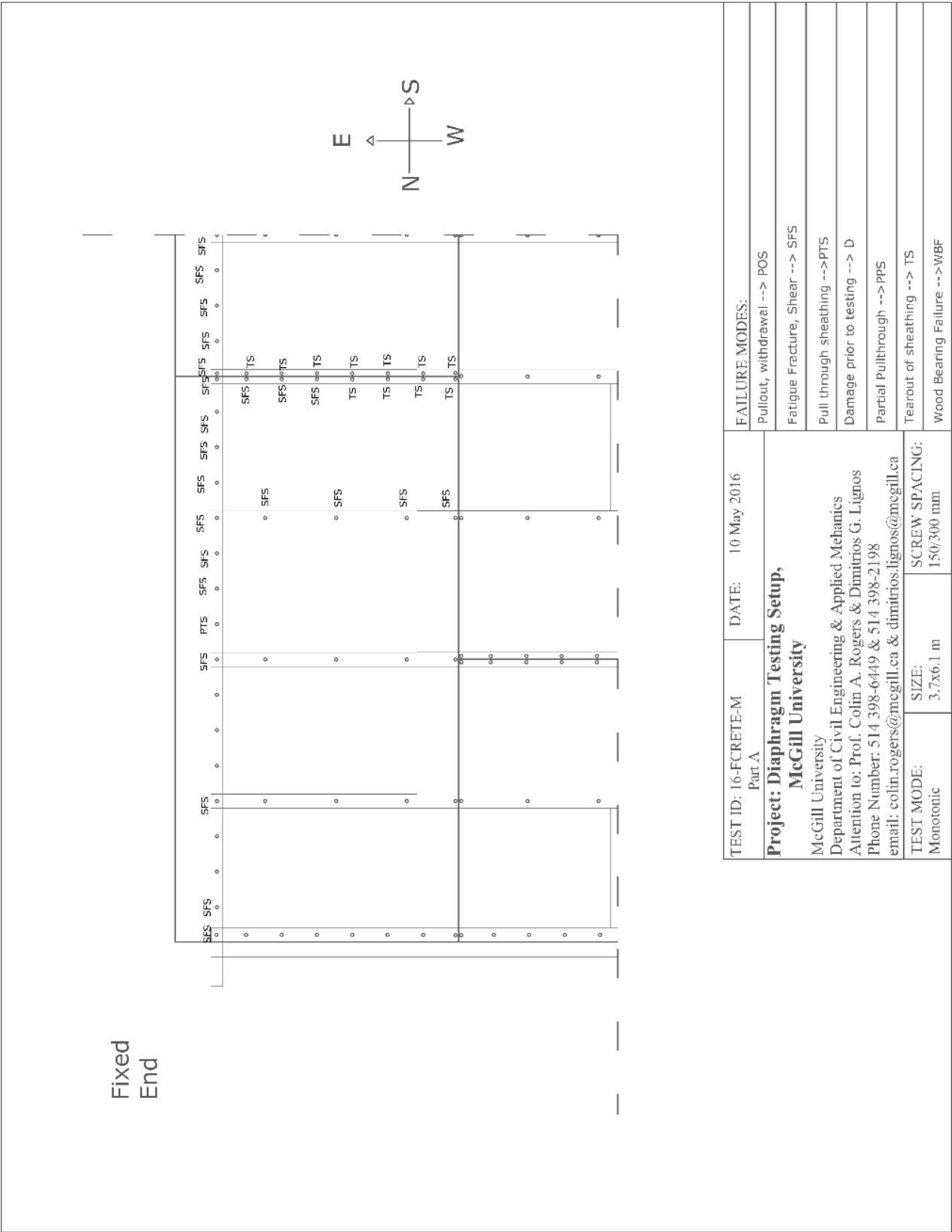


Figure A.27: Sheathing Fastener Failure Modes Part A Specimen 16-FCRETE-M

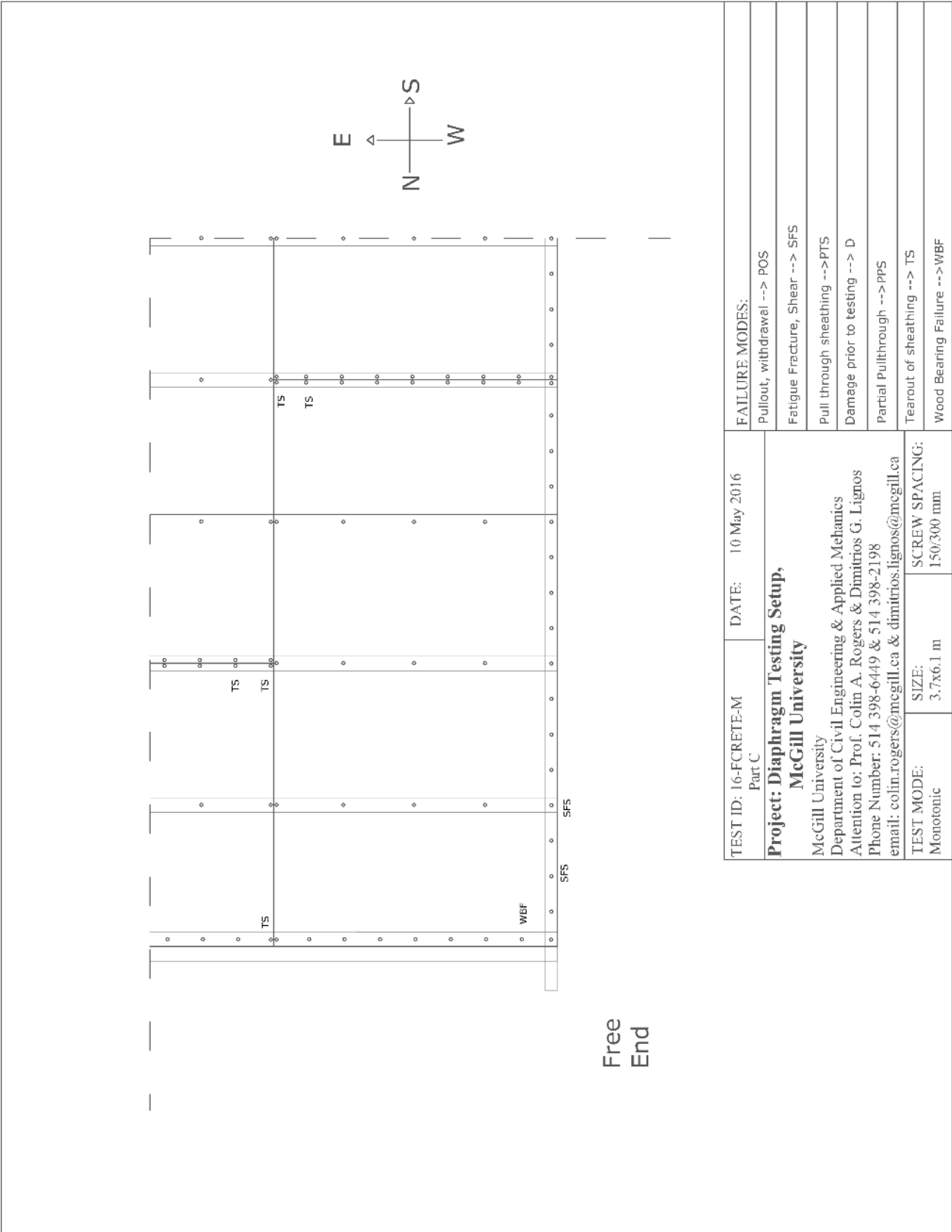


Figure A.29: Sheathing Fastener Failure Modes Part C Specimen 16-FCRETE-M

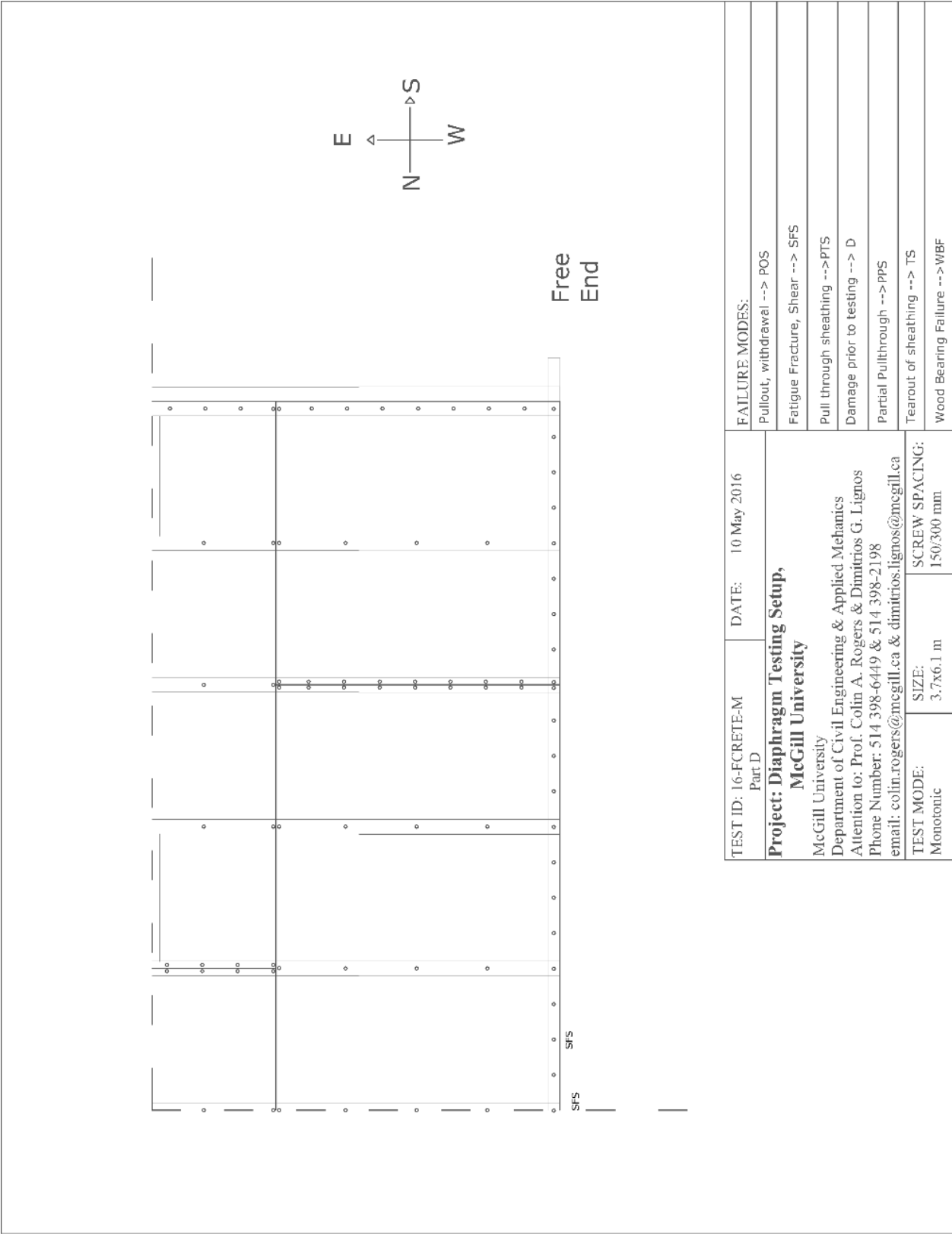


Figure A.30: Sheathing Fastener Failure Modes Part D Specimen 16-FCRETE-M

APPENDIX B:
Tensile Coupon Tests

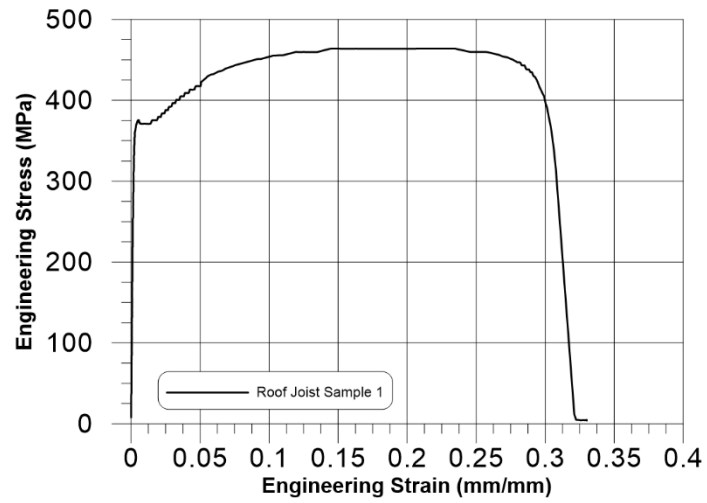


Figure B.1: Tensile Coupon Sample Response: Roof Joist 1

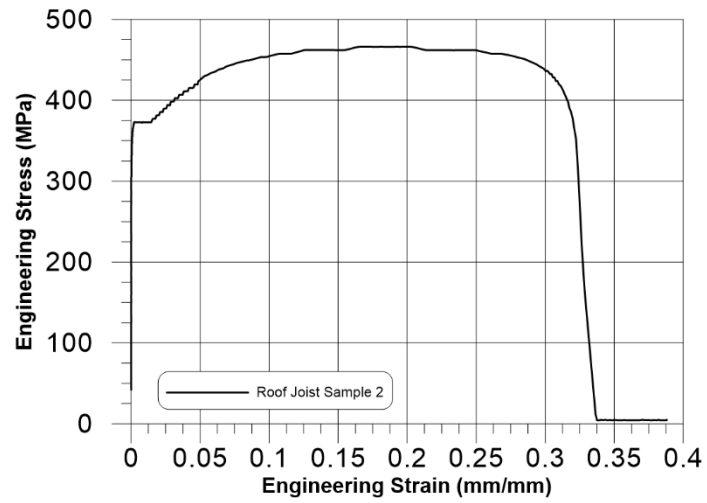


Figure B.2: Tensile Coupon Sample Response: Roof Joist 2

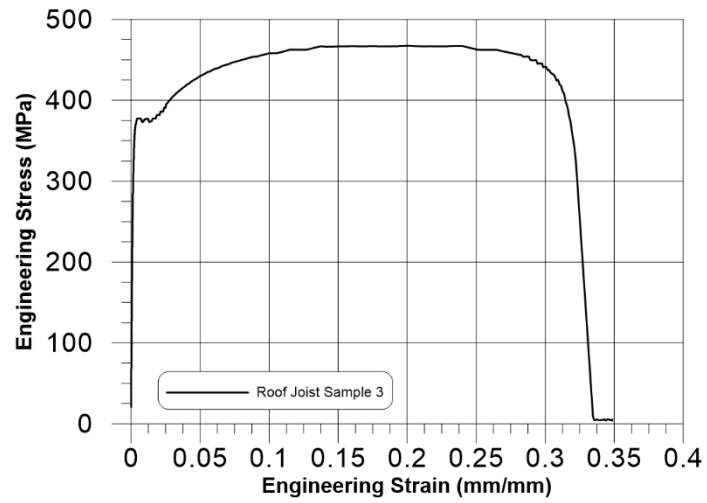


Figure B.3: Tensile Coupon Sample Response: Roof Joist 3

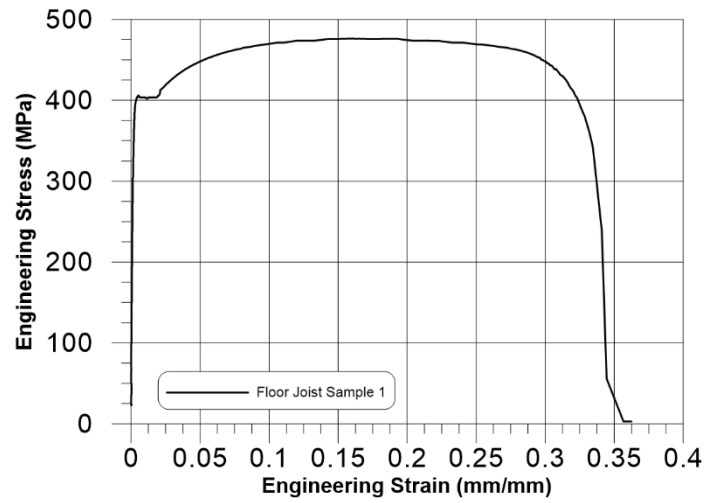


Figure B.4: Tensile Coupon Sample Response: Floor Joist 1

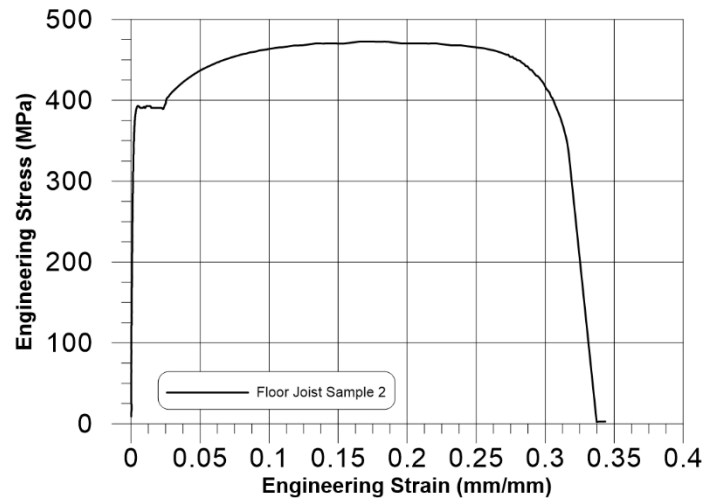


Figure B.5: Tensile Coupon Sample Response: Floor Joist 2

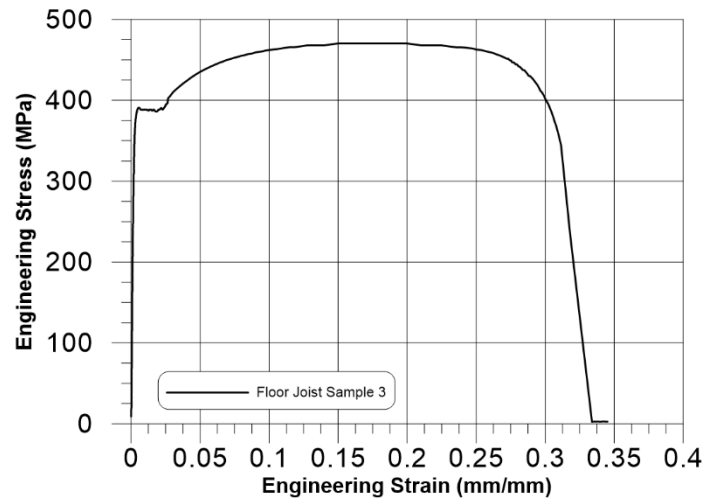


Figure B.6: Tensile Coupon Sample Response: Floor Joist 3

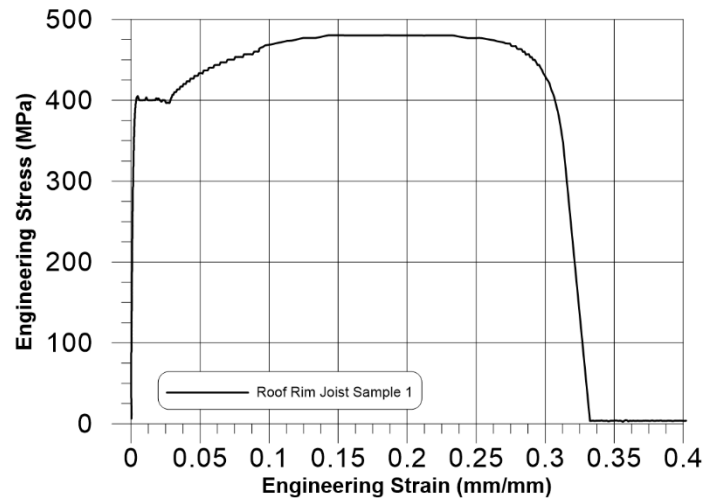


Figure B.7: Tensile Coupon Sample Response: Roof Rim Joist 1

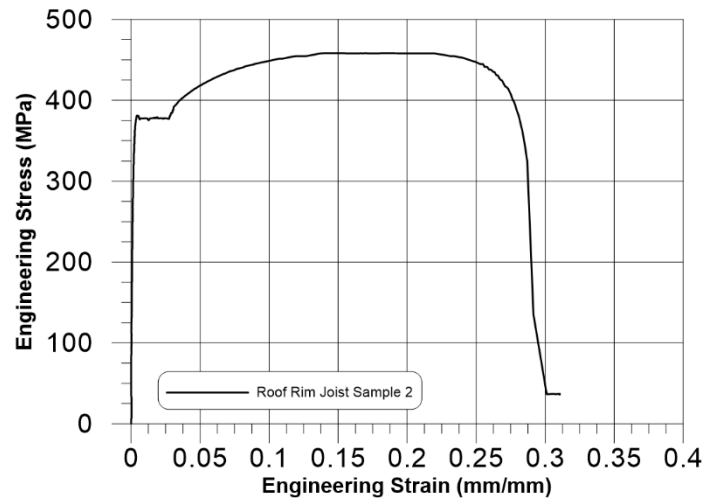


Figure B.8: Tensile Coupon Sample Response: Roof Rim Joist 2

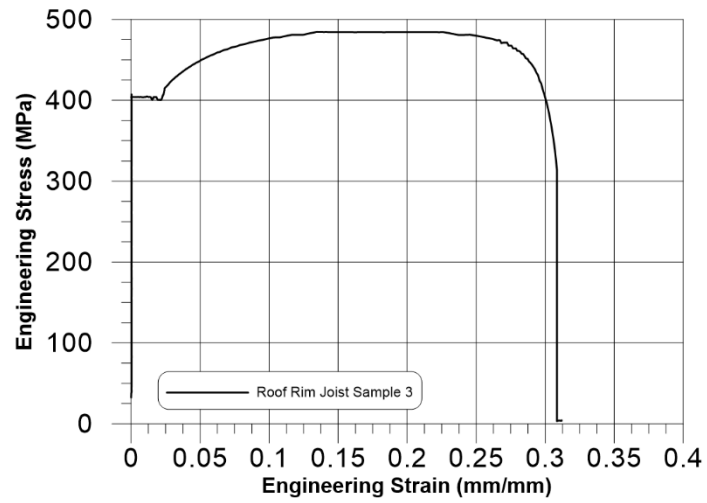


Figure B.9: Tensile Coupon Sample Response: Roof Rim Joist 3

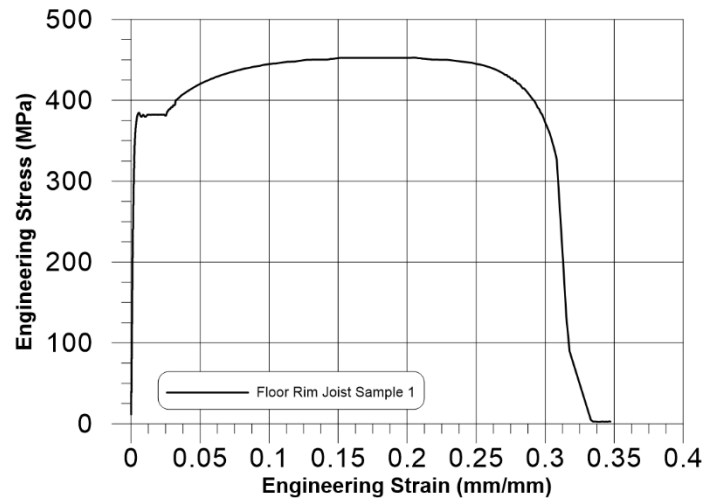


Figure B.10: Tensile Coupon Sample Response: Floor Rim Joist 1

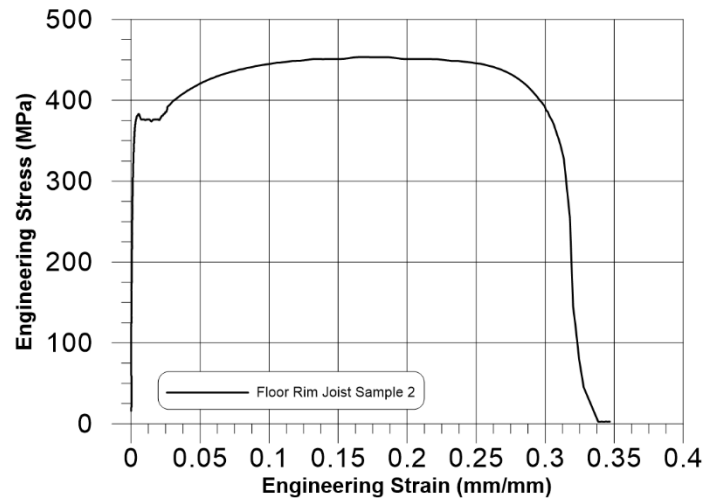


Figure B.11: Tensile Coupon Sample Response: Floor Rim Joist 2

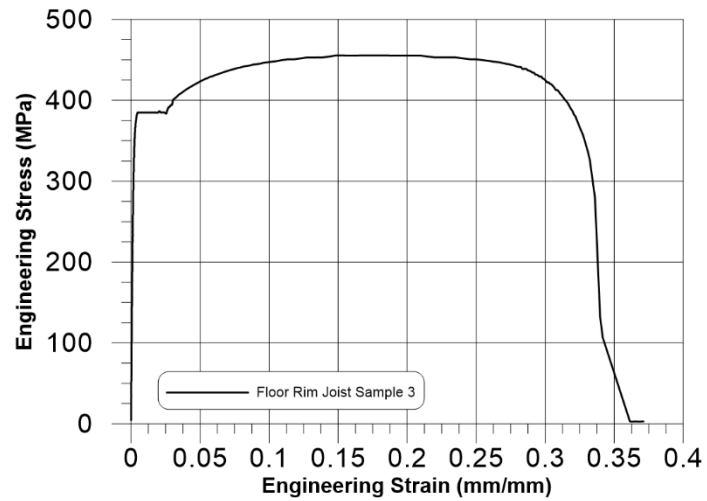


Figure B.12: Tensile Coupon Sample Response: Floor Rim Joist 3

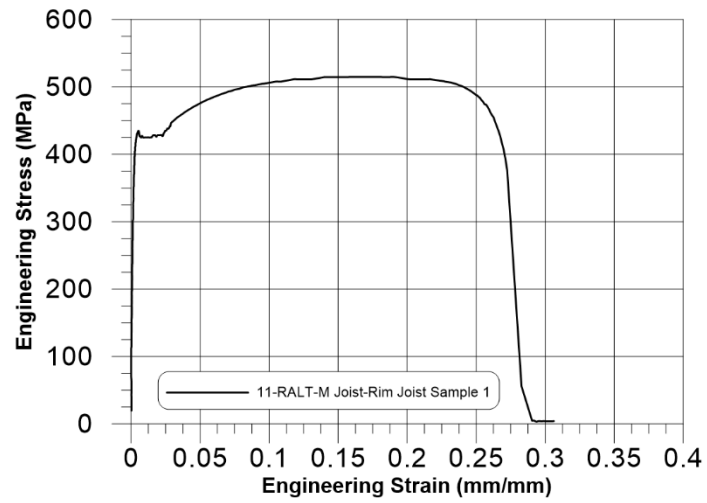


Figure B.13: Tensile Coupon Sample Response: 11-RALT-M Joist-Rim Joist Sample 1

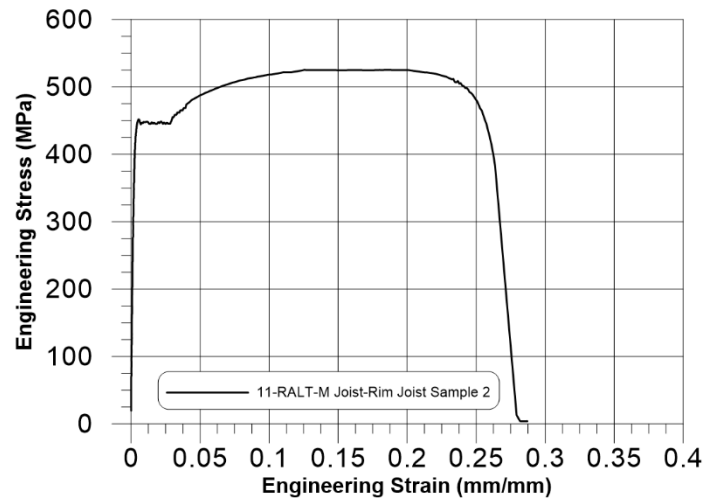


Figure B.14: Tensile Coupon Sample Response: 11-RALT-M Joist-Rim Joist Sample 2

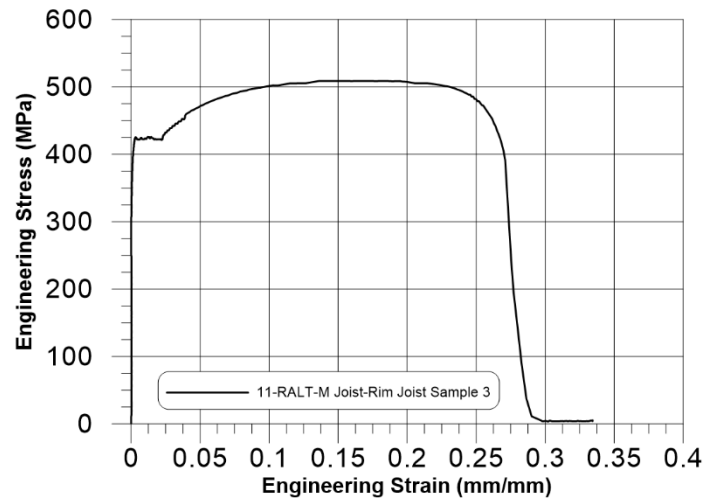


Figure B.15: Tensile Coupon Sample Response: 11-RALT-M Joist-Rim Joist Sample 3

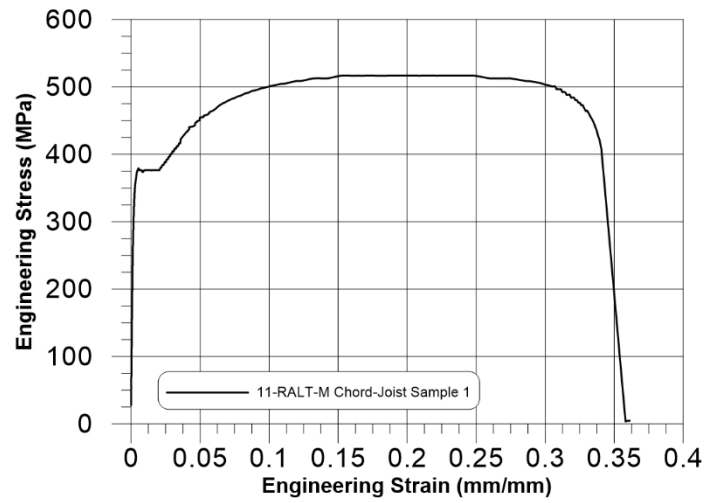


Figure B.16: Tensile Coupon Sample Response: 11-RALT-M Chord-Joist Sample 1

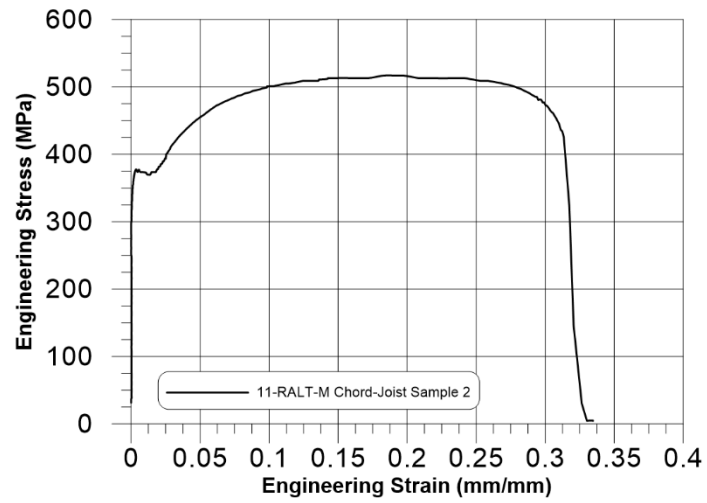


Figure B.17: Tensile Coupon Sample Response: 11-RALT-M Chord-Joist Sample 2

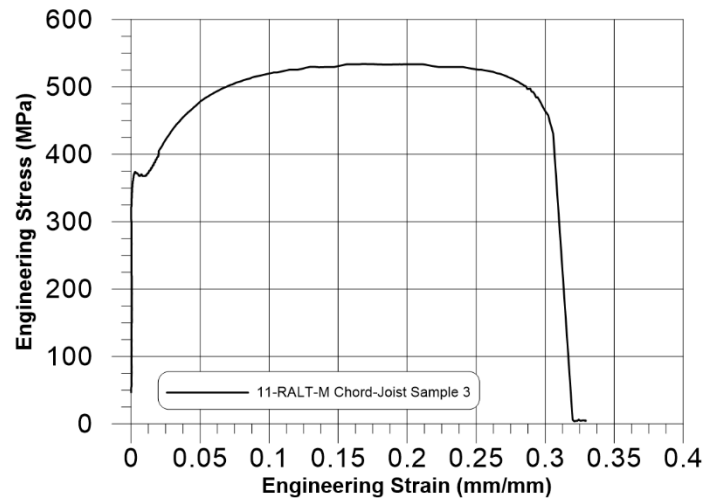


Figure B.18: Tensile Coupon Sample Response: 11-RALT-M Chord-Joist Sample 3

Table B.1: Complete Summary of Tensile Coupon Test Samples

Specimens	Steel Thickness (mm)	E (MPa)	F _y (MPa)	ε _y (mm/mm)	F _u (MPa)	ε _u (mm/mm)	F _u /F _y	Elongation (%)
Roof Joist 1	1.37	208400	375	0.00492	464	0.219	1.24	30.8
Roof Joist 2			372	0.00214	466	0.169	1.25	32.4
Roof Joist 3			377	0.00442	467	0.201	1.24	32.2
Floor Joist 1	2.46	207500	406	0.00516	476	0.160	1.17	33.5
Floor Joist 2			393	0.00506	473	0.172	1.20	31.7
Floor Joist 3			391	0.00520	470	0.199	1.20	31.8
Roof Rim Joist 1	1.73	204800	405	0.00492	480	0.146	1.19	31.4
Roof Rim Joist 2			381	0.00414	458	0.185	1.20	28.7
Roof Rim Joist 3			407	0.00028	485	0.135	1.19	30.9
Floor Rim Joist 1	2.46	201400	384	0.00568	453	0.203	1.18	30.8
Floor Rim Joist 2			383	0.00538	453	0.165	1.18	31.4
Floor Rim Joist 3			385	0.00486	455	0.154	1.18	33.6
11-RALT-M Joist-Rim Joist 1	1.37	203200	435	0.00538	515	0.177	1.18	27.2
11-RALT-M Joist-Rim Joist 2			452	0.00538	525	0.184	1.16	26.4
11-RALT-M Joist-Rim Joist 3			425	0.00316	509	0.150	1.20	27
11-RALT-M Chord-Joist 1	1.73	194700	379	0.00512	517	0.220	1.36	34.1
11-RALT-M Chord-Joist 2			378	0.00366	517	0.187	1.37	32.1
11-RALT-M Chord-Joist 3			374	0.00296	534	0.168	1.43	30.6

APPENDIX C:

Connection Tests

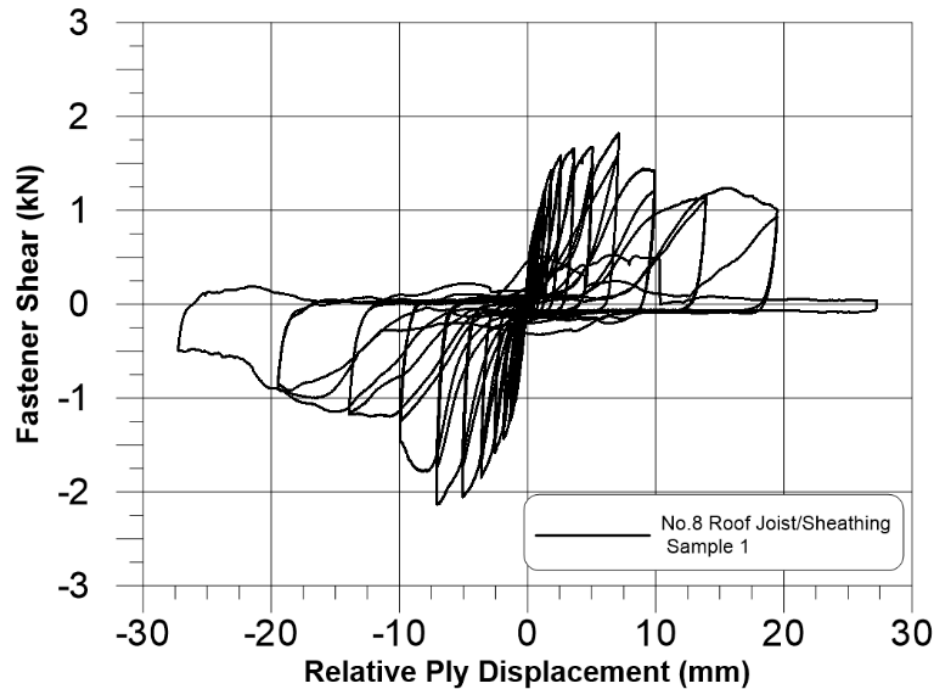


Figure C.1: Roof Joist/Sheathing Connection with #8 Fastener Sample 1

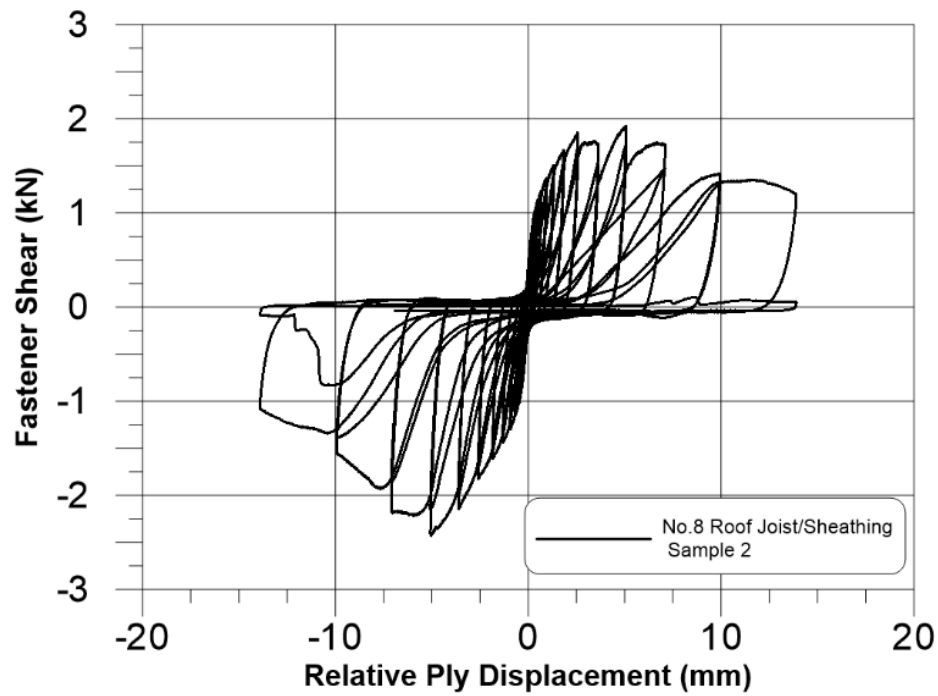


Figure C.2: Roof Joist/Sheathing Connection with #8 Fastener Sample 2

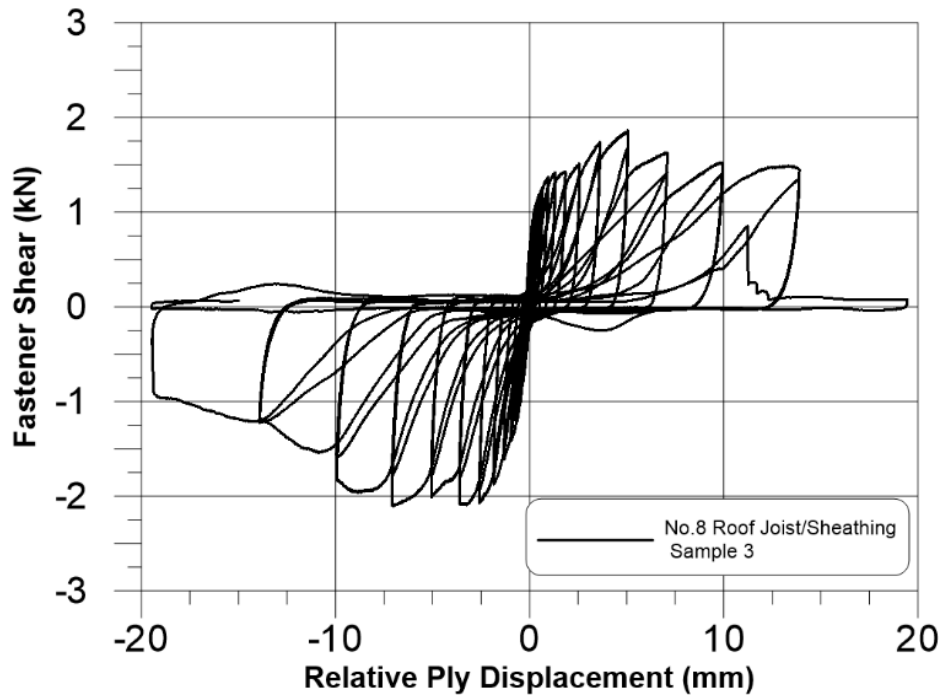


Figure C.3: Roof Joist/Sheathing Connection with #8 Fastener Sample 3

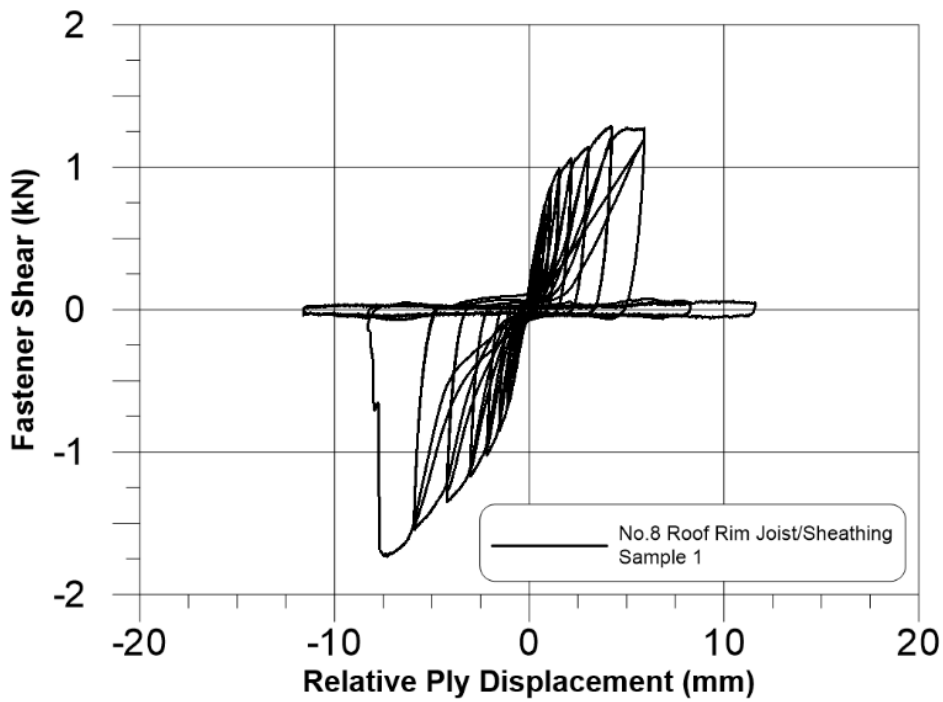


Figure C.4: Roof Rim Joist/Sheathing Connection with #8 Fastener Sample 1

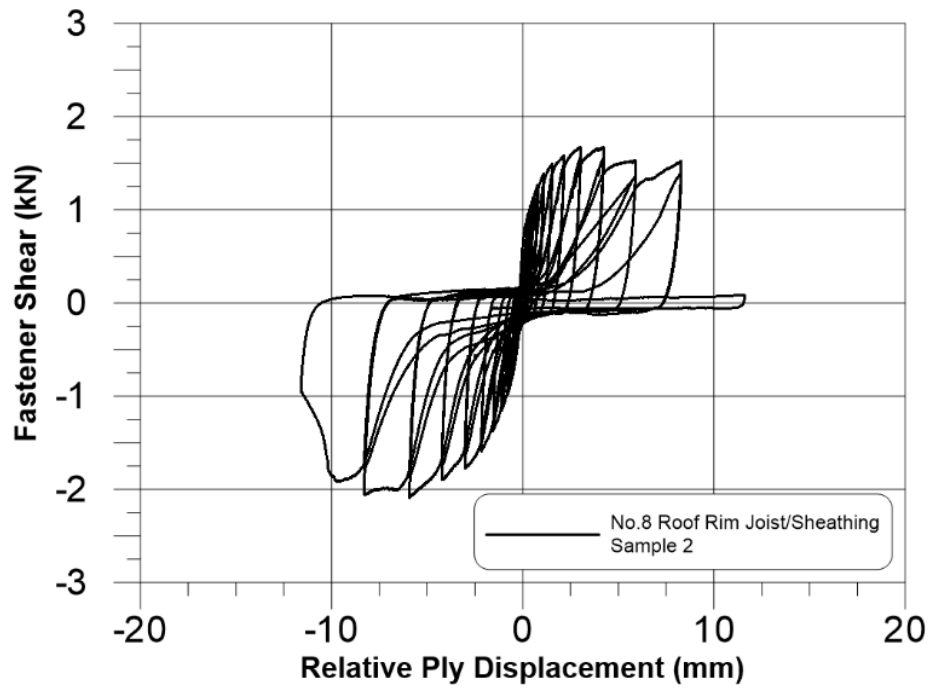


Figure C.5: Roof Rim Joist/Sheathing Connection with #8 Fastener Sample 2

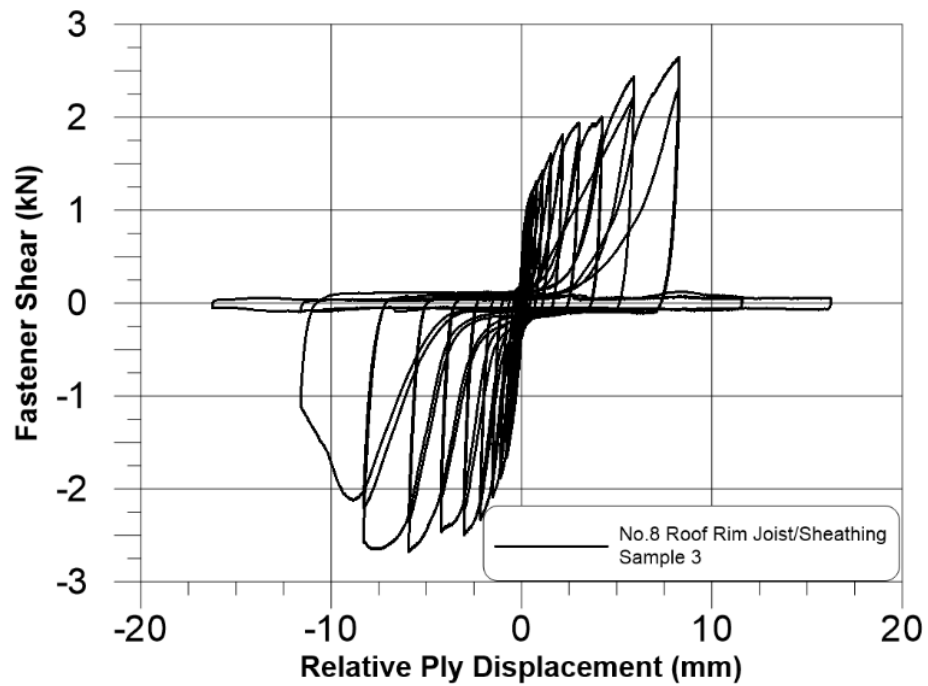


Figure C.6: Roof Rim Joist/Sheathing Connection with #8 Fastener Sample 3

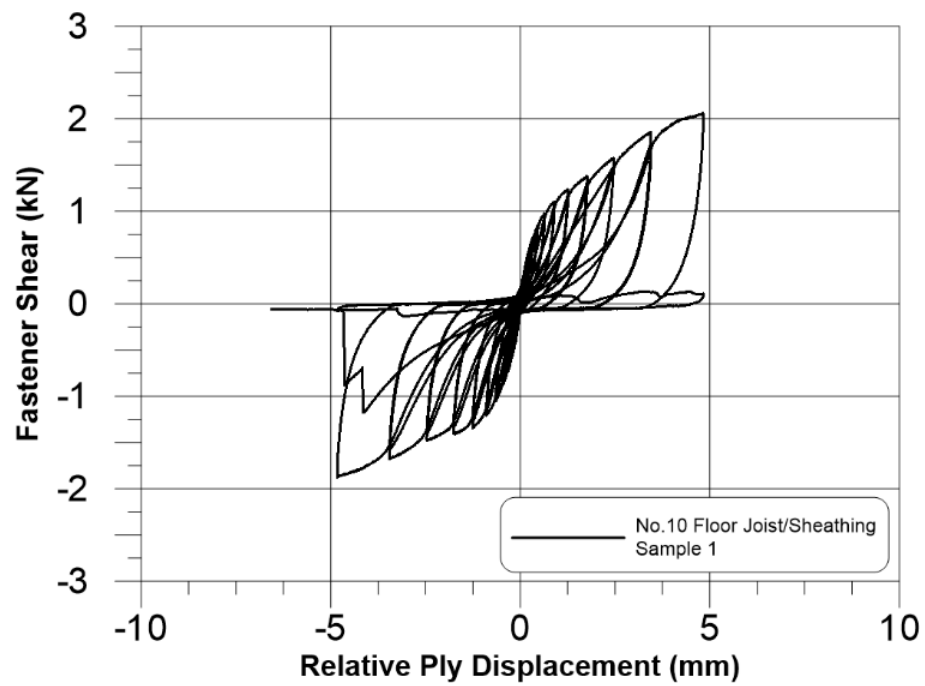


Figure C.7: Floor Joist/Sheathing Connection with #10 Fastener Sample 1

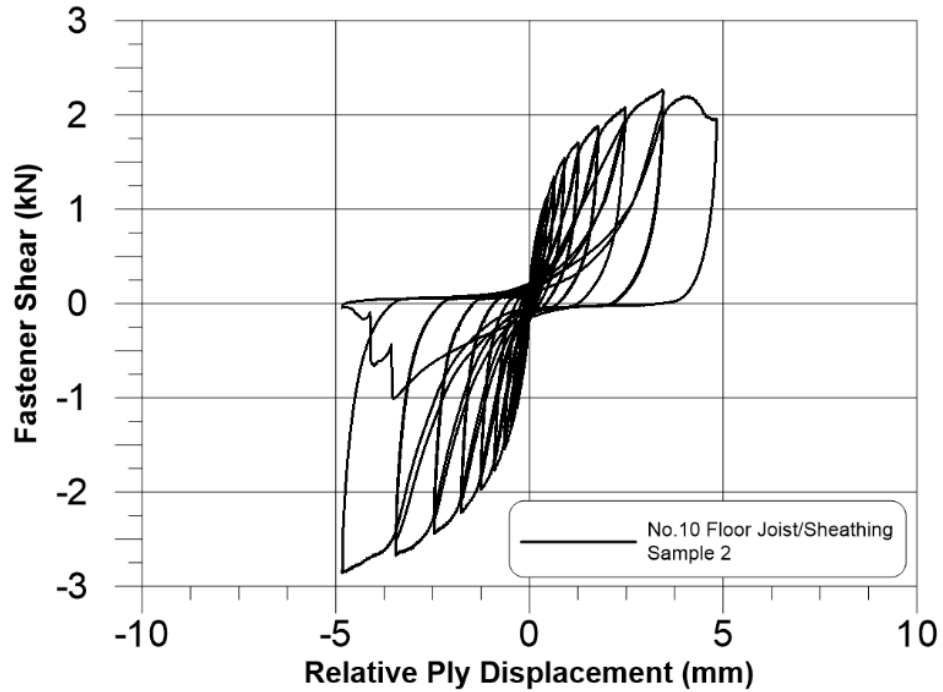


Figure C.8: Floor Joist/Sheathing Connection with #10 Fastener Sample 2

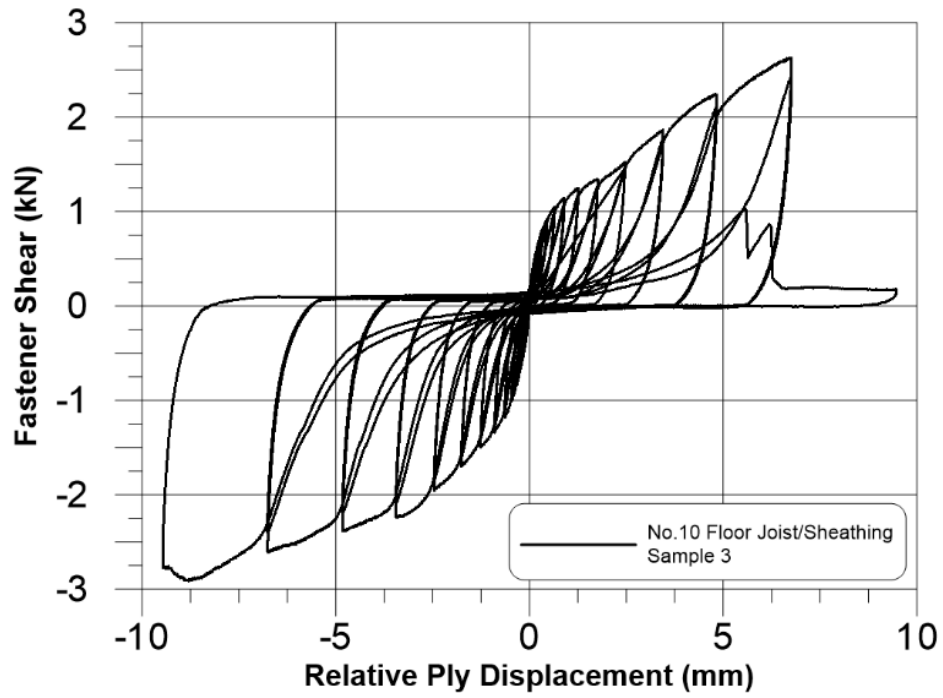


Figure C.9: Floor Joist/Sheathing Connection with #10 Fastener Sample 3

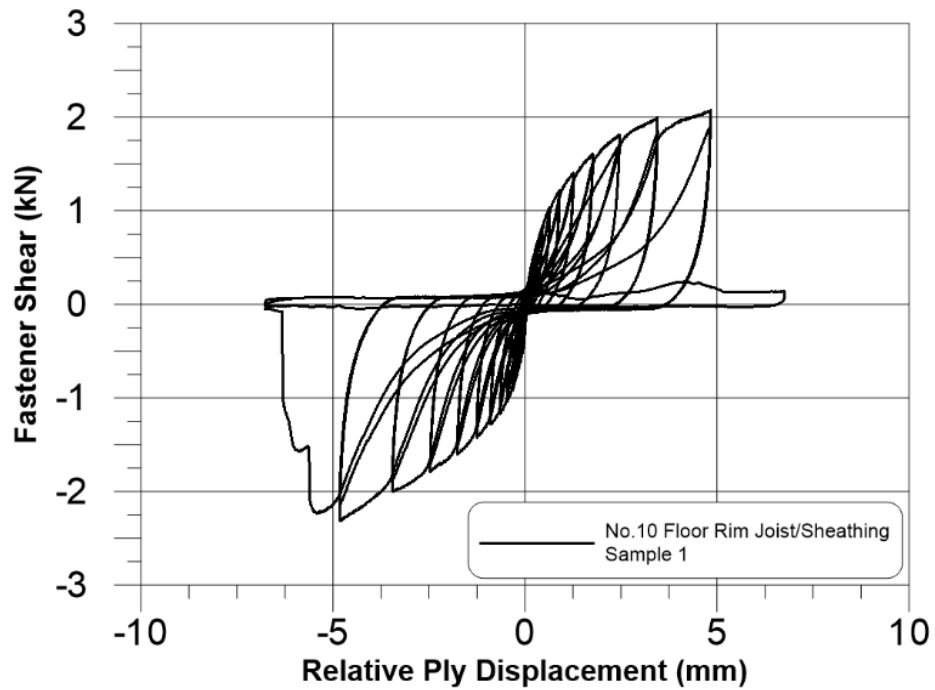


Figure C.10: Floor Rim Joist/Sheathing Connection with #10 Fastener Sample 1

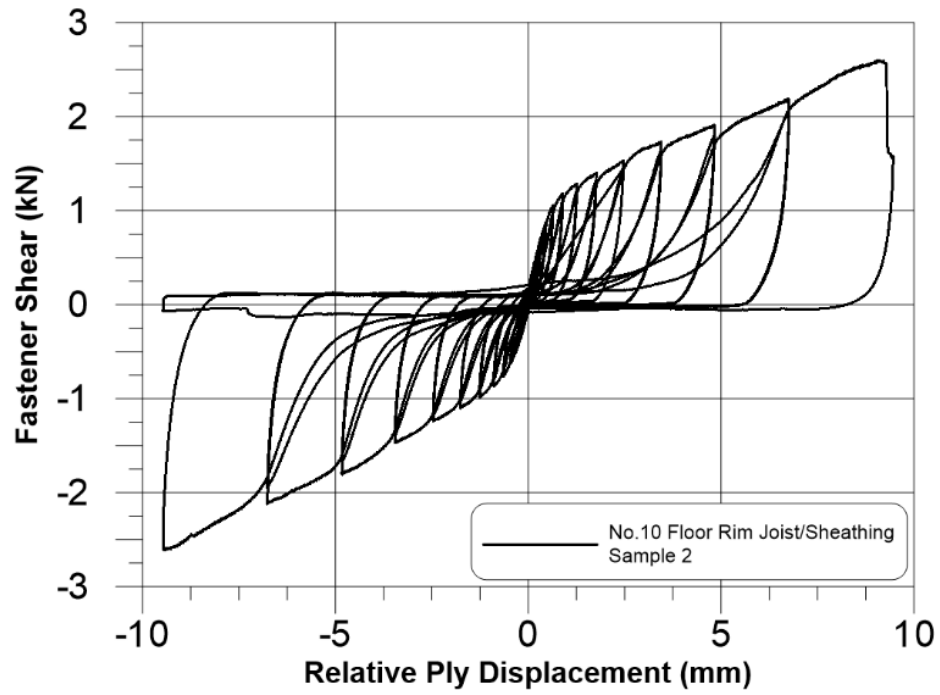


Figure C.11: Floor Rim Joist/Sheathing Connection with #10 Fastener Sample 2

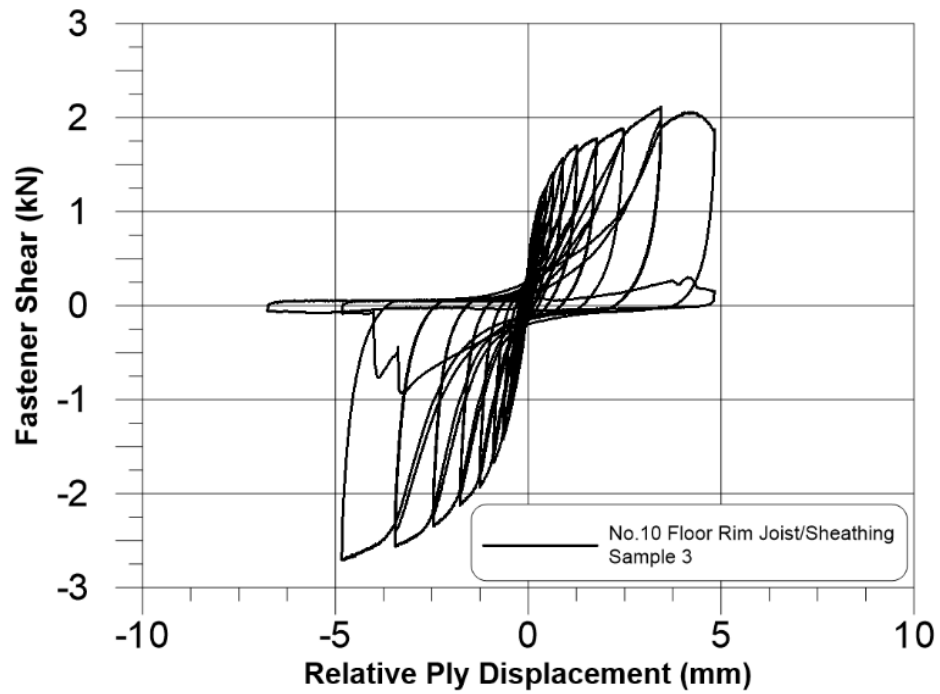


Figure C.12: Floor Rim Joist/Sheathing Connection with #10 Fastener Sample 3

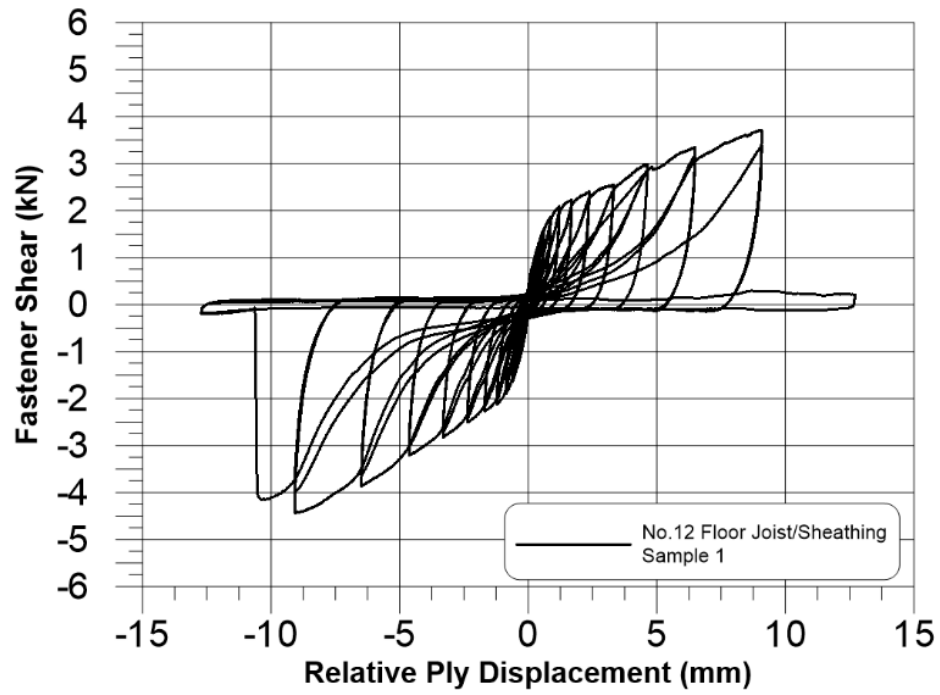


Figure C.13: Floor Joist/Sheathing Connection with #12 Fastener Sample 1

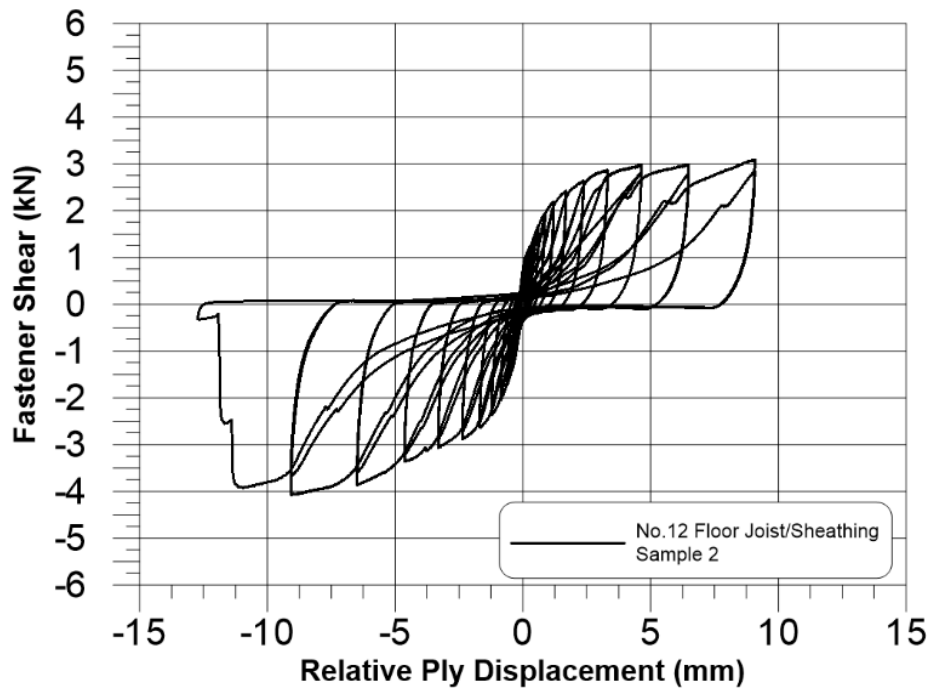


Figure C.14: Floor Joist/Sheathing Connection with #12 Fastener Sample 2

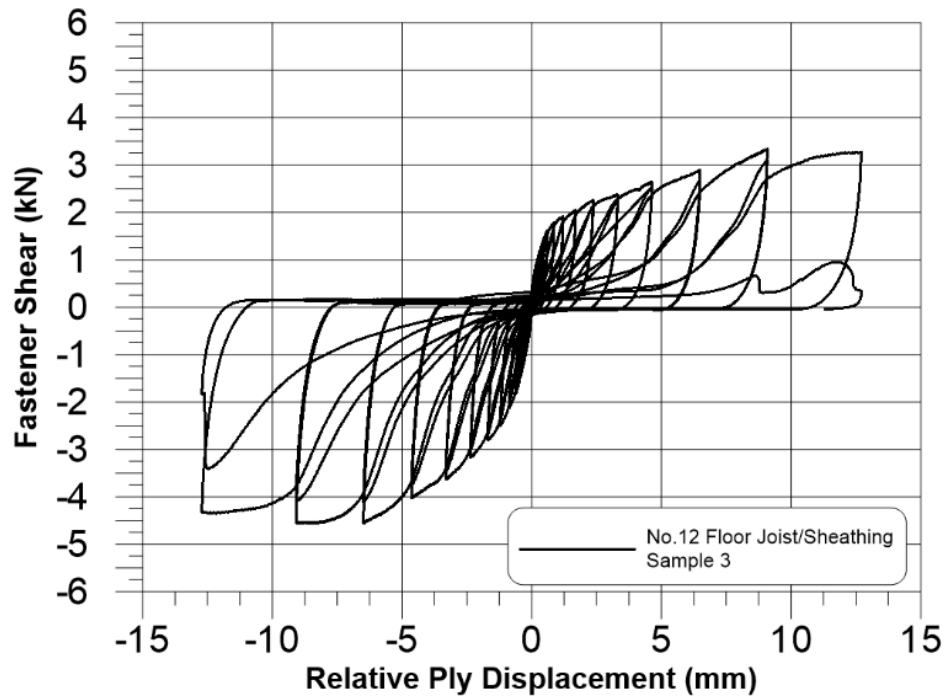


Figure C.15: Floor Joist/Sheathing Connection with #12 Fastener Sample 3

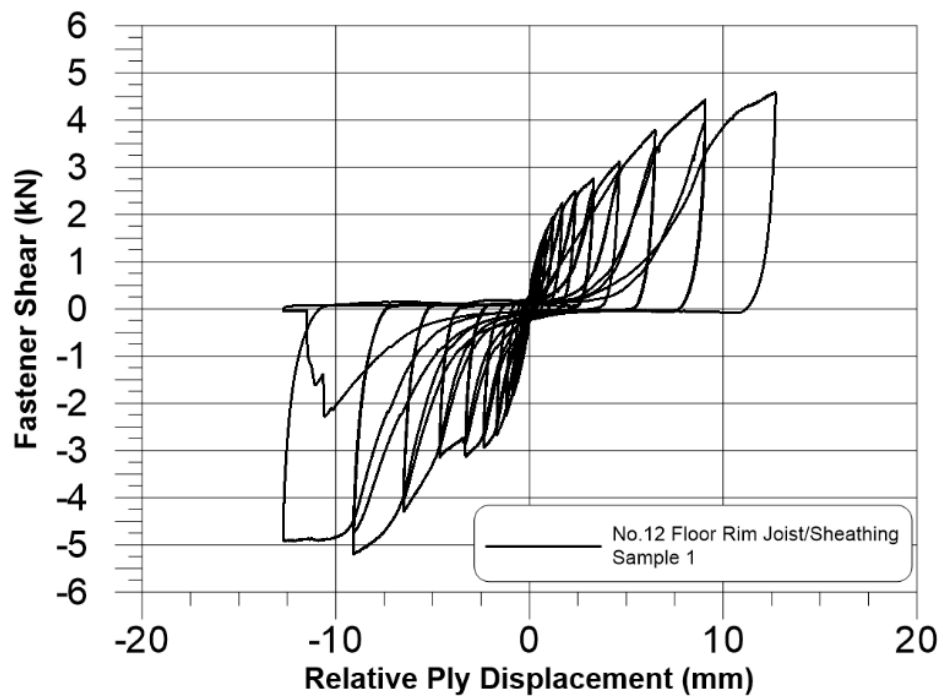


Figure C.16: Floor Rim Joist/Sheathing Connection with #12 Fastener Sample 1

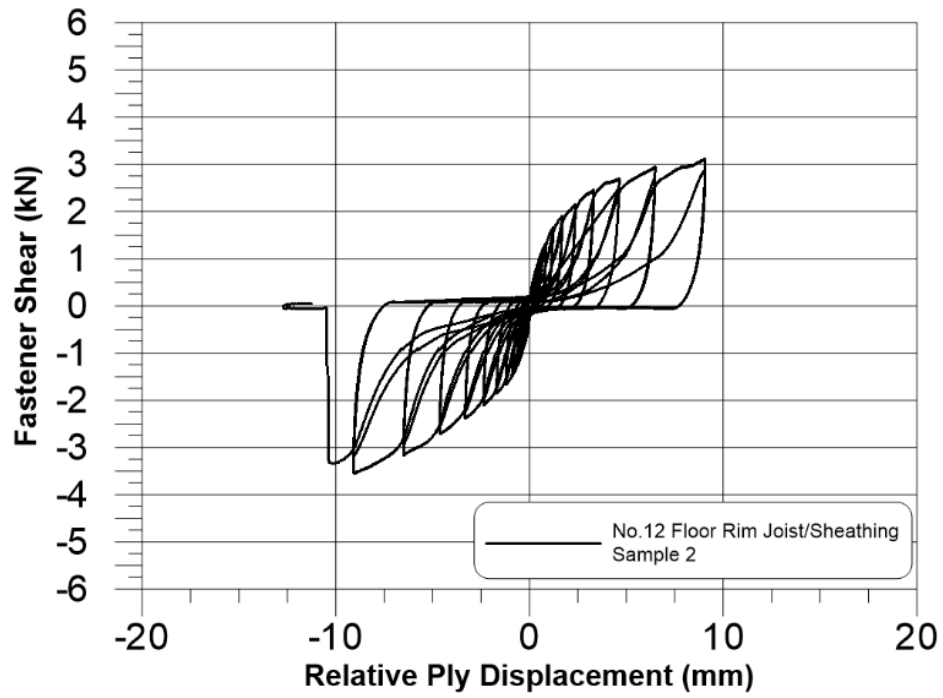


Figure C.17: Floor Rim Joist/Sheathing Connection with #12 Fastener Sample 2

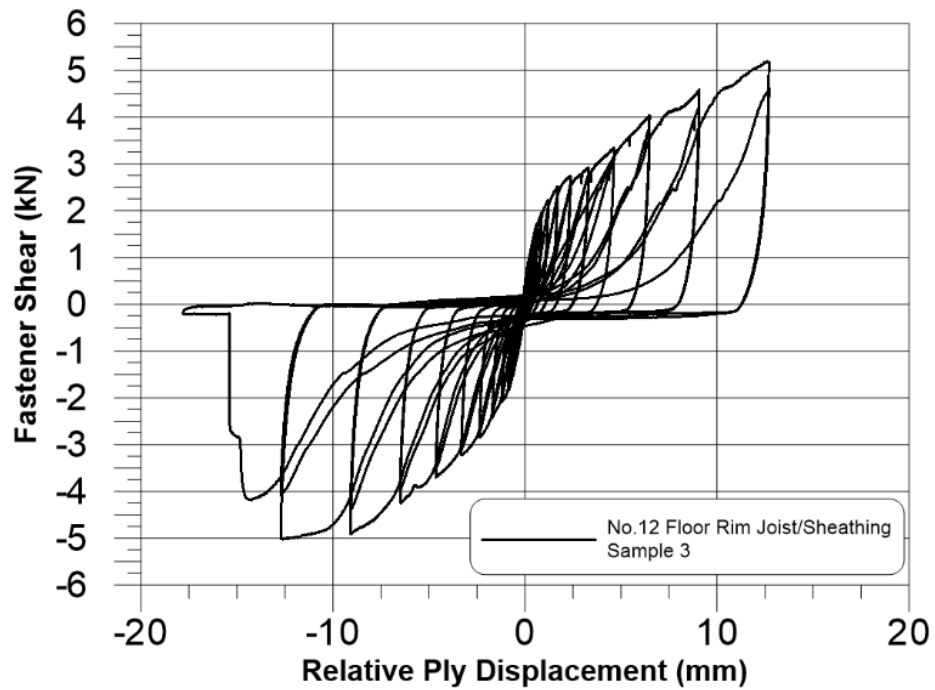


Figure C.18: Floor Rim Joist/Sheathing Connection with #12 Fastener Sample 3

APPENDIX D:
Dowel Bearing Tests

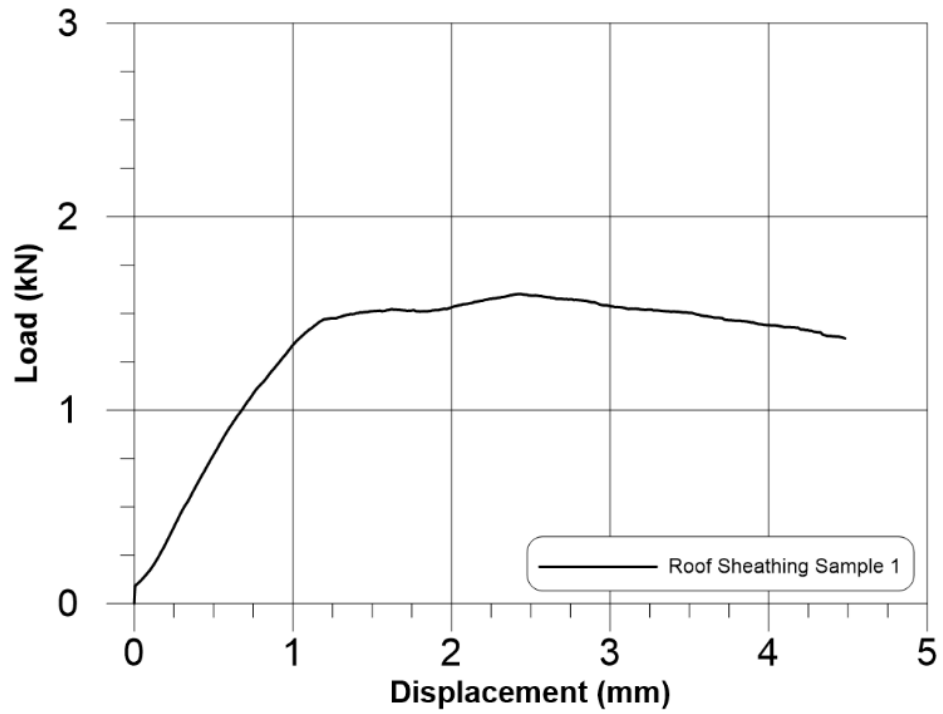


Figure D.1: Roof OSB Sheathing Sample 1

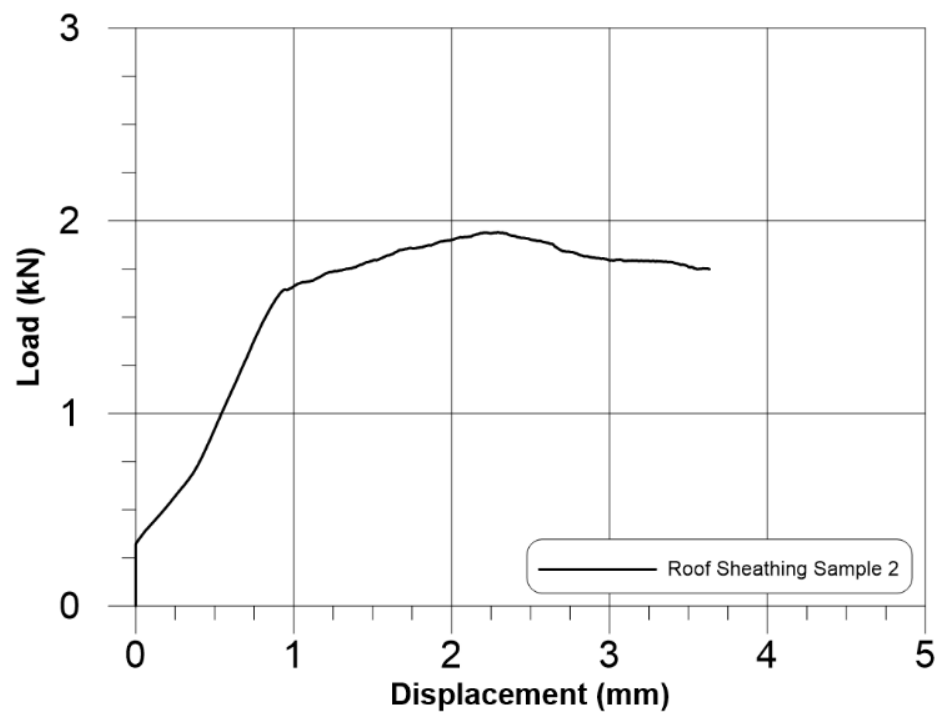


Figure D.2: Roof OSB Sheathing Sample 2

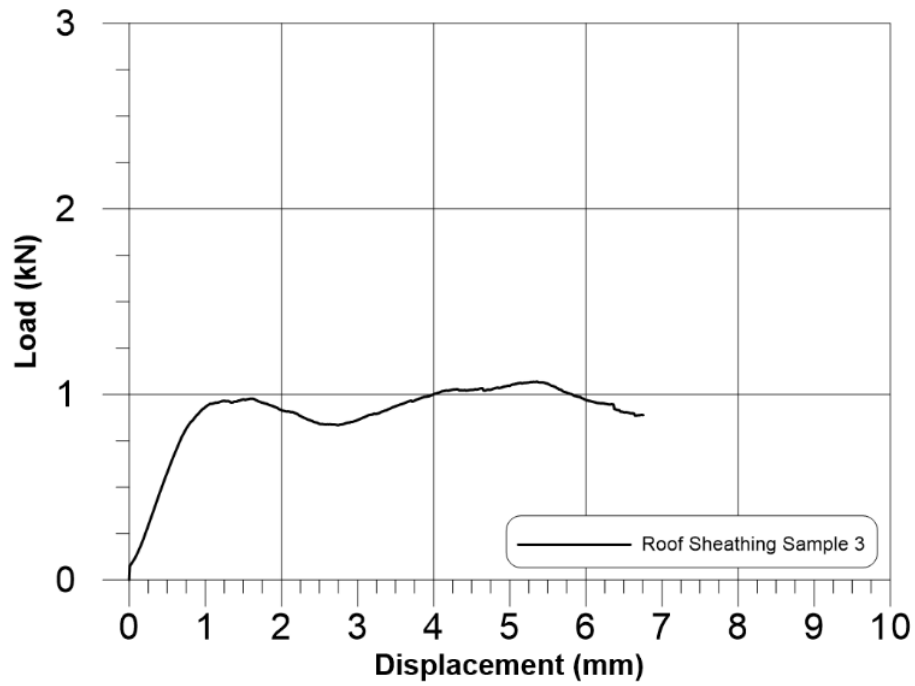


Figure D.3: Roof OSB Sheathing Sample 3

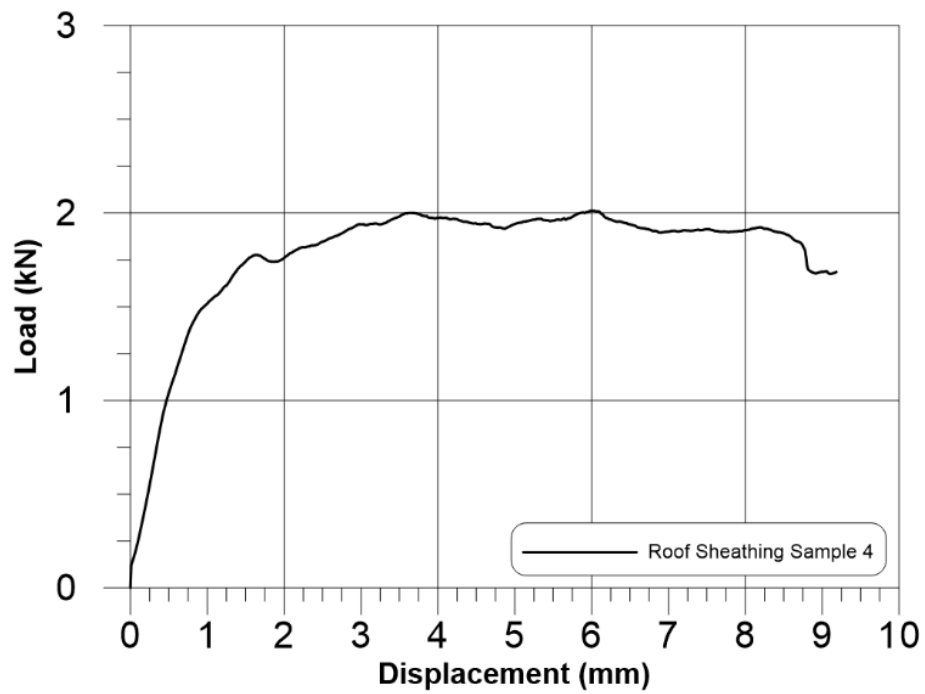


Figure D.4: Roof OSB Sheathing Sample 4

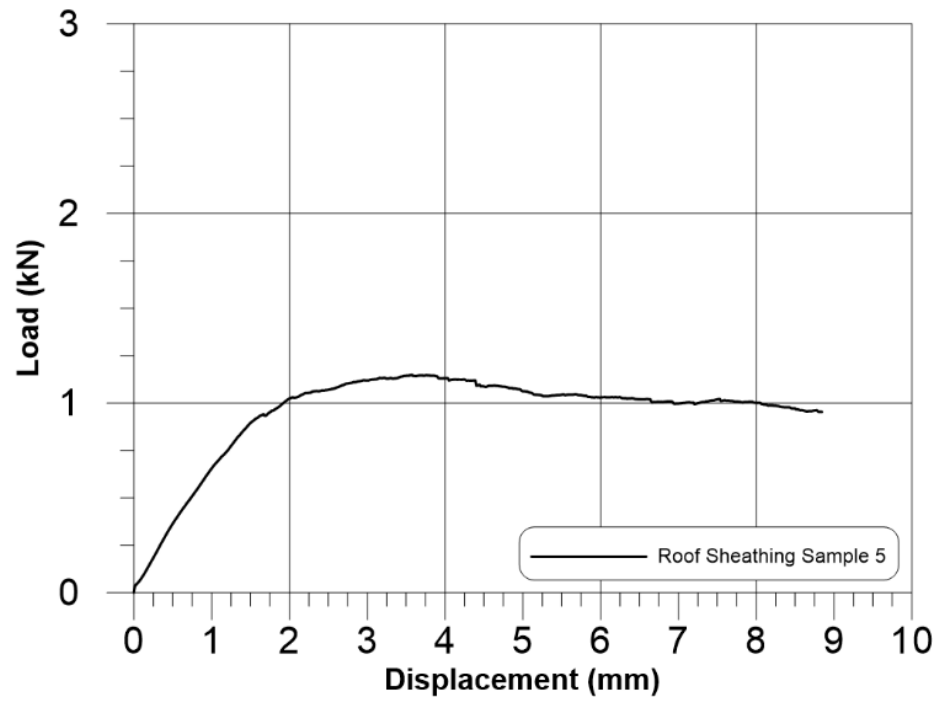


Figure D.5: Roof OSB Sheathing Sample 5

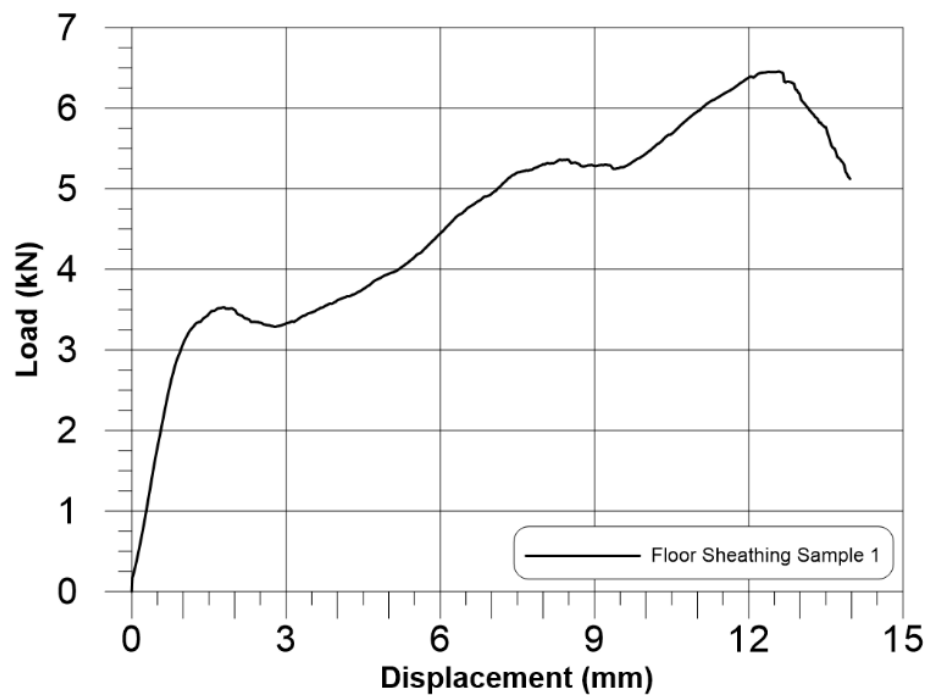


Figure D.6: Floor OSB Sheathing Sample 1

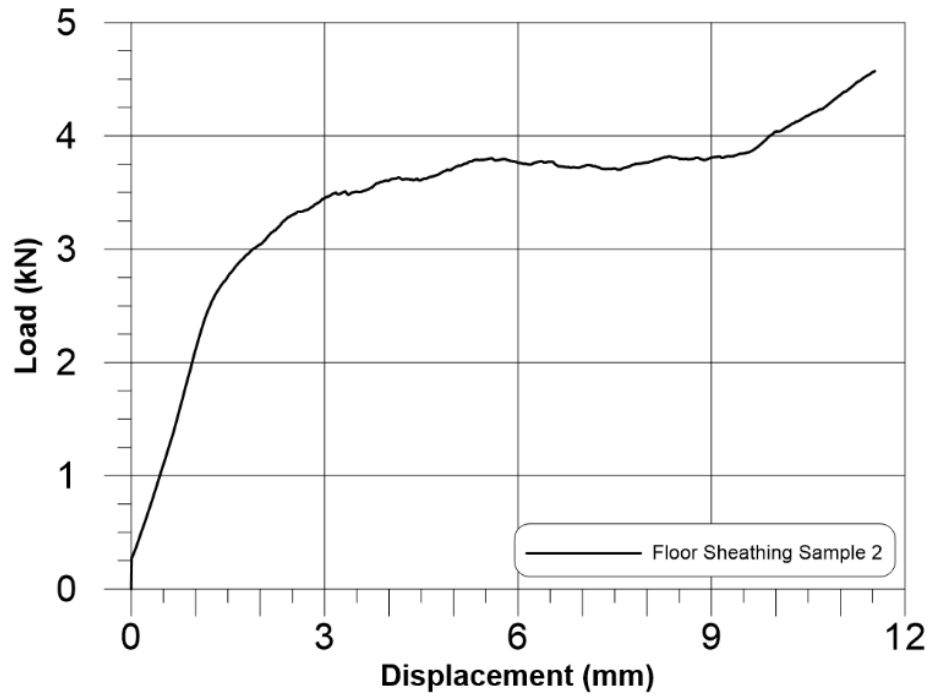


Figure D.7: Floor OSB Sheathing Sample 2

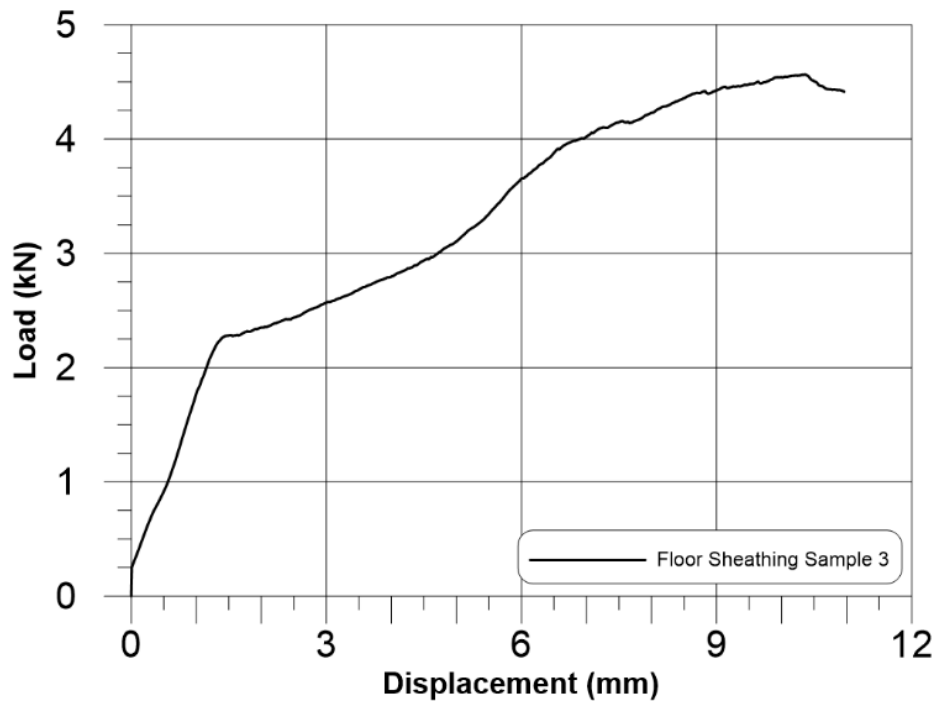


Figure D.8: Floor OSB Sheathing Sample 3

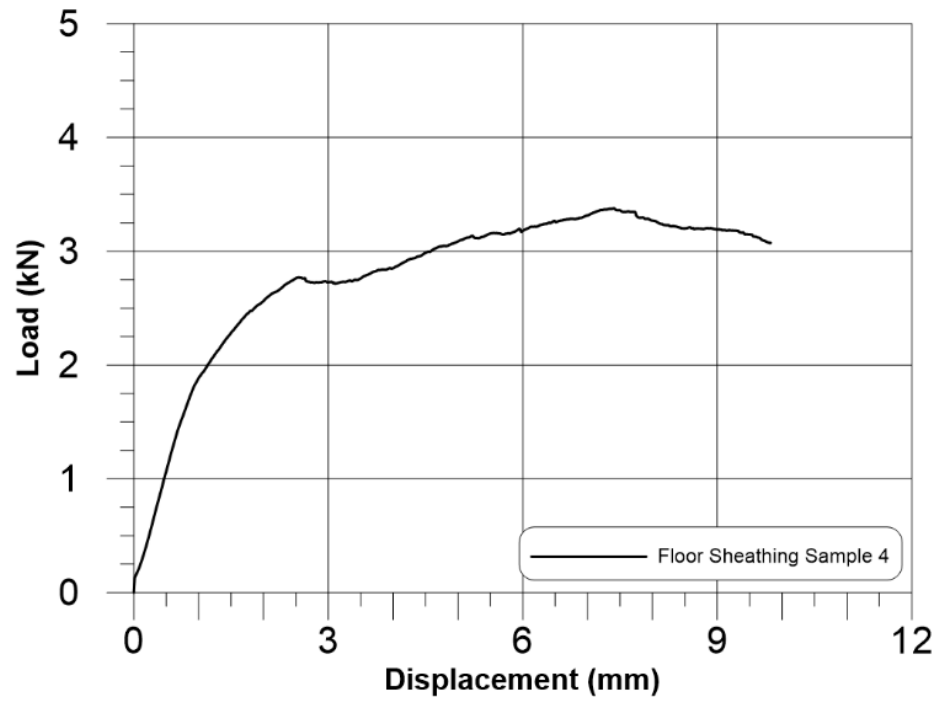


Figure D.9: Floor OSB Sheathing Sample 4

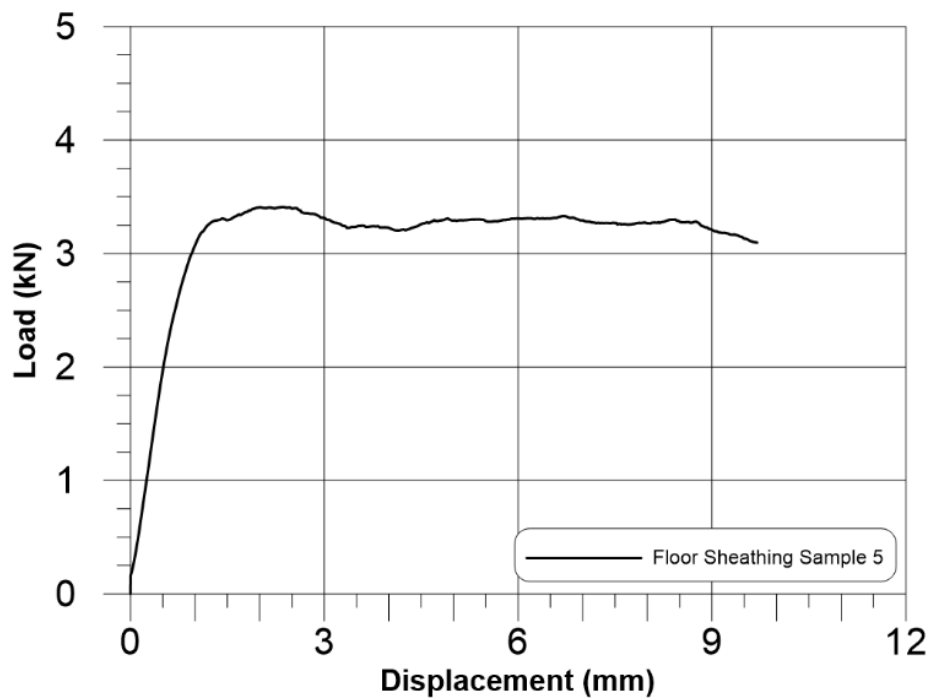


Figure D.10: Floor OSB Sheathing Sample 5